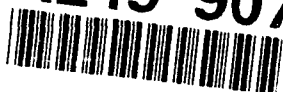AD-A249 907

DTIC
ELECTE
MAY 8 1992
C   D

AD_____

QUANTIFYING THE KINETIC PROCESSES ASSOCIATED
WITH HIV INFECTION OF TARGET CELLS (AIDS)

FINAL REPORT

SCOTT P. LAYNE
MICAH DEMBO

FEBRUARY 11, 1992

Supported by

U.S. ARMY MEDICAL RESEARCH AND DEVELOPMENT COMMAND
Fort Detrick, Frederick, Maryland 21702-5012

MIPR 90MM0545

Los Alamos National Laboratory
Los Alamos, New Mexico 87545

Approved for public release; distribution unlimited.

92   4 29 091

92-11789

REPORT DOCUMENTATION PAGE

Public reporting burden for this collection of information is estimated to average 1 hour per response, including the time for reviewing instructions, searching existing data sources, gathering and maintaining the data needed, and completing and reviewing the collection of information. Send comments regarding this burden estimate or any other aspect of this collection of information, including suggestions for reducing this burden, to Washington Headquarters Services, Directorate for Information Operations and Reports, 1215 Jefferson Davis Highway, Suite 1204, Arlington, VA 22202-4302, and to the Office of Management and Budget, Paperwork Reduction Project (0704-0188), Washington, DC 20503

1. AGENCY USE ONLY (Leave blank)	2. REPORT DATE	3. REPORT TYPE AND DATES COVERED
	February 11, 1992	Final Report 22 Jan 90 – 20 Jan 92

4. TITLE AND SUBTITLE	5. FUNDING NUMBERS
Quantifying the Kinetic Processes Associated with HIV Infection of Target Cells (AIDS)	MIPR 90MM0545
6. AUTHOR(S)	63105A ✓
Scott P. Layne Micah Dembo	3M263105DH29 AD DA331028

7. PERFORMING ORGANIZATION NAME(S) AND ADDRESS(ES)	8. PERFORMING ORGANIZATION REPORT NUMBER
Los Alamos National Laboratory Los Alamos, New Mexico 87545	

9. SPONSORING/MONITORING AGENCY NAME(S) AND ADDRESS(ES)	10. SPONSORING/MONITORING AGENCY REPORT NUMBER
U.S. Army Medical Research & Development Laboratory Fort Detrick Frederick, Maryland 21702-5012	

11. SUPPLEMENTARY NOTES

12a. DISTRIBUTION/AVAILABILITY STATEMENT	12b. DISTRIBUTION CODE
Approved for public release; distribution unlimited	

13. ABSTRACT (Maximum 200 words)

The primary purpose of this project was to develop mathematical models of HIV infection that simulated kinetic processes taking place in viral infectivity assays. The seconday purpose was to develop a series of decisive experimental tests of these kinetic models. The overall goal was to determine whether kinetic modeling improves the quality and reliability of data derived from quantitative infectivity assays, and to see whether the data from model-directed assays lends further insight into in vivo infectious processes. We believe that the specific objectives of this project have been achieved. The findings of this study have practical applications to the standardization of infectivity assays, the testing of therapeutic agents binding to viral gp120 and cellular CD4, and the evaluation of HIV vaccines. We also see improvements in the ability to extrapolate from assays conditions in vitro to physiologic conditions in vivo.

14. SUBJECT TERMS		15. NUMBER OF PAGES
Human immunodeficiency virus (HIV) Acquired immunodeficiency syndrome (AIDS) Kinetic models of infection		
		16. PRICE CODE

17. SECURITY CLASSIFICATION OF REPORT	18. SECURITY CLASSIFICATION OF THIS PAGE	19. SECURITY CLASSIFICATION OF ABSTRACT	20. LIMITATION OF ABSTRACT
Unclassified	Unclassified	Unclassified	Unlimited

FOREWORD

Opinions, interpretations, conclusions, and recommendations are those of the author and are not necessarily endorsed by the U.S. Army.

___E___ Where copyrighted material is quoted, permission has been obtained to use such material.

___N/A___ Where material from documents designated for limited distribution is quoted, permission has been obtained to use the material.

___E___ Citations of commercial organizations and trade names in this report do not constitute an official Department of the Army endorsement or approval of the products or services of these organ ations.

___N/A___ In conducting research using animals, the investigator(s) adhered th the "Guide for the Care and Use of Laboratory Animals," prepared by the Committee on the Care and Use of Laboratory Animals of the Institute of Laboratory Animal Resources, National Research Council (NIH Publication No. 86-23, Revised 1985).

___N/A___ For the protection of human subjects, the investigator(s) have adhered to the policies of applicable Federal Law 45CFR46.

___N/A___ In conducting research utilizing recombinant DNA technology, the investigator(s) adhered to current guidelines promulgated by the National Institutes of Health.

Scott P. Jones 02-11-92
Principal Investigator's Signature   Date

TABLE OF CONTENTS

EXECUTIVE SUMMARY

The primary purpose of this project was to develop mathematical models of HIV infection that simulated kinetic processes taking place in viral infectivity assays. The secondary purpose was to develop a series of decisive experimental tests of these kinetic models. The overall goal was to determine whether kinetic modeling improves the quality and reliability of data derived from quantitative infectivity assays, and to see whether the data from model-directed assays lends further insight into *in vivo* infectious processes. As discussed below, we believe that the specific objectives of this project have been achieved. The findings of this study have practical applications to the standardization of infectivity assays, the testing of therapeutic agents binding to viral gp120 and cellular CD4, and the evaluation of HIV vaccines. We also see improvements in the ability to extrapolate from assays conditions *in vitro* to physiologic conditions *in vivo*.

The simplest models simulated four reactions taking place in infectivity assays: infectious contact between virion and cell, spontaneous shedding of gp120, single-hit viral inactivation, and formation of gp120-blocker complexes (see attached *PNAS* article). By using these models, we developed a series of experiments for investigating the influence of these four reactions on infection. During the course of this project, numerous biological, chemical and physical experiments were undertaken in close collaboration with other laboratories (see APPENDIX for listing of collaborators). The goal of these experiments was to identify agreements or disagreements with the kinetic models, further refine experimental techniques, and reduce the effects of extraneous variables. In general, we found surprisingly close agreement between the simplest kinetic model of HIV infection and quantitative viral infectivity assays. To overcome the remaining disagreements between theory and experiment, we developed a new kinetic model of HIV infection that incorporated a more complete description of viral kinetics. The new features of this model are discussed below (see CONCLUSIONS section).

In this section, we provide an executive summary of the theoretical and experimental accomplishments of this project, and summarize their significance. More complete descriptions of all these points are found in the body of the final report and in the attached publications. We also summarize the papers, presentations and invited talks that were generated from this work.

KINETIC MODELING ACCOMPLISHMENTS AND THEIR APPLICATIONS

■ Formulation of a simple kinetic model of HIV infection that successfully accounts for many experimental observations. This has led to the development of several types of standard infectivity assays, which measure: biological gp120-blocker association constants (K_{assoc}), gp120 shedding rates from virions, and the critical fraction of gp120 molecules.

■ Formulation of a new (or second generation) kinetic model of HIV infection that provides a more complete description of viral behavior. This has facilitated more detailed examinations of the critical number of gp120 molecules, heterogeneities in viral stocks, and initial virus-cell interactions.

■ Development of new methods for reducing assay artifacts and the effects of extraneous variables. This has significantly improved the reproducibility of quantitative infectivity assays with HIV-1 and HIV-2.

■ Development of new and simple criteria for characterizing the "fitness" of HIV stocks. This has lead to improvements in the production of HIV stocks for use in viral infectivity assays and for use as animal challenge stocks in vaccine development programs.

■ Development of new methods for characterizing the blocking activities of soluble CD4 (sCD4), Fab fragments, monoclonal immunoglobulins, and polyclonal sera. This has lead to standardized assay methods between laboratories, permitting the direct comparison of data between investigators.

IMPORTANT EXPERIMENTAL FINDINGS AND THEIR IMPLICATIONS

■ HIV-1 and HIV-2 require a critical number of free gp120 molecules for efficient infection of $CD4^+$ cells. Above the critical number, HIV infects at a rate proportional to the number of free gp120 molecules. Below the critical number, the rate is below proportional (see attached *Nature* article). This finding has two important implications. First, the results of quantitative infectivity assays depend on the age (fitness) of viral stocks. Because of the critical number, old viral stocks which have lost most of their viral-associated gp120 are easier to block than new viral stocks. Without proper controls, viral stocks derived from "chronic" cell cultures can lead to significant

assay artifacts (see Fig. 1). Second, we perceive an inverse relationship between immunoglobulin blocking activity and the critical number of gp120 molecules. Larger critical numbers will require correspondingly smaller humoral responses and *vice versa*. To determine whether this relationship influences the development of HIV vaccines with broad efficacy, it will be important to see how the critical number varies between divergent wild-type strains and CD4$^+$ cells from a number of individuals.

■ As predicted by the kinetic model, the biological blocking activity of sCD4 (a competitive inhibitor) decreases with increasing CD4$^+$ cell density (see Fig. 1). Once HIV infection *in vivo* becomes established in compartments with high CD4$^+$ cell densities (*e.g.*, lymph nodes), it appears that blockers such as immunoglobulins may provide little or no protection. This loss of blocking activity with increasing cell density is a mechanism of persistent HIV infection (see attached *Journal of Virology* article).

■ For HIV-1HXB3, the spontaneous shedding of gp120 and the dissolution of p24 core proteins obey a first order process. This simple form of viral behavior justifies most of the assumptions in kinetic models of HIV infection. In addition, the viral p24 core protein and surrounding lipid membrane are relatively stable compared to the loss of gp120 envelope protein (see BODY section). This means that the loss of HIV infectivity correlates with the spontaneous shedding of gp120. This correlation with gp120 shedding and the requirement for a minimal number of gp120 molecules has led us to postulate that HIV auto-regulates its infectivity and pathogenicity during the extracellular life cycle. See the attached *International Reviews of Immunology* article for a complete discussion of this hypothesis.

■ For monoclonal immunoglobulins and their Fab fragments, small changes in the amino acid sequence of gp120 can lead to rather large changes in biological blocking activity. This finding is preliminary and limited to a small set of murine monoclonals and their Fab fragments (see APPENDIX section). If this finding applies to human immunoglobulins in general, however, it may be impractical to develop HIV vaccines with broad efficacy.

■ The initial phase of HIV infection can be likened to a branching process (see Fig. 2). In this process, each infected target cell generates an average number of progeny virions, V_n, that are released into the extracellular medium. These virions, in turn, infect new target cells with an

average probability, I_n. If the branching number (*i.e.*, the average number of successfully infecting progeny virions) is $V_n \times I_n > 1$, then a growing infection will develop. On the other hand, if the branching number is $V_n \times I_n < 1$, then the initial infection will eventually extinguish. Table 1 summarizes some of the extracellular parameters that determine whether an initial infectious event will result in a "bomb" or "dud." Note that increased humoral blocking activity and increased killing of infected target cells (the latter was not included in the kinetic model) will act in concert to reduce the branching number.
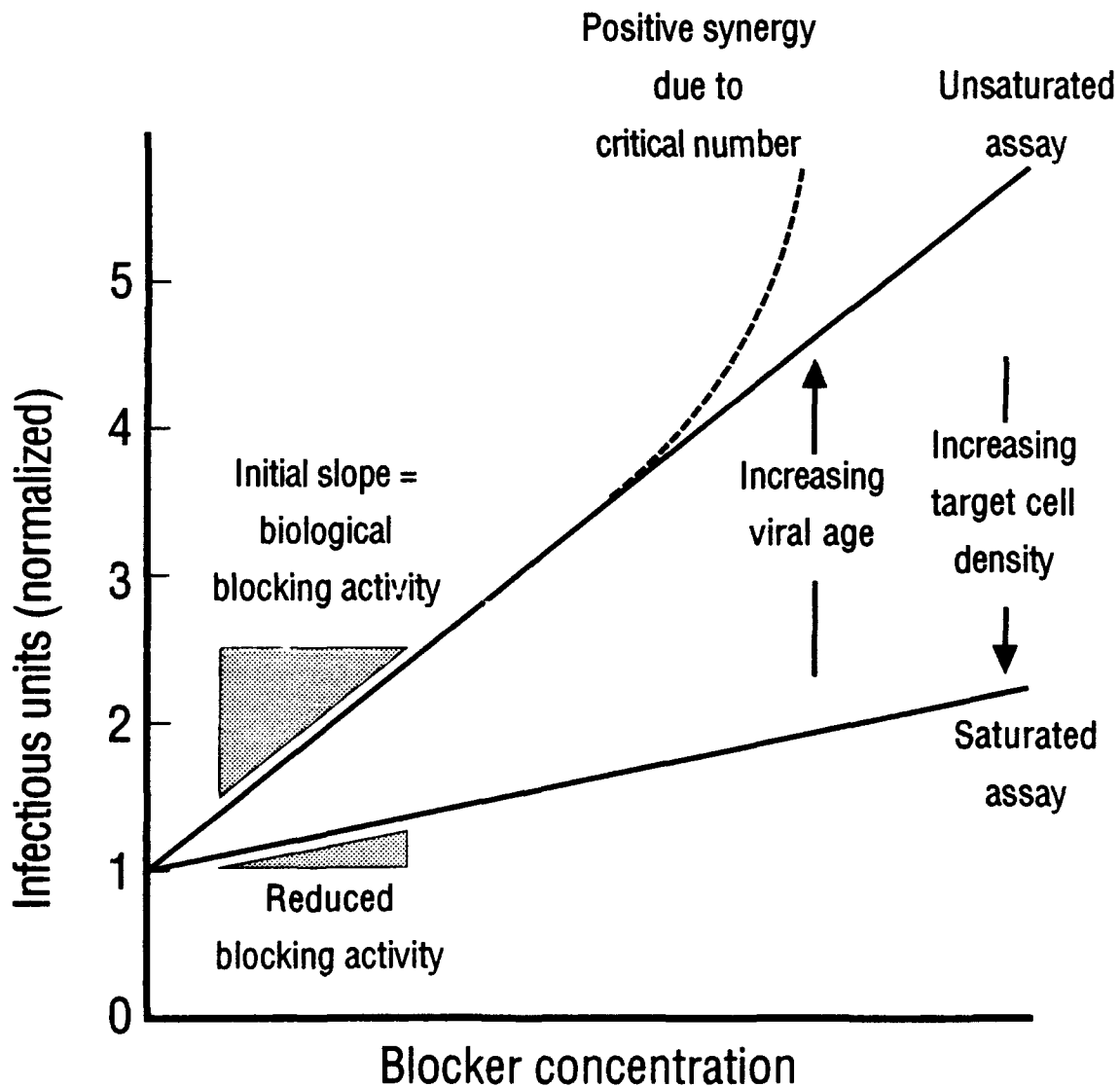
FIG. 1. Summary of the opposing effects of target cell density and viral stock age.
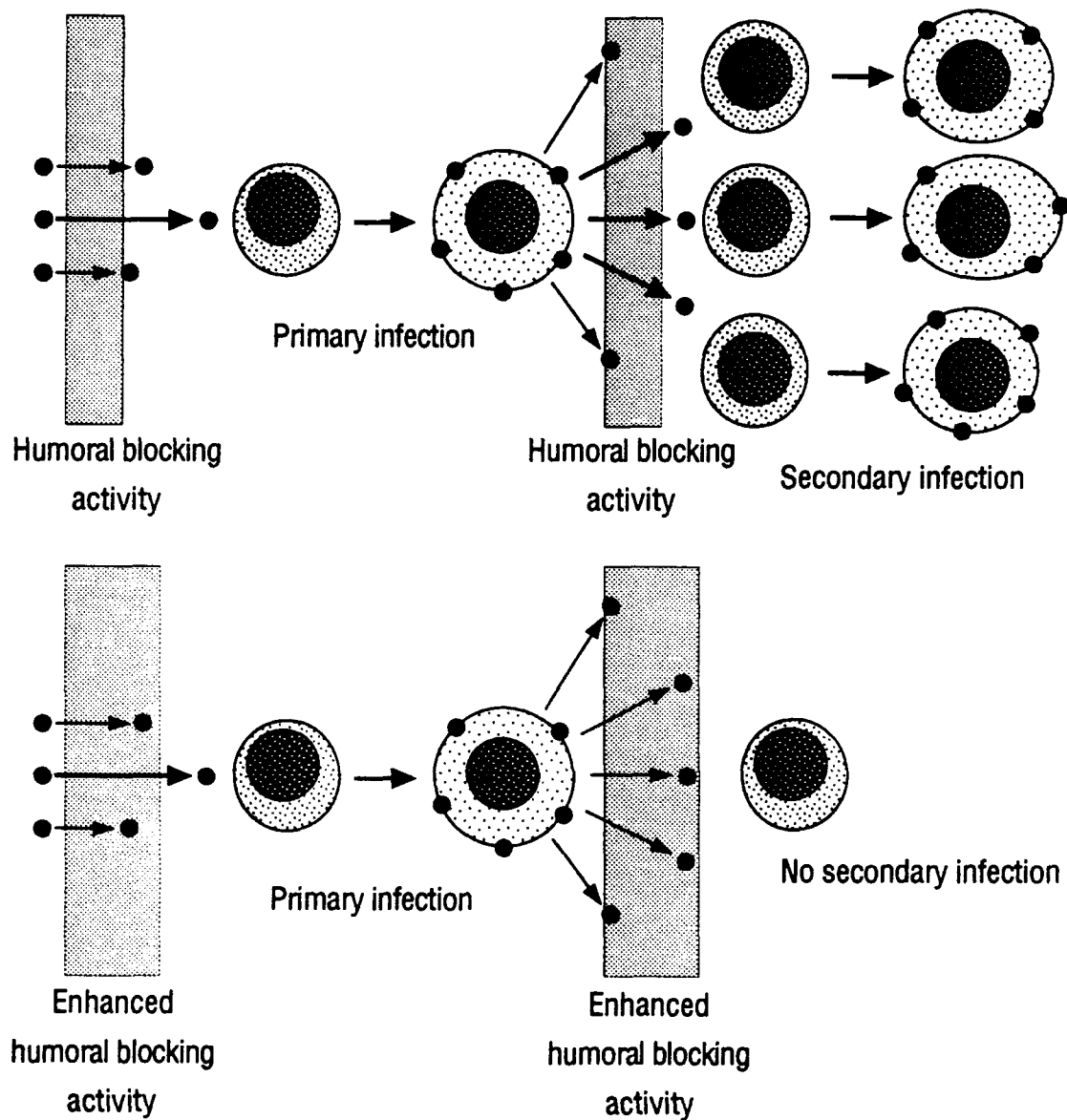
FIG. 2. The initial growth of HIV infection *in vitro* and *in vivo* can be likened to a branching process. Such a process also describes the reactions taking place during nuclear fission. In this case, target cells are analogous to fissionable nuclei, progeny virions are analogous to neutrons, and humoral blockers are analogous to control elements. The figure illustrates the effects of humoral blocking activity. Lower levels of blocking activity (above) permit growth of infection whereas higher levels (below) halt the initial infection. Note that the spread of HIV infection can be arrested even after an initial infectious event. Table 1 summarized other extracellular parameters that influence whether a chain reaction is achieved or not.

Table 1. *Extracellular parameters determining whether the initial branching process leads to a "bomb" or "dud"*

Factors promoting the growth of infection
- increased target cell density (*i.e.*, infection in lymphoid organs)
- increased number of progeny virions
- increased gp120 on active virions
- increased lifetime of infectious particles
- decreased critical number

Factors promoting the extinction of infection
- increased humoral blocker concentration
- increased gp120-blocker K_{assoc}
- increased gp120 shedding rate
- increased nonspecific viral inactivation rate
- increased critical number
- increased killing rate of infected target cells (*i.e.*, cell-mediated immunity)

NEW EXPERIMENTAL OBSERVATIONS FROM THIS PROJECT

■ Measuring the gp120 half life in virions by ELISA and electron microscopy (EM).

■ Measuring the p24 half life in virions by ELISA.

■ Measuring the viral lipid membrane half life by EM.

■ Measuring the RNA polymerase (reverse transcriptase) activity half life in virions.

■ Quantify absolute particle densities by EM.

■ Measuring the absolute p24 content per particle.

■ Measuring the ratio of infectious to noninfectious viral particles.

■ Correlating sCD4 blocking activity with gp120 spontaneous shedding.

■ Correlating the initial slope of viral decay assays with the half life of gp120.

■ Correlating increasing positive synergy in sCD4 blocking with gp120 spontaneous shedding.

■ Showing that CEM-SS cells and H-PBMC have similar HIV-1 infection susceptibilities.

■ Showing that ultracentrifugation does not degrade HIV infectivity.

■ Showing that total concentrations of p24 and gp120 are stable in viral stocks with time.

■ Measuring the loss RNA polymerase activity in viral stocks with preincubation time.

■ Measuring changes in the inhibitory action of phosphonoformate (foscarnet) with time.

PUBLICATIONS ON THIS RESEARCH

1. Scott P. Layne, Michael J. Merges, Micah Dembo, John L. Spouge & Peter L. Nara. HIV requires multiple gp120 molecules for CD4-mediated infection. *Nature* 346, 277–279 (1990).

2. Scott P. Layne, Michael J. Merges, John L. Spouge, Micah Dembo & Peter L. Nara. Blocking of HIV infection depends on cell density and viral stock age. *J. Virology* 65, 3293–3300 (1991).

3. Scott P. Layne & Micah Dembo. The auto-regulation model: A unified concept of how HIV regulates its infectivity, pathogenesis and persistence. *International Reviews of Immunology* 8, 33–64 (1992).

4. Peter L. Nara, Mike Merges, Nancy Dunlop, Wen-Po Tsai, and Scott P. Layne. Unit 11.6. Neutralization, inactivation, and cell-fusion inhibition assays for the study of immunoglobulin and anti-viral immunotherapeutic agents against HIV. *Current Protocols* (1992, in the press).

MANUSCRIPTS IN PREPARATION ON THIS RESEARCH

1. Scott P. Layne, Michael J. Merges, Micah Dembo, John L. Spouge, Shawn R. Conley, John P. Moore, Jawahar L. Raina, Herbert Renz, Hans R. Gelderblom & Peter L. Nara. Spontaneous shedding of gp120 from HIV-1 modulates infectivity. *Virology* (1992, to be submitted).

2. Michael J. Merges, Peter L. Nara, and Scott P. Layne. Measuring the blocking activity and valency of monoclonal immunoglobulins and their Fab fragments against HIV-1. *J. Virology* (1992, in preparation).

3. Herbert Renz, Hans R.Gelderblom, Peter L. Nara, Michael J. Merges, and Scott P. Layne. Electron microscope measurements of HIV particle density and spontaneous gp120 shedding. *Methods in Virology* (1992, in preparation).

MEETING ABSTRACTS ON THIS RESEARCH

1. Scott P. Layne, Michael J. Merges, Micah Dembo, John L. Spouge & Peter L. Nara. HIV gp120 Cooperativity: A New Outlook on Viral Receptor/Anti-Receptor Based Interventive Strategies. *Johns Hopkins Conference on AIDS.* April 2–3 (1990).

2. Scott P. Layne, Michael J. Merges, Micah Dembo, John L. Spouge & Peter L. Nara. GP120 Cooperativity: A New Finding that Pertains to Vaccine Development and Receptor / Anti-Receptor Therapies. *6th International AIDS Conference* Abstract No. F.A.O.317 (1990).

3. Scott P. Layne, Michael J. Merges, Micah Dembo, John L. Spouge Hans R. Gelderblom & Peter L. Nara. Determining Basic Molecular Requirements for Blocking Therapies and HIV Vaccines *in vitro*. *Annual Meeting of the Laboratory of Tumor Cell Biology*. August 11–17 (1990).

4. Scott P. Layne, Michael J. Merges, Micah Dembo, John L. Spouge & Peter L. Nara Determining Basic Molecular Requirements for Blocking Therapies and HIV Vaccines *in vitro*. *Modern Approaches to New Vaccines Including Prevention of AIDS*. Cold Spring Harbor Laboratory. September 12–16 (1990).

5. Scott P. Layne, Michael J. Merges, Micah Dembo, John L. Spouge & Peter L. Nara. Envelope Shedding and High Cell Density: Barriers to Vaccine and Immunotherapy Development. *7th International AIDS Conference* Abstract No. M.A.1270 (1991).

6. Scott P. Layne, Michael J. Merges, Micah Dembo, John L. Spouge & Peter L. Nara. Relationships Between Envelope Shedding, Cell Density, and Humoral Blocking Activity. *Annual Meeting of the Laboratory of Tumor Cell Biology*. September 1–8 (1991).

7. Scott P. Layne, Michael J. Merges, Micah Dembo, John L. Spouge & Peter L. Nara High physiologic cell CD4+ cell densities overcome the neutralizing activity of antibodies — A mechanism of HIV persistence. *Modern Approaches to New Vaccines Including Prevention of AIDS*. Cold Spring Harbor Laboratory. September 19–23 (1991).

ADVISORY COMMITTEES MAKING USE OF THIS RESEARCH

1. *NIAID Primate Challenge Viral Stock Workshop*, October 15, 1991, Marco Island, FL.

2. *NCI AIDS Antiviral Drug Discovery Advisory Meeting*, November 14–15, 1991, Bethesda, MD.

INVITED TALKS ON THIS RESEARCH

DATE	CONTACT	ORGANIZATION & LOCATION
02-15-90	Dr. David Ho	UCLA / Cedars-Sinai Medical Center Los Angeles, CA
02-26-90	Dr. Anthony Fauci	National Institute for Allergy and Infectious Disease Bethesda, MD
03-16-90	Dr. Nancy Haigwood	Chiron Corporation Emeryville, CA
07-16-90	Dr. Donald Burke	Walter Reed Institute of Army Research Rockville, MD
09-24-90	Dr. John Wohlheiter	Walter Reed Institute of Army Research Washington, DC
10-30-90	Dr. Robert Sutherland	SRI International Menlo Park, CA
12-10-90	Dr. Jim Mullins	Stanford University Stanford, CA
04-30-91	Dr. Gerald Eddy	Henry M. Jackson Foundation Rockville, MD
09-16-91	Dr. David Ho	The Aaron Diamond AIDS Research Center New York, NY
10-23-91	Dr. Ron Swanstrom	Lineberger Cancer Center, Univ. North Carolina Chapel Hill, NC
01-22-1992	Dr. Bruce Walker	Massachusetts General Hospital Boston, MA

PERSONNEL RECEIVING PAY FROM THE CONTRACT SUPPORT

Scott P. Layne, M.D.
Biology & Biophysics Group (T–10)
Mail Stop K710
Los Alamos National Laboratory
Los Alamos, New Mexico 87545
(505) 667-7510 TEL
(505) 665-3493 FAX

Micah Dembo, Ph.D.
Biology & Biophysics Group (T–10)
Mail Stop K710
Los Alamos National Laboratory
Los Alamos, New Mexico 87545
(505) 667-4799 TEL
(505) 665-3493 FAX

INTRODUCTION

Human immunodeficiency viruses (HIV) are highly labile and a variety of decay processes are thought to contribute to this property. As described in the kinetic model of HIV infection (Layne *et al.*, 1989), this includes the spontaneous dissociation of gp120 envelope proteins from their underlying gp41 transmembrane proteins, which takes place because the interactions are entirely noncovalent (Gelderblom *et al.*, 1985). The physical breakdown of the lipid shell covering viral particle, which is facilitated by surface active agents in the fluid medium (Nara *et al.*, 1987). The dissolution of p24 core proteins encasing viral RNA, which presumably follows the disappearance of the lipid shell and is hastened by enzymatic attack (McDougal *et al.*, 1985). And the spontaneous loss of RNA polymerase activity, which takes place at physiologic temperature is caused by undefined mechanisms (Lori *et al.*, 1988; Goff, 1990). At present, however, there is little information on the kinetics of these chemical reactions, their rate constants, and how widely these rates vary between viral isolates at physiologic conditions. Furthermore, there is scant understanding of how these reactions influence the activities of antiviral agents that attack extracellular or intracellular events in the viral life cycle (Looney *et al.*, 1990; Layne and Dembo, 1992; Lu *et al.*, 1992; Fernandez-Larsson *et al.*, 1992).

During the past two years, we have undertaken an extensive study of the kinetic reactions of HIV-1HXB3 (Shaw *et al.*, 1984). This laboratory strain was chosen over others because HIV-1HXB3 was relative easy to grow and store large volumes, and because recombinant gp120, p24 and RNA polymerase proteins were available for the absolute calibration of chemical assays. The strategy of this study was to perform a variety of physical, chemical and biological assays on the same viral stock, permitting correlations between the different types of data. Physical measurements of particle density and the number of gp120 knobs per virion were carried out by electron microscopy. Chemical measurements of gp120 envelope and p24 core proteins were carried out by ELISA. Biochemical measurements of RNA polymerase activity were performed by quantitative enzymatic assays. Biological measurements of viral titer, spontaneous viral inactivation and the activities antiviral agents were performed by quantitative infectivity assays. To determine basic kinetic parameters, such as half lives and reaction orders, assays were repeated on

viral stocks that were preincubated for various intervals at 37° C. To investigate how the perturbation of virus-cell binding was influenced by preincubation, sCD4 was used as a blocking agent at concentrations that did not facilitate spontaneous shedding of gp120 (Moore *et al.*, 1990; McKeating *et al.*, 1991; Layne *et al.*, 1991). Also to investigate how the perturbation of reverse transcription was influenced by preincubation, phosphonoformate (foscarnet) was used as a noncompetitive inhibitor of viral RNA polymerase at concentrations that were nontoxic to cells (Majumdar *et al.*, 1978; Öberg, 1983). As explained below, both types of "perturbation" assays were necessary for unraveling how the individual inactivation processes contributed to the loss of HIV infectivity.

Previous studies found that the blocking activity of sCD4 was inversely related to the density of CD4$^+$ cell in viral infectivity assays (Layne *et al.*, 1991; Dimitrov *et al.*, 1992). For "unsaturated" assays at low target cell densities, the biological blocking activity of sCD4 corresponded to the gp120-sCD4 association constant (K_{assoc}) from chemical measurements. That is, the inhibition of infection was proportional to the formation of gp120-sCD4 complexes (Layne *et al.*, 1990). For "saturated" infectivity assays at high target cell densities, on the other hand, the biological blocking activity of sCD4 fell far below the chemical K_{assoc}. This decline occurred because the CD4 receptors on cell surfaces, which mediated infection, competed successfully with the sCD4 molecules in solution for viral-associated gp120 molecules (Layne *et al.*, 1989). Therefore, to permit direct comparisons between chemical and biological measurements, the majority of infectivity assays in this study were carried out at low target cell densities.

Also previous studies indicated that HIV requires a minimal (threshold) number of free gp120 molecules for efficient infection of CD4$^+$ cells (Bym *et al.*, 1989; Layne *et al.*, 1990). When more than this minimal number were present on a virion, the rate of infection was proportional to free gp120. When less than this number were present, the rate of infection was significantly reduced. These studies did not, however, assemble sufficient information to estimate the actual size of this number. Thus, a further goal of this project was to determine the minimal number for HIV-1HXB3 and CEM-SS cells by utilizing the relevant physical, chemical and biological data.

BODY

In this section, we review the experimental methods in sufficient detail to permit the replication of all data. We review the results obtained, with emphasis on how it applies to the kinetic model of HIV infection. We then discuss the results relative to the goals of this project and consider how they apply to the standardization of infectivity assays, the testing of therapeutic agents binding to viral gp120 and cellular CD4, and the evaluation of HIV vaccines.

EXPERIMENTAL METHODS

■ **Culturing human peripheral blood mononuclear cells (H-PBMC)** — Three days before an assay, white cells were isolated from packed blood (one HIV-negative donor) by centrifugation through Ficoll-Paque. The white cells were washed twice [suspended in 50 ml of phosphate-buffered saline (PBS) and centrifuged for 10 minutes at $300 \times g$], the remaining red cells were disrupted with 25 ml of ammonium chloride lysis buffer (Biofluids, Inc.), and the white cells were again washed twice. The white cells were cultured (37° C and 5% CO_2) in polystyrene flasks at 2×10^6 cells ml^{-1} with RPMI 1640 containing 10% fetal bovine serum (FBS) and 2 μg ml^{-1} phytohemagglutinin (PHA). After two days, nonadherent cells were centrifuged (10 minutes at $300 \times g$) to remove PHA and were placed in polystyrene flasks at 1×10^6 cells ml^{-1} with RPMI 1640 containing 10% FBS and 32 units ml^{-1} of IL-2. The next day, these stimulated H-PBMC were used as target cells in viral infectivity assays.

■ **Growing viral stocks** — H9 cells were grown at densities (~5×10^5 ml^{-1}) that maintained exponential growth. A total of 2.5×10^8 H9 cells were suspended in 100 ml of media with 50 nM DEAE-Dextran (Pharmacia) for 30 minutes, centrifuged for 10 minutes at $300 \times g$, and suspended in 50 ml of fresh media containing RPMI 1640, 10% FBS and 1% penicillin, streptomycin, and neomycin antibiotics (PSN). The treated H9 cells were inoculated with 50 ml of freshly thawed HIV-1HXB3 stock (multiplicity of infection, MOI ≈ 0.1). After incubation for one hr at 37°C, the infected H9 cells were washed twice (centrifuged for 10 minutes at $200 \times g$, followed by suspension in 100 ml PBS and again centrifuged), suspended in 500 ml of fresh media, and incubated in a roller bottle at 37° C. Two days later, the infected H9 culture was clarified by

centrifugation (20 minutes at $10,000 \times g$) and frozen ($-70°$ C) in 10 ml aliquots. To monitor the titer of HIV-1HXB3 stocks, infected H9 cultures were incubated for periods of 4 to 6 days. At daily intervals, 5 ml aliquots of supernatant were removed, clarified by centrifugation, and frozen. Subsequently, these samples were assayed in parallel for infectious units.
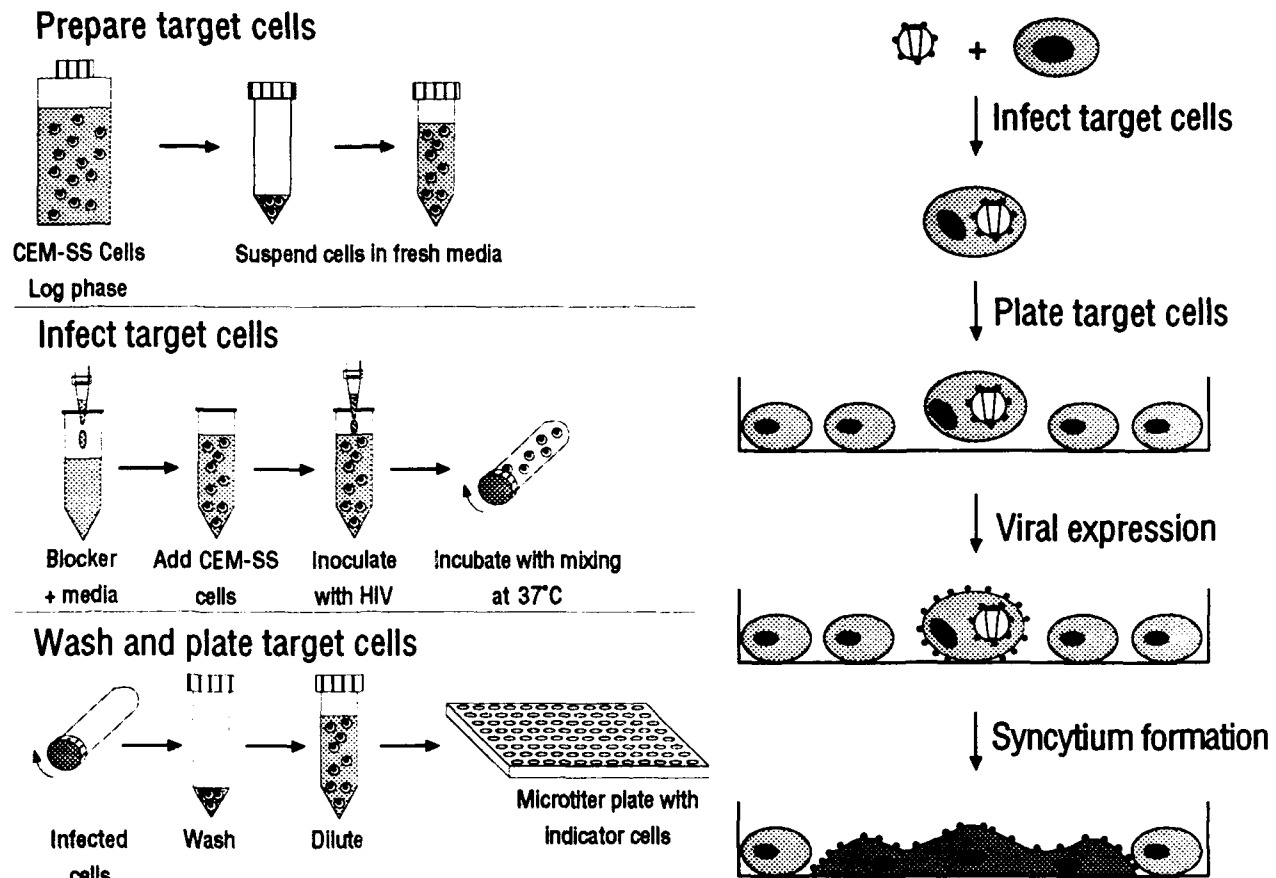
Prepare target cells

CEM-SS Cells
Log phase   Suspend cells in fresh media

Infect target cells

Blocker   Add CEM-SS   Inoculate   Incubate with mixing
+ media   cells   with HIV   at 37°C

Wash and plate target cells

Infected   Wash   Dilute   Microtiter plate with
cells   Indicator cells

Infect target cells

Plate target cells

Viral expression

Syncytium formation

FIG. 3. Schematic diagram of the quantitative syncytium-forming infectivity assay. Note that target cells are manipulated separately from indicator cells.

■ **Quantitative infectivity assays** — CEM-SS cells were grown at densities ($\sim 5 \times 10^5$ ml^{-1}) that maintained their exponential growth (Fig. 3). To perform an assay, CEM-SS cells were suspended in fresh media (RPMI 1640, 10% FBS and 1% PSN) to serve as "indicator" and "target" cells (Layne et al., 1990; Layne et al., 1991). Uninfected cell monolayers were prepared by adding 3.5×10^4 CEM-SS cells to flat-bottomed microplate wells (96 per plate). These indicator cells were then incubated ($37°$ C and 5% CO_2) for later use. CEM-SS target cells (or H-PBMC

target cells from above) were suspended in 50 nM DEAE-Dextran for 30 minutes prior to their use. After removing the DEAE-Dextran, a fixed number of target cells were added to 2 ml micro-centrifuge tubes containing fresh media with different concentrations of sCD4. To hold the inoculum-to-volume ratio constant, identical aliquots of HIV stock were added to each tube. Particular ratios (either 10 or 20%) were selected to give an MOI less than 0.1, a total gp120 concentration less than $0.1 \times K_{assoc}$, and a satisfactory statistical count of infectious units. To assure uniform mixing, tubes were rolled during the infection period (1 hr at 37° C). Next, to remove cell-free virus and blocker, infected target cells were washed once (centrifuged for 1 minute at $10,000 \times g$, suspended in 1 ml of PBS and again centrifuged) and suspended in fresh media. Infected cell monolayers were prepared by adding a small number (from 1250 to 5000) of CEM-SS or H-PBMC target cells to indicator cell monolayers. Thus, in all wells, indicator to target cell ratios were at least 7 to 1. A total of 8 replicate wells were plated per time point and blocker concentration. Syncytial forming units (SFU) representing the infection of individual target cells by cell free virus were counted 3 to 5 days following plating (Nara *et al.*, 1987; Nara *et al.*, 1988).

■ **Viral decay assays** — 250 ml of frozen HIV-1HXB3 stock were thawed and pooled within 10 minutes. The stock was then incubated with gentle mixing at 37° C. At regular intervals (1 to 2 hrs), quantitative infectivity assays were performed with CEM-SS and H-PBMC target cells (1.4×10^4 cells ml^{-1} and 1.8 ml reaction volumes), and with 0 and 0.5 nM sCD4 in the media (four separate assays per time point). Also at regular intervals (4 or 12 hrs), a "prespin" sample of viral stock was frozen (-70° C) for subsequent assays. At the same time, 8 ml aliquots of stock (in duplicate tubes) were ultracentrifuged ($155,000 \times g$ for 40 min) and the resulting "postspin" supernatants were frozen for subsequent assays. After swabbing all remaining supernatant from the ultracentrifuge tubes, the viral pellets (~10 μl volume) were suspended in 0.8 ml of fresh media (10× concentrated) and frozen for subsequent assays (Fig. 4A). Also at regular intervals (4 or 12 hrs), 9.9 ml aliquots of viral stock were thoroughly mixed with 0.1 ml of polystyrene spheres (1490 ± 40 Å dia from Duke Scientific or 2500 ± 130 Å dia from Polysciences), resulting in 1×10^9 spheres ml^{-1}. An 8 ml aliquot of this mixture was ultracentrifuged ($155,000 \times g$ for 40 min), the supernatant was decanted and the pellet was fixed with 2.5% gluteraldehyde (Fig. 4B). Following

this, the frozen prespin samples, postspin supernatants and suspended pellets were thawed and evaluated in parallel by gp120 ELISA, p24 ELISA, RNA polymerase activity assays, and RNA polymerase inhibition assays. Gluteraldehyde-fixed pellets were evaluated by quantitative electron microscopy.

A   B

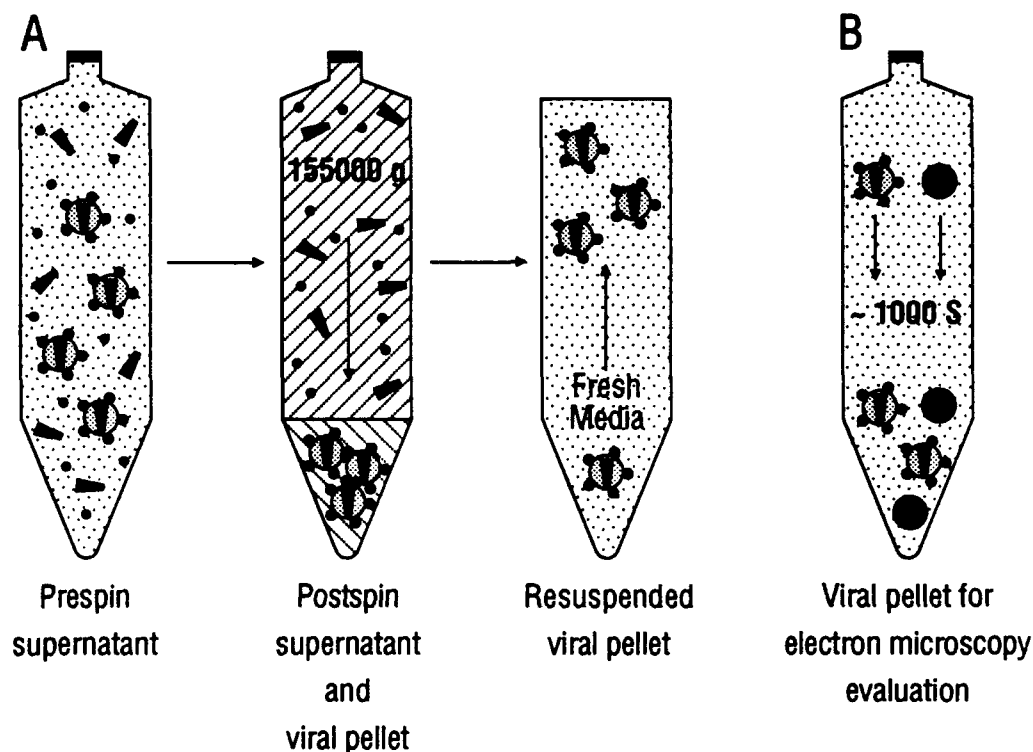| Prespin | Postspin | Resuspended | Viral pellet for |
supernatant	supernatant	viral pellet	electron microscopy
	and		evaluation
	viral pellet		

FIG. 4. (A) Schematic diagram of ultracentrifugation methods for generating prespin, postspin and pellet samples from HIV stocks. (B) Schematic diagram showing the co-sedimentation of latex spheres and viral particles.

■ gp120 ELISA — Frozen samples from viral decay assays (described above) were thawed and lysed with Nonidet P40 (NP40), at a final concentration of 0.5%. To obtain linear gp120 assays, the prespin sample and postspin supernatant were diluted 100 fold and viral pellets were diluted 1000 fold in RPMI 1640 medium containing 10% fetal calf serum and 0.5% NP40. Immulon-II microplate wells (Dynatech) were coated with D7324 capture antibody (Aalto Bioreagents), washed and blocked as previously described (Moore et al., 1988; Moore et al., 1989). Next, 100 μl of each sample was added to 6 replicate wells and incubated for 3 hrs at room temperature. Unbound protein was removed by washing twice with 200 μl of solution containing

144 mM NaCl and 25 mM Tris (pH 7.6). Bound gp120 was detected with a pool of HIV-1–positive human serum, an alkaline-phosphatase conjugated antibody to human IgG (SeraLab), and an AMPAK ELISA amplification system (Novo Nordisk). Reactions were stopped with 50 μl of 0.5 M HCl and optical densities at 492 nm were measured. Protein concentrations were determined against recombinant HIV-1IIIB gp120 derived from CHO cells (Celltech). The gp120 standards were included on all microplates (3 replicates in serial 3 fold dilutions).

■ p24 ELISA — Frozen samples from decay assays (described above) were thawed and lysed with Triton X100, at a final concentration of 0.5%. To obtain linear p24 assays, the prespin sample and postspin supernatant were diluted 5000 fold and viral pellets were diluted 40,000 fold in DuPont "core" diluent containing 0.5% Triton X100. Next, 100 μl of each sample was added to 4 replicate wells in commercial microstrips (NEK-060A, DuPont). All subsequent steps were performed in accordance with the manufacturers instructions (DuPont, 1990). The optical density (492 nm) of developed wells was determined by an automated plate reader (Vmax Kinetics, Molecular Devices). Protein concentrations were determined against recombinant HIV-1IIIB p24 supplied with the ELISA kits. p24 standards were included on all microplates (3 replicates in serial 2 fold dilutions).

■ RNA polymerase activity assays — Frozen samples from decay assays were thawed and lysed with Triton X100, at a final concentration of 0.5%. The prespin samples were used directly in RNA polymerase assays. The postspin supernatants and viral pellets were further diluted 2 fold in fresh media (RPMI 1640, 10% FBS and 1% PSN). 6 μl of each sample were transferred to four replicate wells. 20 μl of reaction solution were added to each well, resulting in 50 mM Tris (pH 7.6), 100 nM NaCl, 6 mM $MgCl_2$, 10 mM Dithiothreitol, 4 μg ml^{-1} Oligo(dT)$_{12-18}$, 40 μg ml^{-1} Poly(A), 0.12 mCi ml^{-1} [^{3}H]TTP and 0.25% NP40 (Baltimore et al., 1971; Goodman et al., 1971). The 96-well polystyrene microplates were then covered and incubated for 1 hr at 37° C. Next, 150 μl of stop solution containing 40 mM sodium pyrophosphate and 15 mM NaCl was added. Radioactive products were then precipitated with 20 μl of 60% trichloroacetic acid (TCA) and the microplates were placed on ice for an additional 30 min. The 196 μl in each well were transferred to 0.45 μm filter papers (Micro Cell Harvester, Skatron) with 5.0 ml of wash solution containing 6% TCA and 40 mM sodium pyrophosphate. Filter papers were dryed in a

vacuum oven, placed in scintillation fluid, and counted for beta activity (LKB Betaplate, Model No. 1205). Viral RNA polymerase activities were quantified against recombinant HIV-1IIIB polymerase derived from *E. coli* (p66/p51 heterodimer, American Bio-Technologies). Recombinant standards were included on all microplates (4 replicates in serial 2 fold dilutions). For 1.5×10^{-7} and 1.17×10^{-9} g of recombinant protein, beta counts were 4.8×10^5 and 3×10^3, respectively. The total counts were proportional to the protein weight and background counts were approximately 1×10^3.

■ **RNA polymerase inhibition assays** — Four prespin samples (preincubation times of 0, 8, 16 and 24 hrs) were thawed all at once. Quantitative infectivity assays were carried out on these samples with 0, 25, 50 and 100 µM trisodium phosphonoformate (foscarnet) in the media, and with CEM-SS target cells (5×10^4 target cells ml^{-1}, 1 ml reaction volumes and total of 16 tubes). To assure that phosphonoformate was in equilibrium in the assays, it was added to the target cells 4 hrs prior to adding the prespin samples (inoculum-to-volume ratio of 10%). After a 1 hr infection period, target cells were washed with fresh media containing phosphonoformate and suspended in fresh media containing phosphonoformate at the same four concentrations. Following this, the infected target cells (5×10^3 per well) were added to indicator cell monolayers containing phosphonoformate at the same concentrations. To evaluate the side effects of phosphonoformate on syncytia formation, 3 tubes without phosphonoformate in the media were inoculated with prespin samples that were preincubated for 0 hrs. Subsequently, these target cells (5×10^3 per well) were added to indicator cell monolayers containing 25, 50 and 100 µM phosphonoformate. Phosphonoformate was classified as a noncompetitive inhibitor of RNA polymerase (Majumdar *et al.*, 1978; Öberg, 1983). It was selected over other antiviral compounds because the parent compound was active, readily penetrated cells and was nontoxic at the concentrations used (Helgstrand *et al.*, 1978; Sandstrom *et al.*, 1985).

■ **Quantitative electron microscopy** — Fixed pellets from the viral decay assays (containing virions and spheres) were prepared for electron microscopy by two methods. Method 1. The pellets were embedded directly in Epon. To enhance visualization of gp120 knobs, specimens were fixed with OsO_4 for 60 minutes, treated with 0.1% tannic acid for 30 minutes, and

stained with 2% uranyl acetate for 90 minutes (all procedures performed at 4° C). Ultra-thin sections (~500 Å) were cut at different depths in the pellet. Method 2. The pellets were first embedded in low-melting argarose and run through an automated tissue processor (Lynx, Austrian Biomedical). This extra step facilitated the arbitrary division of samples before embedding them in Epon. The divided samples were then stained (as described above) and cut into ultra-thin sections. All specimens were mounted on 300 mesh copper grids, post-stained with lead citrate (Venable *et al.*, 1965), and evaluated using Zeiss electron microscopes (EM 902 or 10). From one thin section, 10 to 15 randomly selected areas were photographed, while strictly avoiding the evaluation of consecutive sections. For each negative, the total number of virions and polystyrene spheres were counted. Also the number of gp120 knobs on each virion were counted. To avoid bias, electron microscopy samples were identified by a code name, which was broken only after finishing the evaluation of negatives. Only negatives with more than 5 spheres and 5 virions were used in subsequent statistical analyses of the data.

■ **Biological blocking activities** — To facilitate the analysis of HIV infectivity assays, "normalized SFU" was defined as the mean number of SFU without sCD4 in the media divided by the mean number of SFU with sCD4 in the media (see Fig. 1). To facilitate the analysis of sCD4 blocking, the slope of a normalized SFU versus sCD4 concentration plot, [(normalized SFU) – 1] ÷ (sCD4 concentration), was defined as the "biological blocking activity" of sCD4. Biological blocking activities have units of inverse molar (M^{-1}), which permits comparison to gp120-sCD4 association constants derived from chemical measurements (Layne *et al.*, 1989; Layne *et al.*, 1990; Layne *et al.*, 1991).

■ **Statistical analysis of data** — The data were analyzed by two methods. Method 1. Biological blocking activities were calculated by minimizing $f(a, b) = \Sigma\{[y_i - (ax_i + b)] \div \sigma_i\}^2$, which gave a weighted least-squares fit to the data. y_i was the mean value of 1/SFU at the *i*th sCD4 concentration, σ_i was the standard deviation of 1/SFU, and x_i was the sCD4 concentration at the *i*th data point. For normalized SFU plots, the weighted least-squares fit gave biological blocking activities (slopes) of $a \div b$. Error bars in normalized plots were calculated by adding $\sigma_i \div y_i$ at the first data point to $\sigma_i \div y_i$ the *i*th data point, and then multiplying this sum by the value of normalized SFU at the *i*th data point. Method 2. Half lives and doubling times were also

calculated by minimizing $f(a, b)$. In this case, y_i was the mean value of log10(SFU) at the ith preincubation time concentration, σ_i was the standard deviation of log10(SFU), and x_i was the preincubation time at the ith data point. For log-linear plots, the weighted least-squares fit gave a half life (or doubling time) and intercept of a and b, respectively. Error bars in normalized plots were calculated by adding σ_i without sCD4 at the ith data point to σ_i with sCD4 at the ith data point and then dividing this sum by $sqr(2)$. This value (error) was then incorporated into the quantity $10exp[(y_i$ without sCD4) $- (y_i$ with sCD4) $\pm$ (error)] at each ith data point. For both data analysis methods, unweighed least-squares fits were obtained by setting $\sigma_i = 1$. The 95% confidence limits for biological blocking activities and half lives were calculated by a standard bootstrap algorithm (Efron *et al.*, 1991).

RESULTS

■ **Exponentially growing viral stocks** — Figure 5 shows the expression of infectious HIV-1HXB3 from two separate H9 cultures. Both cultures were prepared with the same continuous cell line, inoculated with the same viral stock and MOI, and rapidly harvested by the same method. For the first 24 hrs, the first culture (□) produced new virus at an exponential rate that was remarkably rapid (doubling time ≈ 2 hrs). From 24 to 48 hrs, however, the growth rate of this culture decreased rapidly and from 48 to 144 hrs, the production rate of new virus was insufficient for maintaining a constant titer. For the first 96 hrs, the second culture (○) produced new virus at an exponential rate that was rapid but somewhat slower (doubling time ≈ 7 hrs). For this culture, samples were not taken for growth times longer than 96 hrs. Thus, the inevitable effects of cell depletion on viral expression were not observed. These two sets of data were selected for presentation because they bracketed typical doubling times and durations of exponential growth. Since H9 cultures always produced HIV-1HXB3 exponentially for the first 48 hrs (data not shown), all viral stocks used in this study were harvested after 48 hrs of growth.

■ **Viral recovery after ultracentrifugation** — To determine the effects of ultracentrifugation on HIV-1HXB3 infectivity, a viral stock was preincubated for increasing intervals of time at 37° C. An 8 ml aliquot of stock was ultracentrifuged (155,000 × g for 40 min), and the resulting postspin supernatant and pellet (suspended in 8 ml of fresh media) were assayed

for SFU. At the same time, a prespin sample of viral stock was also assayed for SFU. Table 2 shows the results of this procedure at three preincubation times. The complete recovery of SFU in the viral pellets, to within experimental uncertainty, was independent of preincubation time. This demonstrated that manipulations such ultracentrifugation and suspension did not perturb HIV-1HXB3 infectivity. In addition, at all preincubation times, no SFU were detected in postspin supernatants. This further demonstrated that sedimentation of HIV-1HXB3 was independent of viral aging. These invariant results were important controls for the subsequent chemical and biological experiments.
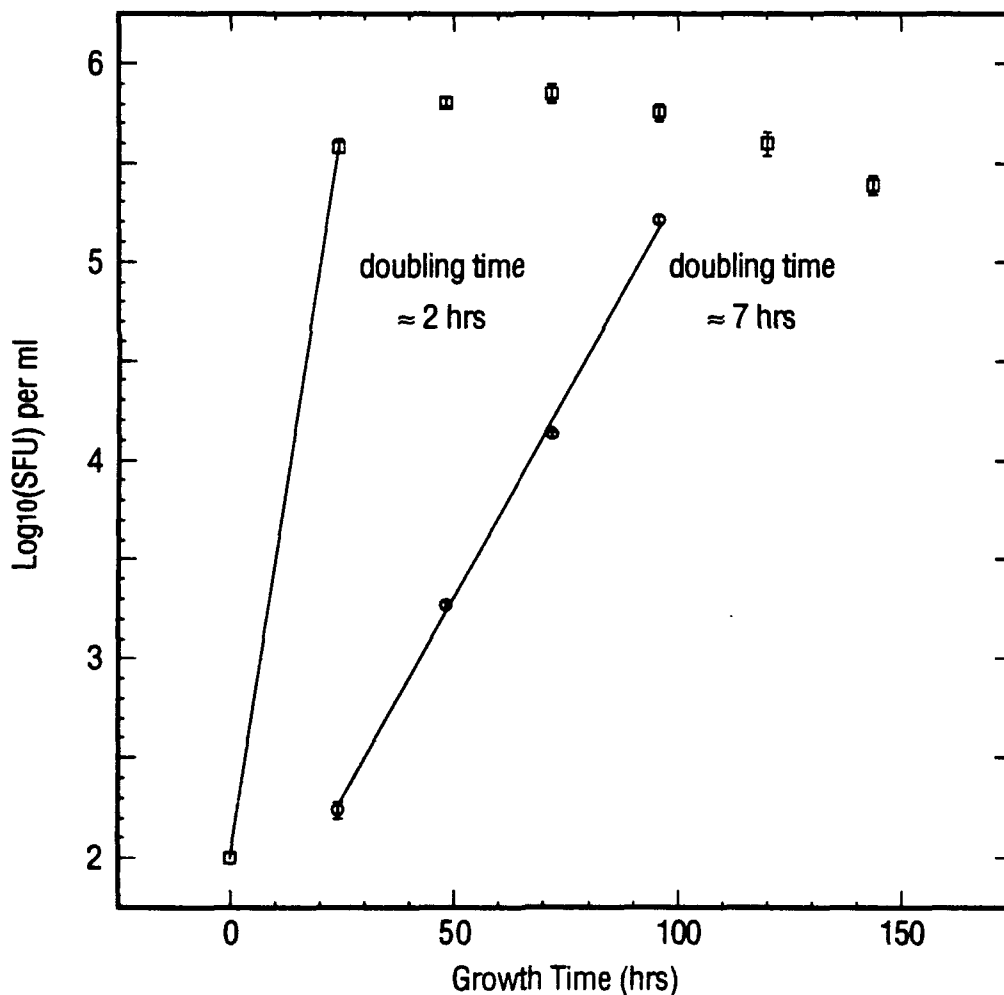

FIG. 5. The figure shows exponential growth of infectious HIV-1HXB3 in two separate H9 cultures (□ and ○). At 24 hr intervals, aliquots of supernatant were removed, clarified by low speed centrifugation and frozen. Subsequently, the frozen samples were thawed and assayed all at once for SFU. Each time point is an average of 8 replicate microtiter wells. Error bars signify ± 1 SD. Doubling times are unweighed least-squares fits to the data.

Table 2. *Effects of ultracentrifugation on infectivity as a viral stock ages*

Preincubation time (hrs)	Prespin SFU Mean ± SD	Supernatant SFU Mean ± SD	Pellet SFU Mean ± SD	Pellet + Prespin ratio Mean ± SD
2	459 ± 17	0	468 ± 45	1.02 ± 0.14
9	279 ± 13	0	234 ± 19	0.84 ± 0.11
17	83 ± 6	0	78 ± 7	0.94 ± 0.15

CEM-SS target cell density was 1.6×10^5 ml^{-1}. SFU were averaged from 8 microtiter wells. After the preincubation period, the processing times (from starting ultracentrifugations to inoculating infectivity assays) ranged from 105 to 110 minutes. At 9 hrs of preincubation, the spontaneous decay of viral infectivity was quite rapid. Thus, small differences in processing times can lead to larger differences in SFU.

Table 3. *Quantifying virion density by electron microscopy*

Preincubation time (hrs)	Number of EM negatives evaluated	Virion to sphere ratio Mean ± SD	Virion density (ml^{-1}) Mean ± SD
0	17	29 ± 10	$(2.9 \pm 1.0) \times 10^{10}$
4	4	42 ± 14	$(4.2 \pm 1.4) \times 10^{10}$
12	4	42 ± 5.3	$(4.2 \pm 0.5) \times 10^{10}$
36	13	42 ± 5.3	$(4.3 \pm 2.2) \times 10^{10}$
Average	—	37 ± 16	$(3.7 \pm 1.6) \times 10^{10}$

For this particular study, there were a mean of 560 virions and 15 latex spheres per EM negative. The sphere diameter was 1490 ± 40 Å.

■ **Quantifying virion density by electron microscopy** — The density of virions was determined by adding a known concentration of latex spheres to viral stocks and then ultracentrifuging the mixture. Since spheres and virions had similar sedimentation coefficients, ~1000 Svedberg (Sharp *et al.*, 1950; Anderson, 1968; Salmeen *et al.*, 1976), they migrated to the bottom of the centrifuge tube in equal proportion. With thin-section electron microscopy (Fig. 6), the ratios of spheres to virions in the pellets were evaluated, permitting calculation of the virion density. Table 3 summarizes the results of this procedure for an HIV-1HXB3 stock used

throughout this study. At all four preincubation times, the average virion density of 3.7×10^{10} ml^{-1} was constant to within experimental uncertainty. Five other HIV-1HXB3 stocks that were grown similarly had virion densities ranging from 1×10^9 to 5×10^9 ml^{-1} (summarized below in Table 5). For these stocks, as well, the densities remained constant for preincubation times ranging from 24 to 60 hrs (data not shown). These results demonstrated that the lipid shells covering viral particles were stable (at 37° C) compared to the other decay processes examined below.
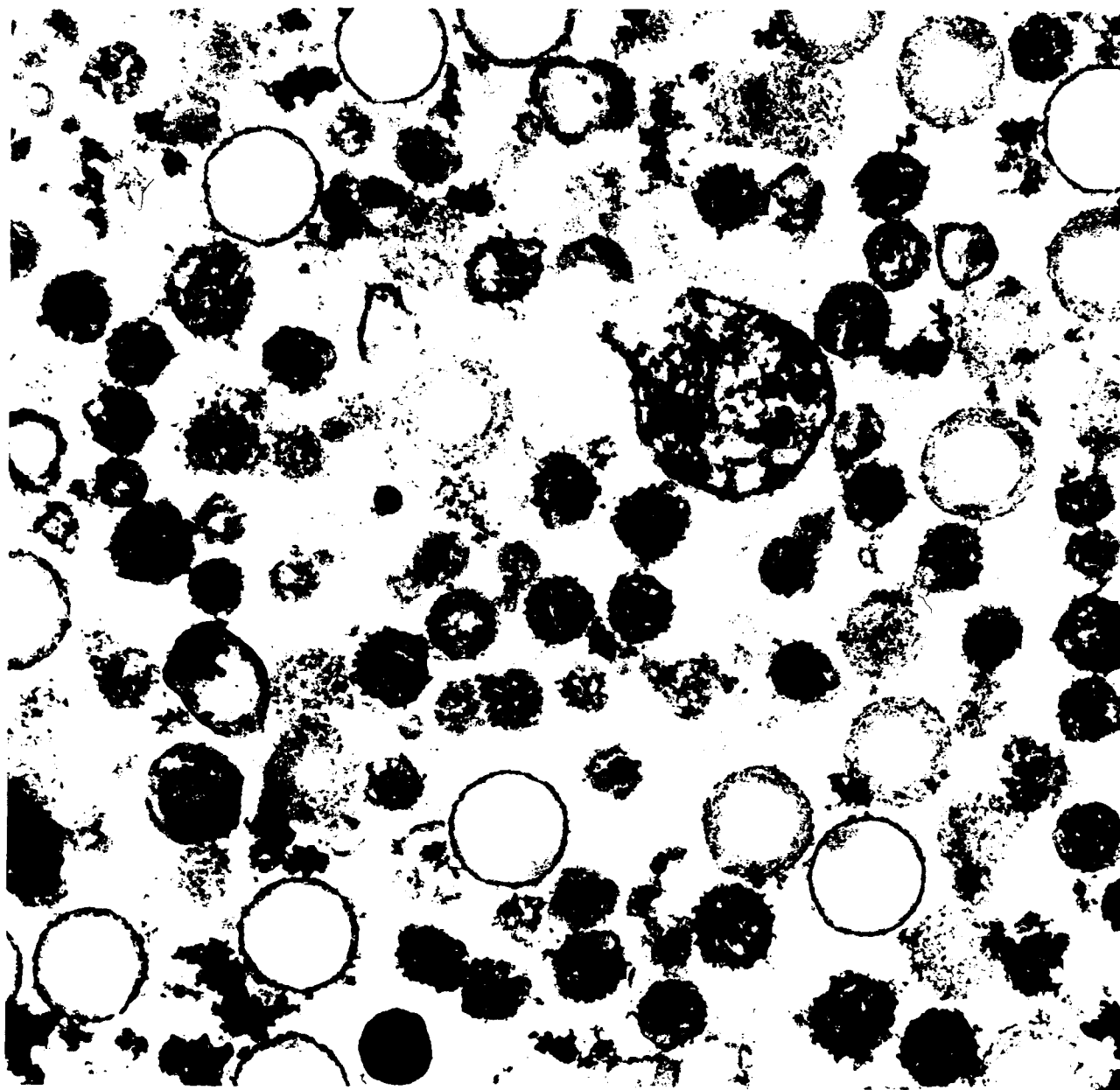

FIG. 6. Determining the virion density from thin-section electron micrographs. The HIV-1HXB3 stock was mixed with latex spheres (1490 ± 40 Å diameter) at a density of 1×10^9 ml^{-1}. Following ultracentrifugation and staining of the sample, the virion to sphere ratio was evaluated. In this negative, there were 34 spheres and 803 virions. This yielded a virion to sphere ratio of 23.6 and a virion density of 2.4×10^{10} ml^{-1}.
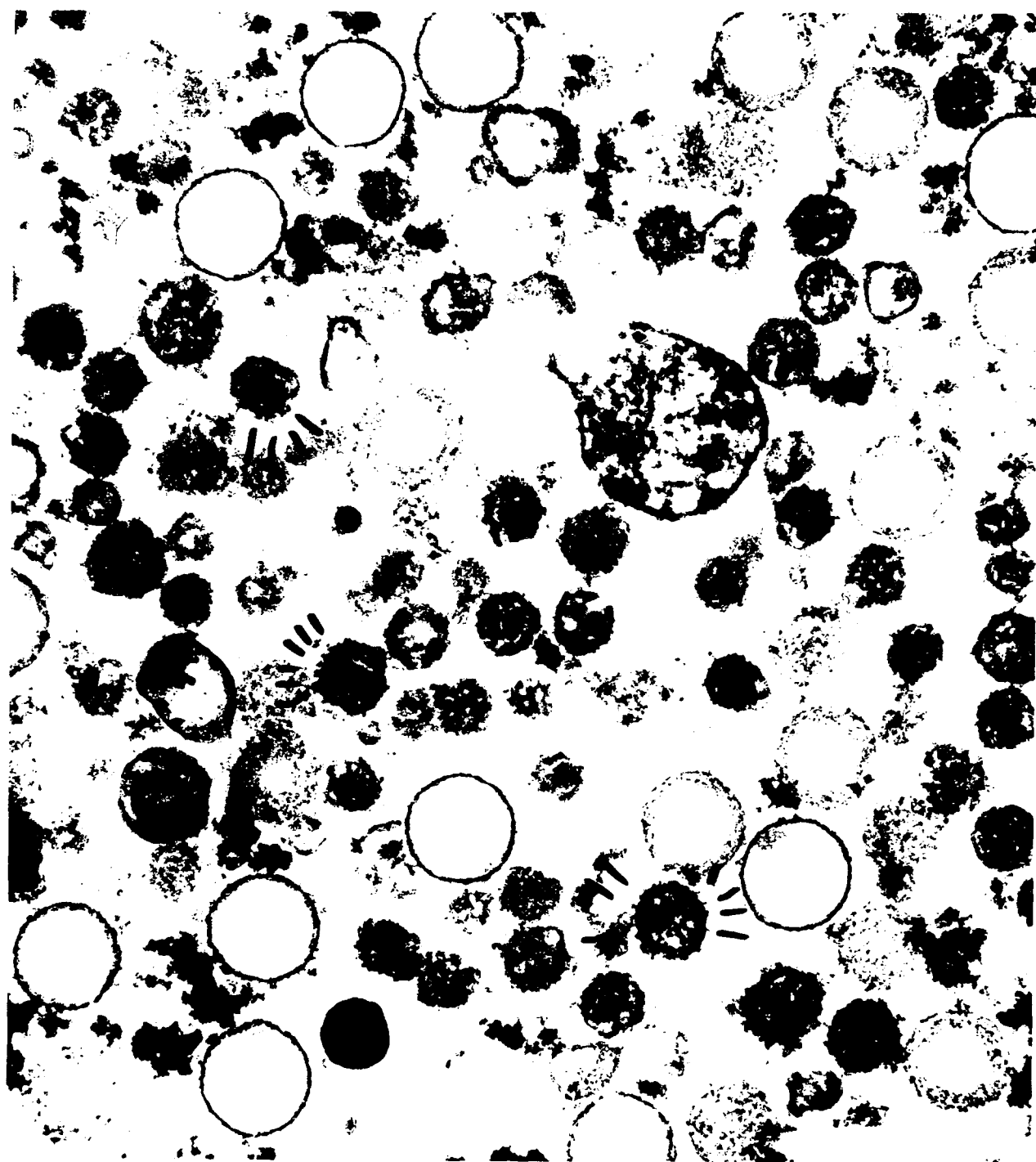
FIG. 7. Determining the number of gp120 knobs from thin-section electron micrographs. For each particle, the number of glycoprotein knobs were counted and recorded for subsequent statistical analysis. Since the 500 Å sections reveal approximately one third of the surface area on a virion. the average number of gp120 knobs per virion was 3 fold larger. The latex spheres diameter was 2500 ± 130 Å.

■ **Quantifying gp120 knob loss by electron microscopy** — The number of gp120 knobs on cell-free virions were also evaluated by thin-section electron microscopy (Fig. 7). Briefly, this was done by examining individual virions on EM negatives and recording the total number of visible knobs. To obtain reliable statistics, 20 to 30 negatives were evaluated at each preincubation time, resulting in the examination of 100 to 500 virions per time point. Figure 8 shows the results of this procedure. The excellent straight line fit to the data (solid line) had a correlation coefficient of 0.99, half life of 57 hrs, and 95% confidence limits of 38 to 144 hrs (dotted lines). Comparable outcomes were also obtained for two similar HIV-1HXB3 stocks (data not shown). These results demonstrated that the spontaneous shedding of gp120 knobs was first-order with time.
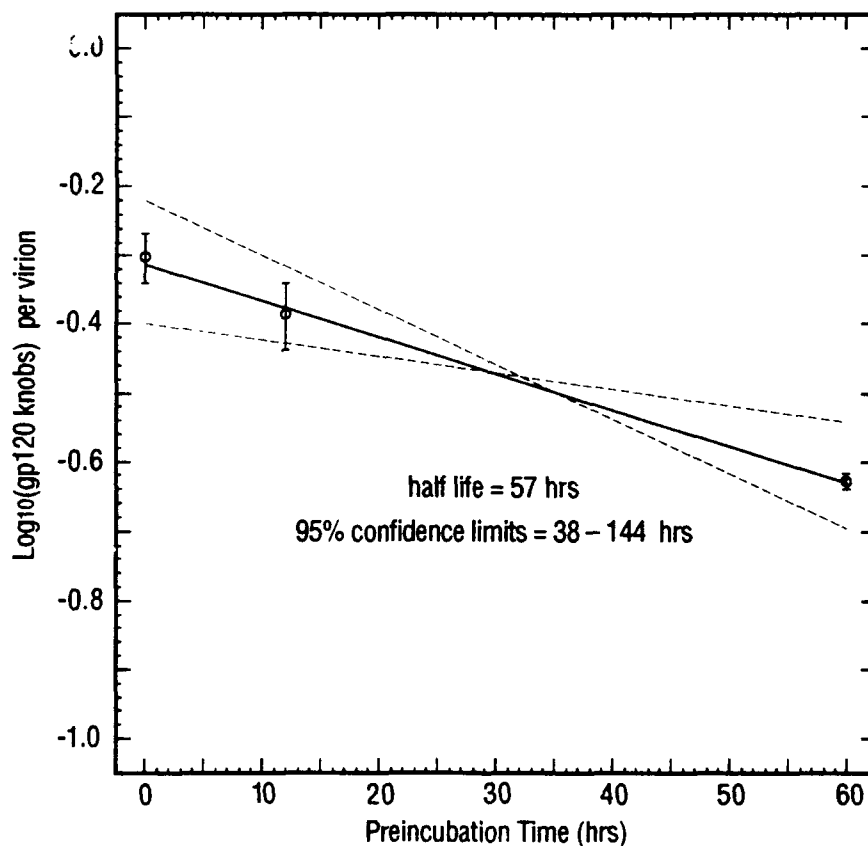

FIG. 8. Determining the gp120 shedding rate by electron microscopy. The number of gp120 knobs on virions were evaluated after preincubating a viral stock for 0, 12 and 60 hrs at 37°C. Subsequently, the mean number of knobs and standard deviation were calculated at each time point. The half life (solid line) is an unweighed least-squares fit to the data. The 95% confidence limits (dotted lines) were calculated by a bootstrap algorithm (see methods). Error bars show ± 1 SD.

■ **Quantifying gp120 and p24 losses by ELISA** — To further examine the kinetics of viral decay, an HIV-1HXB3 stock was harvested after 48 hrs of exponential growth (see Fig. 5) and afterwards it was incubated at 37°C. At regular intervals, aliquots of the stock were ultracentrifuged and the supernatants were separated from the pellets. Subsequently, the pellets were suspended in fresh media and both samples were frozen. At the same time, prespin aliquots of the viral stock were also frozen. To quantify the concentrations of envelope and core proteins, gp120 and p24 ELISA were performed in parallel. Results from these ELISA are shown in Figs. 9 and 10, respectively.
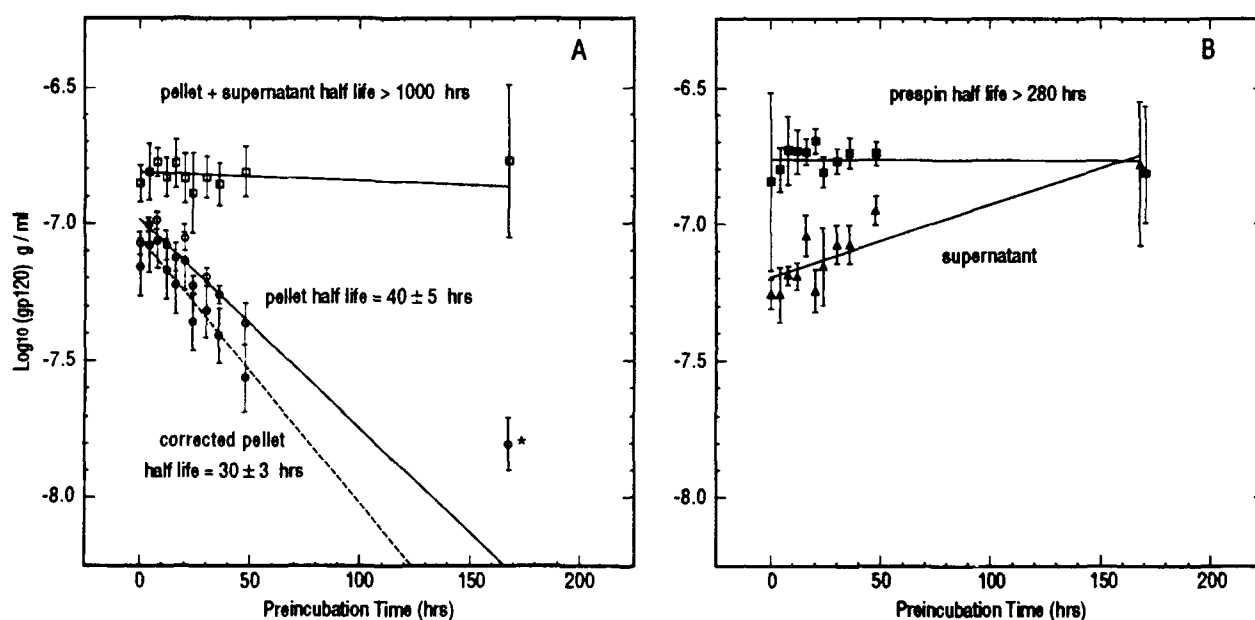
FIG. 9. The graphs show gp120 ELISA data from an HIV-1HXB3 stock that was preincubation at 37° C. Symbols denote prespin samples (■), postspin supernatants (△), viral pellets (○), corrected viral pellets (●) and summed data (□). Results are a mean of 6 replicate wells per time point. Half lives (solid lines) are unweighed least-squares fits to the data. The 95% confidence limits (reported with the half life) were calculated by a bootstrap algorithm (see methods). Error bars show ± 1 SD.

The concentration of viral-associated gp120 in the pellets (○ in Fig. 9A) decreased with increasing preincubation time and reached a baseline level (○*) by 168 hrs. A least-squares fit to the data (from 0 to 48 hrs, lower solid line) yielded a half life of 40 hrs and 95% confidence limits of 35 to 45 hrs. In accordance with this, the concentration of soluble gp120 in the supernatant (△

in Fig. 9B) increased with time. Adding the gp120 concentrations in the pellet and supernatant together gave a total ($\square$ in Fig. 9A) that was constant during the entire experiment. This sum matched the gp120 concentration in the prespin samples ($\blacksquare$ in Fig. 9B), corroborating that gp120 was indeed conserved with time. After subtracting the average gp120 concentration in the pellet at 168 hrs ($\bigcirc^*$ in Fig. 9A) from the data at earlier times, concentrations were obtained that were disentangled from the background ($\bullet$ in Fig. 9A). A least-squares fit to the data (from 0 to 48 hrs, dotted line) yielded a half life of 30 hrs and 95% confidence limits of 27 to 33 hrs. This corrected gp120 shedding rate agreed with direct EM measurements, to within a factor of two, and also agreed with gp120 ELISA measurements from two other decay experiments (summarized in Table 6 below). These results further demonstrated that spontaneous shedding of gp120 was first-order with time.
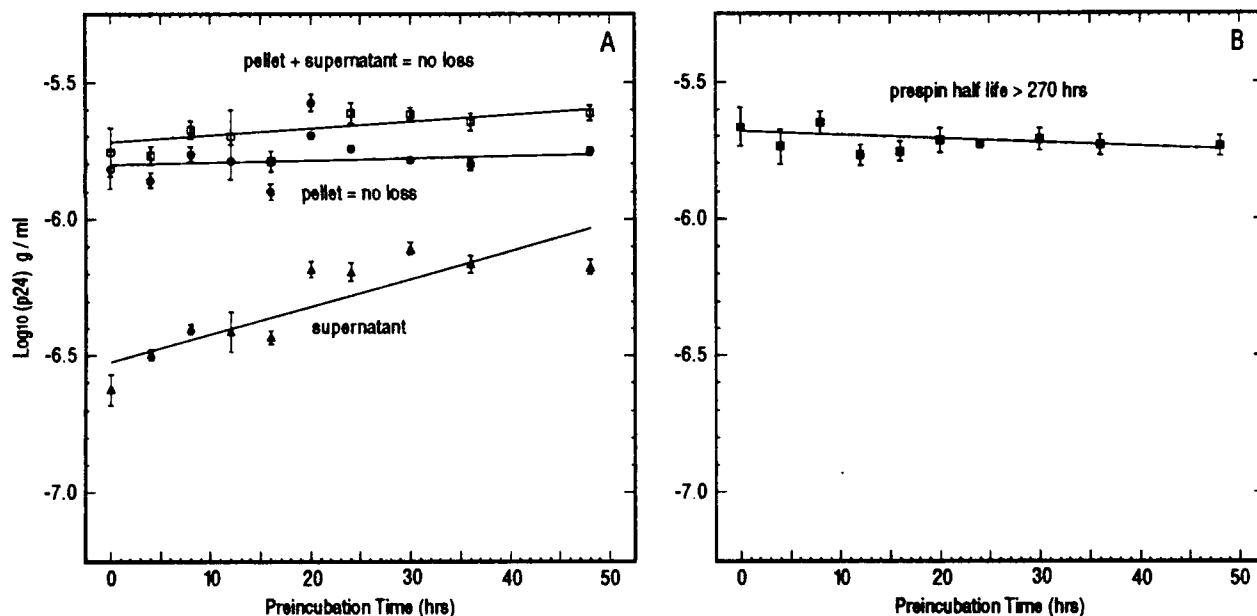

FIG. 10. The graphs show p24 ELISA data from an HIV-1HXB3 stock that was preincubation at 37° C. Symbols denote prespin samples ($\blacksquare$), postspin supernatants ($\triangle$), viral pellets ($\bigcirc$) and summed data ($\square$). Results are a mean of 4 replicate wells per time point. Half lives (solid lines) are unweighed least-squares fits to the data. The 95% confidence limits (reported with the half life) were calculated by a bootstrap algorithm (see methods). Error bars show ± 1 SD.

The concentration of viral-associated p24 in the pellets ($\bigcirc$ in Fig. 10A) remained constant with preincubation time. In spite of this, the concentration of soluble p24 in the supernatant ($\triangle$ in Fig.

10A) increased approximately 2 fold with time. This discrepancy in the data resides within experimental uncertainty but it could also indicate that a small fraction (~20%) of viral particles "dissolved" over the 48 hr interval. Adding the p24 concentrations in the pellet and supernatant together gave a total (□ in Fig. 10A) that was constant with time. This sum matched the p24 concentrations in prespin samples (■ in Fig. 10B), verifying that p24 was indeed conserved with time. These p24 core protein data were consistent with EM measurements (Table 3) indicating that the lipid shell of HIV was relatively stable. The results also demonstrated that p24 was lost from viral pellets at much slower rate than gp120 shedding. Therefore, the dissolution of intact viral particles was an insignificant factor contributing to the rate of gp120 shedding (○ and ● in Fig 9A).

■ **Quantifying RNA polymerase loss at 37° C** — Reverse transcription has been identified as a required step in the life cycle of HIV (Goff, 1990). Quantitative RNA polymerase-activity assays were thus performed on the prespin, postspin and pellet samples, with the goal of determining whether polymerase activity varies with preincubation time. As shown in Fig. 11, the activity of viral-associated RNA polymerase in the pellets (○) decreased with increasing preincubation time. A least-squares fit to the data (upper line) yielded a half life of 40 hrs and 95% confidence limits of 35 to 45 hrs. In addition, the activity of soluble polymerase in the supernatant (△ in Fig. 11B) decreased with time. A least-squares fit to this data (lower line) yielded a half life of 90 hrs and 95% confidence limits of 30 to 150 hrs. Adding the polymerase activities in the pellet and supernatant together gave a total (□ in Fig 11B) that also decreased during the experiment. The half life of the sum was 40 hrs, with 95% confidence limits of 36 to 44 hrs. To within experimental uncertainty, the summed data matched the total polymerase activity in the prespin samples (■ in Fig 11B), corroborating that RNA polymerase activity was not conserved with time. The half life of the prespin sample was 100 hrs, with 95% confidence limits of 30 to 170 hrs.

These results demonstrated that the loss of viral-associated RNA polymerase activity was first-order with time and that the loss rate was comparable to gp120 shedding. Similar data were also obtained for another HIV-1HXB3 stock (data not shown). Since electron microscopy and p24

ELISA indicated that viral particles were relatively stable over the period of this experiment, it was unlikely that appreciable amounts of RNA polymerase were released into the postspin supernatants. Thus, the loss of RNA polymerase activity in the supernatant indicated that solubilized enzyme was also labile.
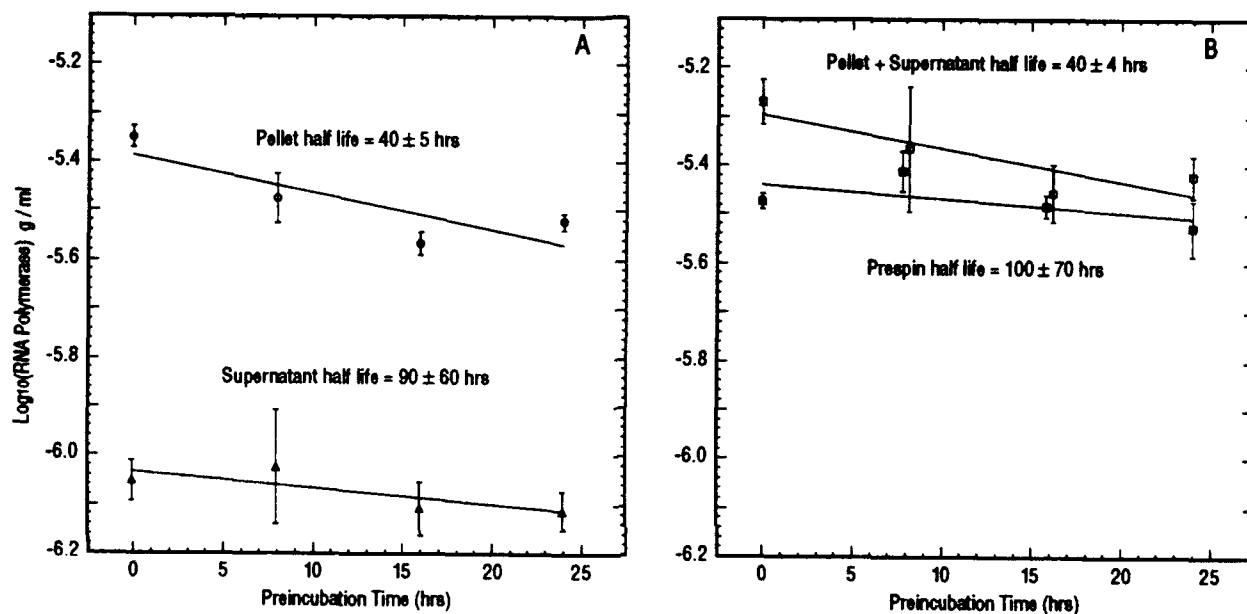

FIG. 11. The graphs show RNA polymerase activity from an HIV-1HXB3 stock that was preincubation at 37° C. Symbols denote prespin samples (■), postspin supernatants (△), viral pellets (○) and summed data (□). Results are a mean of 4 replicate wells per time point. Half lives (solid lines) are unweighed least-squares fits to the data. The 95% confidence limits and half life were calculated by a bootstrap algorithm (see methods). Error bars show ± 1 SD.

■ **Spontaneous viral inactivation at 37° C** — To correlate measurements of gp120 envelope shedding, p24 core dissolution and RNA polymerase loss with the spontaneous inactivation of HIV, a series of quantitative infectivity assays were performed on HIV-1HXB3 stock that was preincubated before use. At each time point, the assays were conducted with CEM-SS and H-PBMC target cells, both in the presence and absence of 0.5 nM sCD4 in the media. As shown in Fig. 12, this amounted to four different assays at each time point.
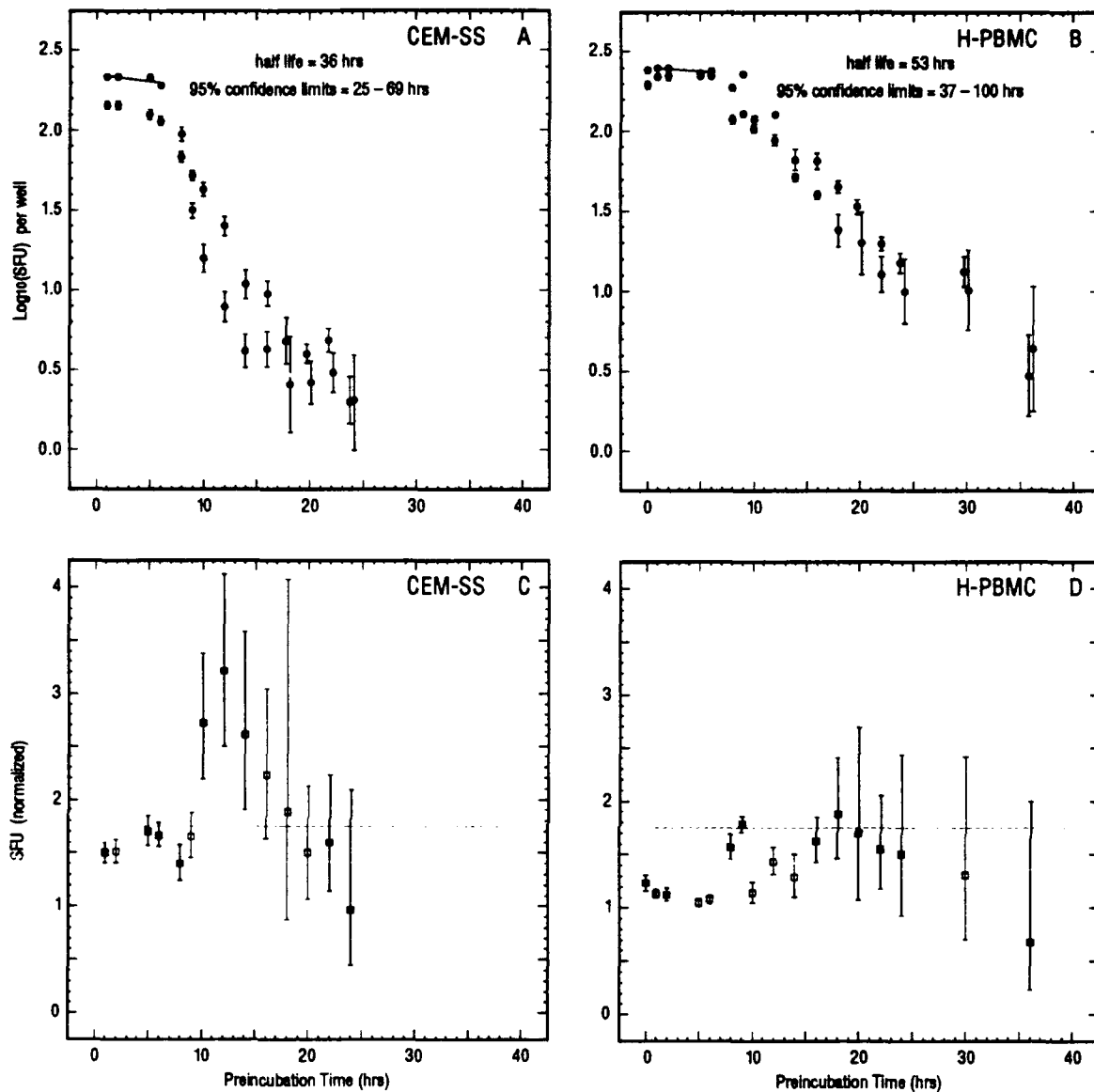
FIG. 12. The graphs show the spontaneous inactivation of HIV-1HXB3 at 37° C. At 1 to 2 hr intervals, the number of SFU in the viral stock were quantified with (A) CEM-SS and (B) H-PBMC target cells. For both target cell types, assays were conducted without (○) and with 0.5 nM sCD4 (●) in the media. Results are a mean of 8 replicate wells per time point. Error bars show ± 1 SD. The half lives of spontaneous inactivation (solid lines) are unweighed least-squares fits to the data (from 0 to 6 hours) for assays without sCD4. The 95% confidence limits were calculated by a bootstrap algorithm (see methods). The ratios between the assays without and with 0.5 nM sCD4 in the media are shown for (C) CEM-SS and (D) H-PBMC target cells. The ratios (normalized SFU) were calculated from data at each time point. Error bars show ± 1 SD in these ratios. Dotted lines correspond to the expected amount of blocking for 0.5 nM sCD4 and a gp120-sCD4 K_{assoc} equalling 1.5×10^9 M^{-1}.

Spontaneous multi-hit inactivation of HIV was observed with both CEM-SS (Fig. 12A) and H-PBMC (Fig. 12B) target cells. At the start of the experiment, both target cell types scored a comparable number of SFU (216 ± 7 for CEM-SS and 241 ± 8 for H-PBMC) to within experimental uncertainty. At the end of the experiment, the magnitude of viral inactivation was also similar (approximately 100 fold) for the four different assays. As shown in Figs. 12A and 12B, the profile of inactivation for both target cell types was was three-phased. There was an initial slow phase (less than 7 hrs), followed by a fast phase (from 10 to 20 hrs), and then another slow phase (greater than 22 hrs). The processes responsible for generating this sigmoidal inactivation profile will be considered in the discussion. Also as shown in Figs. 12C and 12D, the blocking activity of sCD4 with CEM-SS and H-PBMC target cells was comparable in its overall profile. During the fast phase of viral inactivation (from 10 to 18 hrs), sCD4 blocking activity increased significantly above baseline levels.

In spite of these similarities, there were still some observable differences in viral inactivation and sCD4 blocking. The duration of the initial slow phase of inactivation (plateau) was shorter for assays with CEM-SS cells (~6 hrs) than for assays with H-PBMC (~9 hrs). Preincubation times required for the 100 fold drop in infectivity were 2 fold shorter for CEM-SS cells (~18 hrs) than for H-PBMC (~9 hrs). For CEM-SS assays, the initial sCD4 blocking activity (0 to 10 hrs in Fig. 12C) corresponded to the gp120-sCD4 K_{assoc} from chemical measurements (dotted line). For H-PBMC assays, however, the initial sCD4 blocking activity was nearly absent, falling far below the expected chemical K_{assoc} (dotted line). At longer preincubation times, the excursions in sCD4 blocking activity were more pronounced for CEM-SS assays than for H-PBMC assays. In other words, compared to CEM-SS cells, H-PBMC were more difficult to protect with sCD4 in the media. These results indicated that CEM-SS assays were unsaturated at a target cell density of 1.4×10^4 ml^{-1}, whereas the H-PBMC assays were partially saturated at this same target cell density. These observable differences in viral inactivation (Figs. 12A and 12B) were also consistent with the hypothesis that compared to CEM-SS cells, HIV-1HXB3 required a smaller minimal number of unblocked gp120 molecules for efficient infection of H-PBMC. The rationale for this notion will be considered in the discussion.

■ **sCD4 blocking activity with viral preincubation at 37° C** — To further study how sCD4 blocking activity depended on spontaneous viral inactivation, a series of quantitative infectivity assays were performed with HIV-1HXB3 stock that was preincubated before use. This time, however, emphasis was placed on a larger number of sCD4 concentrations rather than a many sequential time points. To generate directly comparable data, assays were conducted with CEM-SS target cells at the same density $(1.4 \times 10^4 \text{ ml}^{-1})$ as the those in Fig. 12 and with the same 10% inoculum-to-volume ratio. As shown in Fig. 13, this amounted to seven different assays at each of the three time points.
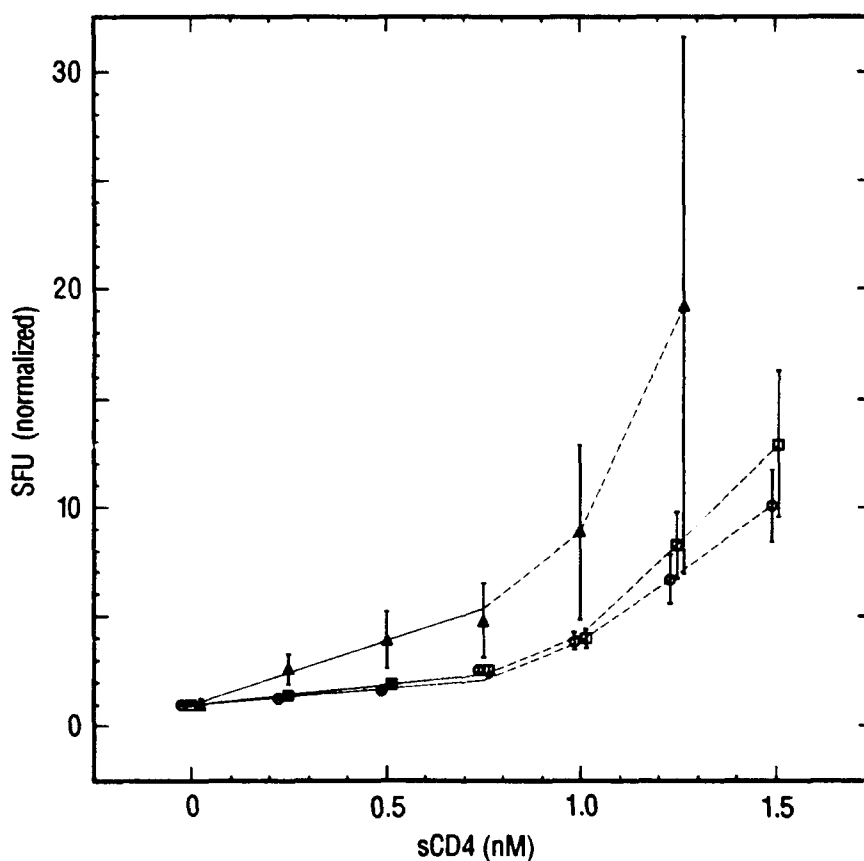
FIG. 13. The biological blocking activities of sCD4 (solid lines) were determined after preincubating an HIV-1HXB3 stock at 37° C. At 0 (○), 8 (□) and 16 (△) hrs, the sCD4 blocking activities were $(1.5 \pm 0.2) \times 10^9$, $(1.8 \pm 0.2) \times 10^9$ and $(5.8 \pm 0.7) \times 10^9$ M^{-1}, respectively. At each preincubation time, the ordinates (normalized SFU) were calculated by dividing the assays without sCD4 by the assays with sCD4. The blocking activities are weighted least-squares fits to the 4 lower sCD4 concentrations. Results are a mean of 8 replicate wells per data point. Error bars show ± 1 SD. The dotted lines were drawn to clarify trends in the data.

For infectivity assays without preincubation (○ in Fig. 13), the initial slope was linear and yielded a biological blocking activity of $(1.5 \pm 0.2) \times 10^9$ M^{-1}. At sCD4 concentrations greater than 0.75 nM, there was a positive synergy in blocking. For assays with 8 hrs of preincubation (□), the initial slope was linear and yielded a slightly increased blocking activity of $(1.8 \pm 0.2) \times 10^9$ M^{-1}. At the 1.25 and 1.5 nM sCD4, there were observable increases in the positive synergy. For assays with 16 hrs of preincubation (△), the initial slope was again linear but yielded a 4 fold increase in blocking activity, $(5.8 \pm 0.7) \times 10^9$ M^{-1}. At the 1.0 and 1.25 nM sCD4, there were correspondingly large increases in the positive synergy and at 1.5 nM sCD4, SFU were completely abolished. In the assays without preincubation (○), sCD4 blocking activity corresponded to the gp120-sCD4 K_{assoc} from chemical measurements (Layne et al., 1990). This results clearly demonstrated that small amounts of sCD4 inhibited infection in proportion to gp120-sCD4 complex formation. With longer preincubation times, the observed increases in sCD4 blocking activity and positive synergy supported the hypothesis that HIV required a critical number of unblocked gp120 molecule for efficient infection of CD4$^+$ cells (Layne et al., 1991).

■ **Phosphonoformate inhibitory activity with viral preincubation at 37° C** — The shedding of gp120 envelope proteins (Figs. 8 and 9) and the loss of RNA polymerase activity (Fig. 11) occurred at rates that resembled the initial rate of HIV inactivation (from 0 to 6 hrs in Figs. 12A and 12B). Since these rates were at least 3 fold faster than the dissolution of p24 core proteins (Fig. 10), it appeared likely that either one or both of these processes governed HIV decay. The observation that sCD4 blocking varied with viral preincubation (Fig. 14) has already implicated gp120 shedding in HIV inactivation (Layne et al., 1991). It thus remained to be settled how the loss of RNA polymerase activity contributed to spontaneous viral decay.

To make this assessment, a series of quantitative infectivity assays were performed on HIV-1HXB3 stock that was preincubated for various intervals before use. At each time point, assays were conducted with CEM-SS target cells and with 0, 25, 50 and 100 μM phosphonoformate (foscarnet) in the media. Afterwards, the infected target cells were plated on indicator cell monolayers containing the same concentrations of phosphonoformate in the media. To evaluate the side effects of phosphonoformate on syncytia formation, infectivity assays without

phosphonoformate were also conducted on the viral stock that was not preincubated. Subsequently, infected cell monolayers were prepared with media containing 25, 50 and 100 μM phosphonoformate. As shown in Fig. 14, this amounted to four phosphonoformate inhibition assays at 0 (○), 8 (□), 16(△) and 24 (◇) hrs, plus three side effect assays (●).
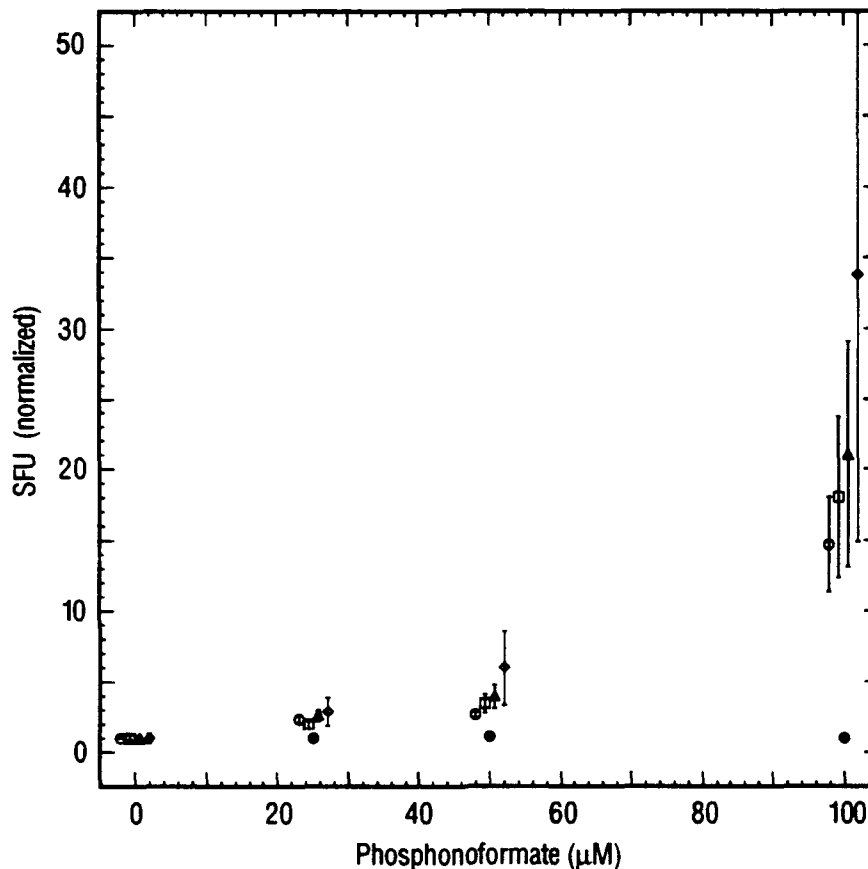
FIG. 14. The graph shows the inhibitory action of phosphonoformate on an HIV-1HXB3 stock that was preincubation at 37° C. Infectivity assays with CEM-SS target cells were conducted on stocks that were preincubated for (○) 0, (□) 8, (△) 16 and (◇) 24 hrs. At each preincubation time, the ordinates (normalized SFU) were calculated by dividing the assays without phosphonoformate by the assays with phosphonoformate. To evaluate the side effects of phosphonoformate on syncytium formation, three additional assays were conducted without viral preincubation and without phosphonoformate in the media. Subsequently, phosphonoformate was added to the media after infecting, washing and plating the target cells. Normalizing these three assays by the relevant control assay without phosphonoformate (○) yielded ordinates ranging from to 0.99 and 1.03 (●). This result demonstrated that phosphonoformate did not inhibit the formation of syncytia in the microtiter wells. For all assays, results are a mean of 8 replicate wells per data point. Error bars show ± 1 SD.

When phosphonoformate was added after infecting and washing the target cells, there was no observable inhibition of infectious events (● in Fig. 14). Thus, the presence of this antiviral agent in microtiter wells did not alter the scoring of SFU. For assays with phosphonoformate in the media during infection, there were observable inhibitions in SFU compared to the relevant controls (Fig. 14). For assays with 25 μM phosphonoformate, the inhibition of SFU ranged from 1.9 to 2.8 fold. The slight differences in inhibitory activity among the four preincubation times, however, resided within experimental uncertainty and did not reveal any strong trends. For assays with 50 μM phosphonoformate, on the other hand, the inhibition of SFU ranged from 1.9 to 2.8 fold and were correlated with preincubation time. For assays with 100 μM phosphonoformate, the inhibition of SFU ranged from 15 to 34 fold and were strongly correlated with preincubation time.

The half life of RNA polymerase activity in intact virions was 40 ± 5 hrs (Fig. 11). Thus, while conducting the viral inactivation assays shown in Fig. 12, approximately half of the RNA polymerase activity was lost. Figure 14 showed that when half of the RNA polymerase activity was inhibited by 25 μM phosphonoformate, there was no observable difference among the four preincubated HIV-1HXB3 stocks. Therefore, for preincubation times less than 40 hours, the results clearly demonstrated that spontaneous HIV inactivation was independent of RNA polymerase activity. In other words, virions contained a redundant amount of active RNA polymerase. For much longer preincubation times, however, the loss of RNA polymerase activity appears to contribute to HIV inactivation (see discussion).

■ **Calculating the protein content per virion** — Data from the foregoing physical, chemical and biological assays permitted direct calculation of the number of p24 molecules per virion, gp120 molecules per virion and active RNA polymerase molecules per virion. The approach to these calculations are briefly described below and summarized in Table 4.

Between 0 and 48 hrs of preincubation, p24 concentrations in the viral pellets were conserved (○ in Fig. 10A). Averaging all the data (40 ELISA determinations over 10 time points) gave the p24 concentration reported in Table 4. Using the average virion density from Table 3, yielded a mean of 5×10^{-17} g of p24 core protein per particle. Converting this number with a molecular weight of 2.4×10^4 g mole^{-1} yielded a mean of 1200 p24 molecules per virion. To within

experimental uncertainty, similar results were also obtained for two independent HIV-1HXB3 stocks (data not shown).

Table 4. *Protein content of HIV-1HXB3 particles*

Preincubation time (hrs)	Protein in viral pellet (g ml^{-1})	Virion density (ml^{-1})	Protein content per virion (g)	No. of molec. per virion
Core p24				
0 – 48	$(1.6 \pm 0.2) \times 10^{-6}$	$(3.7 \pm 1.6) \times 10^{10}$	$(4.4 \pm 2.6) \times 10^{-17}$	1200 ± 700
Envelope gp120				
0	$(6.9 \pm 0.4) \times 10^{-8}$	$(3.7 \pm 1.6) \times 10^{10}$	$(1.9 \pm 0.9) \times 10^{-18}$	10 ± 5
48	$(2.7 \pm 0.2) \times 10^{-8}$	$(3.7 \pm 1.6) \times 10^{10}$	$(7.4 \pm 3.8) \times 10^{-19}$	4 ± 2
RNA polymerase				
0	$(4.5 \pm 0.2) \times 10^{-6}$	$(3.7 \pm 1.6) \times 10^{10}$	$(1.2 \pm 0.6) \times 10^{-16}$	600 ± 300
24	$(3.0 \pm 0.1) \times 10^{-6}$	$(3.7 \pm 1.6) \times 10^{10}$	$(8.1 \pm 3.8) \times 10^{-17}$	400 ± 200

All data are reported as the mean ± 1 SD.

Between 0 and 48 hrs of preincubation, gp120 concentrations in the viral pellets (○ and ● in Fig. 9A) declined at a rate that was first-order with time. Table 4 shows the gp120 concentrations in the viral pellets at 0 and 48 hrs of preincubation, with the background gp120 concentration at 168 hrs subtracted (○* in Fig. 9A). Using the average virion density from Table 3, yielded means of 2×10^{-18} and 7×10^{-19} g of gp120 envelope protein per particle at 0 and 48 hrs, respectively. Converting these numbers with a with molecular weight of 1.5×10^5 g mole^{-1} yielded a mean of 10 and 4 gp120 molecules per virion, respectively. To within experimental uncertainty, similar results were also obtained for another independent HIV-1HXB3 stock (data not shown).

Between 0 and 24 hrs of preincubation, RNA polymerase activity in the viral pellets (○ in Fig. 11A) declined at a rate that was first-order with time. Table 4 shows the RNA polymerase concentration in the viral pellets at 0 and 24 hrs of preincubation. Using the average virion density from Table 3, yielded means of 1×10^{-16} and 8×10^{-17} g of active RNA polymerase per particle at 0 and 48 hrs, respectively. Converting this number with a molecular weight of 1.17×10^5 g mole^{-1} yielded means of 600 and 400 active molecules per virion, respectively. Similar results were also obtained for duplicate assays on the same HIV-1HXB3 stock (data not shown).

■ **Infectious to noninfectious virion ratios** — For viral stocks without preincubation (at 0 hrs in Figs. 12A and 12B), quantitative infectivity assays with CEM-SS and H-PBMC target cells detected 216 ± 7 and 241 ± 8 SFU per microtiter well, respectively. For these assays, 0.18 ml of viral stock was used and 2.5×10^3 infected target cells (from a total of 2.5×10^4 cells) were plated in each microtiter well. Thus, these particular conditions gave a multiplicative factor of 55.6, for converting the number SFU per well to the number SFU per ml of viral stock. This converted data is shown in the first two rows in Table 5. Next, dividing this number by the average virion density (from Table 3) yielded a SFU to virion ratio of approximately 3×10^{-7} for both target cells types.

Table 5. *Ratio of infectious to noninfectious virions*

Target cell type	Target cell density (ml^{-1})	SFU (ml^{-1}) Mean $\pm$ SD	Virion density (ml^{-1}) Mean $\pm$ SD	SFU to virion ratio Mean $\pm$ SD
CEM-SS	1.4×10^4	$(1.2 \pm 0.04)\times10^4$	$(3.7 \pm 1.6)\times10^{10}$	$(3.2 \pm 1.5)\times10^{-7}$
H-PBMC	1.4×10^4	$(1.3 \pm 0.04)\times10^4$		$(3.6 \pm 1.7)\times10^{-7}$
CEM-SS	1.6×10^5	$(1.5 \pm 0.04)\times10^5$	$(4.9 \pm 2.3)\times10^9$	$(3.0 \pm 1.5)\times10^{-5}$
CEM-SS	4.0×10^6	$(1.9 \pm 0.07)\times10^6$		$(3.9 \pm 1.9)\times10^{-4}$
CEM-SS	5.0×10^5	$(8.5 \pm 0.4)\times10^4$	$(2.6 \pm 0.8)\times10^9$	$(3.3 \pm 1.2)\times10^{-5}$
CEM-SS	2.0×10^6	$(2.6 \pm 0.1)\times10^5$		$(1.0 \pm 0.4)\times10^{-4}$
CEM-SS	2.0×10^6	$(5.0 \pm 0.24)\times10^5$	$(1.2 \pm 0.6)\times10^9$	$(4.1 \pm 2.2)\times10^{-4}$

The table shows results for four separate HIV-1HXB3 stocks. All the stocks were assayed without preincubation. SFU were averaged from 8 microtiter wells.

Table 5 also shows converted data for quantitative infectivity assays with three other HIV-1HXB3 stocks. Among all these stocks, the ratio of infectious to noninfectious virion ranged from a low of 3×10^{-7} to a high of 1×10^{-4}. These results clearly demonstrated that the ratios depended on the target cell density. As expected, lower target cell densities (unsaturated assays) were associated with smaller ratios and higher target cell densities (saturated assays) were associated with larger ratios (Layne *et al.*, 1989).

■ Comparing the results from three decay assays — Table 6 summarizes the results of gp120 ELISA, p24 ELISA and RNA polymerase activity assays for three separate HIV-1HXB3 stocks. Stock number 1 was already examined in detail (see Figs. 9 – 11). Stocks 2 and 3 provide useful comparisons for evaluating the reproducibility and uncertainty in the data. The results from all three stock demonstrate that the total amounts (prespin and summed data) of p24 and gp120 protein in the assays were conserved with time. The results also demonstrate that the p24 half lives in the viral pellets were 3 to 4 fold larger than the half lives of gp120 and RNA polymerase activity. Finally, the half lives for gp120 shedding in the viral pellets were remarkable similar (mean of 28 hrs) among all three stocks.

Table 6. *Half life of p24, gp120 and RNA polymerase activity (hrs)*

Stock	p24 core protein			gp120 envelope protein			RNA polymerase activity		
	Prespin	Summed	Pellet	Prespin	Summed	Pellet	Prespin	Summed	Pellet
No. 1	> 270	no loss	no loss	> 280	> 1000	30 ± 3	100 ± 70	40 ± 4	40 ± 5
No. 2	> 170	430 ± 60	100 ± 20	no loss	> 500	25 ± 5	—	—	—
No. 3	no loss	no loss	> 110	> 240	60 ± 10	29 ± 5	—	—	—

Summed data are the postspin supernatant and pellet data added together. No loss corresponds to least-squares fit to the data having either zero or positive slope with preincubation time. All data are the reported as mean ± 95% confidence limits.

DISCUSSION

For this project, we collected a variety of physical, chemical and biological data on HIV-1 stocks that multiplied exponentially in cell cultures. This permitted us to draw correlations between different types of data and determine the number of gp120 envelope, p24 core and RNA polymerase molecules per virion. To our knowledge, such comprehensive investigations have not been previously reported for HIV. nor perhaps for other related lentiviruses and retroviruses. All the rate constants measured in th. .tudy were first order with time (Table 6). This simple form of viral behavior justified most of the assumptions in mathematical models of HIV infection (Layne *et al.*, 1989). Such models considered that viral inactivating processes obeyed first order kinetics, and that gp120 molecules were independent and equivalent with respect to infection. However,

since HIV required a minimal (or threshold) number of gp120 molecules for efficient infection of CD4$^+$ cells, the notion that infection proceeded at a rate proportional to unblocked gp120 requires some revision (see below).

Direct measurements of the envelope shedding rate by electron microscopy (Fig. 8) and gp120 ELISA (Fig. 9) were comparable to within a factor of two. In conjunction, we found that the loss of RNA polymerase activity (Fig. 11) took place at rate that was similar to gp120 shedding. To ascertain how the loss of RNA polymerase activity contributed to spontaneous HIV inactivation, a series of phosphonoformate inhibition assays were performed. The results from these experiments demonstrated that a 2 fold perturbation of RNA polymerase activity (by 25 µM phosphonoformate) did not distinguish viral stocks with 24 hrs preincubation from those without preincubation (Fig. 14). Therefore, for the preincubation times used in this study (up to 36 hrs in Fig. 12), the loss of RNA polymerase activity did not contribute significantly to HIV inactivation. In addition, we found that the lipid bilayer covering virions (Table 3) and p24 core proteins within virions (Fig. 10) were stable compared to shedding and loss of RNA polymerase activity. This demonstrated that the physical breakup of viral particles did not contribute significantly to the rates of envelope shedding and polymerase loss. When considered altogether, the data demonstrated that the loss of HIV-1 infectivity was most closely correlated with the spontaneous shedding of gp120. Further below, we will consider the kinetics of HIV inactivation at longer preincubation times.

For independent and equivalent gp120 molecules, mathematical models of HIV infection predicted that plots of normalized SFU versus sCD4 concentration should yield a straight line (Layne et al., 1989). When the data for such plots came from unsaturated infectivity assays, the initial slopes were both expected and found to equal the gp120-sCD4 K_{assoc} from chemical measurements (Layne et al., 1990). Upward curvature in normalized SFU plots indicated blocking greater than proportional to gp120-sCD4 complex formation (positive synergy). Conversely, downward curvature indicated blocking less than proportional to complex formation (negative synergy). In Fig. 13, the initial linear slopes (at preincubation times of 0 and 8 hrs) were similar to the sCD4-gp120 K_{assoc} from chemical measurements. This result demonstrated that sCD4 blocking activity was proportional to complex formation, for sCD4 concentrations less than

0.75 nM, and verified that the viral infectivity assays were indeed unsaturated. At higher concentrations, however, the positive synergy and its increase with preincubation time supports the hypothesis that HIV required a minimal number of unblocked gp120 molecules for efficient infection of CD4$^+$ cells. The increasing positive synergy appeared with time because gp120 shedding acted as a surrogate for sCD4 blocking.

For unsaturated infectivity assays, mathematical models predicted that the initial slope of a viral decay plot should correspond to the combined rates of gp120 shedding and particle dissolution (Layne *et al.*, 1989). In agreement with this, the initial rates of viral decay (0 to 6 hrs in Figs. 12A and 12B) were similar to the combined rates to within a factor of two. After this initial phase, however, the multi-hit inactivation rate was much faster than expected from simple assumptions of independent and equivalent gp120 molecules. This finding further corroborated the minimal number hypothesis, because virions falling below a threshold would accentuate the observed rate of multi-hit inactivation. During the final phase of viral decay (preincubation times greater than 20 hrs), there was a slowing in the rate for both types of target cells. This slowing was consistent with the single-hit inactivation of virions that were far below the minimal number threshold. In this case, the inactivation rate of these minimally infectious particles should equal the combined rates of gp120 shedding and particle dissolution. The data in Figs. 12A and 12B were certainly consistent with this prediction, but their large uncertainties did not permit reliable calculations of half lives and confidence limits.

As HIV infectivity decreased with time, there was a peculiar up-and-down profile in the blocking activity of sCD4 (Figs 12C and 12D). The upward portion of this profile was analogous to an increasing positive synergy with preincubation time. To understand the downward portion, however, we must consider how sCD4 blocking was affected by the distribution of gp120 molecules in the viral population. At short preincubation times, there was a "homogeneous" population of virions with more than the minimal number of free gp120 molecules. The small amounts of sCD4 in the infectivity assays (● in Figs. 12A and 12B) did not push the population below threshold. Thus, relative to the infectivity assays without sCD4 (○ in Figs. 12A and 12B), blocking was proportional to gp120-sCD4 complex formation. At intermediate preincubation times, there was a "heterogeneous" population of virions that were both above and below the

minimal number. In this case, sCD4 pushed a larger fraction of the population below threshold. Thus, relative to infectivity assays without sCD4, blocking was greater than proportional to complex formation. At long preincubation times, there was a "homogeneous" population of virions with less than the minimal number of free gp120 molecules. The sCD4 in the assays acted on a viral population that was already below threshold. Thus, relative to infectivity assays without sCD4, blocking was again proportional to complex formation. By this reasoning, we would expect the positive synergy in sCD4 blocking (Fig. 13) to subside with longer preincubation times. Decisive tests of this prediction are now underway.

At long preincubation times (Fig. 12), both the reduced rate of HIV decay and the up-and-down blocking profile were most consistent with the notion of minimally infectious particles that were below threshold. For completeness, however, we also considered two alternative explanations for these data. The first was that there was a subfraction of virions (about 10^{-2} of the infectious population) that were highly resistant to blocking by sCD4. This resistant population became evident only after the disappearance of the more labile and susceptible population. Since higher sCD4 concentrations (5 nM) blocked infection by more than 500 fold (data not shown), this explanation seemed unlikely. The second was that there was a subfraction of target cells (about 10^{-2} of the total population) that were highly susceptible to infection. Since the overall magnitude of HIV inactivation was similar for both CEM-SS and H-PBMC target cells, however, that this latter explanation also seemed unlikely.

At short and long preincubation times, both CEM-SS and H-PBMC target cells detected similar numbers of SFU (Figs. 12A and 12B). Also both cell types had sigmoidal profiles of HIV decay, reflecting the influence of a threshold for efficient infection. There were, nevertheless, several noteworthy differences in these infectivity assays. First, the time interval in which the 100 fold loss of viral infectivity took place was nearly 2 fold longer for H-PBMC (~36 hrs) than for CEM-SS (~18 hrs) target cells. For the H-PBMC assays, the initial phase of slow inactivation was several hours longer and the intermediate multi-hit phase had a slower rate. Second, for identical target cell densities and assay conditions, the blocking activity of sCD4 was less for H-PBMC target cells than for CEM-SS target cells (Figs 12C and 12D). For H-PBMC assays, the initial

sCD4 blocking activity was below the gp120-sCD4 K_{assoc} (dotted line), indicating the effects of saturation. For CEM-SS assays, the initial sCD4 blocking activity equalled K_{assoc}, indicating unsaturated conditions. Third, the up-and-down profile of sCD4 blocking activity was less pronounced for assays with H-PBMC target cells than for assays with CEM-SS target cells. All these seemingly incongruent observations, however, are consistent with the idea that HIV-1HXB3 required a smaller minimal number of gp120 molecules for efficient infection of H-PBMC than for CEM-SS target cells. This follows because the effects of multi-hit inactivation are directly related to the minimal number of gp120 molecules. Smaller thresholds have less pronounced effects on viral decay and vice versa. Furthermore, the effects of assay saturation are inversely proportional to the minimal number. Thus, at a particular density, target cells with a smaller threshold are more likely to underestimate the gp120-sCD4 K_{assoc}.

The surfaces of both HIV and $CD4^+$ cells are studded with adhesion molecules and covered by a diffuse coat of sugar molecules (glycocalyx) that are negatively charged (Fenouillet et al., 1988; Springer et al., 1990). These similar features suggest that the initial binding of HIV to a target cell is, in many ways, parallel to the adhesive interaction between two immune cells. For such cell-cell interactions, it was shown that adhesion between two surfaces represents a first-order thermodynamic phase transition which takes place only when a certain threshold number of interactions between adhesion molecules is exceeded (Bell et al., 1984; Dembo et al., 1987). If the density of adhesion molecules is below this critical number, the cellular surfaces will simply not adhere (Plunkett et al., 1987). The exact value of the critical number is a function of several variables, most importantly the strength of the repulsive electrostatic potential between the surfaces and the association constant of the adhesion molecules for their complementary receptors. Thus, this viewpoint suggests that the critical number of gp120 molecules for efficient infection arises from repulsive forces between viral and cellular glycocalyces and attractive ones between gp120 and CD4. In order to overcome the protective barrier that enshrouds $CD4^+$ cells, a critical number of gp120-CD4 interactions must form. Once gp120 falls below the critical number, a virion may still infect a cell (for example, by colliding with cells or at regions on cells having thinner barriers) but the odds of this happening will be slim (Layne and Dembo, 1992). Hence, for the H-PBMC and CEM-SS assays (Fig. 12), we believe that the observed differences in the sigmoidal profile of

HIV decay and sCD4 blocking were caused by smaller and larger cell-surface barriers, respectively.

From this study, there were sufficient data for estimating the minimal number of gp120 molecules for efficient infection of CEM-SS target cells. To perform this calculation, we first had to ascertain several conversion factors. At zero preincubation time, electron microscopy detected a mean of 0.5 knobs per virion (Fig. 8) and found that approximately 90% of virions were devoid of knobs (data not shown). Since these specimens were approximately 500 Å thick (one third of a viral diameter) they revealed about one third of the knobs on virions. From the work of others (Schawaller *et al.*, 1989; Earl *et al.*, 1990), we also know that these knobs were either trimers or tetramers. Based on these data, we used multiplication factors of 10, 3 and 3 − 4 for the distribution, visualization and multimer conversions, respectively. This gave an overall multiplication factor of 90 to 120 for converting gp120 knobs per virion to gp120 molecules per virion. Using a mean of 0.5 knobs per virion yielded a total of 45 to 60 gp120 molecules per virion. In addition, at zero preincubation time, gp120 ELISA detected a mean of 10 ± 5 gp120 molecules per virion (Table 4). Since approximately 90% of virions in these samples were also devoid of knobs (data not shown) we used a multiplication factor of 10 for converting the data. This independent estimate yielded a total of 50 to 150 gp120 molecules per virion, which agreed with the electron microscopy estimates to within a factor of 2. When more than 0.75 nM sCD4 was added to infectivity assays with CEM-SS target cells, there was a positive synergy (Fig. 13). Using a gp120-sCD4 K_{assoc} of 1.5×10^9 M^{-1} and the sCD4 concentration at which upward curvature began, permitted us to directly estimate the minimal fraction of unblocked gp120 molecules. For equilibrium blocking conditions, this estimate gave a free gp120 fraction of $[1+(1.5 \times 10^9$ M$^{-1}) \times (7.5 \times 10^{-10}$ M$)]^{-1} \approx 0.47$, or approximately 50% for the minimal fraction. Multiplying the total number of gp120 per virion by the minimal fraction gave minimal numbers of 23 to 30 and 25 to 75 gp120 molecules per virion for electron microscopy and ELISA data, respectively. Since HIV-1 can have a maximum (Gelderblom, 1991) of 210 to 280 gp120 molecules on its surface (*i.e.*, trimers or tetramers and up to 70 knobs), we calculated a minimal fraction of 10% to 30% for virions with all their knobs. This result should be viewed as

meaningful only within the rather limited confi... ... *in vitro* assays. The minimal number in more "physiologic" target cells remains to be determined as well as range of minimal numbers for different field isolates of HIV.

For viral stocks without preincubation, we found that there were 600 ± 300 active RNA polymerase molecules per virion (Table 4). This result was based on the enzymatic activity of a known amount of recombinant RNA polymerase from HIV-1IIIB, which closely resembles the HIV-1HXB3 clone. The recombinant enzyme was a highly purified p66/p51 heterodimer, resembling the native enzyme found in virions (Veronese *et al.*, 1986; Furman *et al.*, 1991). For other retroviruses, such as moloney murine leukemia virus (Panet *et al.*, 1978), rauscher mouse leukemia virus (Krakower *et al.*, 1977) and avian myleoblastosis virus (Panet *et al.*, 1975; Bauer *et al.*, 1980; Kacian *et al.*, 1971), the RNA polymerase contents were found to range between 17 and 110 molecules per virion. Thus, the number of polymerase molecules per HIV particle was larger than for other retroviruses. In this study, the number of polymerase molecules per virion was based on enzymatic activities from viral stocks that multiplied exponentially in cell cultures. In previous studies, the number of RNA polymerase molecules were determined by anti-polymerase immunoglobulins (radioimmunoassay) and on stocks with unknown growth histories. Thus, the discrepancies between this study and previous ones may be due to the differences in assay technique and viral stock preparation. On the other hand, it may simply indicate that HIV-1 has a larger number of RNA polymerase molecules per virion.

To our knowledge, the half life of RNA polymerase activity has not been previously reported for HIV at 37° C. Temperature-sensitive RNA polymerases have been characterized from moloney leukemia virus (MLV) but they were selected from mutant viral strains rather than a cloned laboratory isolate (Goff *et al.*, 1981). For MLV, previous studies also found that RNA polymerase activity was highly labile at 44° C and that the loss of RNA polymerase activity correlated with the spontaneous decay of infectivity at 44° C (Gerwin *et al.*, 1977). In addition, inhibiting the incorporation of RNA into virions by actinomycin D had no measurable effects on thermolability. It was thus concluded that the thermal properties of MLV RNA polymerase were independent of the viral genome. Since the loss of polymerase activity and its decay were investigated at elevated temperatures, however, the relevance of these MLV findings to the present

ones must await further clarification. Other studies with HIV-1 have found that recombinant RNA polymerase was not autolytic *in vitro* (Mizrahi *et al.*, 1989) and that recombinant protease did not degrade heterodimeric p66/p51 RNA polymerase *in vitro* (Meek *et al.*, 1989). Thus, for HIV-1, several plausible mechanisms for the loss of RNA polymerase activity have already been ruled out by the investigations of others. Thus, the mechanisms responsible for the spontaneous loss of RNA polymerase activity in virions remain undefined at present.

The phosphonoformate inhibition assays demonstrated that a 2 fold perturbation of RNA polymerase activity did not distinguish viral stocks with 24 hrs preincubation from those without preincubation ($25\mu M$ in Fig. 14). Thus, at short preincubation times, we believe that virions possessed redundant amounts of RNA polymerase activity. This conclusion was further supported by the rather large number of active RNA polymerase molecules per virion in viral stocks without preincubation (Table 4). At higher phosphonoformate concentrations (50 and 100 μM), however, there were clear difference in the preincubated viral stocks. As shown in Fig. 14, the inhibitory activity of phosphonoformate was directly correlated with preincubation at 37° C. This result suggested that the loss of RNA polymerase activity contributed to HIV decay at preincubation times greater than the polymerase half life (about 40 hrs in Fig. 11). This additional mechanism of HIV inactivation helps to account for the small ratio of infectious to noninfectious virions in viral stocks that were grown exponentially (Table 5). From the limited number of phosphonoformate inhibitions assays, though, we cannot tell whether HIV inactivation was proportional to the loss of RNA polymerase activity or whether there was a threshold number for efficient infection. Further experiments will be required for clarifying this matter.

In this study, the ratios of infectious-to-noninfectious virions ranged from 10^{-4} to 10^{-7} and were correlated with the density of CD4$^+$ target cells in the infectivity assays (Table 5). At the lower cell densities, the ratios were smaller and vice versa. Four of the viral infectivity assays were carried out at CD4$^+$ cell densities that were 10 – 100 fold smaller than those of blood, where typical densities are around 5×10^6 cells ml^{-1}. Thus, these particular results (Table 5) may underestimate the infectious-to-noninfectious ratios that are characteristic of blood. In lymph and lymph nodes, typical CD4$^+$ cell densities are 10^7 to 10^9 cells ml^{-1}, respectively. It therefore

remains unclear whether a significantly larger fraction of the so-called "noninfectious" virions would infect at higher target cell densities. Recently, it was shown that viral burdens in lymphoid organs (*i.e.*, the fraction of infected CD4$^+$ cells) were approximately 10 fold larger than the ones in blood (Pantaleo *et al.*, 1991). With this finding, it is tempting to speculate that larger ratios of infectious-to-noninfectious virions in lymphoid organs may contribute to this elevated burden.

Three-dimensional electron microscope tomography of HIV-1 indicated that a p24 shell covers the viral genome (Gelderblom, 1991). The volume of this shell was approximately 3×10^7 Å^3, which corresponds to a hollow cylinder with a length of 1200 Å, diameter of 200 Å and thickness of 50 Å. Since proteins have a mean density of 1.23 daltons Å^{-3} and one dalton equals 1.67×10^{-24} g (Barrow, 1974), we estimated that an individual virion contains approximately 4×10^{-17} g of p24. In this study, it was found that HIV-1 contains approximately 5×10^{-17} g of p24 per virion (Table 4), which agrees closely with our estimate.

The remarkable stability of the p24 core (Table 6) and lipid shell covering HIV-1 (Table 3) suggested that these data may have some use in ascertaining the stability of virions in the plasma of infected persons. In some cases, clinical studies found correlations between the viral titers and p24 concentrations in plasma (Ho *et al.*, 1989; Coombs *et al.*, 1989; Clark *et al.*, 1991; Daar *et al.*, 1991) In these instances, the viral titers ranged from 10^1 to 10^4 TCID$_{50}$ ml^{-1} and the corresponding p24 concentrations in plasma ranged from 10 to 1000 pg ml^{-1}. Based on 5×10^{-17} g of p24 per virion, these plasma p24 concentrations correspond to 2×10^5 to 2×10^7 virions ml^{-1}, respectively. Thus, in the plasma of infected individuals, we estimate that the ratio of infectious to noninfectious virions varied from 5×10^{-5} to 5×10^{-4}. These ratios were comparable to the ones shown in Table 5, suggesting that human plasma does not contain surface-active factors with pronounced viricidal activities. Nevertheless, further clinical studies are warranted that correlate direct particle counts and p24 concentrations with HIV titers from a range of physiologic CD4$^+$ cell densities.

Among HIV researchers, there has been some debate on how to grow "optimal" viral stocks for use in antiviral screening assays and vaccine trials in animals (Cohen, 1989). Resolving this debate is important, because the physical state of viral particles can greatly influence the activities of antiviral agents that attack extracellular (Fig. 13) and intracellular (Fig. 14) targets. We believe

that the close correlation between gp120 shedding (Fig. 9) and initial HIV decay (Fig. 12) provides a straightforward method for judging whether stocks are indeed optimal. To do this, two pieces of information are required. The first is a measure of the doubling time for viral stocks multiplying exponentially in cell cultures. A good method for making such an estimate is illustrated in Fig. 5. The second is a measure of the half life of gp120 shedding. Such a determination can come from physical measurements with electron microscopy (Fig. 7), from chemical measurements with gp120 ELISA (Fig. 9), or from unsaturated infectivity assays (see the initial slopes in Figs. 12A and 12B). From these data, it is simple to see whether the doubling time to half life ratio is smaller or larger than one. If this ratio is smaller than one, then new virions are expressed at a rate that outpaced their spontaneous decay. Conversely, if this ratio is larger than one, then new virions are expressed at a rate that lagged behind their spontaneous decay. From this perspective, it is also simple to see that the mean number of gp120 molecules per virion will be larger in stocks with smaller growth-to-decay ratios. Therefore, to maximize the number gp120 molecules per virion, HIV stocks must be grown such that the doubling time is much smaller than the half life for spontaneous shedding. Based on a gp120 half life of 30 hrs (Fig. 9), we calculate grow-to-decay ratios of 0.067 and 0.23 for the fastest and slowest HIV-1HXB3 stocks, respectively (Fig. 5). Thus, for growth times less than 48 hrs, both viral stocks meet our criteria for optimization. In previous growth studies *in vitro* (Fenyö et al., 1989), HIV strains were categorized as rapid-high or slow-low. Because of its simplicity, this older classification still has some utility. We believe, however, that doubling times, half lives and growth-to-decay ratios provide a more complete classification of viral characteristics.

In this study, we found that the processes governing the decay of HIV infectivity were first-order with time. Whether this simple behavior is particular to HIV-1HXB3 or applicable to other viral strains must await future studies. To gain greater confidence, these experiments will be carried out with "physiologic" infectivity assays and wild-type viral strains. That is, the infectivity assays will use freshly isolated H-PBMC target cells and media consisting of human sera. The gp120 blocking agents will consist of monoclonal immunoglobulins and polyclonal sera from HIV-infected individuals. The wild-type stocks will come from single-pass primary cell cultures

and have grow-to-decay ratios that are minimized. The goal of these studies will be to determine the overall range of kinetic rates for HIV. This includes correlations between the rates of particle lysis, p24 dissolution, gp120 shedding, RNA polymerase loss, and spontaneous HIV decay. For a number of wild-type strains, a further goal will be to determine the minimal number of gp120 molecules for efficient infection of $CD4^+$ cells. This number is particularly important, because we perceive an inverse relationship between immunoglobulin blocking activity and the critical number. Larger critical numbers will require correspondingly smaller humoral responses and vice versa. Therefore, to determine whether this relationship influences the development of HIV vaccines with broad efficacy, it will be important to see how the critical number varies between divergent wild-type strains and $CD4^+$ cells from a number of individuals.

CONCLUSIONS

Simple mathematical models of HIV have clarified our understanding of the kinetic processes in viral infectivity assays. The unique data from model-directed assays have practical applications to the standardization of infectivity assays, the testing of therapeutic agents binding to viral gp120 and cellular CD4, and the evaluation of HIV vaccines. We also see improvements in the ability to extrapolate from assays conditions *in vitro* to physiologic conditions *in vivo*. Many of these improvements would not have been realized without the use of such models. Furthermore, we envision that model-directed assays will continue to make unique contributions to HIV research.

Based on our past two years of experimental work, we have developed a new kinetic model of HIV infection that incorporates a more complete description of viral kinetics, and overcomes disagreements between theory and experiment. We have also formulated four questions (listed below) that will be useful for applying the model to *in vitro* experiments. These questions are discussed in detail in the attached *International Reviews of Immunology* article.

■ **New Kinetic Model** — In the quantitative infectivity experiments, most but not all predictions of the original kinetic model were corroborated. By scrutinizing the departures from predicted outcomes, we were led to formulate a new model of HIV infection. Below, we describe this refined and generalized model with emphasis on the evidence that led us to propose each of its novel features (Fig. 15).
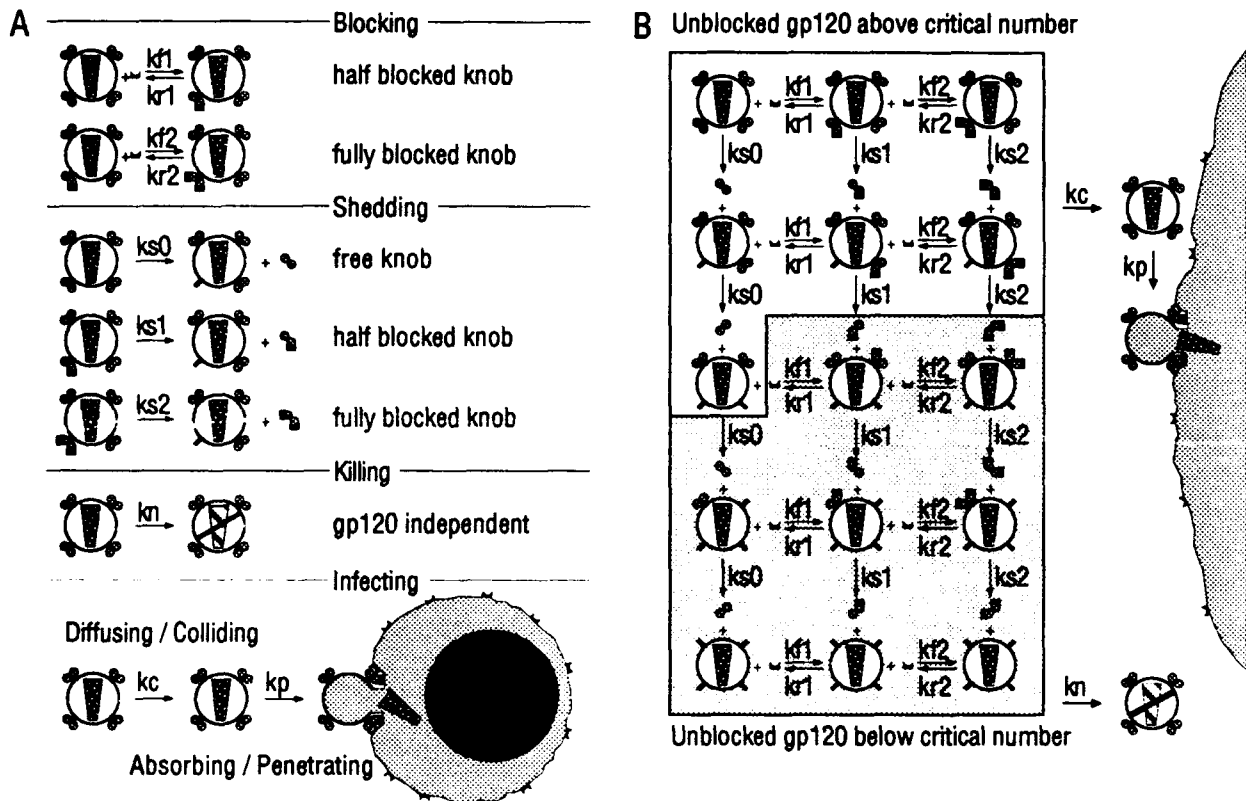
FIG. 15. (A) Basic reactions in the new kinetic model. k_{f1} and k_{f2} are rates for the formation of half-blocked and fully-blocked gp120 dimers, respectively. k_{r1} and k_{r2} are rate constants for the dissociation of half-blocked and fully-blocked gp120 dimers, respectively. k_{s0}, k_{s1} and k_{s2} are rates for spontaneous shedding of unblocked, half-blocked and fully-blocked gp120 dimers, respectively. k_n is the rate of nonspecific viral inactivation. k_c is the rate of collision between a viral particle and a cell. k_p is the rate of absorption and penetration for a viral particle at the cell surface. (B) Combined reactions in the new model. When viral particles are above a critical number of gp120 knobs (unshaded region), they infect at a rate proportional to the number of unblocked gp120s. When viral particles are below the critical fraction (shaded), they infect at a rate less than proportional to the number of unblocked gp120s. In this figure, for example, virions start out with four gp120 knobs and the critical number is two unblocked knobs.

First, in the original model, it was assumed that infection proceeded at a rate proportional to unblocked gp120 molecules. This rate was independent of the total number of gp120s in the viral envelope. However, the positive synergy in the biological blocking activity of sCD4 (Fig. 13), the large amplification factor relating gp120 shedding to loss of infectivity (Figs. 12A and 12B), and the increasing positive synergy with preincubation time (Fig. 13) are most consistent with the notion that HIV requires a critical number of unblocked gp120 molecules for efficient infection of

CD4$^+$ cells. Therefore, in the new model, the rate of infection depends on an adjustable threshold. Above it, the rate is proportional to unblocked gp120s and below it, the rate depends on a cutoff function that is less than proportional (Fig. 16). As described in Fig. 17, there are good molecular reasons for the existence of the critical number (Layne and Dembo, 1992).

Second, in the original model, the distribution of gp120 on viral particles was irrelevant because it was assumed that each gp120 was equivalent and independent in promoting infection. Introducing a critical number, however, means that it is no longer possible to conform to this equivalent site approximation. Therefore, in the new model, any distribution of gp120 on particles (all combinations of numbers and ages) are analyzable. This flexibility is needed for studying the influence of viral stock heterogeneity on assay results. It is also useful for determining whether particular outcomes from infectivity assays are representative for all viral stocks or are stock dependent.
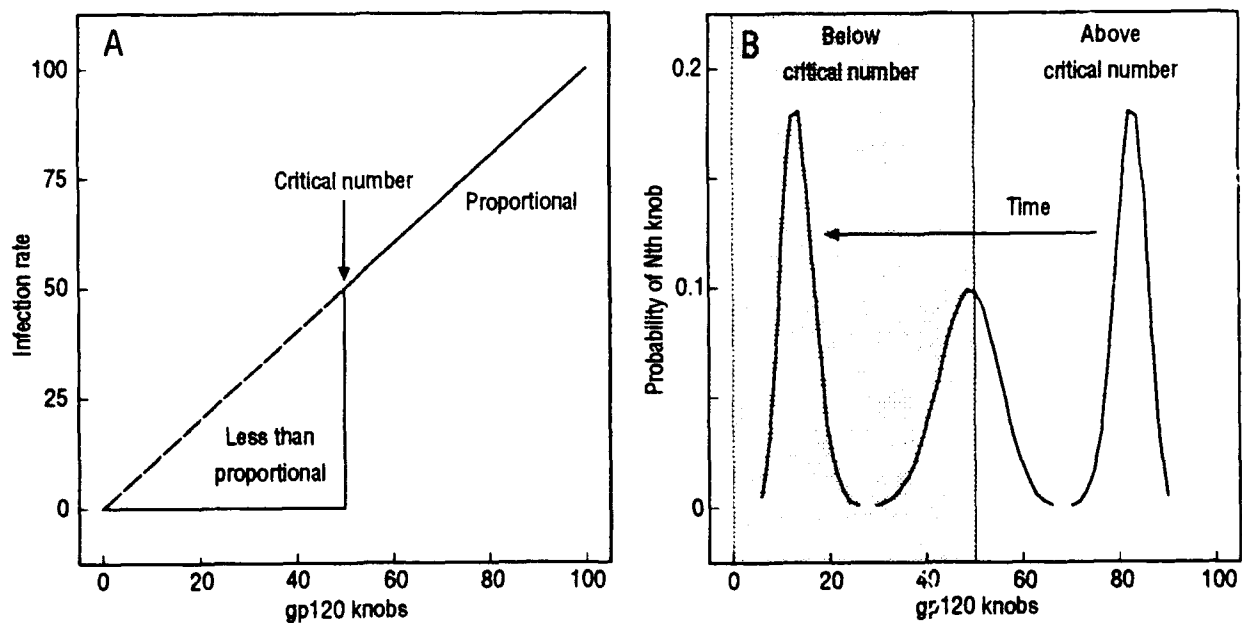

FIG. 16. (A) Above the critical number, the infection rate is proportional to the number unblocked gp120 knobs. Below the critical number, the rate is less than proportional to the number unblocked gp120 knobs. That is, the actual infection rate falls somewhere within the triangle. (B) As viral particles age, they spontaneously fall below the critical number by the shedding of gp120. The figure illustrates a hypothetical distribution of gp120 on particles at three preincubation times. Initially, all particles are above the critical number. At the intermediate time, equal numbers of particles are above and below this number. At the longer preincubation time, all particles are below the critical number.

Third, in the old model, a single lumped parameter governed the rate of infectious collision between a viral particle and target cell. Although this was a reasonable starting point, it nevertheless did not permit us to distinguish kinetic processes taking place before a particle and cell collide from those taking place afterward. Therefore, the new model divides this lumper parameter into two components. The first characterizes the rate at which particles diffuse and collide with cells. The second characterizes the rate at which particles absorb and penetrate at cell surfaces. The relative size of these two rates permits infection to be categorized as either "collision" or "attachment" limited. In collision-limited infections (Berg, 1977), sCD4 will have no biological blocking activity in unsaturated assays. In attachment-limited infections (Goldstein, 1989; Goldstein et al., 1989), on the other hand, sCD4 will have a blocking activity equal to the gp120-sCD4 K_{assoc}. Thus, the new model will be useful for analyzing how changes at the cell surface influence the blocking of infection, and for distinguishing pre-binding from post-binding neutralization.

Fourth, in the original model, gp120 knobs were considered as monomers. However, biochemical (Schawaller et al., 1989; Earl et al., 1990) and electron microscopy (Gelderblom et al., 1988) studies of gp120 have shown that knobs on HIV are multimers. Therefore, in the new model, we will consider a knob as a dimer, which is the simplest form of a multimer. The association constant for blocking individual gp120 monomers within a dimer may depend on whether knobs are free or half blocked. Thus, two sets of forward and reverse rate constants are defined for governing these reactions, which allows for allosteric interactions between sites.

Fifth, in the old model, the shedding rate of gp120 was independent of the formation of gp120-sCD4 complexes. However, we found that biological blocking activity of sCD4 at high concentrations was noncompetitive (Layne et al., 1991). As shown by other investigators, an enhanced rate of spontaneous shedding of gp120 accounts for this noncompetitive activity (Moore et al., 1990; McKeating et al., 1991). Therefore, in the new model, the shedding rate of a gp120 knob depends on the number of molecules bound to it. Thus, there are three separate shedding rates corresponding to free, half and fully blocked dimers. This permits greater flexibility and precision in the analysis of noncompetitive blocking activity.

Sixth, the role of nonspecific inactivation (Nara *et al.*, 1987) is unchanged in the new model. It thus continues to represent single-hit processes that are independent of the number of gp120 dimers on a viral particle.
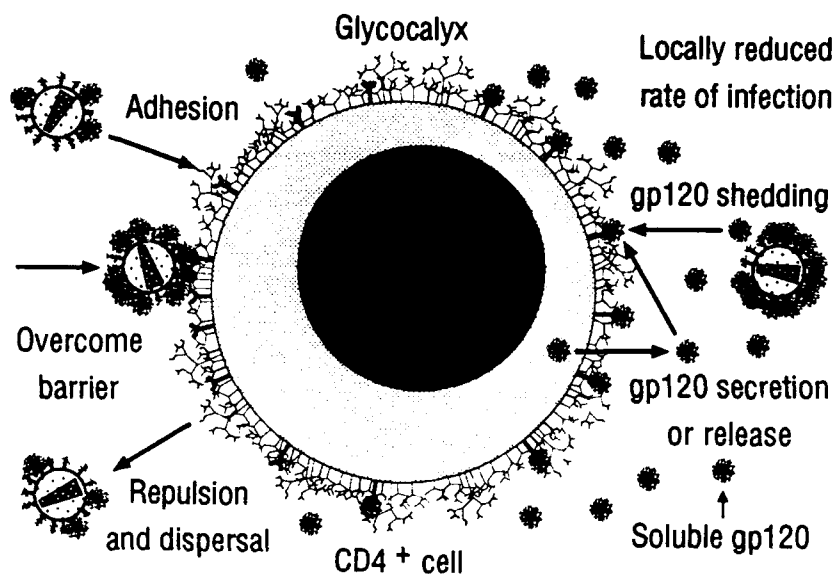

FIG. 17. The critical number of gp120s for efficient infection of CD4$^+$ cells arises from a balance of forces. Repulsive forces from viral and cellular glycocalyces are opposed by attractive ones from gp120 and CD4 interaction. The shedding of gp120 from particles and its secretion or release from infected cells results in high local concentrations of gp120 and the blocking of CD4 receptors on cell surfaces. This will locally reduce the rate of infection, prevent superinfection of progenitor cells, and promote viral export from infected tissues. These actions will permit HIV infection to persist within the host without causing excessive cytolytic damage or cell fusion, which is characteristic of lentiviral infections.

OPEN QUESTIONS FOR THE KINETIC MODEL

■ **Role of the Glycocalyx** — *What factors on the viral envelope and cell-surface glycocalyx determine the critical number of gp120 knobs?*

■ **Examining Physiologic Target Cells** — *Does the model of HIV infection kinetics apply to other types of target cells?*

■ **Characterizing Immunoglobulin Blocking Activity** — *Are neutralization mechanisms by sCD4, monoclonal immunoglobulins and polyclonal sera from HIV-infected persons similar or fundamentally different?*

■ **Variations Between HIV Strains** — *What range of critical numbers, shedding rates and neutralization susceptibilities typify wild-type strains of HIV?*

REFERENCES

Anderson, N. G. (1968). Analytical techniques for cell fractions VIII. Analytical differential centrifugation in angle-head rotors. *Analytical Biochem.* **23,** 72–83.

Baltimore, D., and Smoler, D. (1971). Primer requirements and template specificity of the DNA polymerase of RNA tumor viruses. *Proc. Natl.Acad. Sci. USA* **68,** 1507–1511.

Barrow, G. M. (1974). Physical chemistry for the life sciences. McGraw-Hill, New York.

Bauer, G., and Temin, H. M. (1980). Radioimmunological comparison of the DNA polymerases of avian retroviruses. *J. Virol.* **33,** 1046–1057.

Bell, G. I., Dembo, M., and Bongrand, P. (1984). Cell adhesion: competition between nonspecific repulsion and specific binding. *Biophys. J.* **45,** 1051–1064.

Berg, H. C., and Purcell, E. M. (1977). Physics of chemoreception. *Biophys. J.* **20,** 193–219.

Byrn, R. A., Sekigawa, I., Chamow S. M., Johnson J. S., Gregory, T. J., Capon, D. J., and Groopman, J. E. (1989). Characterization of in vitro inhibition of human immunodeficiency virus by purified recombinant CD4. *J. Virology* **63,** 4370–4375.

Clark, S. J., Saag, M. S., Decker, W. D., Campbell-Hill, S., Roberson, J. L., Veldkamp, P. J., Kappes, J. C., Hahn, B. H., and Shaw, G. M. (1991). High titers of cytopathic virus in plasma of patients with symptomatic primary HIV-1 infection. *New Engl. J. Med.* **324,** 954–960.

Cohen, J. (1991). Is NIH failing an AIDS "challenge"? *Science* **251,** 518–520.

Coombs, R. W., Collier, A. C., Allain, J.-P., Nikora, B., Leuther, M., Gjerset, G. F., and Corey, L. (1989). Plasma viremia in human immunodeficiency virus infection. *New Engl. J. Med.* **321,** 1626–1631.

Daar, E. S., Moudgil, T., Meyer, R. D., and Ho, D. D. (1991). Transient high levels of viremia in patients with primary human immunodeficiency virus type 1 infection. *New Engl. J. Med.* **324,** 961–964.

Dembo, M., and Bell, G. I. (1987). The thermodynamics of cell adhesion. *Current Topics in Membranes and Transport* **29,** 71–89.

DuPont Chemical, Inc. (1990). *HIV-1 p24 core profile ELISA.* Catalog number NEK-060A.

Dimitrov, D. S., Hillman, K., Manischewitz, J., Blumenthal, R., and Golding, H. (199#). Kinetics of sCD4 binding to cells expressing HIV-1 envelope glycoprotein. *J. Virology* 66, 132–138.

Earl, P. L., Doms R. W., and Moss, B. (1990). Oligomeric structure of the human immunodeficiency virus type 1 envelope glycoprotein. *Proc. Natl. Acad. Sci. USA* 87, 648–652.

Efron, B., and Tibshirani, R. (1991). Statistical data analysis in the computer age. *Science* 253, 390–395.

Fenouillet, E., Clerget-Raslain, B., Gluckman, J. C., Guétard, D., Montagnier, L., and Bahraoui, E. (1898). Role of N-linked glycans in the interaction between the envelope glycoprotein of human immunodeficiency virus and its cellular CD4 receptor. *J. Exp. Med.* 169, 807–822.

Fenyö, E. M., Albert, J., and Åsjö, B. (1989). Replicative capacity, cytoplasmic effect and cell tropism of HIV. *AIDS (suppl 1)* 3: S5–S12.

Fernandez-Larsson, F., Srivastava, K. K., Lu, S., and Robinson, H. L. (1992). Replication of patient isolates of human immunodeficiency virus type 1 in T cells: A spectrum of rates and efficiencies of entry. *Proc. Natl. Acad. Sci. USA* 89, 000–000.

Furman, P. A., Painter, G., Wilson, J. E., Cheng, N., and Hopkins, S. (1991). Substrate inhibition of the human immunodeficiency virus type 1 reverse transcriptase. *Proc. Natl. Acad. Sci. USA* 88, 6013–6017.

Gelderblom, H. R., Reupke, H., and Pauli, G. (1985). Loss of envelope antigens of HTLV-III/LAV, a factor in AIDS pathogenesis? *Lancet* ii, 1016–1017.

Gelderblom, H. R.,Özel, M., Hausmann, E. H. S., Winkel, T., Pauli, G., and Koch, M. A. (1988). Fine structure of human immunodeficiency virus (HIV), immunolocalization of structural proteins and virus–cell relation. *Micron and Microscopica* 19, 41–60.

Gelderblom, H. R. (1991). Assembly and morphology of HIV: potential effect of structure on function. *AIDS* 5, 617–638.

Gerwin, B. L., and Levin, J. G. (1977). Interactions of murine leukemia virus core components: characterization of reverse transcriptase packaged in the absence of 70S genomic RNA. *J. Virol.* 24, 478–488.

Goff, S., Traktman, P., and Baltimore, D. (1981). Isolation and properties of Moloney Murine Leukemia Virus mutants: use of a rapid assay for release of virion reverse transcriptase. *J. Virol.* 38, 239–248.

Goff, S. (1990). Retroviral reverse transcriptase: synthesis, structure, and function. *J. Acquired Immune Defic. Syndr.* 3, 817–831.

Goldstein, B. (1989). Diffusion limited effects of receptor clustering. *Comments on Theoretical Biol.* 1, 109–127.

Goldstein, B., Posner, R. G., Torney, D. C., Erickson, J., Holowka, D., and Baird, B. (1989). Competition between solution and cell surface receptors for ligand. *Biophys. J.* 56, 955–966.

Goodman, N. C., and Spiegelman, S. (1971). Distinguishing reverse transcriptase of an RNA tumor virus from other known DNA polymerases. *Proc. Natl.Acad. Sci. USA* 68, 2203–2206.

Helgstrand, E., Eriksson, B., Johansson, N. G., Lannerö, B., Larsson, A., Misiorny, A., Norén, J. O., Sjöberg, B., Stenberg, K., Stening, G., Stridh, S., Öberg, B., Alenius, S., and Philipson, L. (1978). Trisodium Phosphonoformate, a new antiviral compound. *Science* 201, 819–821.

Ho, D. D., Moudgil, T., Alam, M. (1989). Quantitation of human immunodeficiency virus type 1 in the blood of infected persons. *New Engl. J. Med.* 321, 1621–1625.

Kacian, D. L., Watson, K. F., Burny, A., and Spiegelman, S. (1971). Purification of the DNA polymerase of avian myleoblastosis virus. *Biochem. Biophys. Acta* 246, 365–383.

Krakower, J. M., Barbacid, M., and Aaronson, S. A. (1977). Radioimmunoassay for mammalian type C viral reverse transcriptase. *J. Virol.* 22, 331–339.

Layne, S. P., Spouge, J. L., and Dembo, M. (1989). Quantifying the infectivity of human immunodeficiency virus. *Proc. Natl. Acad. Sci. USA* 86, 4644–4648.

Layne, S. P., Merges, M. L., Dembo, M., Spouge, J. L., and Nara, P. L. (1990). HIV requires multiple gp120 molecules for CD4-mediated infection. *Nature* 346, 277–279.

Layne, S. P., Merges, M. L., Spouge, J. L., Dembo, M., and Nara, P. L. (1991). Blocking of human immunodeficiency virus infection depends on cell density and viral stock age. *J.*

Virology 65, 3293–3300.

Layne, S. P., and Dembo, M. (1992). The auto-regulation model: A unified concept of how HIV regulates its infectivity, pathogenesis and persistence. *International Reviews of Immunology* 8, 33–64.

Looney, D. J., Hayashi, S., Nicklas, M., Redfield, R. R., Broder, S., Wong-Staal, F., and Mitsuya, H. (1990). Differences in the interaction of HIV-1 and HIV-2 with CD4. *J. Acquired Immune Defic. Syndr.* 3, 649–657.

Lori, F., Scovassi, A. I., Zella, D., Achilli, G., Cattaneo, E., Casoli, C., an Bertazzoni, U. (1987). Enzymatically active forms of reverse transcriptase of the huma . immunodeficiency virus. *AIDS Res. Hum. Retroviruses* 4, 393–398.

Lu, S., Putney, S. D., and Robinson, H. L. (1992). Human immunodeficiency virus type 1 entry into T cells: more-rapid escape from an anti-V3 loop than from antireceptor antibody. *J. Virol* 66, 000–000.

Majumdar, C., Abbotts, J., Broder, S., and Wilson, S. H. (1988). Studies on the mechanism of human immunodeficiency virus reverse transcriptase. *J. Biol. Chem.* 263, 15657–15665.

McDougal, J. S., Martin, L. S., Cort, S. P., Mozen, M., Heldebrant C. M., and Evatt, B. L. (1985). Thermal inactivation of the acquired immunodeficiency syndrome virus, human T lymphotropic virus-III/lymphadenopathy-associated virus, with special reference to antihemophilic factor. *J. Clin. Invest.* 76, 875–877.

Meek, T. D., Dayton, B. D., Metcalf, B. W., Dreyer, G. B., Strickler, J. E., Gorniak, J. G., Rosenberg, M., Moore, M. L., Magaard, V. W., and Debouck, C. (1989). Human immunodeficiency virus 1 protease expressed in Escherichia coli behaves as a dimeric aspartic protease. *Proc. Natl. Acad. Sci. USA* 86, 1841–1845.

McKeating, J. A., A. McKnight, and J. P. Moore. 1991. Differential loss of envelope glycoprotein gp120 from virions of human immunodeficiency virus type 1 isolates: effects on infectivity and neutralization. *J. Virology* 65, 852–860.

Mizrahi, V., Lazazus, G. M., Miles, L. M., Meyers, C. A., and Debouck, C. (1989). Recombinant HIV-1 reverse transcriptase: purification, primary structure, and polymerase/ribonuclease H activities. *Arch. Bio chem. Biophys.* 273, 347–358.

Moore, J. P., and Jarrett, R. F. (1988). Sensitive ELISA for the gp120 and gp160 surface glycoproteins of HIV-1. *AIDS Res. Hum. Retroviruses* **4**, 369–379.

Moore, J. P., Wallace, L. A., Follett, E. A. C., and McKeating, J. A. (1989). An enzyme-linked immunosorbent assay for antibodies to the envelope glycoproteins of divergent strains of HIV-1. *AIDS* **3**, 155–163.

Moore, J. P., McKeating, J. A., Weiss, R. A., and Sattentau, Q. J. (1990). Dissociation of gp120 from HIV-1 virions induced by soluble CD4. *Science* **250**, 1139–1142.

Nara, P. L., Dunlop, N. M., Robey, W. G., Callahan, R., and Fischinger, P. J. (1987). Lipoprotein-associated oncornavirus-inactivating factor in the genus *Mus*: effects on murine leukemia viruses of laboratory and exotic mice. *Cancer Res.* **47**, 667–672.

Nara, P. L., Hatch, W. C., Dunlop, N. M., Robey, W. G, Arthur, L. O., Gonda, M. A., and Fischinger, P. J. (1987). Simple, rapid, quantitative, syncytium-forming microassay for the detection of human immunodeficiency virus neutralizing antibody. *AIDS Res. Hum. Retroviruses* **3**, 283–302.

Nara, P. L., and Fischinger, P. J. (1988). Quantitative infectivity assay for HIV-1 and -2. *Nature* **332**, 469–470.

Öberg, B. (1983). Antiviral effects of phosphonoformate (PFA, foscarnet sodium). *Pharmac. Ther.* **19**, 387–415.

Panet, A., Baltimore, D., and Hanafusa, T. (1975). Quantitation of avian RNA tumor virus reverse transcriptase by radioimmunoassay. *J. Virol.* **16**, 146–152.

Panet, A., and Kra-Oz, Z. (1978). A competition immunoassay for characterizing the reverse transcriptase of mammalian RNA tumor viruses. *Virology* **89**, 95–101.

Pantaleo, G., Graziosi, C., Butini, L., Pizzo, P. A., Schnittman, S. M., Kotler, D. P., and Fauci, A. S. (1991). Lymphoid organs function as major reservoirs for human immunodeficiency virus. *Proc. Natl. Acad. Sci. USA* **88**, 9838–9842.

Plunkett, M. L., Sanders, M. E., Selvaraj, P., Dustin, M. L., and Springer, T. A. (1987). Rosetting of activated human T lymphocytes with autologous erythrocytes. *J. Exp. Med.* **165**, 664–676.

Salmeen, I., Ramai, L., Luftig, R. B., Liebes, L., Retzel, E., Rich, M., and McCormick, J. J. (1976). Hydrodynamic diameters of murine mammary, rous sarcoma, and feline leukemia RNA tumor viruses: studies by laser beat frequency light-scattering spectroscopy and electron microscopy. *J. Virol.* 17, 584–596.

Sandstrom, E. G.,Kaplan, J. C., Byington, R. E., and Hirsch, M. S. (1985). Inhibition of human T-cell lymphotropic virus type III in vitro by phosphonoformate. *Lancet* i, 1480–1482.

Sharp, D. G., and Beard, J. W. (1950). Size and density of polystyrene particles measured by ultracentrifugation. *J. Biol. Chem.* 185, 247–253.

Shaw, G. M., Hahn, B. H., Arya, S. K., Groopman, J. E., Gallo, R. C., and Wong-Staal, F. (1984). Molecular characterization of human T-cell leukemia (lymphotropic) virus type III in the acquired immune deficiency syndrome. *Science* 226, 1165–1171.

Springer, T. A. (1990). Adhesion receptors of the immune system. *Nature* 346, 425–434.

Venable, J. H., and Coggeshall, R. (1965). A simplified lead citrate stain for use in electron microscopy. *J. Cell Biol.* 25, 407–408.

Veronese, F. M., Copeland, T. D., DeVico, A. L., Rahman, R., Oroszlan, S., Gallo, R. C., and Sarngadharan, M. G. (1986). Characterization of highly immunogenic p66/p51 as the reverse transcriptase of HTLV-III/LAV. *Science* 231, 1289–1291.

Schawaller, M., Smith, G. E., Skehel, J. J., and Wiley, D. C. (1989). Studies with crosslinking reagents on the oligomeric structure of the env glycoprotein of HIV. *Virology* 172, 367–369.

APPENDIX

COLLABORATORS

An important component of this project was collaboration with leading HIV researchers. Without their unique talents and contributions, this work would not have been possible. Mathematical analyses of the kinetic models of HIV infection were undertaken in collaboration with Dr. John L. Spouge (National Library of Medicine, Bethesda, MD). Quantitative infectivity assays and chemical measurements were undertaken in collaboration with Dr. Peter L. Nara, Michael J. Merges, and Shawn R. Conley (National Cancer Institute, Frederick, MD). Electron microscopy studies were undertaken in collaboration with Drs. Hans R. Gelderblom and Herbert Renz (Robert Koch-Institute, Berlin, Germany). The gp120 enzyme linked immunosorbent assays (ELISA) were undertaken in collaboration with Drs. John P. Moore (Aaron Diamond AIDS Research Center, New York, NY) and Jawahar L. Raina (American Bio-Technologies, Cambridge, MA).

PRELIMINARY MONOCLONAL Ig AND Fab FRAGMENT STUDIES

Blocking can be understood in terms of a forward rate constant (k_f), a reverse rate constant (k_r) and an equilibrium association constant (K_{assoc}). For most immunoglobulins, the size of the forward rate constant is independent of the size of the reverse rate constant. Thus, blocking is best understood in terms of the reverse rate constant and equilibrium association constant. Monoclonal immunoglobulins (mIg) directed against gp120 have the potential for forming bivalent attachments. Such bivalent interactions can reduce the rate at which mIg molecules dissociate from gp120 and increase the effective mIg-gp120 K_{assoc} (sometimes called the immunoglobulin avidity).

To investigate these issues, we performed a number of infectivity assays with murine monoclonal immunoglobulins and their Fab fragments. For HIV-1HXB3 and HIV-1HX10, we used the monoclonal immunoglobulin called 0.5β, which binds to the V3 loop on gp120. For HIV-1MN, we used the monoclonal immunoglobulin called F50.1, which also binds to the V3 loop.

Before conducting infectivity assays, virus and mIg (or Fab) were mixed and incubated for 1 hour at 37°C. The mixture was ultracentrifuged (155,000 × g for 40 min) and the supernatant was

completely removed. The viral pellet with volume of ~10 µl was then suspended to its original volume of 8000 µl with fresh media without immunoglobulin. This washing procedure reduced the concentration of mIg and Fab fragments in the fresh media by about 800 fold. At 0, 2 and 4 hours following this wash, quantitative infectivity assays were performed with CEM-SS target cells at low density (1.4×10^4 ml^{-1}) to assure unsaturated conditions. The results of these experiments are summarized in Tables 7, 8 and 9.

For HIV-1HXB3 (Table 7), both 0.5β IgG and Fab had similar blocking ratios at the concentrations of 0, 10^{-11} and 10^{-8} M. These blocking ratios were unchanged at 2 and 4 hours following the wash (data not shown). These results indicated that 0.5β IgG and Fab were completely reversible at the concentrations used.

Table 7. *Inhibition of HIV-1HXB3 infectivity by 0.5β monoclonal immunoglobulin and its Fab fragment after removing the blocker from viral particles by ultracentrifugation.*

HIV-1 strain	Form of monoclonal	Post-removal time (hrs)	Blocker conc. (molar)	SFU* Mean ± 1 SD	Blocking ratio
HXB3	0.5β – IgG	0	0	58.6 ± 4.6	1.0
			10^{-11}	56.4 ± 5.3	1.0
			10^{-8}	58.6 ± 5.2	1.0
	0.5β – Fab	0	0	58.0 ± 6.5	1.0
			10^{-11}	57.5 ± 5.4	1.0
			10^{-8}	56.3 ± 6.1	1.0

* SFU are a mean of 8 microtiter wells.

For HIV-1HX10 (Table 8), 0.5β IgG and Fab had slightly different blocking ratios at 10^{-9} M and significantly different ones at 10^{-6} M. In all instances, the blocking ratios were larger for intact IgG than for the corresponding Fab fragment. This result suggested that 0.5β IgG formed bivalent attachments whereas 0.5β Fab only formed monovalent attachments. With increasing time after the wash, the blocking ratio for 0.5β IgG (at 10^{-9} M) fell by approximately 3 fold, indicating that there was a slow reversible component. At the higher IgG concentration (10^{-6} M), however, there was no

evidence for a reversible component. This observation was again consistent with the notion bivalent binding. At the higher Fab concentration (10^{-6} M), the blocking ratio fell with time after the wash, indicating a reversible component due to monovalent binding.

Table 8. *Inhibition of HIV-1HX10 infection by 0.5β monoclonal immunoglobulin and its Fab fragment after removing the blocker from viral particles by ultracentrifugation.*

HIV-1 strain	Form of monoclonal	Post-removal time (hrs)	Blocker conc. (molar)	SFU* Mean ± 1 SD	Blocking ratio
HX10	0.5β – IgG	0	0	50.3 ± 4.6	1.0
			10^{-9}	16.5 ± 3.0	3.1
			10^{-6}	0.4 ± 0.7	130
		2	0	48.3 ± 4.2	1.0
			10^{-9}	31.9 ± 2.0	1.5
			10^{-6}	0.3 ± 0.5	160
		4	0	26.0 ± 2.0	1.0
			10^{-9}	26.3 ± 1.6	1.0
			10^{-6}	0.1 ± 0.4	260
	0.5β – Fab	0	0	50.5 ± 5.0	1.0
			10^{-9}	41.9 ± 5.2	1.2
			10^{-6}	19.3 ± 2.1	2.6
		2	0	48.1 ± 4.7	1.0
			10^{-9}	44.3 ± 2.9	1.1
			10^{-6}	25.3 ± 2.5	1.9
		4	0	25.9 ± 2.6	1.0
			10^{-9}	24.5 ± 2.1	1.1
			10^{-6}	17.1 ± 1.6	1.5

* SFU are a mean of 8 microtiter wells.

Overall, the gp120 amino acid sequence for HIV-1HXB3 and HIV-1HX10 differ by less than 0.5%. In the V3 loop, there is a single site change in the amino acid sequence. From these results, we conclude that slight alterations in the envelope sequence induce major changes in immunoglobulin binding characteristics.

Table 9. *Inhibition of HIV-1MN infectivity by F50.1 monoclonal immunoglobulin and its Fab fragment after removing the blocker from viral particles by ultracentrifugation.*

HIV-1 strain	Form of monoclonal	Post-removal time (hrs)	Blocker conc. (molar)	SFU* Mean ± 1 SD	Blocking ratio
MN	F50.1 – IgG	0	0	85.5 ± 4.5	1.0
			10^{-9}	43.6 ± 4.7	2.0
			10^{-7}	0	large
		2	0	77.8 ± 4.8	1.0
			10^{-9}	35.5 ± 4.0	2.2
			10^{-7}	0	large
		4	0	71.3 ± 4.7	1.0
			10^{-9}	20.0 ± 3.6	3.6
			10^{-7}	0	large
	F50.1 – Fab	0	0	84.8 ± 3.7	1.0
			10^{-8}	86.0 ± 3.5	1.0
			10^{-6}	86.0 ± 4.9	1.0
		2	0	80.6 ± 4.0	1.0
			10^{-8}	80.3 ± 3.1	1.0
			10^{-6}	80.3 ± 3.4	1.0
		4	0	70.3 ± 3.6	1.0
			10^{-8}	73.3 ± 3.0	1.0
			10^{-6}	71.6 ± 4.8	1.0

* SFU are a mean of 8 microtiter wells.

For HIV-1MN (Table 9), F50.1 IgG had very different blocking activities at 10^{-9} and 10^{-7} M. The lower concentration gave a 2–3 fold reduction in HIV infectivity whereas the higher concentration completely blocked infectious events. At both IgG concentrations, there was no evidence for a reversible component. On the other hand, the F50.1 Fab fragment was completely reversible at the concentrations used. These results indicated that F50.1 IgG formed bivalent attachments that were completely irreversible whereas 0.5β Fab formed monovalent attachments that were completely reversible. We must note that it remains to be determined whether F50.1 IgG induces the spontaneous shedding of gp120.

In summary, these data indicate that intact immunoglobulins can form bivalent attachments with gp120 on HIV-1. These attachments display both slowly reversible and irreversible components which are consistent with the notion of bivalent binding. The corresponding Fab fragments display lesser degrees of blocking and have reversible components that are more rapid. This finding is preliminary and limited to a small set of murine monoclonals and their Fab fragments. If this finding applies to human immunoglobulins in general, however, it may be impractical to develop HIV vaccines with broad efficacy. We believe that direct measurements of the forward and reverse rate constants by plasmon resonance spectroscopy would be useful for better understanding the blocking activities of these monoclonal immunoglobulins.

ATTACHED PUBLICATIONS

- Layne *et al. Proc. Natl. Acad. Sci. USA* **86**, 4644–4648 (1989).
- Layne *et al. Nature* **346**, 277–279 (1990).
- Layne *et al. J. Virol.* **65**, 3293–3300 (1991).
- Layne & Dembo. *International Reviews of Immunology* **8**, 33–64 (1992).

Quantifying the infectivity of human immunodeficiency virus

(viral infectivity assay/human immunodeficiency virus kinetics/gp120 blocking protein)

SCOTT P. LAYNE*, JOHN L. SPOUGE†, AND MICAH DEMBO*

*Theoretical Division, Los Alamos National Laboratory, Los Alamos, NM 87545; and †Laboratory of Mathematical Biology, National Cancer Institute, National Institutes of Health, Bethesda, MD 20892

Communicated by Stirling A. Colgate, March 8, 1989 (received for review January 9, 1989)

ABSTRACT   We have developed a mathematical model that quantifies lymphocyte infection by human immunodeficiency virus (HIV) and lymphocyte protection by blocking agents such as soluble CD4. We use this model to suggest standardized parameters for quantifying viral infectivity and to suggest techniques for calculating these parameters from well-mixed infectivity assays. We discuss the implications of the model for our understanding of the infectious process and virulence of HIV *in vivo*.

Subsets of lymphocytes, monocytes, and macrophages expressing CD4 are the primary targets for infection by human immunodeficiency virus (HIV) (1), and three overall steps have been suggested for the infective process. First, HIV diffuses to the cell surface; second, gp120 (120-kDa glycoprotein) on the virus' surface and CD4 on the target cell's surface form a bimolecular complex; third, interactions involving CD4, gp120, and gp41 promote fusion of HIV envelope with target cell membrane, resulting in entry of the viral core (2–4). Given this mechanism, blocking some or all gp120 molecules on the viral surface should inhibit infection (5), and, consequently, soluble forms of CD4 (sCD4) have been suggested as potential therapeutic agents. In fact, several studies have demonstrated that sCD4 blocks HIV infection *in vitro* (6–10).

In this paper, we develop a mathematical model quantifying the kinetics of target cell infection by HIV and target cell protection by sCD4. The model is concerned with infection from the fluid phase and does not address direct cell-to-cell transmission—e.g., syncytia formation (11). We show how the model can be used to analyze the results of well-mixed viral infectivity assays and to determine parameters that influence the initial steps in infection. The model also has implications for our understanding of the infectious process and virulence of HIV *in vivo* and on the prospects for therapy with sCD4.

THE MODEL

Consider a stock solution prepared from the supernatant of a cell culture infected with a particular strain of HIV. Such a stock solution can be regarded as a mixture of "homogeneous cohorts" of virions (i.e., populations of virions that were born simultaneously and that have been treated identically ever since). At birth, all members of a homogeneous cohort are assumed to be identical. A virion is said to remain "live" at time T, if it has neither participated in an infective event nor been nonspecifically killed. As time progresses, some cohort members will die and the "infectivity" of those remaining live will diverge due to random processes.

Now suppose that V_0 random members of a homogeneous cohort are selected at birth. These virions are allowed to preincubate for time T_p and are then inoculated at $T = 0$ into a chamber containing a large excess of CD4⁺ target cells (see Fig. 1A). The objective of this procedure is to count the

number of virions that successfully infect, I, which then yields the probability that a single virion will successfully infect, $i \equiv I/V_0$. Considering each homogeneous cohort separately involves no loss of generality, since the behavior of a mixture of cohorts is obtained by taking a weighted average.

Fig. 1B illustrates the random processes acting on a cohort. Of these, blocking, shedding, and infection depend on gp120; nonspecific killing does not. The "equivalent site approximation" from polymer chemistry gives a manageable formulation of Fig. 1B with a minimal loss of detail (15–17). According to this approximation, each gp120 molecule on the surface of a "live" virion has the same chance of being shed, of binding to CD4 on a target cell, or of binding to sCD4 in solution (i.e., each gp120 has the same cross section for reaction). Furthermore, nonspecific killing operates independently on each live virion, regardless of its number of gp120 molecules.

Let N be the initial number of gp120 molecules on each virion at birth and let g be the probability that a particular gp120 remains at a later time. Since gp120s can be either free or complexed with sCD4, $g \equiv (F + C)/NV$, where F and C are the numbers of free and complexed gp120 molecules on live virions and V is the number of live virions. Because of the equivalent site approximation, the probability that a live virion's surface will present exactly J gp120s is always given by a binomial distribution:

$$P(J) = \binom{N}{J} g^J (1 - g)^{N-J}. \tag{1}$$

Since F/NV is the probability that a given gp120 on a live virion is free and C/NV is the probability that a given gp120 on a live virion is complexed, it follows that each infective event causes the loss (on average) of $[1 + (N - 1)F/NV]$ free gp120 molecules and $[(N - 1)C/NV]$ complexed gp120 molecules.

Now let L and B be the respective concentrations of target cells and sCD4 in the reaction chamber. Because the viral inoculum is small, both L and B remain unperturbed and the kinetics in the reaction chamber are governed by:

$$\frac{dI}{dT} = k_i LF, \tag{2}$$

$$\frac{dV}{dT} = -k_i LF - k_n V, \tag{3}$$

$$\frac{dF}{dT} = -k_f BF + k_r C - (k_s + k_n)F \\ -k_i LF \left[1 + (N - 1)\frac{F}{NV}\right]. \tag{4}$$

$$\frac{dC}{dT} = k_f BF - k_r C - (k_s + k_n)C - k_i LF \left[(N - 1)\frac{C}{NV}\right]. \tag{5}$$

Fig. 1B defines the five rate constants: k_i, k_n, k_s, k_f, and k_r. The terms $k_i LF$ and $k_n V$ are the rates of loss of live viral

Abbreviations: HIV, human immunodeficiency virus; sCD4, soluble CD4 protein.

particles due to infection and nonspecific killing, respectively. The terms $k_f BF$ and $k_r C$ are the rates of formation and disassociation of gp120–sCD4 complexes, respectively. The terms $(k_s + k_n)F$ and $(k_s + k_n)C$ are the respective rates of loss of free and complexed gp120 from live virions due to the combined effects of spontaneous shedding and nonspecific killing of virus. Finally, the terms $k_i LF[1 + (N - 1)F/NV]$ and $k_i LF[(N - 1)C/NV]$ are the respective rates of loss of free and complexed gp120 from live virions due to infective events.

The initial conditions for Eqs. 2–5 depend on circumstances during the preincubation phase. In most assays, virions have no opportunity to infect target cells during preincubation $(L = 0)$ and are not exposed to sCD4 $(B = 0)$. The conditions at $T = 0$ are then: $I = 0$, $V = V_0 \exp\{-k_n T_p\}$, $F = NV_0 \exp\{-(k_n + k_s)T_p\}$, and $C = 0$.

To facilitate analysis, introduce nondimensional variables $i \equiv I/V_0$, $v \equiv V/V_0$, $f \equiv F/NV$, and $c \equiv C/NV$. Also introduce nondimensional time, $t \equiv (k_s + k_n)T$, and nondimensional parameters $\sigma \equiv k_s/(k_s + k_n)$, $\lambda \equiv k_i L/(k_s + k_n)$, $\gamma \equiv k_r/(k_s + k_n)$, and $\beta \equiv k_f B/k_r$. Then Eqs. 2–5 take the form:

$$\frac{di}{dt} = N\lambda f v, \tag{6}$$

$$\frac{dv}{dt} = -[N\lambda f + 1 - \sigma]v, \tag{7}$$

$$\frac{df}{dt} = -\gamma(\beta f - c) - \sigma f - \lambda f(1 - f), \tag{8}$$

$$\frac{dc}{dt} = \gamma(\beta f - c) - \sigma c + \lambda f c. \tag{9}$$

The quantity i is the probability that an infectious virion born at $-t_p$ infects by time t. This is the main quantity of biological interest derived from infectivity assays.

Parameter Estimation. T lymphocytes used in viral infectivity assays typically display $r \approx 2 \times 10^4$ CD4 receptors (18). According to Berg and Purcell (19), the probability that a viral gp120 diffusing to a lymphocyte will find a CD4 receptor is $rR_b/(rR_b + \pi R_l) \approx 0.8$ (Table 1). Electron microscope studies (20–22) estimate that 70–80 gp120 complexes cover a mature virion (a single gp120 complex covers $\approx 1/100$th of a virion's surface). Therefore, we take $N = 80$ and the Smoluchowski formula for diffusional collision between two spherical particles (23) gives the rate constant for infection: $k_i \leq (0.8)(0.01)4\pi(D_s + D_l)(R_s + R_l) \approx 8.0 \times 10^{-13}$ cm^3·sec^{-1}. Experiments with other viruses indicate that k_i is unlikely to be more than 1000 times smaller than this upper limit (24).

The Smoluchowski equation along with estimates from Table 1 also yield an upper limit for the forward rate constant of the blocking reaction: $k_f \leq 4\pi(D_s + D_b)(R_g + R_b) \approx 3.0 \times 10^{-12}$ cm^3·sec^{-1}. Again, we would not expect k_f to be more than 1000 times smaller than this upper limit.

The association constant between sCD4 and gp120 (6, 25) ranges from 0.25×10^9 to 1.4×10^9 M^{-1}. Accordingly, we take $k_{assoc} = k_f/k_r \approx 1.2 \times 10^9$ M$^{-1} = 2.0 \times 10^{-12}$ cm^3·molecule^{-1}. Given the fixed ratio k_{assoc}, the reverse rate constant for the blocking reaction is $k_r = k_f/k_{assoc} \leq 1.5$ sec^{-1}.

HIV-1 strains IIIB and RFII lose half of their infectivity in 4–6 hr at 37°C [P. L. Nara and J. Kessler, personal communication (using the assay in ref. 26)]. This gives $(k_s + k_n) \approx 10^{-4}$ sec^{-1}·molecule^{-1} to within a factor of 2. Unless specified, we use the above parameters for all numerical calculations.

Numerical Solutions. Fig. 2 illustrates numerical solutions of the model for typical parameters: Fig. 2A shows a case with no blocker; Fig. 2B shows the effect of adding a low concentration of blocker; Fig. 2C shows the effect of adding a higher concentration of blocker; and Fig. 2D shows the effect of a high concentration of blocker in conjunction with nonspecific killing—e.g., by nonoxynol-9 (27).
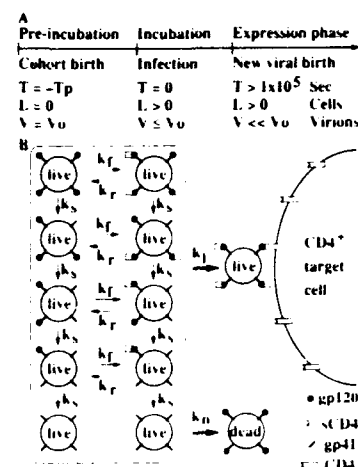

FIG. 1. (A) The three phases in a viral infectivity assay. Virions are born at $T = -T_p$. During the preincubation phase, $-T_p \leq T \leq 0$, shedding and nonspecific killing occur but target cell infection does not occur since $L = 0$. During the incubation phase, $0 \leq T \leq 1 \times 10^5$ sec, all three processes of shedding, nonspecific killing, and target cell infection occur. At $T > 1 \times 10^5$ sec, new virions start emerging from infected cells and secondary infections occur. (B) The kinetic processes in a viral infectivity assay. k_i is the rate constant for successful infective contact between viral gp120 and CD4 on a target cell, defined on a per gp120 basis. When a virion sheds all of its gp120, it is considered live but not infectious. k_n is the rate constant for nonspecific killing of virions, which includes mechanisms such as enzymatic degradation, dissolution by soaps, and neutralization by lipoprotein vesicles (12). Complement does not appear to contribute to nonspecific killing of HIV (13). The processes of infection and nonspecific killing result in the disappearance of virions together with their associated free and complexed gp120s. k_s is the rate constant for spontaneous disassociation of gp120 from gp41 (14). Although such "shedding" causes progressive inactivation of virions, it does not cause the actual disappearance of virions. k_f and k_r are the forward and reverse rate constants for gp120–sCD4 complex formation, respectively. These processes result in the masking and unmasking of gp120s but do not result in the net loss of gp120 or in the disappearance of virions.

In Fig. 2A, the number of infected target cells rises linearly until $T \approx 1 \times 10^3$ sec. Subsequently, at the characteristic shedding time $k_s^{-1} \approx 1 \times 10^4$ sec, there is a drop in the number of gp120 molecules on the surface of virions and the rate of target cell infection diminishes. The obvious decline in the number of virions at $T \approx 1 \times 10^4$ sec is due to target cell infection. When target cell infection stops, $T \approx 1 \times 10^5$ sec, 72% of initial virions have infected target cells; the remaining 28%, now completely lacking gp120 molecules and hence noninfectious, remain in the media. In this computation, there is no nonspecific killing and, at least in theory, these live but noninfectious particles remain in solution indefinitely.

Fig. 2B shows the effects of adding a small concentration of sCD4 to the culture medium. The initial rate of target cell infection is unchanged from Fig. 2A until viral gp120 and sCD4 begin to equilibrate at $T \approx 1 \times 10^{-1}$ sec. Immediately

Table 1. Summary of diffusion rates

Object	Radius, cm	Diffusion rate, cm^2·sec^{-1}
HIV virion (20–22)	$R_v \approx 5.0 \times 10^{-6}$	$D_v \approx 2.0 \times 10^{-8}$
CD4$^+$ lymphocyte	$R_l \approx 4.0 \times 10^{-4}$	$D_l \approx 2.5 \times 10^{-10}$
gp120	$R_g \approx 3.3 \times 10^{-7}$	$D_g \approx 3.0 \times 10^{-7}$
sCD4 molecule (50 kDa)	$R_b \approx 2.5 \times 10^{-7}$	$D_b \approx 4.0 \times 10^{-7}$

The diffusion rate of a sphere of radius R is approximately $k\tau/6\pi\eta R$, where k is the Boltzman constant, τ is temperature, and η is viscosity (23). We use $\tau \approx 300$ K, $\eta \approx 2 \times 10^{-2}$ poise, and assume that protein occupies ≈ 1.23 Å^3 per Da.
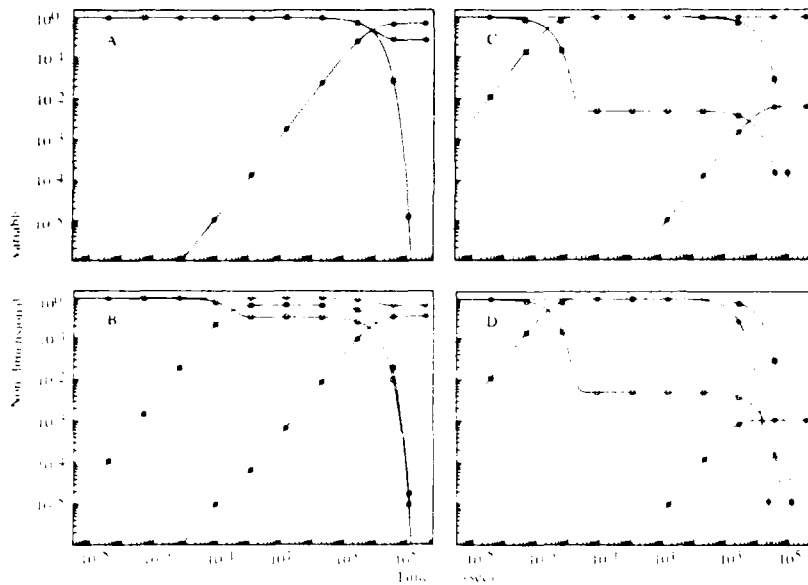
FIG. 2. Four numerical solutions of the model illustrating the progress of an untreated infection, an infection treated with two different concentrations of sCD4, and an infection treated with sCD4 plus an agent that enhances nonspecific killing. The corresponding parameters are $B = 0$ and $k_n = 0$ (A), $B = 1 \times 10^{12}$ molecules·cm^{-3} and $k_n = 0$ (B), $B = 1 \times 10^{14}$ molecules·cm^{-3} and $k_n = 0$ (C), $B = 1 \times 10^{14}$ molecules·cm^{-3} and $k_n = 5 \times 10^{-4}$ sec^{-1} (D). ■, $c \equiv C/NV$; □, $f \equiv F/NV$; ●, $i \equiv I/V_0$; , $v \equiv V/V_0$. For all solutions, $T_p = 0$ and $L = 2 \times 10^6$ cells·cm^{-3}, which is a typical lymphocyte concentration for infectivity assays.

following this, the rate of target cell infection declines by a factor of 2–3 and, because of this decline, only 35% of the initial virions ultimately find target lymphocytes, a decline comparable to the blocking ratio.

In Fig. 2C, the concentration of sCD4 is 100-fold higher than in Fig. 2B. Consequently, equilibration of the blocker with gp120 occurs in only 3×10^{-3} sec and 199 of 200 gp120 molecules are blocked. The rate of infectious events declines by the same proportion but the gp120 shedding is unchanged. Therefore, the final proportion of infecting virions is only 0.6%.

Fig. 2D shows the synergy of a high concentration of sCD4 with nonspecific killing of virus. Let us presume a rate constant for nonspecific killing, $k_n = 5 \times 10^{-4}$ sec^{-1}, that is 5-fold faster than the rate constant for gp120 shedding, $k_s = 1 \times 10^{-4}$ sec^{-1}. As in Fig. 2C, binding of sCD4 to viral gp120 and the shedding of viral gp120 are independent of nonspecific killing and occur on a "per live virion" basis. Nonspecific killing causes the disappearance of virions and so infection stops before virions shed all of their gp120 molecules. As a result, the final proportion of infecting virions is diminished by a factor of 6 relative to Fig. 2C.

Analytical Solutions. In Fig. 2, viral gp120 and sCD4 reach equilibrium rapidly compared to target cell infection, a property holding for the full range of physically relevant parameters. Consequently, the usual quasi steady-state approximation, $k_f BF \approx k_r C$, permits asymptotic solutions to Eqs. 6–9. This approximation holds for time scales longer than the gp120–sCD4 equilibration time (derivation given in ref. 28).

Recall that $g \equiv f + c$ is the nondimensional concentration of both free and complexed gp120 on live virions. Because of the quasi steady-state approximation, $c \approx \beta g/(1 + \beta)$ and $f \approx g/(1 + \beta)$. Adding Eqs. 8 and 9 and applying these relations gives the Bernoulli equation:

$$\frac{dg}{dt} = -\sigma g - \lambda(1 + \beta)^{-1}g(1 - g). \quad [10]$$

The nondimensional form of the initial conditions at $t = 0$ is: $i_0 = 0$, $v_0 = \exp\{-(1 - \sigma)t_p\}$ and $g_0 = \exp\{-\sigma t_p\}$.

Eq. 10 is solvable by separation of variables, and integral forms of $v(t)$ and $i(t)$ are obtained as described elsewhere (28). When $N \gg 1$, these forms lead to a good estimate of the value of $i(t)$ as $t \to \infty$:

$$i_x = e^{-(1-\sigma)t_p} \frac{\zeta N}{N-1} e^{-\zeta\delta} \sum_{j=0}^{\infty} \frac{(\zeta/\delta)^j}{(1 + \delta j)j!}, \quad [11]$$

where $\zeta \equiv \exp\{-\sigma t_p\}(N - 1)\lambda/(\lambda + 1 + \beta)$ and $\delta \equiv [\lambda + \sigma(1 + \beta)]/(\lambda + 1 + \beta)$. Notice that $\zeta \leq N - 1$ and $\delta \leq 1$. The parameter ζ is a measure of the degree to which assay conditions promote target cell infection. The expansions of Eq. 11 for both $\zeta \to 0$ and $\zeta \to N - 1$ lead to the expressions

$$i_x \approx \frac{NV_0 k_1 L\, e^{-(k_s + k_n)t_p}}{k_1 L + (k_s + k_n)(1 + B k_{assoc})}$$
$$\times \left\{ 1 - \frac{\zeta}{1 + \delta} + O(\zeta^2) \right\}. \quad [12]$$

and

$$i_x \approx \frac{V_0 N\, e^{-k_n t_p}}{N - 1} \left\{ 1 - \frac{1 - \delta}{\zeta} + O(\zeta^{-2}) \right\}. \quad [13]$$

respectively. Notice that δ appears only in the higher-order terms.

The main use of Eqs. 12 and 13 is for design and analysis of experiments to measure the viral parameters k_{assoc}, k_s, k_n, k_1, and NV_0. Fig. 3 illustrates the transition from the regime of Eq. 12 (small ζ) to the regime of Eq. 13 (large ζ).
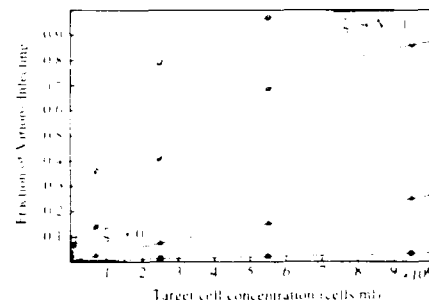

FIG. 3. Numerical solutions of the model illustrating a progression from small to large ζ (Eqs. 12 and 13). The four solutions correspond to different sCD4 concentrations: □, $B = 0$; ○, 1×10^{12}; △, 1×10^{13}; ■, 1×10^{14} molecules·cm^{-3}. The life of a virion consists of a race between finding a target cell and inactivation. Small values of ζ reflect a situation in which a given virion is likely to have only one chance to infect a target cell in its lifetime. Conversely, large values of ζ reflect a situation in which a given virion has multiple chances to infect a target cell. The figure shows the effects of adding various concentrations of sCD4. Notice that the region of transition between linear and nonlinear behavior depends strongly on the blocker concentration. For all solutions $k_n = 0$, $k_s = 1 \times 10^{-4}$ sec^{-1}, and the incubation time $T = 6.48 \times 10^4$ sec.

FINAL REPORT   MIPR # 90MM0545   ATTACHMENT

Immunology: Layne *et al.*   *Proc. Natl. Acad. Sci. USA* 86 (1989)   4647

Consider an experiment to determine k_{assoc}. In such an experiment, I_x would be measured at various values of the blocker concentration, B, with all other variables held constant. When target cell concentration L is moderate, Eq. 12 implies that a plot of $I_x(B = 0)/I_x(B \geq 0)$ versus B will be linear with slope $= k_{assoc}/(1 + \lambda)$ and intercept $= 1$. Fig. 4 shows five plots generated by numerical solutions of Eqs. 2–5, simulating such an experiment at different lymphocyte concentrations, L. Although the plots for all values of L appear linear, the fact that $\lambda \propto L$ means that the slopes seriously underestimate k_{assoc} except at the lowest cell concentrations. Hence, when determining k_{assoc} from the inhibition of viral infectivity, the experiment must be performed within the regime where the results are independent of cell concentration—i.e., $\lambda << 1$.

Measuring the decay of viral infectivity with increasing preincubation times allows estimation of k_n and k_s. Fig. 5 shows five curves generated by numerical solution of Eqs. 2–5 simulating such experiments at different choices of nonspecific killing, k_n. Target cell concentration is made as large as possible and no blocker is added ($B = 0$). Under these conditions, it can be shown (Eq. 13) that the initial decay rate gives k_n and that the final decay rate gives $k_s + k_n$ (Eq. 12). The increase in decay rate with preincubation is a consequence of a fundamental kinetic difference between nonspecific killing and shedding. The former is a so-called "single-hit" process, whereas the latter is a "multi-hit" process inactivating the virus via incremental steps (i.e., loosing a few gp120s makes little difference to the initial infection rate). The lumped quantity, $k_s + k_n$ is a direct measure of the ability of a viral strain to survive until it finds a target cell. A change in either k_n or $k_s + k_n$ provides an objective measure of the potencies of viricidal agents.

Conducting two "preincubation assays" as described above with different target cell concentrations yields estimates of both NV_0 and k_1 (Fig. 6). The quantity NV_0 is useful for estimating the number of "infectious" virions in the inoculum. The rate constant k_1 is important because it quantifies the susceptibility of a particular target cell type to infection by a particular HIV strain. A decrease in k_1 can be caused by a number of independent factors—e.g., a decrease in the surface density of CD4, an increase in the viral uncoating and penetration time, or an increase in the abortive disassociation of the initial virus–target cell complex. Fisher *et al.* (29)
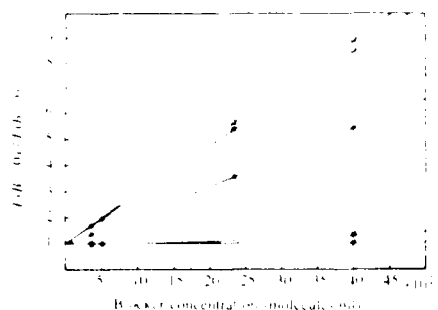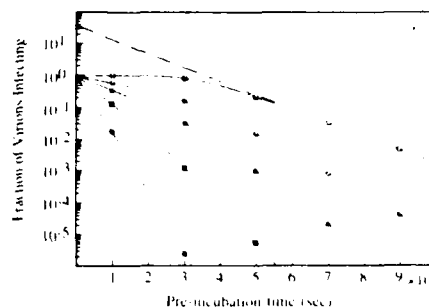

FIG. 5. Five numerical solutions of the model simulating a series of experiments to determine k_s and k_n. In all five simulations, virions are allowed to preincubate for various times T_p and are then inoculated into a reaction chamber. The five plots correspond to increasing amounts of nonspecific killing: $\square$, $k_n = 0$; $\bigcirc$, 0.5×10^{-4}; $\triangle$, 1×10^{-4}; $\blacksquare$, 2×10^{-4}; $\bullet$, 4×10^{-4} sec^{-1}. The ordinate is normalized by the initial number of virions, which is equivalent to taking $V_0 = 1$ in Eqs. 12 and 13. Initially, the slope of each plot is k_n but at longer preincubation times, the slope increases and approaches $k_s + k_n$. Based on Eq. 13, extrapolating the final slope to $T_p = 0$ (top curve) gives the intercept $NV_0 k_1 L/(k_1 L + k_s + k_n)$. For all solutions $k_s = 1 \times 10^{-4}$ sec^{-1}, $B = 0$, $L = 1 \times 10^8$ cm^{-3}, and the incubation time $T = 6.48 \times 10^4$ sec.

and Cheng-Mayer *et al.* (30) report that different HIV isolates vary markedly in their capacity to propagate *in vitro*. A numerical ranking of virus–target cell "tropism" according to the value of k_1 would help to clarify whether such variations are due to increased transmission or increased reproduction of virions.

DISCUSSION

Five publications report that sCD4 blocks HIV infection of CD4$^+$ lymphocytes (6–10) but, of these, only two provide sufficient information to determine k_{assoc}. From figure 4 of Deen and co-workers (9, 31) the ratio of infection between "delayed control" and "experiment" yields $k_{assoc} \approx 3.4 \times 10^{-12}$ cm^3·molecule^{-1}. Figure 3 of Hussey *et al.* (8) gives $k_{assoc} \approx 3.8 \times 10^{-12}$ cm^3·molecule^{-1} for both sCD4 derivatives.

These results should be compared to values of k_{assoc} measured for different analogs of sCD4 using direct physical methods (6, 25): $0.42 \times 10^{-12} \leq k_{assoc} \leq 2.3 \times 10^{-12}$ cm^3·molecule^{-1}. The fair agreement of k_{assoc} as determined by physical and biological methods, strongly supports the fundamental assumption that infection proceeds at a rate proportional to the number of unblocked gp120s on a virion's surface (i.e., the equivalent site approximation). In particu-
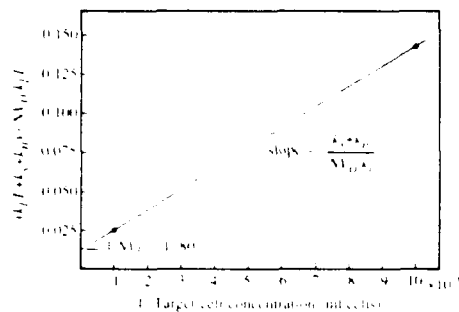

FIG. 4. Numerical solutions simulating a series of infectivity assays for quantifying k_{assoc}. Affinity is measured by comparing an assay without blocker to an assay with blocker, holding other conditions identical. This control/experiment ratio is expressed by $I(B = 0)/I(B > 0)$. The five straight lines correspond to increasing concentrations of target cells: $\square$, $L = 2 \times 10^4$; $\bigcirc$, 2×10^5; $\triangle$, 2×10^6; $\blacksquare$, 2×10^7; $\bullet$, 2×10^8 cells·cm^{-3}. The corresponding slopes for these solutions are 2.0×10^{-12}, 1.9×10^{-12}, 1.1×10^{-12}, 8.0×10^{-14}, and 0 cm^3·molecule^{-1}, respectively. According to Eq. 12, these slopes provide estimates of the quantity $k_{assoc}/(1 + k_1 L/(k_s + k_n))$, which is the effective association constant between blocker and gp120. The decline of the slopes with increasing target cell concentration occurs because $k_1 L/(k_s + k_n)$ increases. For all solutions $T_p = 0$, $k_n = 0$, $k_s = 1 \times 10^{-4}$ sec^{-1}, and the incubation time $T = 6.48 \times 10^4$ sec.

FIG. 6. Estimation of NV_0 and k_1 using data from at least two different preincubation assays. In the top curve of Fig. 5, extrapolating the final slope to $T_p = 0$ gives $NV_0 k_1 L/(k_1 L + k_s + k_n) \approx 40$, when $L = 10^8$ cm^{-3}. Performing a similar extrapolation when $L = 10^7$ cm^{-3} (with all other conditions identical) gives $NV_0 k_1 L/(k_1 L + k_s + k_n) \approx 7$ (not shown). Plotting $(k_1 L + k_s + k_n)/NV_0 k_1 L$ versus $1/L$ gives a straight line with intercept $= 1/NV_0$ and slope/intercept $= (k_s + k_n)/k_1$. Since $k_s + k_n$ is given by the final slope in Fig. 5, k_1 can be estimated directly.

lar, this agreement would not ensue if infection from the fluid phase did not require gp120 or if blocking essentially all viral receptors were necessary to diminish infection. The fact that sCD4 inhibits viral infection despite long incubation times confirms the existence of spontaneous nonspecific killing or shedding processes, $k_n + k_s$, and the importance of such processes in limiting viral infection. If virions did not lose activity with time, then eventually all live virions would infect despite blocker.

The expression phase of an infectivity assay can be likened to a branching process. In this process, each primary infection generates (on average) V_n secondary virions that enter the culture medium without preincubation ($T_p = 0$). These secondary virions, in turn, infect new target cells with probability i_x. A growing infection develops if the branching number (the average number of successfully infecting secondary virions) is $V_n i_x > 1$.

Blocking secondary infection with sCD4 permits estimation of the branching number for an unblocked infection. Define B_{min} as the minimum sCD4 concentration extinguishing the branching process. Under many circumstances (Eq. 12), it can be shown that $V_n i_x \approx NV_n k_1 L/(k_s + k_n) \approx (1 + B_{min} k_{assoc})$. Estimating $B_{min} > 10\,\mu g\cdot cm^{-3} = 1 \times 10^{14}$ molecules·cm^{-3} from Deen *et al.* (9) and using $k_{assoc} \approx 3 \times 10^{-12}$ cm^3·molecule^{-1} yields $1 + B_{min} k_{assoc} > 300$, which is surprisingly large.

We note that Deen *et al.* (9) stimulated the CD4$^+$ lymphocytes in their assay with phytohemagglutinin and recent work by Gowda *et al.* (32) indicates that activation by mitogens increases the rate of CD4$^+$ lymphocyte infection. Based on this, it is conceivable that activation increased both the probability of target cell infection, i_x, and the number of secondary virions, V_n. Experiments measuring the branching number of unstimulated and stimulated target cells are needed.

Since the branching number, $NV_n k_1 L/(k_s + k_n)$, is proportional to target cell concentration, we can extrapolate from the conditions of Deen *et al.* (9) ($L \approx 10^6$ cells·cm^{-3} and $B_{min} > 10\,\mu g\cdot cm^{-3}$) to the conditions in blood ($L \approx 10^6$ cells·cm^{-3}) and lymph node ($L = 10^8$ cells·cm^3). Such extrapolation indicates a minimum therapeutic dose of $\approx 1000\,\mu g\cdot cm^{-3}$ of sCD4 to treat established infections *in vivo*. Even more pessimistically, target cell infection from direct cell-to-cell contacts (e.g., via major histocompatibility complex-restricted interactions) is probably less easily blocked than infection from the fluid medium. Experiments examining this situation are also required.

These results hold if the primary mechanism of action of sCD4 is simply to block the infective process by steric hindrance. Siliciano *et al.* (33) and Lanzavecchia *et al.* (34) indicate that sCD4 may protect CD4$^+$ lymphocytes from indirect or autoimmune effects of gp120. If this is the case, much lower concentrations of sCD4 may be of therapeutic use.

The branching process can also be used for estimating the immune response that an anti-gp120 vaccine must induce to protect against HIV infection. In this instance, k_{assoc} is the association constant between gp120 and neutralizing immunoglobulin, and B_{min} is the minimum concentration of immunoglobulin required to extinguish the spread of infection. Assuming that neutralizing immunoglobulin has a k_{assoc} identical to that of sCD4 (a rather high-affinity immunoglobulin), a molecular weight of $\approx 150,000$, and $V_n i_x \approx 300$ yields $B_{min} \approx 0.03$ mg·cm^{-3} for blood. For lymph node, we calculate that ≈ 3 mg·cm^{-3} may be required to prevent growth of infection. Normally, serum contains ≈ 20 mg·cm^{-3} of all classes of immunoglobulin. Thus, an anti-gp120 vaccine must induce and maintain an extremely high titer of blocking antibody.

1. Fauci, A. S. (1988) *Science* 239, 617–622.
2. Kowalski, M., Potz, J., Basiripour, L., Dorfman, T., Goh, W. C., Terwilliger, E., Dayton, A., Rosen, C., Haseltine, W. & Sodroski, J. (1987) *Science* 237, 1351–1355.
3. Bedinger, P., Moriarty, A., von Borstel, R. C., II, Donovan, N. J., Steimer, K. S. & Littman, D. R. (1988) *Nature (London)* 334, 162–165.
4. McCune, J. M., Rabin, L. B., Feinberg, M. B., Lieberman, M., Kosek, J. C., Reyes, G. R. & Weissman, I. L. (1988) *Cell* 53, 55–67.
5. Weiss, R. A. (1988) *Nature (London)* 331, 15.
6. Smith, D. H., Byrn, R. A., Marsters, S. A., Gregory, T., Groopman, J. E. & Capon, D. J. (1987) *Science* 238, 1704–1707.
7. Fisher, R. A., Bertonis, J. M., Meier, W., Johnson, V. A., Costopoulos, D. S., Liu, T., Tizard, R., Walker, B. D., Hirsch, M. S., Schooley, R. T. & Flavell, R. A. (1988) *Nature (London)* 331, 76–78.
8. Hussey, R. E., Richardson, N. E., Kowalski, M., Brown, N. R., Chang, H.-C., Siliciano, R. F., Dorfman, T., Walker, B., Sodroski, J. & Reinherz, E. L. (1988) *Nature (London)* 331, 78–81.
9. Deen, K. C., McDougal, J. S., Inacker, R., Folena-Wasserman, G., Arthos, J., Rosenberg, J., Maddon, P. J., Axel, R. & Sweet, R. W. (1988) *Nature (London)* 331, 82–84.
10. Traunecker, A., Luke, W. & Karjalainen, K. (1988) *Nature (London)* 331, 84–86.
11. Lifson, J. D., Feinberg, M. B., Reyes, G. R., Rabin, L., Banapour, B., Chakrabarti, S., Moss, B., Wong-Staal, F., Steimer, K. S. & Engleman, E. G. (1986) *Nature (London)* 323, 725–728.
12. Nara, P. L., Dunlop, N. M., Robey, W. G., Callahan, R. & Fischinger, P. J. (1987) *Cancer Res.* 47, 667–672.
13. Harada, S., Yoshiyama, H. & Yamamoto, N. (1985) *J. Clin. Microbiol.* 22, 908–911.
14. Schneider, J., Kaaden, O., Copeland, T. D., Oroszlan, S. & Hunsmann, G. (1986) *J. Gen. Virol.* 67, 2533–2538.
15. Flory, P. J. (1941) *J. Am. Chem. Soc.* 63, 3083–3100.
16. Stockmayer, W. H. (1943) *J. Chem. Phys.* 11, 45–55.
17. Perelson, A. S. & DeLisi, C. (1980) *Math. Biosci.* 48, 71–110.
18. Stein, B. S., Gowda, S. D., Lifson, J. D., Penhallow, R. C., Bensch, K. G. & Engleman, E. G. (1987) *Cell* 49, 659–668.
19. Berg, H. C. & Purcell, E. M. (1977) *Biophys. J.* 20, 193–219.
20. Gelderblom, H. R., Hausmann, E. H. S., Özel, M., Pauli, G. & Koch, M. A. (1987) *Virology* 156, 171–176.
21. Gelderblom, H. R., Özel, M., Hausmann, E. H. S., Winkel, T., Pauli, G. & Koch, M. A. (1988) *Micron Microsc.* 19, 41–60.
22. Özel, M., Pauli, G. & Gelderblom, H. R. (1988) *Arch. Virol.* 100, 255–266.
23. Chandrasekhar, S. (1943) *Rev. Mod. Phys.* 15, 1–89.
24. Nir, S., Stegmann, T. & Wilschut, J. (1986) *Biochemistry* 25, 257–266.
25. Lasky, L. A., Nakamura, G., Smith, D. H., Fennie, C., Shimasaki, C., Patzer, E., Berman, P., Gregory, T. & Capon, D. J. (1987) *Cell* 50, 975–985.
26. Nara, P. L., Hatch, W. C., Dunlop, N. M., Robey, W. G., Arthur, L. O., Gonda, M. A. & Fischinger, P. J. (1987) *AIDS Res. Hum. Retrov.* 3, 283–302.
27. Hicks, D. R., Martin, L. S., Getchell, J. P., Heath, J. L., Francis, D. P., McDougal, J. S., Curran, J. W. & Voeller, B. (1985) *Lancet* ii, 1422–1423.
28. Spouge, J. L., Layne, S. P. & Dembo, M. (1989) *Bull. Math. Biol.*, in press.
29. Fisher, A. G., Ensoli, B., Looney, D., Rose, A., Gallo, R. C., Saag, M. S., Shaw, G. M., Hahn, B. H. & Wong-Staal, F. (1988) *Nature (London)* 334, 444–447.
30. Cheng-Mayer, C., Seto, D., Tateno, M. & Levy, J. A. (1988) *Science* 240, 80–82.
31. McDougal, S. J., Mawle, A., Cort, S. P., Nicholson, J. K. A., Cross, G. D., Scheppler-Campbell, J. A., Hicks, D. & Sligh, J. (1985) *J. Immunol.* 135, 3151–3162.
32. Gowda, S. D., Stein, B. S., Mohagheghpour, N., Benike, C. J. & Engleman, E. G. (1989) *J. Immunol.* 142, 773–780.
33. Siliciano, R. F., Lawton, T., Knall, C., Karr, R. W., Berman, P., Gregory, T. & Reinherz, E. L. (1988) *Cell* 54, 561–575.
34. Lanzavecchia, A., Roosnek, E., Gregory, T., Berman, P. & Abrignani, S. (1988) *Nature (London)* 334, 530–532.

HIV requires multiple gp120 molecules for CD4-mediated infection

Scott P. Layne*, Michael J. Merges†, Micah Dembo*, John L. Spouge‡ & Peter L. Nara†

* Theoretical Division, Los Alamos National Laboratory, Los Alamos, New Mexico 87545, USA
† Virus Biology Section, Laboratory of Tumor Cell Biology, NCI-FCRF, Frederick, Maryland 21701, USA
‡ National Center for Biotechnology Information, National Library of Medicine, Bethesda, Maryland 20894, USA

BINDING of glycoprotein gp120 to the T cell-surface receptor CD4 is a crucial step in CD4-dependent infection of a target cell by the human immunodeficiency virus (HIV)[1-5]. Blocking some or all gp120 molecules on the viral surface should therefore inhibit infection. Consequently, competitive receptor inhibitors, such as soluble synthetic CD4 (sCD4), synthetic CD4 peptides and immunoglobulins, have been investigated *in vitro*[6-17] and *in vivo*[18-20], but little is known about the molecular mechanisms of these inhibitors. We have now quantitatively examined blocking by soluble CD4 in the hope of gaining insight into the complex process of viral binding, adsorption and penetration. At low sCD4 concentrations, the inhibition in three HIV strains is proportional to the binding of gp120. The biological association constant (gp120-sCD4 K_{assoc}) for HIV-2$_{NIHZ}$ is $(8.5 \pm 0.5) \times 10^7 \, M^{-1}$, whereas K_{assoc} for HIV-1$_{HXB3}$ (1.4 ± 0.2) and HIV-1$_{MN}$ $(1.7 \pm 0.1) \times 10^9 \, M^{-1}$ are 15–20-fold larger. For all three viral strains, the biological K_{assoc} from infectivity assays is comparable to the chemical K_{assoc}. The inhibitory action of sCD4 at high concentrations, however, is not fully explained by simple proportionality with the binding to gp120. Positive synergy in blocking of infection occurs after about half the viral gp120s molecules are occupied, and is identical for all three viral strains, despite the large differences in K_{assoc}. Our method of measuring the viral–cell receptor K_{assoc} directly from infectivity assays is applicable to immunoglobulins, to other viruses and to assays using primary or transformed cell lines.

A quantitative infectivity assay requires the number of infectious events to be linear (unsaturated) in the target cell concentration[21,22]. Figure 1 shows results for six concentrations of CEM-SS cells[23,24]. Results were linear at lower cell concentrations and showed only minor assay saturation at higher concentrations. The multiplicity of infection in all assays was less than 0.025 (see Fig. 1, methods).

To distinguish among the possible mechanisms by which sCD4 blocks gp120-mediated infection, we previously analysed a kinetic model of the initial events of infection[21,22], in which each gp120 monomer within an oligomer is functionally independent and equivalent. This neutral hypothesis predicts that for an unsaturated assay, a plot of inverse infection (1/SFU, where SFU are syncytial-forming units) versus sCD4 concentration should be a straight line. That is, inhibition is proportional to binding. Dividing the slope of an inverse infection plot by its intercept gives the gp120-sCD4 K_{assoc}. Upward curvature in the inverse infection plot indicates positive synergy between gp120 molecules as they promote infection or between sCD4

FIG. 1 Examining the linearity of infectivity assays. To compare one assay with another they must scale linearly with target cell concentration, because saturated assays make blockers seem ineffective[21,22]. The graphs for HIV-1$_{HXB3}$ (○), HIV-1$_{MN}$ (□) and HIV-2$_{NIHZ}$ (△) show SFU plotted against target cell concentration. For each viral strain, assays were conducted at six target-cell and seven sCD4 concentrations (see Table 1). All results are the mean of eight microtitre wells (bars show ± 1 s.d.). Results without sCD4 are shown; similar results were obtained when sCD4 was added to the assays. The dotted lines are weighted least-squares fits. At all sCD4 concentrations, correlation coefficients were ≥0.89 for HIV-1$_{HXB3}$, ≥0.97 for HIV-1$_{MN}$, and ≥0.98 for HIV-2$_{NIHZ}$, substantiating that the infectivity assays were linear at the lower, more heavily weighted cell concentrations.

METHODS. The HIV-1 and HIV-2 stocks were acutely collected from H9 cells to optimize infectivity[23]. HIV-1 *in vivo* is a mixture of closely related viral subpopulations with minor envelope variations[31]. To address the influence of envelope microheterogeneity on infectivity[32-34], we studied both a molecularly cloned viral stock (HIV-1$_{HXB3}$) and two uncloned viral stocks (HIV-1$_{MN}$ and -2$_{NIHZ}$)[26]. HIV-1$_{MN}$ was selected because of its dominance in recent seroprevalence surveys[35]. In typical viral stocks, gp120 is not only present on virions as oligomers[36] but also exists as soluble gp120 monomers[37]. Thus, soluble gp120 may cause artefacts if it competes significantly with viral-associated gp120 for sCD4 or cell-surface CD4. In the present study, radioimmunoassay[38] was used to measure the total gp120 (soluble plus viral-associated) in all HIV stocks tested. The total gp120 in the viral inocula was 1×10^{-10}, 6×10^{-11} and 3×10^{-12} M for HIV-1$_{HXB3}$, HIV-1$_{MN}$ and HIV-2$_{NIHZ}$, respectively. These concentrations of total gp120 were, in the worst case, more than sevenfold smaller than $1/K_{assoc}$. Hence, the association of soluble gp120 with sCD4 or cell-surface CD4 was negligible in all viral stocks[23] used in this study. Infectious events were quantified by a modified version of the syncytium-forming assay[23,24]. The modifications minimized artefacts associated with high cell concentrations in conjunction with sCD4 in the assay. Before the assay, CEM-SS cells were grown at low concentrations ($<5 \times 10^5 \, ml^{-1}$) to assure logarithmic growth. On the day of an assay, cells were suspended in fresh medium at densities of 4.5×10^5 and $2 \times 10^6 \, ml^{-1}$ to serve as 'indicator' and 'target' cell stocks, respectively. Target cells (0.5 ml) were then transferred to culture tubes containing six different volumes of fresh medium and seven different sCD4 concentrations (total of 42 tubes). The final target-cell densities in the culture tubes were 1×10^6, 5×10^5, 2.5×10^5, 1.25×10^5, 6.25×10^4 and $3.13 \times 10^4 \, ml^{-1}$. The respective reaction volumes were 1, 2, 4, 8, 16 and 32 ml. Identical multiplicities of infection (in graded volumes of viral stock) were added to each tube, resulting in a constant viral inoculum to reaction volume of 10%. To assure uniform mixing, culture tubes were rolled (~10 turns per min) during the 2-hour infection period. Next, the infected target cells were washed three times (centrifugation for 5 min, 200g, followed by suspension in 40 ml fresh medium and another centrifugation) and suspended in fresh medium at 5×10^4 cells ml^{-1}. This thorough washing of sCD4 from the target cells prevented subsequent inhibition of syncytium formation in the monolayer of target and indicator cells (two washes removed all sCD4, data not shown). Cell monolayers were prepared by adding 4.5×10^4 indicator cells (0.1 ml) and 5×10^3 target cells (0.1 ml) to flat-bottomed microtitre wells (indicator target cell ratio of 9:1). A total of eight wells were plated per sCD4 and target-cell concentration. Syncytia (representing the infection of individual target cells by cell-free virus) were counted on days three (HIV-2) or five (HIV-1) after infection. The above description applies to HIV-1$_{HXB3}$ assays (an indicator to target-cell ratio of 90:1 gave identical results to the 9:1 ratio used here, data not shown). For HIV-1$_{MN}$ assays, target-cell stocks were prepared at 1×10^6 cells ml^{-1} and target-cell densities in the culture tubes were twofold smaller. For HIV-2$_{NIHZ}$ assays, indicator-cell stocks were prepared at 6.5×10^5 cells ml^{-1}; infected target-cells were washed and suspended at 1×10^5 cells ml^{-1} (indicator target-cell ratio of 6.5:1). For assays with reaction volumes of 1, 2, 4, 8, 16 and 32 ml the comparative number of SFU were calculated by multiplying actual number of SFU in each well by 32, 16, 8, 4, 2 and 1 respectively. Minimizing $f(a,b) = \Sigma \{[y - (ax + b)]/\sigma\}^2$ gives a weighted least-squares linear fit to the data (y is the mean value of SFU at the ith sCD4 concentration, σ is the s.d. of SFU and x is the blocker concentration at the ith data point). Terms in the correlation coefficient[39] were weighted by $1/\sigma^2$. A weighted correlation coefficient = 1 means that the least-squares line fits the data perfectly

SFU ($\times 10^3$)

Target cells (100,000 ml^{-1})
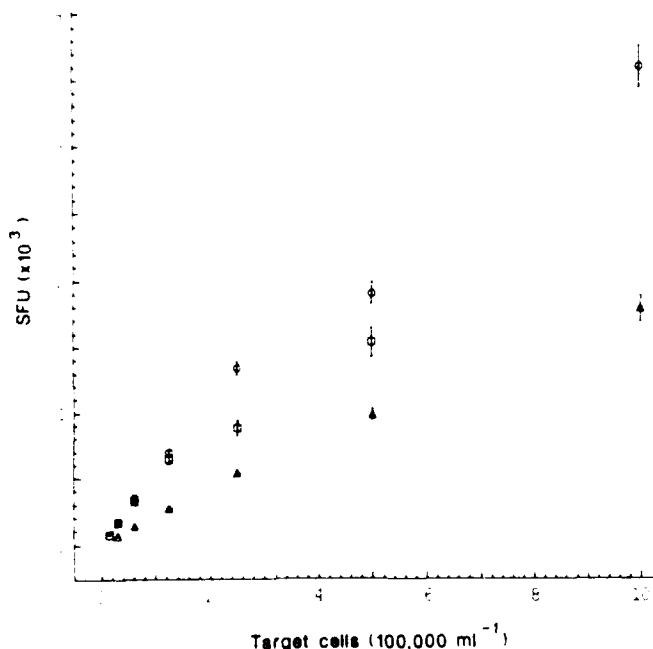
molecules as they bind to and block gp120. Downward curvature indicates corresponding negative synergy.

Figure 2 shows the inverse infection plot for HIV-2$_{NIHZ}$ at 1×10^6 target cells per ml. The plot curves progressively upward at higher sCD4 concentrations, indicating positive synergy in sCD4 blocking. Nevertheless, the data are linear at lower blocker concentrations and allow the determination of K_{assoc}. For example, the straight line in Fig. 2 gives a K_{assoc} of about 8.56×10^7 M^{-1} and the five other target cell concentrations gave comparable K_{assoc} (Table 1). K_{assoc} was also independent of the target cell concentration for the two strains of HIV-1 studied.

A chemical association constant for gp120-sCD4 binding cannot be presumed to measure a biological K_{assoc}, but it can be compared with the biological K_{assoc} as shown in Table 1. Despite a 20-fold difference in K_{assoc} between the viral types, the chemical measurements agree quite closely with our own. This difference agrees with reports of reduced blocking activity by sCD4 for HIV-2 in comparison with HIV-1[12,25,41]. Thus, the initial slope of the inverse infection plot[21,22] demonstrates that the biological activity of sCD4 (at low concentrations) is primarily due to reversible blocking of viral gp120 cell-surface CD4 interactions.

To analyse the synergistic blocking activity at higher concentrations, we normalized the inverse infection plot as follows. The inverse infection is divided by its control—inverse infection without blocker. The concentration of sCD4 is multiplied by
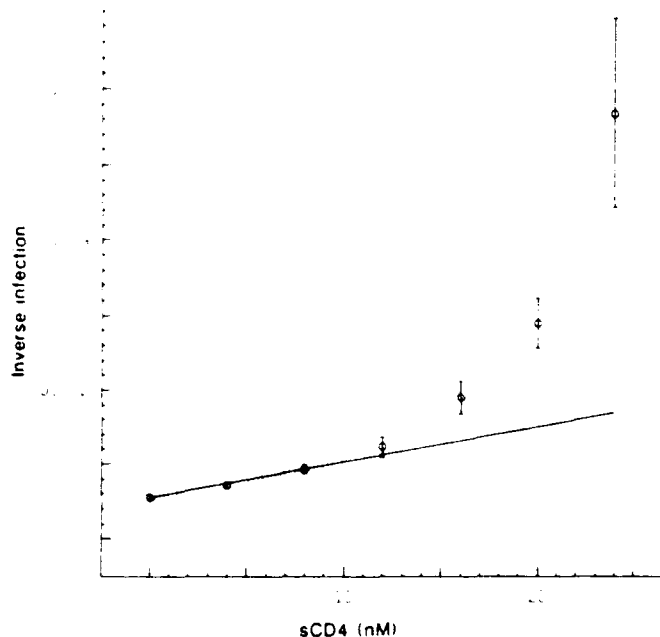

FIG 2 Calculating the gp120-sCD4 K_{assoc} from infectivity assays. When infectivity assays scale linearly with target cell concentration, a plot of inverse infection (1/SFU) versus sCD4 concentration should yield a straight line with slope/intercept ≈ K_{assoc} (refs 21, 22). An example of this inverse infection plot is illustrated for HIV-2$_{NIHZ}$ when target cell concentration is 1×10^6 cells ml^{-1}. The solid line is a weighted least-squares fit to the data (bars show mean ± 1 s d.) at sCD4 concentrations of 0, 4, 8 and 12 nM. The fit has weighted correlation coefficient of ~0.99, slope of ~4.75 × 10^4 M^{-1} and intercept of ~5.56 × 10^4, giving K_{assoc} ≈ 8.56 × 10^7 M^{-1} (y, is the mean value of 1/SFU, see Fig. 1 methods). The dotted lines are the 95% confidence limits for the fit. Both limits were calculated by a standard bootstrap method[40] and, in this example, give 7.47 × 10^7 ≤ K_{assoc} ≤ 8.86 × 10^7 M^{-1}. For the three viral strains, we calculated K_{assoc} from the lower four sCD4 concentrations in Table 1. The weighted correlation coefficients for all the fits are ≥0.85 for HIV-1$_{HXB3}$, ≥0.98 for HIV-1$_{MN}$ and ≥0.99 for HIV-2$_{NIHZ}$, indicating nearly complete explanations of the data at the lower sCD4 concentrations.

TABLE 1   Summary of the gp120-sCD4 K_{assoc}

Viral strain	Target cells (ml^{-1})	K_{assoc} ± 1 s.d. (M^{-1})	Mean K_{assoc} ± 1 s.d. (M^{-1})
HIV-1$_{HXB3}$	3.13×10^4	$(1.38 \pm 0.17) \times 10^8$	
	6.25×10^4	$(1.34 \pm 0.15) \times 10^8$	
	1.25×10^5	$(1.34 \pm 0.17) \times 10^8$	
	2.50×10^5	$(1.30 \pm 0.18) \times 10^8$	
	5.00×10^5	$(1.16 \pm 0.15) \times 10^8$	
	1.00×10^6	$(1.90 \pm 0.39) \times 10^8$	
			$(1.4 \pm 0.20) \times 10^9$
HIV-1$_{MN}$	1.56×10^4	$(1.46 \pm 0.10) \times 10^9$	
	3.13×10^4	$(1.82 \pm 0.14) \times 10^9$	
	6.25×10^4	$(1.84 \pm 0.14) \times 10^9$	
	1.25×10^5	$(1.65 \pm 0.09) \times 10^9$	
	2.50×10^5	$(1.89 \pm 0.14) \times 10^9$	
	5.00×10^5	$(1.45 \pm 0.15) \times 10^9$	
			$(1.7 \pm 0.13) \times 10^9$
HIV-2$_{NIHZ}$	3.13×10^4	$(9.46 \pm 0.64) \times 10^7$	
	6.25×10^4	$(9.16 \pm 0.42) \times 10^7$	
	1.25×10^5	$(8.89 \pm 0.76) \times 10^7$	
	2.50×10^5	$(7.67 \pm 0.38) \times 10^7$	
	5.00×10^5	$(7.48 \pm 0.42) \times 10^7$	
	1.00×10^6	$(8.56 \pm 0.64) \times 10^7$	
			$(8.5 \pm 0.54) \times 10^7$

For each viral strain and target cell concentration, target cells were infected at seven sCD4 concentrations. For HIV-1$_{HXB3}$, sCD4 concentrations were 0, 4.0×10^{-10}, 8.0×10^{-10}, 1.2×10^{-9}, 1.6×10^{-9}, 2.0×10^{-9}, 2.4×10^{-9} M. For HIV-1$_{MN}$, sCD4 concentrations were 0, 2.0×10^{-10}, 4.0×10^{-10}, 6.0×10^{-10}, 8.0×10^{-10}, 1.0×10^{-9}, 1.2×10^{-9} M. For HIV-2$_{NIHZ}$, sCD4 concentrations were 0, 4.0×10^{-9}, 8.0×10^{-9}, 1.2×10^{-8}, 1.6×10^{-8}, 2.0×10^{-8}, 2.4×10^{-8} M. Using the same soluble CD4 (CD4T) as our study and Scatchard analysis, methods based on the chemical K_{assoc} for HIV-1$_{IIIB}$ was reported as $(1.19 \pm 0.14) \times 10^9$ M^{-1} (ref. 7). Using enzyme-linked immunosorbent assay (ELISA), the chemical K_{assoc} for HIV-1$_{IIIB}$ and HIV-2$_{ROD}$ was $(8.0 \pm 4.8) \times 10^8$ and $(2.2 \pm 1.1) \times 10^7$ M^{-1}, respectively[41]. HIV-1$_{IIIB}$ and HIV-1$_{HXB3}$ differ by 0.5% in their gp120 nucleotide sequence; HIV-2$_{ROD}$ and HIV-2$_{NIHZ}$ differ by 12% (ref. 26). On the basis of nucleotide similarity, the HIV-1 strains permit the most direct comparison between biological and chemical K_{assoc}.

K_{assoc}, giving a numerical value of one to the sCD4 concentration at which half the gp120 molecules are blocked (see Fig. 3). Surprisingly, after normalization, the shape of the inverse infection plot is independent of the target cell concentration, the value of K_{assoc}, and the viral type.

When sCD4 blocks less than half of the gp120 molecules on virus optimized for infectivity[23] ($\beta < 1$, so $1/(1 + \beta) > 1/2$, where $\beta = [sCD4] \times K_{assoc}$), the normalized infection plot (Fig. 3) is linear, indicating each gp120 molecule independently and equivalently contributes to infection[21,22]. But when more than half the gp120 molecules are blocked ($\beta > 1$), the assumption of equivalent and independent gp120 monomers cannot explain all the blocking of infection in vitro.

Some explanations can be excluded immediately. Because the cloned viral stock (HIV-1$_{HXB3}$) gave the same results as the two uncloned viral stocks (HIV-1$_{MN}$ and -2$_{NIHZ}$)[26], the cooperativity is probably not caused by heterogeneous gp120s with differing K_{assoc}. Assay artefacts causing spurious cooperativity, such as interference by soluble gp120, have been ruled out (see legend to Fig. 1). Soluble CD4 might have enhanced the shedding or direct inactivation of viral gp120, but a simple extension of our model[21,22] shows the slope of the inverse infection plot would simply overestimate K_{assoc} and would not produce the upward curvature shown in Fig. 3.

One possibility is that a single gp120-CD4 interaction initiates viral binding, whereas viral adsorption and penetration require subsequent recruitment of additional gp120-CD4 interactions. Recruitment accounts for cooperativity and is consistent with experiments using sCD4 and immunoglobulins to inhibit infection after initial binding[12,17,27]. The recruitment hypothesis predicts that aged viral stocks (with virions that have shed most of
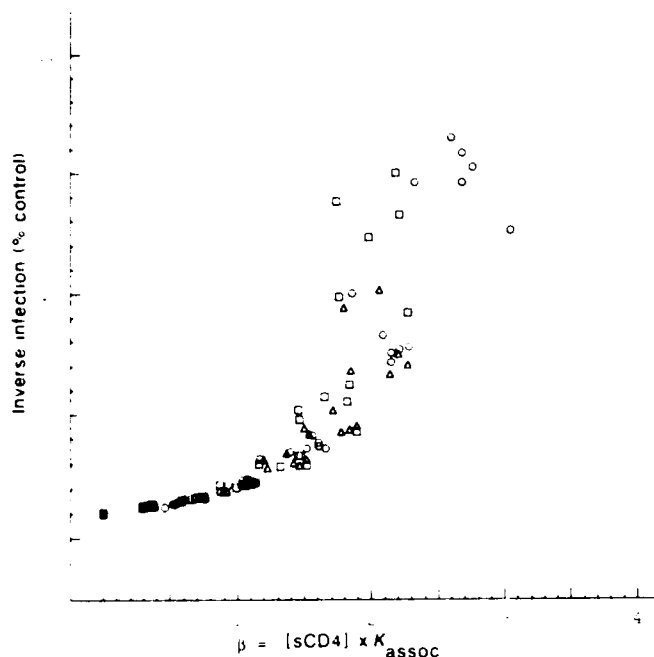
LETTERS TO NATURE

$$\beta = [sCD4] \times K_{assoc}$$

FIG 3 Analysing the cooperative blocking activity of sCD4. Dividing inverse infection (Fig 2) by its control (inverse infection without blocker) and multiplying sCD4 concentrations by the apparent K_{assoc} yields a normalized plot of inverse infection. Each normalization used the K_{assoc} calculated from the same target cell concentration (Table 1). The fraction of gp120 molecules that are either free or blocked by a particular concentration of sCD4 is given by $1/(1 + \beta)$ and $\beta/(1 + \beta)$ respectively, where $\beta = [sCD4] \times K_{assoc}$. Results at all six target cell concentrations for HIV-1$_{HXB3}$ (○), HIV-1$_{MN}$ (□) and HIV-2$_{NEHZ}$ (△). The dotted line represents blocking based on independent and equivalent gp120s (refs 21, 22). When less than half the gp120 molecules are blocked, the points lie on the dotted line. When half the gp120 molecules are blocked, deviations indicating sCD4 blocking synergy begin to occur. The synergies are identical for each viral strain.

their gp120) will be more easily blocked, thus enhancing the cooperativity in Fig. 3. Another explanation is that there are allosteric interactions between gp120s on the viral coat. This, in contrast to the recruitment model, predicts that the cooperativity of aged viral stocks will be unchanged or even decreased.

The upward curvature of the inverse infection plot is apparent only after half of the gp120 binding sites are blocked. Thus, the HIV envelope is covered by a highly redundant number of gp120 molecules which act independently at low sCD4 concentrations. Unlike HIV, viruses such as polio and influenza are covered by interacting (metastable) capsid polypeptide subunits and interacting glycoprotein subunits, respectively, which present relatively few critical neutralization sites. When a fraction of these sites are blocked by neutralizing antibodies, a non-local transition in subunit orientation is induced that inactivates the virus[28-30]. This property may contribute to the humoral efficacy of vaccines against polio and influenza. Neutralizing HIV, however, seems to be fundamentally different.   □

1 Dalgleish A G et al Nature 312, 763-767 (1984)
2 Klatzmann D et al Nature 312, 767-768 (1984)
3 McDougal J S et al Science 231, 382-385 (1986)
4 Kowalski M et al Science 237, 1351-1355 (1987)
5 Bedinger P et al Nature 334, 162-165 (1988)
6 Lasky L A et al Cell 50, 975-985 (1987)
7 Smith D H et al Science 238, 1704-1707 (1987)
8 Fisher R A et al Nature 331, 76-78 (1988)
9 Hussey R E et al Nature 331, 78-81 (1988)
10 Deen K C et al Nature 331, 82-84 (1988)
11 Traunecker A. Luke W & Karjalainen K Nature 331, 84-86 (1988)
12 Clapham P R et al Nature 337, 368-370 (1989)

13 Capon. D J et al Nature 337, 525-531 (1989)
14 Traunecker. A. Schneider, J. Kiefer, H & Karjalanen. K Nature 339, 68-70 (1989)
15 Nara. P L., Hwang. K M., Rausch, D M., Lifson, J D & Eiden, L E Proc natn Acad Sci USA 86, 7139-7143 (1989)
16 Sun, N.-C et al J Virology 63, 3579-3585 (1989)
17 Byrn, R. A et al J Virology 63, 4370-4375 (1989)
18 Watanabe, M et al Nature 337, 267-270 (1989)
19 Schooley, R T et al Ann. intern Med 112, 247-253 (1990)
20 Kahn, J. O. et al Ann. intern. Med 112, 254-261 (1990)
21 Layne, S P., Spouge, J L & Dembo, M Proc natn Acad Sci USA 86, 4644-4648 (1989)
22 Spouge, J L., Layne, S P & Dembo, M Bull math Biol 51, 715-730 (1989)
23 Nara, P L et al AIDS Res hum Retroviruses 3, 283-302 (1987)
24 Nara, P L & Fischinger, P J Nature 332, 469-470 (1988)
25 Sweet, R et al Fifth Int Conf AIDS Abstr W C O 12 (1989)
26 Myers, G et al Human Retroviruses and AIDS Section III, 9-12 (Los Alamos National Laboratory, New Mexico, 1990)
27 Nara, P L in Vaccines 89 (eds Lerner, R A., Ginsberg, H., Chanock, R M & Brown F) 137-144 (Cold Spring Harbor Laboratory, New York, 1989)
28 Icenogle, J et al Virology 127, 412-425 (1983)
29 Emini, E A., Ostapchuk, P & Wimmer, E J Virology 48, 547-550 (1983)
30 Taylor, H P., Armstrong, S J & Dimmock, N J Virology 159, 288-298 (1987)
31 Goudsmit, J et al Proc UCLA Symposia (in the press)
32 Looney, D J et al Science 241, 357-359 (1988)
33 Saag, M S et al Nature 334, 440-444 (1989)
34 Cordonnier, A. Montagnier, L & Emerman, M Nature 340, 571-574 (1989)
35 Zwart, G et al Lancet I, 474 (1990)
36 Özel, M., Pauli, G & Gelderblom, H R Arch Virology 100, 255-266 (1988)
37 Earl, P L., Doms, R W & Moss, B Proc natn Acad Sci USA 87, 648-652 (1990)
38 Pyle, S W et al AIDS Res Hum Retroviruses 3, 387-400 (1987)
39 Kendall, M & Stuart, A The Advanced Theory of Statistics Vol 2 (Griffin, London, 1979)
40 Efron, B & Tibshirani, R Stat Sci 1, 54-77 (1986)
41 Moore, J P AIDS 4, 297-305 (1990)

Blocking of Human Immunodeficiency Virus Infection Depends on Cell Density and Viral Stock Age

SCOTT P. LAYNE,[1*] MICHAEL J. MERGES,[2] JOHN L. SPOUGE,[3] MICAH DEMBO,[1] AND PETER L. NARA[2]

*Theoretical Biology and Biophysics Group, Theoretical Division, Los Alamos National Laboratory, Los Alamos,
New Mexico 87545[1]; Virus Biology Section, Laboratory of Tumor Cell Biology, National Cancer Institute-
Frederick Cancer Research and Development Center, Frederick, Maryland 21701[2]; and National Center
for Biotechnology Information, National Library of Medicine, Bethesda, Maryland 20894[3]*

Quantitative infectivity assays were used to study how the blocking activity of soluble CD4 (sCD4) is affected by sCD4 concentration, target cell density, and viral stock age. During incubation with 20 nM sCD4, human immunodeficiency virus type 1 (HIV-1) stocks underwent irreversible inactivation. In contrast, inactivation with 2 nM sCD4 was almost entirely reversible. At lower sCD4 concentrations ($\leq$2 nM) and target cell densities of 6.25×10^4 ml^{-1}, sCD4 blocking activity for HIV-1 gave a gp120-sCD4 association constant (K_{assoc}) of 1.7×10^9 M^{-1}, which agrees with chemical measurements. At the higher density of 1.6×10^7 cells ml^{-1}, however, the blocking activity was 20-fold less. During incubation of HIV-1 stock optimized for infectivity by rapid harvest, sCD4 blocking activity increased 20-fold during a 3-h window. These results show that competitive blocking activity depends strongly on target cell density and virion age. Thus, unappreciated variations in HIV stocks and assay conditions may hinder comparisons of blockers from laboratory to laboratory, and the age of HIV challenge stocks may influence studies of drug and vaccine efficacy. The results also suggest that blocking of viral particles in lymphoid compartments will require very high competitive blocker concentrations, which may explain the refractory outcomes from sCD4-based drug trials in humans.

Human immunodeficiency virus types 1 and 2 (HIV-1 and HIV-2) share two properties that are important for understanding immunity and therapy. First, HIV preferentially infects CD4$^+$ target cells (9, 29, 37, 41), which have a wide range of densities in lymphoid, reticuloendothelial, and nervous tissues. For example, typical CD4$^+$ cell densities in blood and lymph node are 10^6 to 10^7 and 10^7 to 10^{10} ml^{-1}, respectively. Second, the density of glycoprotein knobs covering the surface of HIV particles decreases with time. This spontaneous shedding occurs because the gp120 surface and gp41 transmembrane glycoproteins are associated by noncovalent interactions (30, 39). After observing this gp120 loss by electron microscopy, Gelderblom et al. (13, 14) suggested that knob density might influence the biological properties (e.g., infection and blocking) of HIV.

To address this hypothesis, we previously used a quantitative infectivity assay to determine how the binding of soluble CD4 (sCD4) (3, 6, 10, 12, 22, 58, 61, 64) to gp120 inhibited viral infectivity (32, 34). At low sCD4 concentrations, the inhibition of HIV-1 and -2 infection was proportional to binding. At slightly higher concentrations, there was a positive synergy in the inhibition of infection. One possible explanation for this concentration-dependent blocking activity was that HIV required a critical density of free gp120 glycoproteins for efficient infection of CD4$^+$ cells. When more than this critical density was present on HIV, infection proceeded at a rate proportional to free gp120 glycoproteins. In agreement with these findings, McKeating et al. (42) demonstrated a connection between the spontaneous shedding of gp120 and the loss of HIV-1 infectivity. Moore et al. (45, 46) have also shown that preincubation of HIV-1 stocks with high sCD4 concentrations (>5 nM) facilitated rapid shedding of gp120 that was accompanied by loss

of infectivity. This facilitation was not observed at low sCD4 concentrations (<5 nM). These studies clearly demonstrated a relationship between gp120 and HIV infectivity. They did not, however, reveal the effects of target cell density on infection and blocking.

We therefore undertook an investigation of how sCD4 blocking activity depends on target cell density, viral stock age, and sCD4 concentration. sCD4 was selected as a model blocking agent for three reasons. First, chemical measurements of the gp120-sCD4 association constant (K_{assoc}) have been published by several groups (44, 58). As previously described (32, 34, 59), such measurements allow correlations between biological activity and the thermodynamic properties of the binding reaction. Second, crystallographic (55, 63) and biological studies indicate that CD4 has one high-affinity binding region for gp120 involving the CDR2 (7, 31, 43) and CDR3 (18, 35, 49) domains. This interaction represents a great simplification over the complexities inherent in multivalent blockers, such as immunoglobulins. Third, two large sCD4-based drug trials in humans are now under way, and to date only refractory outcomes have been reported (8, 25, 56). By examining sCD4 blocking activity with assay conditions mimicking physiologic ones (e.g., a range of target cell densities), we expected to gain some insight into the clinical outcomes.

Understanding how assay conditions influence sCD4 blocking activity has applications to investigations of other gp120 blocking agents and neutralization domains. Examples of such blockers include CD4 fragments (35, 49), CD4-immunoglobulin conjugates (2, 4, 62), monoclonal immunoglobulins (20, 27, 38, 57, 60), and some vaccine-induced immunoglobulins (1). The other blocking domains on gp120 include the third variable region (V3 loop) (15, 23, 24, 52-54), conformational epitopes (16, 17, 20, 50), and conserved sequences (5, 19, 21).

* Corresponding author

MATERIALS AND METHODS

Quantitative infectivity assays. Infectious events were quantified by a modified version of the syncytium-forming viral infectivity assay (32, 47, 48) that minimized artifacts associated with high cell density. Before the assay, CEM-SS cells were grown at densities ($<5 \times 10^5$ ml^{-1}) to ensure their exponential growth. On the day of an assay, cells were suspended in fresh medium to serve as target and indicator cells. Target cells (5×10^5) were transferred to tubes containing four different volumes of fresh media and seven different sCD4 concentrations: 0, 0.4, 0.8, 1.2, 1.6, 2.0, and 2.4 nM. The final target cell densities in the tubes were 1.6×10^5, 4×10^5, 1×10^5, and 6.25×10^4 ml^{-1}. The reaction volumes were 3.13×10^{-2}, 1.25×10^{-1}, 5×10^{-1}, and 8 ml, respectively. Graded volumes of HIV-1HXB3 stock were then added to each tube, resulting in a constant inoculum-to-volume ratio of 10%. To ensure uniform mixing, tubes were rolled during the 1-h infection period at 37°C. Next, the infected target cells were washed once (sufficient to remove sCD4 and cell-free virus) and suspended in fresh media at 5×10^4 cells per ml. Cell monolayers were prepared by adding 5×10^3 target cells and 3.5×10^4 indicator cells to flat-bottom microtiter wells. A total of eight wells were plated per sCD4 and target cell concentration. Syncytia, representing the infection of individual target cells by cell-free virus (47, 48), were counted on day 4 following plating. For the assays in Fig. 2, conditions were modified so the target cell density was 2×10^6 ml^{-1}, the reaction volume was 1 ml, and inoculum-to-volume ratio was 20% in all tubes. Thus, for the experimental stock, 1.4 and 0.28 nM sCD4 were present during incubation and assay, respectively. Cell monolayers were prepared by adding 1×10^4 target cells and 4.5×10^4 indicator cells to flat-bottom microtiter wells. For the assays in Fig. 3, conditions were modified so the target cell density was 5×10^5 ml^{-1}, the reaction volume was 1 ml, and inoculum-to-volume ratio was 20% in all tubes. The six sCD4 concentrations were 0, 0.4, 0.8, 1.2, 1.6, and 2.0 nM. Cell monolayers were prepared by adding 2.5×10^3 target cells and 3.5×10^4 indicator cells to flat-bottom microtiter wells.

Viral stocks. After H9 cells were inoculated at a multiplicity of infection equaling 0.1, the titer of infectious HIV-1HXB3 virions increased exponentially for 2 to 3 days (33). Hence, this multiplicity of infection was chosen for the preparation of optimized viral stocks. Before infection, H9 cells were grown at densities ($<5 \times 10^5$ ml^{-1}) to ensure their exponential growth. H9 cells were treated with DEAE-dextran (25 μg ml^{-1} for 30 min followed by centrifugation for 10 min at 200 × g) and incubated with virus for 1 h. The infected H9 cells were washed twice (centrifugation for 10 min at 200 × g, suspension in phosphate-buffered saline, and another centrifugation), suspended in fresh medium (5×10^5 cells ml^{-1}), and incubated with mixing at 37°C. Two days later, the infected H9 culture was clarified by centrifugation (20 min, 10,000 × g) and placed in an incubator. Infectivity assays were conducted either immediately following clarification or after specified intervals of incubation with mixing at 37°C.

Soluble gp120 in viral stocks. Typically, after ultracentrifugation of day 2 HIV-1HXB3 stocks (40 min, 155,000 × g), the concentration of soluble gp120 in the supernatant was ≤5 × 10^{-10} M by gp120 enzyme-linked immunosorbent assay (ELISA) (American Bio-Technologies). Thus, for inoculum-to-volume ratios of ≤20%, the average concentrations of soluble gp120 were at least sixfold smaller than $1/K_{acrobat}$. For all infectivity assays, this ensured that soluble gp120 did not

compete significantly (32) with virus-associated gp120 for sCD4 or cell surface CD4 during quantitative infectivity assays.

Removing sCD4 from preincubated viral stocks. To assess sCD4 blocking activity, 8-ml aliquots of HIV-1HXB3 stock were preincubated with 0, 2, and 20 nM sCD4 for 80 min at 37°C. sCD4 was then reduced 1,000-fold by ultracentrifuging the preincubated stock (40 min, 155,000 × g), removing the supernatant, and suspending the pellet in 8 ml of fresh medium. The numbers of syncytium-forming units (SFU) remaining after these manipulations are shown in Table 1.

Quantifying blocking activity. To assess the inhibitory effects of sCD4 on HIV infectivity, plots of normalized inverse infection, 1/SFU with blocker multiplied by SFU without blocker, versus sCD4 concentration were constructed (32, 34). For unsaturated and saturated infectivity assays, the slope of such plots, [normalized inverse infection − 1]/[sCD4], is the molar blocking activity. This definition applies to each concentration of blocker and does not require that inverse infection plots be linear.

Statistical analysis. Minimizing $f(a, b) = \Sigma\{[y_i - (ax_i - b)]/\sigma_i\}^2$ gives a weighted least-squares linear fit to the data (26). y_i is the mean value of 1/SFU at the ith sCD4 concentration, σ_i is the standard deviation of 1/SFU, and x_i is the sCD4 concentration at the ith data point. For normalized inverse infection plots, the weighted least-squares fit gives slope = a/b. In Fig. 1b and 3a, weighted least-squares linear fits were calculated from all data. In Fig. 3b, because of upward curvature, fits were calculated from data at the lower four sCD4 concentrations. In Fig. 1a, the unweighted least-squares fit was obtained by setting $\sigma_i = 1$ at the lower three target cell densities. Confidence limits for the blocking activities in Table 2 were calculated by a standard bootstrap method (11).

RESULTS

Reversibility of the blocking activity of sCD4. Agents that block HIV by binding to gp120 are either reversible after removal (competitive) or irreversible (noncompetitive). To evaluate sCD4 with respect to these categories, we preincubated HIV stocks with increasing concentrations of blocker (Table 1). After removal of sCD4 from these stocks, the number of infectious units was assessed with a quantitative infectivity assay. Compared with the control, 2 and 20 nM sCD4 inactivated HIV in 2 h by 1.1- and 63-fold, respectively. Thus, at high concentrations, sCD4 caused irreversible viral inactivation, as already reported by Kirsh et al. (28) and Moore et al. (45, 46). At low concentrations, however, sCD4 blocked HIV competitively.

Effects of assay saturation on competitive blocking activity. It has been well established that HIV particles lose their infectivity with time (36, 40, 42). Assaying the infectivity of virions therefore reflects the race between spontaneous viral

TABLE 1. Classifying the blocking activity of sCD4[a]

sCD4 concn (nM)	SFU/ml (mean ± SEM)[b]	Irreversible inactivation of HIV (fold)
0	$(1.26 \pm 0.01) \times 10^4$	None
2	$(1.15 \pm 0.02) \times 10^4$	1.1
20	$(2.0 \pm 0.2) \times 10^2$	63

[a] Day 2 viral stock was used.
[b] Results are averages of data for 16 microtiter wells for each sCD4 concentration.

TABLE 2. Summary of sCD4 blocking activity

Target cell density (ml⁻¹)	Viral stock	Incubation (h)	Blocking activity[a] ± 1 SD (M⁻¹)	Blocking activity ratio
Fig. 1b				
6.25×10^4	Day 2	0	$(1.7 \pm 0.1) \times 10^9$	1.0
1.00×10^6			$(3.5 \pm 1.0) \times 10^8$	0.21
4.00×10^6			$(1.3 \pm 0.3) \times 10^8$	0.077
1.60×10^7			$(8.5 \pm 7.0) \times 10^7$	0.050
Fig. 3a				
5.00×10^5	Day 2	0.5	$(1.0 \pm 0.1) \times 10^8$	1.0
		6	$(3.3 \pm 0.1) \times 10^8$	3.3
		13	$(8.4 \pm 0.2) \times 10^8$	8.4
Fig. 3b				
5.00×10^5	Day 6	0.5	$(1.8 \pm 0.2) \times 10^8$	1.0
		6	$(5.4 \pm 0.5) \times 10^8$	2.3
		13	$(1.7 \pm 0.2) \times 10^9$	9.4

[a] Using strain HIV-1HXB3 and the same formulation of sCD4, previous measurements of the gp120-sCD4 K_{assoc} yielded $(1.4 \pm 0.2) \times 10^9$ M⁻¹ from unsaturated infectivity assays (32).

inactivation and target cell infection. Figure 1a plots SFU versus target cell density for quantitative assays of HIV-1HXB3. At low target cell densities, every virion has at most a single chance to infect before inactivation. In such unsaturated assays, blockers will perturb single infectious events. At higher target cell densities, virions may have several chances to infect before inactivation. In such saturated assays, blockers must inhibit several potential infectious events. Hence, we expected that competitive blockers would appear significantly less effective at high target cell densities (32, 59).

To test this hypothesis, we conducted quantitative infectivity assays at low sCD4 concentrations and for a range of target cell densities. In unsaturated assays and at low sCD4 concentrations, previous work (32) showed that sCD4 blocking activity (defined in Materials and Methods) gave the gp120-sCD4 K_{assoc}. In this study, when the target cell density was 6.25×10^4 ml⁻¹, sCD4 blocking activity of 1.7×10^9 M⁻¹ (Table 2) agreed with previous biological (32) and chemical (44, 58) measurements of K_{assoc}. As target cell densities increase, however, the blocking activity of sCD4 declined progressively with assay saturation (Fig. 1b). At a target cell density of 1.6×10^7 ml⁻¹, the blocking activity declined 20-fold (Table 2). Target cell density therefore directly influenced competitive blocking activity to HIV.

Effects of viral stock age on competitive blocking activity. Figure 2a shows the spontaneous inactivation curve for a single HIV-1HXB3 stock at 37°C that was rapidly grown and harvested at optimal infectivity. The lower curve shows inactivation in the presence of 1.4 nM sCD4, while the upper curve is the control. Both curves show a 2-h transient phase followed by a initial phase of slow inactivation lasting 6 h. This phase is then followed by a pronounced shoulder, suggesting multihit inactivation. This pattern occurred with either CEM-SS cells (47, 48) or freshly isolated human peripheral blood lymphocytes, and both target cell types measured similar losses of SFU or 50% inhibitory dose over time (33). During the initial phase, 1.4 nM sCD4 did not measurably increase the rate of inactivation compared with the control. During the final phase, however, a marked increase in the rate of inactivation occurred in the presence of sCD4. To determine whether other soluble factors like
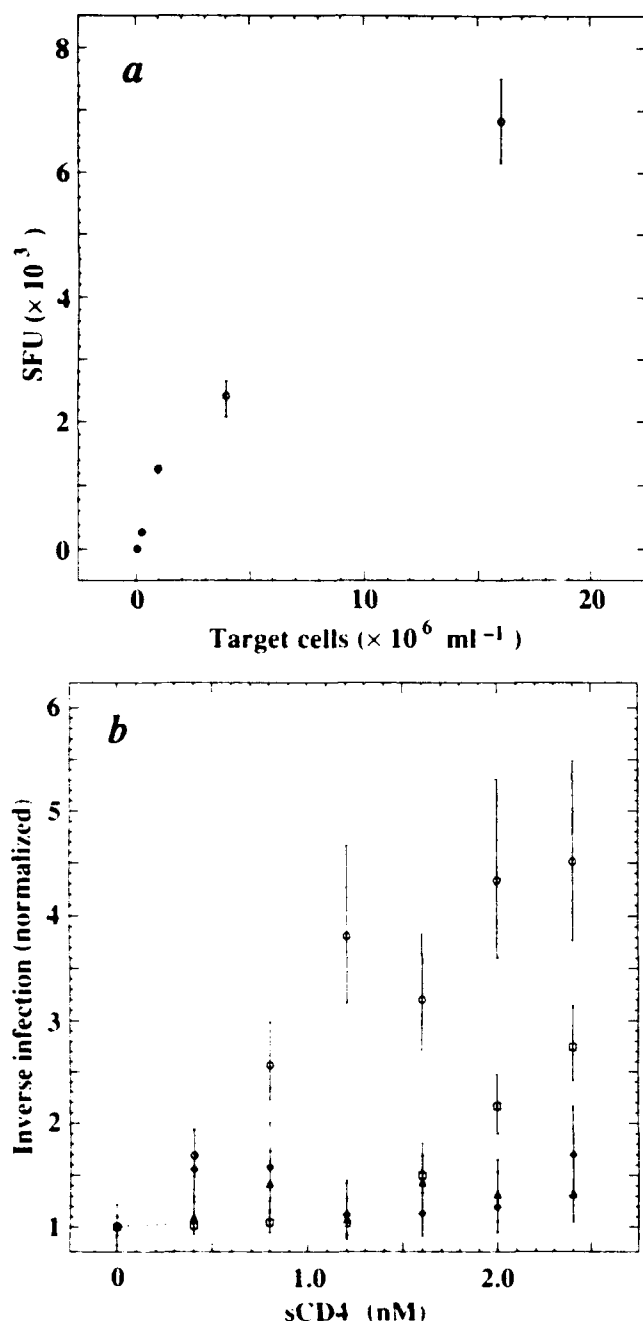
FIG. 1. Measurement of sCD4 blocking activity. (a) Detection of assay saturation in the absence of blocker. The figure plots SFU versus target cell (CEM-SS) density for assays without sCD4. For unsaturated assays, SFU are proportional to target cell density (32). As assays become saturated, SFU are less than proportional to target cell density (34, 59). The dotted line is an unweighted least-squares fit to data at the lower three target cell densities. (b) Measurement of infectious events in the presence of blocker. The figure plots normalized inverse infection. 1/SFU with blocker multiplied by SFU without blocker, versus sCD4 concentration. The slope, [(normalized inverse infection)−1]/[sCD4], is the molar blocking activity. The figure shows results at target cell densities of 6.25×10^4 (●), 1×10^6 (□), 4×10^6 (△), and 1.6×10^7 (○) ml⁻¹. Dotted lines are weighted least-squares fits to the data. Results are means of eight microtiter wells (bars show ± 1 standard deviation). As target cell densities increase, the assays become saturated and the blocking activity decreases.
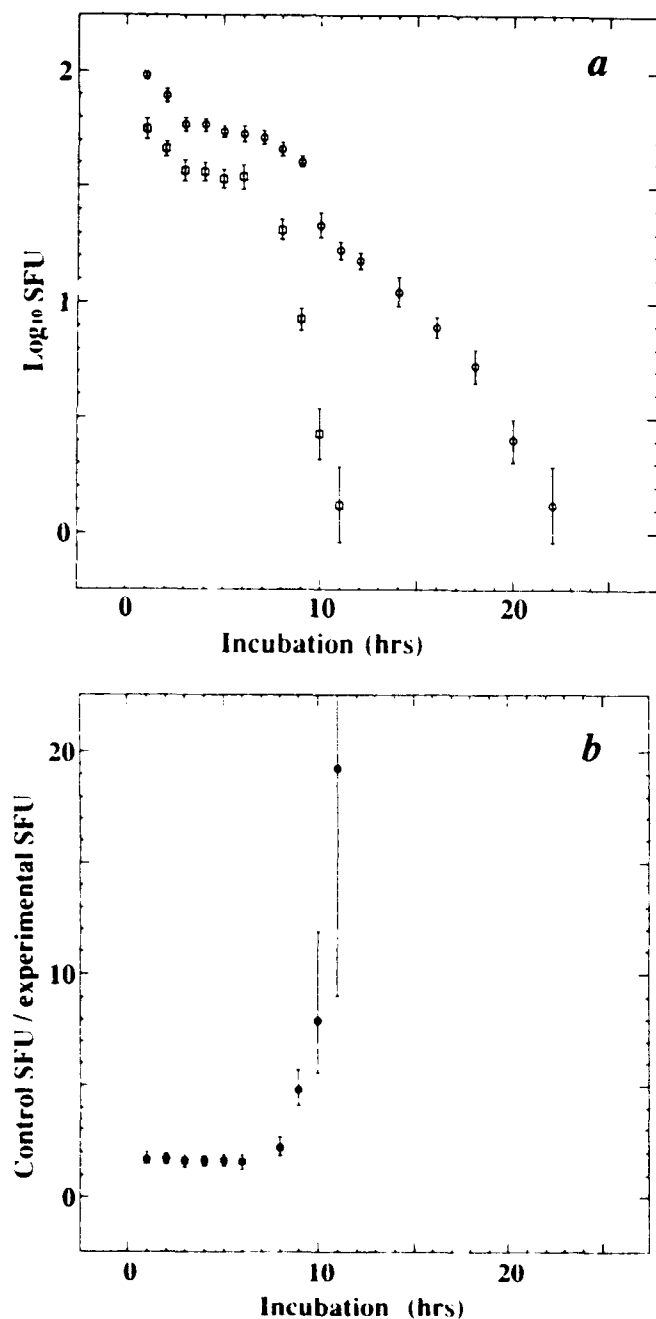
FIG. 2. Measurement of sCD4 blocking activity as viral stocks spontaneously inactivate. After 2 days of exponential viral replication, equal volumes of clarified HIV-1HXB3 stock were added to separate flasks. To the experimental stock, blocker in medium was added to obtain 1.4 nM sCD4; to the control stock, an equal volume of medium without blocker was added. Afterwards, both flasks were incubated at 37°C with gentle mixing. At hourly intervals, the number of SFU in the experimental ( ) and control ( ) stocks were measured by using an unsaturated infectivity assay. (a) Results are the geometric means of eight microtiter wells (bars show ± 1 standard deviation). (b) Ratio of control SFU divided by experimental SFU (bars show ± 1 standard deviation). The dotted line is the expected ratio of control to experimental stocks, based on assay conditions and a gp120-sCD4 K_{assoc} of $1.7 \times 10^9 M^{-1}$. During the first 8 h, sCD4 blocking remained constant (1.5 ≤ ordinate ≤ 2.3). Thereafter, over 3 h, the blocking activity of sCD4 increased by more than 20-fold.

proteases and surface-active agents contributed to degradation, the viral stock was diluted fivefold with fresh medium and incubated at 37°C. Dilution did not affect inactivation (33), ruling out significant contributions by soluble factors.

Figure 2b shows the ratio of SFU in the control and experimental stocks. During the first 6 h, the sCD4 blocking activity was constant and equaled $K_{assoc} \approx 1.7 \times 10^9 M^{-1}$. This blocking activity agrees with unsaturated assays in Fig. 1b, verifying that the Fig. 2 assays were also unsaturated. With longer incubation, however, sCD4 blocking activity increased by more than 20-fold during a 3-h window. This rapid increase in sCD4 blocking activity at low concentrations was consistently observed with three other optimized HIV-1HXB3 stocks (33). Figure 2b demonstrates that sCD4 blocks aged viral stocks more readily than fresh viral stocks. Since HIV spontaneously sheds its envelope (42), the increase in sCD4 blocking activity with incubation suggests that some minimal number of unblocked gp120s is required for infection to occur (32). The multihit kinetics in Fig. 2a also supports this idea.

Combined effects of assay saturation and viral stock age. We further examined the combined effects of assay saturation and spontaneous viral inactivation on sCD4 blocking activity. Figures 3a and b show assay results for HIV-1HXB3 stocks established identically but then allowed to replicate virus for 2 and 6 days, respectively. After incubation (without sCD4) for 30 min at 37°C, the blocking activities (Table 2) for both assays underestimate K_{assoc}, indicating assay saturation. After 6 h, both blocking activities increased two- to threefold but their values still indicated saturation. After 13 h, the day 6 blocking activity equaled K_{assoc}, whereas the day 2 blocking activity still reflected assay saturation. These results clearly show that spontaneous viral inactivation reduces assay saturation (34, 59) and increases blocking activity.

DISCUSSION

These studies indicate that increasing target cell density decreases blocking activity (Fig. 1b). In contrast, spontaneous viral inactivation increases blocking activity (Fig. 2b). Thus, the opposing influence of these variables can completely confound measurements of blocking activity that lack proper controls. These finding have important implications for understanding blocking activity in vivo and standardizing its measurement in vitro.

The data in Table 1 (from Fig. 1b) show that infectivity assays were unsaturated and partially saturated at target cell densities of 6.25×10^4 and $1.0 \times 10^6 ml^{-1}$, respectively. Thus, somewhere between these two target cell densities, a transition in sCD4 blocking activity took place. However, a previous study of sCD4 blocking activity with HIV-1HXB3 found that assays were unsaturated over this same range of target cell densities (32). That is, blocking activity agreed with chemical measurements of K_{assoc} and no transition took place. For both studies, the method of viral stock preparation and detection of infectious events were similar. Nevertheless, the blocking activities at 1.0×10^6 target cells ml^{-1} were clearly dissimilar. These significant differences from two similar but separate studies demonstrate the need for standardizing assay conditions.

To compare blocking activities between studies or from one agent to another, quantitative infectivity assays must be unsaturated (32, 34, 59). One practical approach for meeting this requirement is to produce and store a large volume of viral stock in small aliquots. With these aliquots, a series of
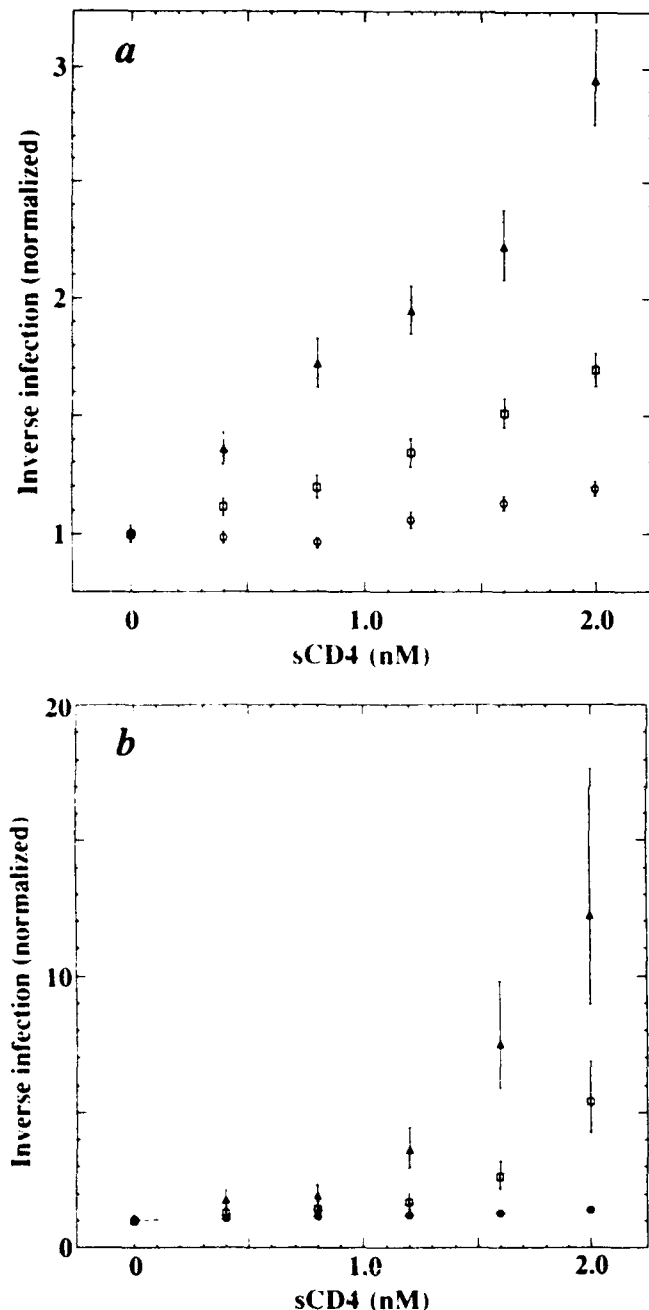
a

b

FIG. 3. Decrease in assay saturation as viral stocks spontaneously inactivate. Equivalent H9 cell cultures were inoculated with HIV-1HXB3 and harvested simultaneously after either 2 days of exponential or 6 days of chronic viral replication. The clarified stocks were then incubated at 37°C with gentle mixing. sCD4 blocking activity for day 2 (a) and day 6 (b) stocks was measured after incubation for 0.5 (○), 6 (□), and 13 (△) h, using the same assay conditions. Results are the means of eight microtiter wells (bars show ± 1 standard deviation). Dotted lines are weighted least-squares fits to the data. As HIV inactivates, sCD4 blocking increases. The blocking activity for the day 6 stock is consistently higher than for the day 2 stock (Table 2). After 13 h, the plot for the day 6 stock curves progressively upward at higher sCD4 concentrations, indicating positive synergy in blocking. This upward curvature corresponds to an increase in the molar blocking activity (defined in the legend to Fig. 1b). For the day 6 stock at 13 h, the synergy at 2.0 nM sCD4 equals 12.2/4.4 = 2.8-fold. The positive synergy suggests that the day 6 stock had fewer gp120 glycoproteins per particle (on average at harvest) than did the day 2 stock.

assays at increasing target cell densities can then be performed to establish the range at which infection is proportional to cell density (Fig. 1a). As shown by the data in Table 2, sCD4 blocking activity in this range is reproducible and permits reliable measurements of K_{assoc}, even for viral stocks displaying positive synergy (Fig. 3b). Since laboratory (rapid-high) strains of HIV are easier to store and assay than field (slow-low) isolates, this approach to standardization will be considerably easier to apply to laboratory isolates. At present, however, we are unaware of any alternative method for quantitative comparisons between HIV strains.

Initial in vitro measurements of sCD4 blocking activity (10, 12, 22, 58, 61) suggested that nanomolar concentrations might have therapeutic effects in vivo. Subsequent to this, two separate sCD4-based drug trials in humans (25, 56) found that nanomolar sCD4 levels in plasma had, unexpectedly, no therapeutic effects (8). To investigate the cause of this outcome, Daar et al. (8) conducted a series of sCD4 sensitivity assays on fresh HIV-1 isolates from infected patients. Their results indicated that fresh HIV-1 isolates were 100- to 1,000-fold less sensitive to sCD4 blocking than were laboratory isolates. Although the biochemical basis for differences between field and laboratory strains was not determined, the decreased sensitivity was consistent with reductions in the chemical gp120-sCD4 K_{assoc}. Since HIV-1 and HIV-2 gp120-sCD4 K_{assoc} differ by 20-fold (32, 44), Daar et al. (8) suggested that large differences in K_{assoc} within HIV-1 might also be possible. We do not disagree with this biochemical explanation of decreased sCD4 blocking activity for fresh HIV-1 isolates. However, Fig. 1b also demonstrates that assay saturation results in significant reductions in sCD4 blocking activity. Assay saturation thus provides an alternative explanation for their observations with fresh HIV-1 isolates in vitro.

Decreasing blocking activity with increasing target cell density unifies two observations regarding therapeutic blockers and humoral immunity. First, it provides a reasonable explanation for the failure of sCD4-based therapies in vivo. Figure 1b shows that sCD4 blocking activity declines rapidly at target cell densities typical of blood, 10^6 to 10^7 ml^{-1}. Hence, sCD4 is unlikely to affect the in vivo spread of HIV in lymphoid compartments that have CD4$^+$ cell densities of 10^7 to 10^9 ml^{-1}. This suggests that therapeutic blockers (8, 25, 56) in these microenvironments need to be essentially irreversible, with K_{assoc} at least 100-fold greater than 10^9 M^{-1}. Second, this decrease also provides a disconcerting explanation for the failure of immunoglobulins to clear initial HIV infection in vivo. Preliminary investigations of 0.5β, a monoclonal immunoglobulin binding to the V3 loop in gp120 (23, 24, 54, 57), demonstrated that inverse infection plots (see Fig. 1b) were linear in concentration and sensitive to HIV-1HXB3 stock age (see Fig. 3) (33). Thus, the blocking activity of 0.5β appears to mimic that of sCD4. If other gp120-binding immunoglobulins are similar to 0.5β, this finding suggests that they will also provide little or no protection to the spread of infection in lymphoid compartments. Persistence of infection is commonly observed for viruses that infect lymphocytes and monocytes (51). The inability of gp120-binding immunoglobulins to block infection at high target cell densities therefore provides new insights into the mechanisms of such persistence.

Figures 2 and 3 show that sCD4 blocking activity increases with preincubation of viral stocks. Since spontaneous shedding of gp120 has been shown to accompany the loss of HIV infectivity (42, 45, 46), the increasing blocking activity in

both figures is presumably due to fewer gp120 knobs per active virion. Beyond this, however, the underlying explanations for these increasing activities are fundamentally different. Figure 2 shows an increasing blocking activity for unsaturated assays, whereas Fig. 3 shows it for saturated ones. For unsaturated assays, increasing sCD4 blocking activity suggests that HIV requires a critical density (or minimal number) of gp120 molecules for efficient infection of CD4⁺ cells. This agrees with earlier observations of concentration-dependent sCD4 blocking activity, which showed enhancements after ~50% of gp120 molecules were bound (32). For saturated assays, increasing blocking activity suggests that the loss of gp120 is accompanied by a reduction in the number of chances that a virion has to infect before inactivation. This idea is consistent with the linear relationship (Fig. 1b) between sCD4 concentration and the blocking of infection in unsaturated assays.

Animal testing is a necessary step in developing an HIV vaccine. Like human transmission, experimental transmission probably takes place with HIV particles having different ages (time elapsed after budding). Consequently, immunoglobulins induced by a vaccine will have to block particles of all ages. The data in Fig. 3 suggest that newer HIV particles will be more difficult to block than older ones. Aged animal challenge stocks may thus give inappropriately high estimates of humoral efficacy in animals. In addition, the 20-fold increase in sCD4 blocking activity (from 8 to 11 h in Fig. 2b) that is accompanied by only a 2.7-fold decrease in SFU (control stock in Fig. 2a) demonstrates that increases in blocking activity are not represented by decreases in viral titer. Hence, losses in a challenge stock's titer may not accurately reflect increasing blocking activity by immunoglobulins. Consideration should therefore be given to optimizing animal challenge stocks and finding new yardsticks for evaluating such stocks. Investigations of gp120-to-p24 and gp120-to-particle ratios for assessing and monitoring challenge stock fitness in vitro are now under way.

Finally, our results indicate a need to develop rigorous screening procedures for evaluating potential HIV therapies and vaccines. The methods described in this report provide a standard and quantitative means for evaluating gp120-binding therapeutics and immunoglobulins over a variety of target cell densities that are found in vivo.

REFERENCES

1. Berman, P. W., T. J. Gregory, L. Riddle, G. R. Nakamura, M. A. Champe, J. P. Porter, F. M. Wurm, R. D. Hershberg, E. K. Cobb, and J. W. Eichberg. 1990. Protection of chimpanzees from infection by HIV-1 after vaccination with recombinant glycoprotein gp120 but not gp160. Nature (London) 345:622–625.

2. Byrn, R. A., J. Mordenti, C. Lucas, D. Smith, S. A. Marsters, J. S. Johnson, P. Cossum, S. M. Chamow, F. M. Wurm, T. Gregory, J. E. Groopman, and D. J. Capon. 1990. Biological properties of CD4 immunoadhesin. Nature (London) 344:667–670.

3. Byrn, R. A., I. Sekigawa, S. M. Chamow, J. S. Johnson, T. J. Gregory, D. J. Capon, and J. E. Groopman. 1989. Characterization of in vitro inhibition of human immunodeficiency virus by purified recombinant CD4. J. Virol. 63:4370–4375.

4. Capon, D. J., S. M. Chamow, J. Mordenti, S. A. Marsters, T. Gregory, H. Mitsuya, R. A. Byrn, C. Lucas, F. M. Wurm, J. E. Groopman, S. Broder, and D. H. Smith. 1989. Designing CD4 immunoadhesins for AIDS therapy. Nature (London) 337:525–531.

5. Chanh, T. C., G. R. Dreesman, P. Kanda, G. P. Linette, J. T. Sparrow, D. D. Ho, and R. C. Kennedy. 1986. Induction of anti-HTLV-III/LAV neutralizing antibodies by synthetic peptides. EMBO J. 5:3065–3071.

6. Clapham, P. R., J. N. Weber, D. Whitby, K. McIntosh, A. G. Dalgleish, P. J. Maddon, K. C. Deen, R. W. Sweet, and R. A. Weiss. 1989. Soluble CD4 blocks the infectivity of diverse strains of HIV and SIV for T cells and monocytes but not for brain and muscle cells. Nature (London) 337:368–370.

7. Clayton, L. K., R. E. Hussey, R. Steinbrich, H. Ramachandran, Y. Husain, and E. L. Reinherz. 1988. Substitution of murine for human CD4 residues identifies amino acids critical for HIV-gp120 binding. Nature (London) 335:363–366.

8. Daar, E. S., X. L. Li, T. Moudgil, and D. D. Ho. 1990. High concentrations of recombinant soluble CD4 are required to neutralize primary human immunodeficiency virus type 1 isolates. Proc. Natl. Acad. Sci. USA 87:6574–6578.

9. Dalgleish, A. G., P. C. L. Beverley, P. R. Clapham, D. H. Crawford, M. F. Greaves, and R. A. Weiss. 1984. The CD4 (T4) antigen is an essential component of the receptor for the AIDS retrovirus. Nature (London) 312:763–767.

10. Deen, K. C., J. S. McDougal, R. Inacker, G. Folena-Wasserman, J. Arthos, J. Rosenberg, P. J. Maddon, R. Axel, and R. W. Sweet. 1988. A soluble form of CD4 (T4) protein inhibits AIDS virus infection. Nature (London) 331:82–84.

11. Efron, B., and R. Tibshirani. 1986. Bootstrap methods for standard errors, confidence intervals, and other measures of statistical accuracy. Stat. Sci. 1:54–77.

12. Fisher, R. A., J. M. Bertonis, W. Meier, V. A. Johnson, D. S. Costopoulos, T. Liu, R. Tizard, B. D. Walker, M. S. Hirsch, R. T. Schooley, and R. A. Flavell. 1988. HIV infection is blocked in vitro by recombinant soluble CD4. Nature (London) 331:76–78.

13. Gelderblom, H. R., E. H. S. Hausmann, M. Ozel, G. Pauli, and M. A. Koch. 1987. Fine structure of human immunodeficiency virus (HIV) and immunolocalization of structural proteins. Virology 156:171–176.

14. Gelderblom, H. R., H. Reupke, and G. Pauli. 1985. Loss of envelope antigens of HTLV-III/LAV, a factor in AIDS pathogenesis? Lancet ii:1016–1017.

15. Goudsmit, J., C. Debouck, R. H. Meleon, L. Smit, M. Bakker, D. M. Asher, A. V. Wolff, C. J. Gibbs, and D. C. Gajdusek. 1988. Human immunodeficiency virus type 1 neutralization epitope with conserved architecture elicits early type-specific antibodies in experimentally infected chimpanzees. Proc. Natl. Acad. Sci. USA 85:4478–4482.

16. Goudsmit, J., C. L. Kuiken, and P. L. Nara. 1989. Linear versus conformational variation of V3 neutralization domains of HIV-1 during experimental and natural infection. AIDS 3(Suppl. 1): S119–S123.

17. Haigwood, N. L., C. B. Barker, K. W. Higgins, P. V. Skiles, G. K. Moore, K. A. Mann, D. R. Lee, J. W. Eichberg, and K. S. Steimer. 1990. Evidence for neutralizing antibodies directed against conformational epitopes of HIV-1 gp120. Vaccines 90: 313–320.

18. Hayashi, Y., K. Ikuta, N. Fujii, K. Ezawa, and S. Kato. 1989. Inhibition of HIV-1 replication and syncytium formation by synthetic CD4 peptides. Arch. Virol. 105:129–135.

19. Ho, D. D., J. C. Kaplan, I. E. Rackauskas, and M. E. Gurney. 1988. Second conserved domain of gp120 is important for HIV infectivity and antibody neutralization. Science 239:1021–1023.

20. Ho, D. D., J. A. McKeating, X. L. Ling, T. Moudgil, E. S. Daar, N.-C. Sun, and J. E. Robinson. 1991. Conformational epitope on gp120 important in CD4 binding and human immunodeficiency virus type 1 neutralization identified by a human monoclonal

antibody. J. Virol. 65:489–493.

21. Ho, D. D., M. G. Sarngadharan, M. S. Hirsch, R. T. Schooley, T. R. Rota, R. C. Kennedy, T. C. Chanh, and V. Sato. 1987. Human immunodeficiency virus neutralizing antibodies recognize several conserved domains on the envelope glycoproteins. J. Virol. 61:2024–2028.

22. Hussey, R. E., N. E. Richardson, M. Kowalski, N. R. Brown, H.-C. Chang, R. F. Siliciano, T. Dorfman, B. Walker, J. Sodroski, and E. L. Reinherz. 1988. A soluble CD4 protein selectively inhibits HIV replication and syncytium formation. Nature (London) 331:78–81.

23. Javaherian, K., A. J. Langlois, G. J. LaRosa, A. T. Profy, D. P. Bolognesi, W. C. Herlihy, S. D. Putney, and T. J. Matthews. 1990. Broadly neutralizing antibodies elicited by the hypervariable neutralizing determinant of HIV-1. Science 250:1590–1593.

24. Javaherian, K., A. J. Langlois, C. McDanal, K. L. Ross, L. I. Eckler, C. L. Jellis, A. T. Profy, J. R. Rusche, D. P. Bolognesi, S. D. Putney, and T. J. Matthews. 1989. Principle neutralizing domain of the human immunodeficiency virus type 1 envelope protein. Proc. Natl. Acad. Sci. USA 86:6768–6772.

25. Kahn, J. O., J. D. Allan, T. L. Hodges, L. D. Kaplan, C. J. Arri, H. F. Fitch, A. E. Izu, J. Mordenti, S. A. Sherwin, J. E. Groopman, and P. A. Volberding. 1990. The safety and pharmacokinetics of recombinant soluble CD4 (rCD4) in subjects with the acquired immunodeficiency syndrome (AIDS) and AIDS-related complex. Ann. Intern. Med. 112:254–261.

26. Kendall, M., and A. Stuart. 1979. The advanced theory of statistics, vol. 2, p. 320. Griffin, London.

27. Kinney-Thomas, E., J. N. Weber, J. McClure, P. Clapham, M. Singhal, K. Shriver, and R. A. Weiss. 1988. Neutralizing monoclonal antibodies to AIDS virus. AIDS 2:25–29.

28. Kirsh, R., T. K. Hart, H. Ellens, J. Miller, S. A. Petteway, D. M. Lambert, J. Leary, and P. J. Bugelski. 1990. Morphometric analysis of recombinant soluble CD4-mediated release of the envelop glycoprotein gp120 from HIV-1. AIDS Res. Hum. Retroviruses 6:1209–1212.

29. Klatzmann, D., E. Champagne, S. Chamaret, J. Gruest, D. Guetard, T. Hercend, J.-C. Gluckman, and L. Montagnier. 1984. T-lymphocyte T4 molecules behave as the receptor for human retrovirus LAV. Nature (London) 312:767–768.

30. Kowalski, M., J. Potz, L. Basiripour, T. Dorfman, W. C. Goh, E. Terwilliger, A. Dayton, C. Rosen, W. Haseltine, and J. Sodroski. 1987. Functional regions of the envelope glycoprotein of human immunodeficiency virus. Science 237:1351–1355.

31. Landau, N. R., M. Warton, and D. R. Littman. 1988. The envelope glycoprotein of the human immunodeficiency virus binds to the immunoglobulin-like domain of CD4. Nature (London) 334:159–162.

32. Layne, S. P., M. L. Merges, M. Dembo, J. L. Spouge, and P. L. Nara. 1990. HIV requires multiple gp120 molecules for CD4-mediated infection. Nature (London) 346:277–279.

33. Layne, S. P., M. J. Merges, and P. L. Nara. Unpublished data.

34. Layne, S. P., J. L. Spouge, and M. Dembo. 1989. Quantifying the infectivity of human immunodeficiency virus. Proc. Natl. Acad. Sci. USA 86:4644–4648.

35. Lifson, J. D., K. M. Hwang, P. L. Nara, B. Fraser, M. Padgett, N. M. Dunlop, and L. E. Eiden. 1988. Synthetic CD4 peptide derivatives that inhibit HIV infection and cytopathicity. Science 241:712–716.

36. Looney, D. J., S. Hayashi, M. Nicklas, R. R. Redfield, S. Broder, F. Wong-Staal, and H. Mitsuya. 1990. Differences in the interaction of HIV-1 and HIV-2 with CD4. J. Acquired Immune Defic. Syndr. 3:649–657.

37. Maddon, P. J., A. G. Dalgleish, J. S. McDougal, P. R. Clapham, R. A. Weiss, and R. Axel. 1986. The T4 gene encodes the AIDS virus receptor and is expressed in the immune system and the brain. Cell 47:333–348.

38. Matsushita, S., M. Robert-Guroff, J. Rusche, A. Koito, T. Hattori, H. Hoshino, K. Javaherian, and S. Putney. 1988. Characterization of a human immunodeficiency virus monoclonal antibody and mapping of the neutralizing epitope. J. Virol. 62:2107–2114.

39. McCune, J. M., L. B. Rabin, M. B. Feinberg, M. Lieberman,

J. C. Kosek, G. R. Reyes, and I. L. Weissman. 1988. Endoproteolytic cleavage of gp160 is required for the activation of human immunodeficiency virus. Cell 53:55–67.

40. McDougal, J. S., L. S. Martin, S. P. Cort, M. Mozen, C. M. Heldebrant, and B. L. Evatt. 1985. Thermal inactivation of the acquired immunodeficiency syndrome virus, human T lymphotropic virus-III/lymphadenopathy-associated virus, with special reference to antihemophilic factor. J. Clin. Invest. 76:875–877.

41. McDougal, S. J., A. Mawle, S. P. Cort, J. K. A. Nicholson, G. D. Cross, J. A. Scheppler-Campbell, D. Hicks, and J. Sligh. 1985. Cellular tropism of the human retrovirus HTLV-III/LAV. J. Immunol. 135:3151–3162.

42. McKeating, J. A., A. McKnight, and J. P. Moore. 1991. Differential loss of envelope glycoprotein gp120 from virions of human immunodeficiency virus type 1 isolates: effects on infectivity and neutralization. J. Virol. 65:852–860.

43. Mizukami, T., T. R. Fuerst, E. A. Berger, and B. Moss. 1988. Binding region for human immunodeficiency virus (HIV) and epitopes for HIV-blocking monoclonal antibodies of the CD4 molecule defined by site-directed mutagenesis. Proc. Natl. Acad. Sci. USA 85:9273–9277.

44. Moore, J. P. 1990. Simple methods for monitoring HIV-1 and HIV-2 gp120 binding to soluble CD4 by enzyme-linked immunosorbent assay: HIV-2 has a 25-fold lower affinity than HIV-1 for soluble CD4. AIDS 4:297–305.

45. Moore, J. P., J. A. McKeating, W. A. Norton, and Q. J. Sattentau. 1991. Direct measurement of soluble CD4 binding to human immunodeficiency virus type 1 virions: gp120 dissociation and its implications for virus-cell binding and fusion reactions and their neutralization by soluble CD4. J. Virol. 65:1133–1140.

46. Moore, J. P., J. A. McKeating, R. A. Weiss, and Q. J. Sattentau. 1990. Dissociation of gp120 from HIV-1 virions induced by soluble CD4. Science 250:1139–1142.

47. Nara, P. L., and P. J. Fischinger. 1988. Quantitative infectivity assay for HIV-1 and -2. Nature (London) 332:469–470.

48. Nara, P. L., W. C. Hatch, N. M. Dunlop, W. G. Robey, L. O. Arthur, M. A. Gonda, and P. J. Fischinger. 1987. Simple, rapid, quantitative, syncytium-forming microassay for the detection of human immunodeficiency virus neutralizing antibody. AIDS Res. Hum. Retroviruses 3:283–302.

49. Nara, P. L., K. M. Hwang, D. M. Rausch, J. D. Lifson, and L. E. Eiden. 1989. CD4 antigen-based antireceptor peptides inhibit infectivity of human immunodeficiency virus in titer at multiple stages of the viral life cycle. Proc. Natl. Acad. Sci. USA 86:7139–7143.

50. Nara, P. L., L. Smit, N. Dunlop, W. Hatch, M. Merges, D. Waters, J. Kelliher, R. C. Gallo, P. J. Fischinger, and J. Goudsmit. 1990. Emergence of viruses resistant to neutralization by V3-specific antibodies in experimental human immunodeficiency virus type 1 IIIB infection of chimpanzees. J. Virol. 64:3779–3791.

51. Oldstone, M. B. A. 1989. Viral persistence. Cell 56:517–520.

52. Parker, T. J., M. E. Clark, A. J. Langlois, T. J. Matthews, K. J. Weinhold, R. R. Randall, D. P. Bolognesi, and B. F. Hayes. 1988. Type-specific neutralization of the human immunodeficiency virus with antibodies to env-encoded synthetic peptides. Proc. Natl. Acad. Sci. USA 85:1932–1936.

53. Putney, S. D., T. J. Matthews, W. G. Robey, D. L. Lynn, M. Robert-Guroff, W. T. Mueller, A. J. Langlois, J. Ghrayeb, S. R. Petteway, K. J. Weinhold, P. J. Fischinger, F. Wong-Staal, R. C. Gallo, and D. P. Bolognesi. 1986. HTLV-III/LAV-neutralizing antibodies to an E. coli-produced fragment of the virus envelope. Science 234:1392–1395.

54. Rusche, J. R., K. Javaherian, C. McDanal, J. Petro, D. L. Lynn, R. Grimaila, A. Langlois, R. C. Gallo, L. O. Arthur, P. J. Fischinger, D. P. Bolognesi, S. D. Putney, and T. J. Matthews. 1988. Antibodies that inhibit fusion of human immunodeficiency virus-infected cells bind a 24-amino-acid sequence of the viral envelope, gp120. Proc. Natl. Acad. Sci. USA 85:3198–3202.

55. Ryu, S.-E., P. D. Kwong, A. Truneh, T. G. Porter, J. Arthos, M. Rosenberg, X. Dai, N-h. Xuong, R. Axel, R. W. Sweet, and W. A. Hendrickson. 1990. Crystal structure of an HIV-binding recom-

binant fragment of human CD4. Nature (London) **348**:419–425.
56. Schooley, R. T., T. C. Merrigan, P. Gaut, M. S. Hirsch, M. Holodniy, T. Flynn, S. Liu, R. E. Byington, S. Henochowicz, E. Gibish, D. Spriggs, D. Kufe, J. Schindler, A. Dawson, D. Thomas, D. G. Hanson, B. Letwin, T. Liu, J. Gulinello, S. Kennedy, R. Fisher, and D. D. Ho. 1990. Recombinant soluble CD4 therapy in patients with the acquired immunodeficiency syndrome (AIDS) and AIDS-related complex. Ann. Intern. Med. **112**:247–253.
57. Skinner, M. A., R. Ting, A. J. Langlois, K. J. Weinhold, H. K. Lyerly, K. Javaherian, and T. J. Matthews. 1988. Characteristics of a neutralizing monoclonal antibody to the HIV envelope glycoprotein. AIDS Res. Hum. Retroviruses **4**:187–197.
58. Smith, D. H., R. A. Byrn, S. A. Marsters, T. Gregory, J. E. Groopman, and D. J. Capon. 1987. Blocking of HIV-1 infectivity by a soluble, secreted form of the CD4 antigen. Science **238**:1704–1707.
59. Spouge, J. L., S. P. Layne, and M. Dembo. 1989. Analytic results for quantifying HIV infectivity. Bull. Math. Biol. **51**:715–730.

60. Sun, N.-C., D. D. Ho, C. R. Y. Sun, R.-S. Liou, W. Gordon, M. S. Fung, X.-L. Li, R. C. Ting, T.-H. Lee, N. T. Chang, and T.-W. Chang. 1989. Generation and characterization of monoclonal antibodies to the putative CD4-binding domain of human immunodeficiency virus type 1 gp120. J. Virol. **63**:3579–3585.
61. Traunecker, A., W. Lüke, and K. Karjalainen. 1988. Soluble CD4 molecules neutralize human immunodeficiency virus type 1. Nature (London) **331**:84–86.
62. Traunecker, A., J. Schneider, H. Kiefer, and K. Karjalainen. 1989. Highly effective neutralization of HIV with recombinant CD4-immunoglobulin molecules. Nature (London) **339**:68–70.
63. Wang, J., Y. Yan, T. P. J. Garrett, J. Liu, D. W. Rodgers, R. L. Garlick, G. E. Tarr, Y. Husain, E. L. Reinherz, and S. C. Harrison. 1990. Atomic structure of a fragment of human CD4 containing two immunoglobulin-like domains. Nature (London) **348**:411–418.
64. Watanabe, M., K. A. Reimann, P. A. DeLong, T. Liu, R. A. Fisher, and N. L. Letvin. 1989. Effects of recombinant soluble CD4 in rhesus monkeys infected with simian immunodeficiency virus of macaques. Nature (London) **337**:267–270.

The Auto-Regulation Model: A Unified Concept of How HIV Regulates its Infectivity, Pathogenesis and Persistence

SCOTT P. LAYNE and MICAH DEMBO

Biology and Biophysics Group, Theoretical Division, University of California, Los Alamos National Laboratory, Los Alamos, New Mexico, 87545, USA

The life cycle of HIV can be divided into two distinct stages: intracellular and extracellular. The prevailing view is that the intracellular stage provides the only locus for regulating the virus in response to physiologic stimuli. Such regulation is accomplished by modulating the rates of transcription, translation and viral assembly. The extracellular stage consists of physical processes such as diffusion, adhesion and penetration of cells by viral particles. These latter processes are commonly thought to be "automatic" and not subject to regulation. For the past several years, we have developed means of more carefully measuring and characterizing the extracellular stage of HIV infection, and we have obtained evidence indicating that novel regulatory processes do, in fact, take place during this extracellular stage. We believe that this extracellular regulation permits HIV to adapt to a wide range of physiologic cell densities, to maintain persistent but slow growing infection, and to defeat the protective activity of humoral blockers. The overall purpose of this review is to consider our evidence for this hypothesis.

KEYWORDS. *human immunodeficiency virus, infectivity assay, soluble CD4, immunoglobulin, humoral immune response*

INTRODUCTION

The maintenance of persistent HIV infection requires that a balance be struck between seemingly contradictory objectives. HIV must reproduce and evade immune surveillance, yet it must not overly attack the host to the point of premature death. To accomplish this balance, we believe that HIV auto-regulates its extracellular stage of infection. This view arose from a series of studies conducted over the past several years to identify the processes occurring during the extracellular stage of HIV infection and to understand their physiologic significance. The essential tools for this work have been kinetic models of HIV infection and quantitative infectivity assays. The models simulate four reactions taking place during an assay: infectious contact between virion and cell, spontaneous shedding of gp120, single viral inactivation, and formation of gp120-blocker complexes. By using these models, we developed a series of experiments for investigating the influence of these four reactions on infection [1–4]. Subsequently, quantitative HIV assays were carried out with different cell densities and blocker concentrations, and with viral stocks that were either fresh or aged. Assay results were then used to identify agreements or disagreements

34   S. P. LAYNE AND M. DEMBO

with the models, further refine experimental techniques, and reduce the effects of extra-
neous variables [5, 6].

After analyzing numerous infectivity assays with "laboratory" strains of HIV-1 and -2,
an overall picture of extracellular infection kinetics and auto-regulation has begun to
emerge. It is based on the recognition that the initial binding of HIV to a target cell is, in
many ways, similar to the adhesive interaction between two immune cells. For such cell-cell
interactions, Bell, Dembo and Bongrand [7, 8] have shown that adhesion between two
surfaces represents a first-order thermodynamic phase transition which takes place when a
certain "critical number" of interactions between adhesion molecules is exceeded. If the
density of adhesion molecules is below this critical number, the cellular surfaces will simply
not adhere [9, 10]. The exact value of the critical number is a function of several variables,
most importantly the strength of the repulsive electrostatic potential between the surfaces
and the association constant of the adhesion molecules for their complementary receptor
(see the review by Springer [9]).

In the case of HIV, the adhesion molecule is gp120 and the cellular receptor is CD4. In
view of the requirement for a critical number of interactions, it is not surprising that HIV is
studded with a high density of gp120 molecules. On the other hand, it is rather puzzling that
spontaneous shedding of gp120 takes place and is correlated with the progressive "multi-
hit" loss of viral infectivity (see next section). This finding contradicts the "classic" single-
hit model of viral inactivation, where whole viral particles (rather than individual envelope
proteins) are considered as the elemental unit of infection and neutralization [11, 12]. More
fundamentally, however, the seemingly "suicidal" propensity of HIV to shed an essential
protein is difficult to understand if the virus is locked in a mortal struggle against the host's
defenses [13].

In order to rationalize the functional role of gp120 shedding, let us consider the
hypothesis that the host's immune defenses play a relatively minor role in limiting infection.
In this case, survival of the host, and thus transmission of infection, must depend on auto-
regulatory mechanisms that are intrinsic to HIV. In terms of such an auto-regulation
hypothesis, the spontaneous shedding of gp120 makes perfect sense. Without this shedding,
it would be only a matter of time before every viral particle collided with and infected a
target cell. This would lead to an overwhelming infection within the host. Thus, gp120
shedding creates a limited interval during which a viral particle must either infect or die.
This race against time creates the context within which other regulatory factors are able to
modulate the probability that a viral particle will infect before it inactivates. It becomes
conceivable that there are means of switching a virion's infectiousness on and off.

Our experimental evidence implicates several variables in determining whether a viral
particle will infect a cell before it spontaneously inactivates [5, 6]. One of these variables is
target cell density. Low target cell densities are obviously associated with small proba-
bilities of encounter between virions and susceptible cells. Because HIV spontaneously
sheds gp120, it is likely that the gp120 content of a virion will fall below the critical number
before it encounters a susceptible cell. Conversely, high densities are associated with large
probabilities, which favors infection. (Virologists often term these two conditions as
"unsaturated" and "saturated," respectively. This is an entirely distinct notion from the
multiplicity of infection, MOI.) Examples of other factors which modulate the probability
that a viral particle will infect before it inactivates are: the concentration of humoral
blockers, the density of CD4 on target cell surfaces, the affinity of gp120 for CD4, and the
magnitude of the repulsive barrier between virion and cell. The role of these various factors
are discussed in greater detail below.

Let us now see how this perspective applies to physiology. Like other lentiviruses, HIV infects cells that are located in lymphoid, reticuloendothelial and nervous tissues [14–16]. The microscopic anatomies of these tissues are all different and thus they contain a wide range of cell densities. For example, typical $CD4^+$ cell densities in blood and lymph nodes are 10^6 to 10^7 and 10^7 to 10^9 ml^{-1}, respectively [17]. At the densities in lymph node, the rate of infectious collisions will be high. Hence, particles will rarely escape from this space unless they retain very small amounts of gp120. Conversely, when HIV particles enter the blood, the rate of infectious collisions will be much smaller. This will permit time for viral particles to diffuse away from their site of release, even when they retain large amounts of gp120. Thus, it is reasonable to expect that HIV will require different amounts of gp120 in these diverse physiologic environments.

Recently, gp120 shedding from viral particles was shown to be accelerated by exposure to high sCD4 concentrations [18–21]. It was proposed that this shedding was required to expose fusion domains within gp41. This hints that fusion domains within gp41 are labile and must be exposed at the very moment of virus-cell interaction. The auto-regulatory implications of this observation are not clear but it is interesting to speculate that facilitated shedding could provide yet another means of modulating infectivity.

Both shedding and overproduction of gp120 have been implicated in disrupting normal immune function [22–24]. This is borne up by experiments showing that uptake and presentation of gp120 fragments on T cell surfaces is accompanied by cell-mediated killing of uninfected "bystander" cells [25, 26]. If this mechanism applies *in vivo*, it is complementary to and in no way contradicts our hypothesis regarding the functional significance of gp120 shedding.

FIRST KINETIC MODEL

The essential tools for our work have been kinetic models of HIV infection and quantitative infectivity assays, which we will describe below. When we formulated the original kinetic model of HIV infection (Fig. 1), the available evidence suggested that four reactions were relevant to our work: infectious contact between virion and cell, spontaneous shedding of gp120, single-hit viral inactivation, and formation of gp120-blocker complexes [1–4]. Infectious contact between virions and cells was described by a single rate constant, k_i. This lumped parameter represented a number of viral-cell interactions culminating with the detection of a single infectious event. For a particular type of target cell, we expected that each viral strain would express a unique rate. Pictures from electron microscopy showed approximately 80 gp120 knobs covering the surface of budding HIV particles. These knobs subsequently disappeared with aging [27–30]. We therefore assumed that the shedding rate, k_s, was first-order with time and that the knobs were monomers. Experiments with other retroviruses showed that immunoglobulin-free serum contained surface-active agents and proteases that neutralized infectivity [31]. We thought it likely that similar nonspecific factors neutralized HIV by first-order processes, k_n, and that such processes were gp120-independent. Blocking of gp120 by monovalent agents was represented by forward and reverse rate constants for complex formation, k_f and k_r respectively. The ratio of these rates equalled the gp120-sCD4 association constant [32].

To apply these four reactions to the analysis of infectivity assays, we introduced two simplifying conditions [1–4]. The first was that all viral particles were members of a single homogenous cohort. In other words, all particles were born at the same time and started out

36   S. P. LAYNE AND M. DEMBO
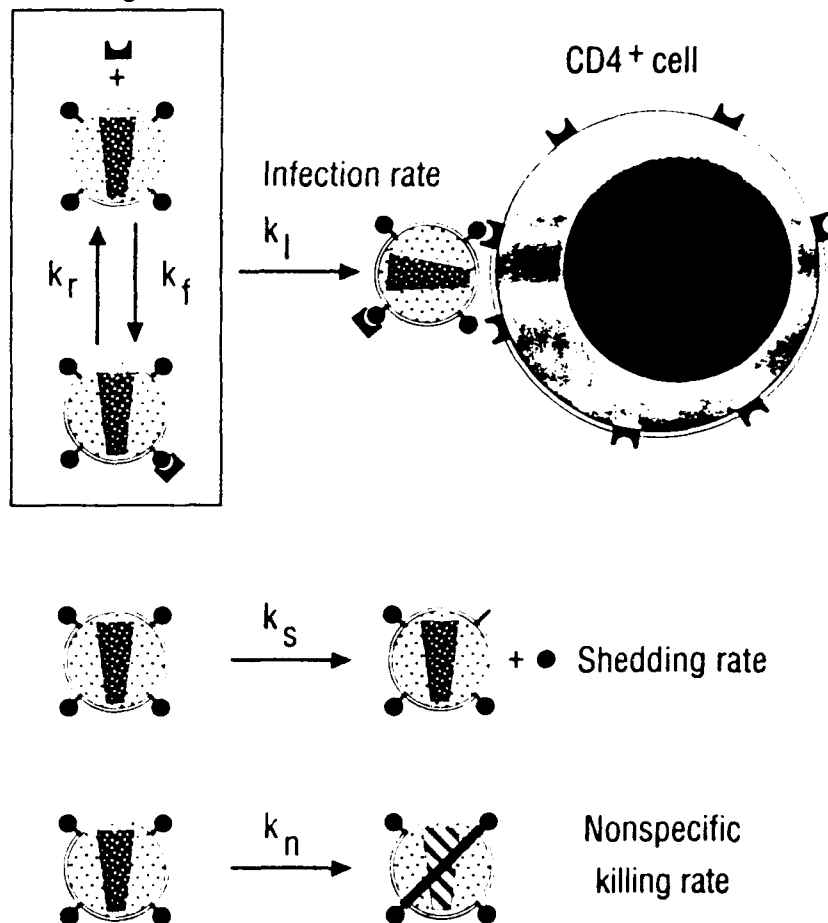
Forward and reverse
blocking rates

FIGURE 1   There are four reactions in the original kinetic model of HIV infection. k_i is rate of infectious contact between a virion and target cell. k · ·he rate of spontaneous shedding of gp120 from virions, which causes multi-hit inactivation. k_n is rate of nonspecific killing of virions, which causes single-hit inactivation. k_f and k_r are the forward and reverse rates of gp120-sCD4 complex formation, respectively. The rates of blocking take place on time scales that are rapid compared to the rate of infection.

with the same number of gp120 knobs. The second condition was that each knob on a viral particle was "equivalent" and "independent" with respect to infection, shedding, single-hit inactivation, and blocking. Thus, viral particles had rates of infectious contact that were proportional to the number of free gp120 knobs on their surfaces. Under these conditions, viral particles could lose their infectivity in small increments by shedding knobs (multi-hit) and all at once by sustaining single-hit inactivation. Finally, we considered infectivity assays that were conducted with small HIV inocula to insure low multiplicities of infection and to prevent soluble gp120 (shed knobs) from blocking a significant fraction of CD4 receptors on target cell surfaces.

In analyzing the kinetic model, we initially chose to examine the blocking of HIV infection by sCD4 [33–37]. We made this choice for three reasons. First, sCD4 was monovalent [38, 39], which conformed to the framework of our original analysis. Second, chemical measurements of the gp120-sCD4 K_{assoc} were available for HIV-1 [33] and HIV-2 [40]. These measurements were essential for making comparisons between biological responses and fundamental thermodynamic parameters. Third, initial calculations by us [1] and subsequent experimental measurements by Ashkenazi et al. [41] and Dimitrov et al. [42] showed that gp120-sCD4 complexes were in a state of equilibrium when a viral particle and target cell collide. In other words, the forward and reverse rates of blocking, k_f and k_r respectively, occurred on time scales that were rapid compared to the rate of infection, k_i. From steady-state calculations, the fraction of free and complexed gp120 molecules was $1/(1+\beta)$ and $\beta/(1+\beta)$, respectively, where $\beta = [sCD4] \times K_{assoc}$. These quasi-equilibrium relationships afforded us considerable utility in analyzing infectivity assay data [5, 6].

QUANTITATIVE INFECTIVITY ASSAYS

There were two approaches for quantifying infection by HIV. The first is to calculate an infectious dose 50% (ID-50) using statistical methods, such as those by Kärber [43] and Spearman [44]. The second is to count infectious events directly from syncytium-forming assays. The principal advantage of the ID-50 method is flexibility. A variety of target cells, HIV strains and viral antigens can be used to score infection as positive or negative. The disadvantage, however, is that large numbers of wells are required for accuracy. The advantages of the syncytial method are rapidity and precision, but these practical attributes are constrained to a small number of HIV strains which form countable syncytia.

Given our requirements for precision, we initially selected to use the syncytium-forming infectivity assay developed by Nara [45, 46]. In the original version of this assay, all manipulations of cells were performed in microtiter wells. Thus, it was not suited for accommodating an extensive range of experimental conditions. In collaboration with Peter Nara (National Cancer Institute), we therefore undertook a large series of experiments with HIV-1 and -2 to develop a new version of the assay [5]. This version separated CEM-SS cells into two groups: "target" and "indicator" cells (Fig. 2). Target cells were manipulated (diluted, infected and washed) in a number of individual tubes. Subsequently, these infected cells were added to monolayers of uninfected indicator cells for readout. The new version of the assay facilitated the addition and removal of blocking agents, accommodated a wide range of target cell densities, and significantly reduced artifacts [6]. All results presented below come from this new version of the infectivity assay. We have also performed a small number of assays with freshly isolated human peripheral blood mononuclear cells (PBMC) as target cells. These PBMC assays gave similar results to CEM-SS assays (data not shown).

Assay Protocol

CEM-SS cells are grown at densities ($\sim 5 \times 10^5$ ml^{-1}) that maintain exponential growth. To perform an assay, cells are suspended in fresh media to serve as "indicator" and "target" cells. Uninfected cell monolayers are prepared by adding 3.5×10^4 CEM-SS cells to flat-bottomed microtiter wells (96 wells per plate). These indicator cells are then incubated at 37°C for later use. A fixed number of target cells are added to tubes containing different volumes of fresh media and amounts of sCD4 (for a range of target cell densities and

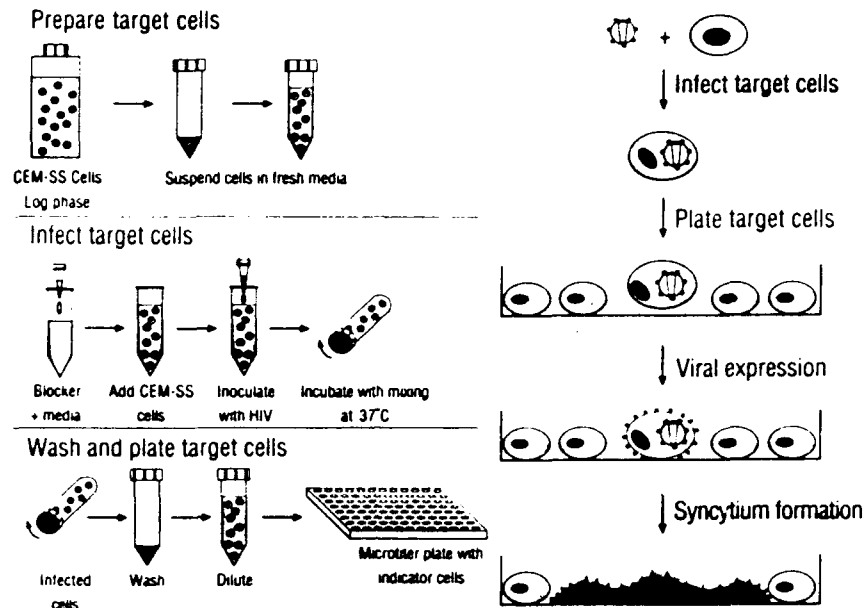38   S. P. LAYNE AND M. DEMBO

FIGURE 2   Schematic diagram of the quantitative syncytium-forming infectivity assay. Note that target cells are manipulated separately from indicator cells.

blocker concentrations). To obtain a constant inoculum to volume ratio for all tubes, graded amounts of HIV stock are then added to each tube. A particular ratio is selected to give a MOI less than 0.1, a total gp120 concentration less than $0.1 \times K_{assoc}$, and a satisfactory statistical count of syncytia. To assure uniform mixing, tubes are rolled during the infection period (either 1 or 2 hours) at 37°C. Next, to remove cell-free virus and blocker, infected target cells are washed once by centrifuging and suspending them in fresh media. Infected cell monolayers are prepared by adding a small number of target cells (2500 to 5000) to indicator cell monolayers. Thus, in all wells, indicator to target cell ratios are at least 7 to 1. A total of 8 wells are plated per target cell and blocker concentration. Syncytial forming units, SFU, representing the infection of individual target cells by cell free virus are counted 3 to 5 days following plating [5, 6]

Statistical Analysis of Data

The slope of a normalized inverse infection plot, [(normalized inverse infection) − 1] ÷ [blocker concentration), is defined as the "biological blocking activity" [5, 6]. Biological ⋯ ⋯ ⋯ ⋯ ⋯ ⋯ ⋯ ⋯ ⋯ $f(a, b) = \sum \{[y_i - (ax_i + b)] \div \sigma_i\}^2$, which gives a weighted least-squares fit to the data. y_i is the mean value of 1/SFU at the ith sCD4 concentration, σ_i is the SD of 1/SFU, and x_i is the sCD4 concentration at the ith data point. For normalized inverse infection plots, the weighted least-squares fit gives slope = $a \div b$. Unweighed least-squares fits are obtained by setting $\sigma_i = 1$. Confidence limits for the biological blocking activities are calculated by a standard bootstrap method [47].

Infection Versus Target Cell Density

In fluid suspensions, the rate of encounter between a viral particle and target cell is proportional to cell density [1–4]. At low cell densities, particles will have small rates of collision. Conversely, at high densities, the rates will be large. If a fixed number of particles and cells are added to a series of tubes containing various volumes of media, then after a period of time we will expect to observe quantitatively different outcomes. At low cell densities, the number of infectious events will grow in proportion to density; but at higher densities, this growth will be less than proportional. When the cells reached sufficiently high density, all active particles will infect and we will observe a plateau in the assays. Figure 3A illustrates this full range of "unsaturated", "partially saturated" and "saturated" behavior for the kinetic model. In close comparison, Figure 3B demonstrates unsaturated and partially saturated behavior for quantitative infectivity assays of HIV-1HXB3. As we can see, the density of 1.6×10^7 cells ml^{-1} is not sufficient for reaching complete saturation.

Now if a small amount of sCD4 is added to the media in the assays, there will be some blocking of gp120 and the rate of infection will diminish. According to the assumption of "independent" and "equivalent" gp120s, the new rate will be proportional to the number of unblocked (free) gp120 molecules on viral particles. As a result, we expect unsaturated behavior to extend to higher cell densities. Once again, Figure 3A illustrates this behavior for the model and Figure 3B demonstrates comparable behavior for assays of HIV-1HXB3 containing 2.4 nanomolar (nM) sCD4. As we can see, a small concentration of sCD4 in the assays means that higher cell densities are needed for achieving assay saturation. This agreement between the kinetic model and quantitative infectivity assays has been demonstrated for both HIV-1 and HIV-2 [5, 6].

In principle, the absolute concentration of infectious particles in HIV stocks can be measured with saturated assays. In practice, however, we have been unable to perform such assays because of the inherent limitations in culturing target cells at high densities for more than several hours. Therefore, to estimate the upper limit for this number, we collaborated
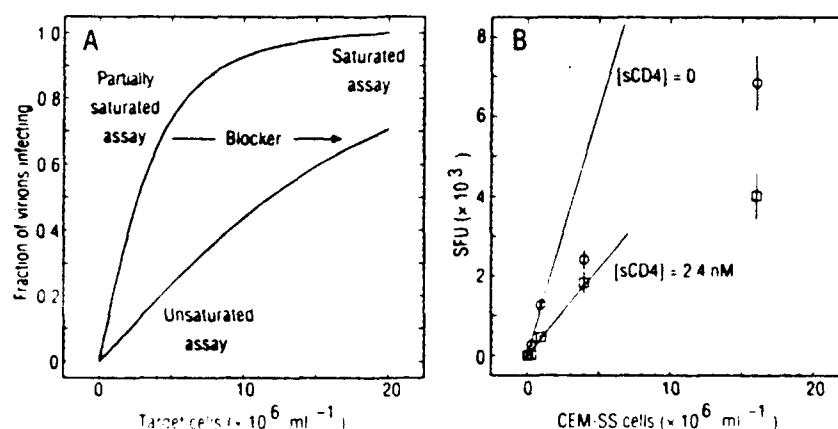

FIGURE 3   (A) Numerical solution of the kinetic model illustrating the progression from "unsaturated" to "saturated" assay behavior. The lower curve shows the predicted effects of adding sCD4. (B) Quantitative infectivity assays of HIV-1HXB3 in the presence (O) and absence (□) of 2.4 nM sCD4, respectively. SFU are the mean of 8 microtiter wells, error bars show ± 1 SD. Lines are weighted least squares fits to the data at the 4 lower cell densities.

40   S. P. LAYNE AND M. DEMBO

with Hans Gelderblom and Herbert Renz (Robert Koch Institute, Berlin) in counting all the particles in optimized viral stocks. Briefly, this was done by adding a known concentration of latex spheres to viral stocks and ultracentrifuging the mixture. Since the spheres and viral particles had similar sedimentation coefficients (~1000 Svedberg), they migrated to the bottom of the centrifuge tube in equal proportion. Next, with ultra thin-section electron micrographs, the ratio of particles to spheres in the pellet was measured, which permitted calculations of the absolute particle concentration. In one (typical) partially saturated infectivity assay, the ratio of infectious to total particles was $(2 \times 10^6$ SFU ml$^{-1}) \div (1 \times 10^{10}$ particles ml$^{-1}) \approx 2 \times 10^{-4}$ SFU particle^{-1}. This ratio sets an upper bound on the fraction of infectious particles. As expected, this limit was much smaller for unsaturated assays, where the ratios ranged from 1×10^{-5} to 1×10^{-6} SFU particle^{-1}. It is certainly conceivable that a sizable fraction of these minimally infectious or "defective" particles would infect at the cell densities (10^8 to 10^9 ml^{-1}) found in lymphoid organs. In other words, the best current methods of measuring infectious particles may be detecting only the "tip of the iceberg." Let us keep these underestimates in mind when considering the notion that HIV requires a critical number of gp120s for efficient infection of cells.

Blocking Activity Versus Target Cell Density and sCD4 Concentration

According to the assumption of "independent" and "equivalent" gp120 molecules, the rate at which a viral particle infects is proportional to the number of unblocked gp120s on its surface [1–4]. This neutral hypothesis predicts that a plot of "normalized inverse infection" (1/SFU with blocker multiplied by SFU without blocker) versus sCD4 concentration will be a straight line. In other words, inhibition proportional to formation of gp120-sCD4 complexes. Upward curvature in normalized inverse infection plot indicates positive synergy in the blocking of infection by sCD4. On the other hand, downward curvature indicates negative synergy. To facilitate analysis, let us define the slope of such plots, [(normalized inverse infection) − 1] ÷ [sCD4], as the "biological blocking activity" of sCD4. This definition will apply to all sCD4 concentrations and does not require the plots to be linear.

Let us now use this definition to see whether the kinetic model passes two decisive tests. The first is measuring the biological blocking activity of sCD4 from unsaturated infectivity assays. In such assays, viral particles will have at most a single chance to infect before inactivation. Thus, the assumption of equivalent and independent gp120s implies that sCD4 blocking activity will equal the gp120-sCD4 K_{assoc} from chemical measurements [5]. The second test is measuring the biological blocking activity in partially saturated assays. In this case, particles will have several chances to infect before inactivation and sCD4 will have to inhibit several potential infectious events. As a result, the kinetic model predicts that sCD4 blocking activity will decline monotonically with increasing degrees of saturation [6].

Figure 4A illustrates this behavior for solutions of the model at two cell densities. At the lower cell density (upper plot), conditions are unsaturated and the slope of 1×10^9M^{-1} equals the K_{assoc} used in the simulations. At the higher cell density (lower plot), conditions are partially saturated and the slope underestimates K_{assoc} by fourfold. As we can see, Figure 4B shows equivalent behavior for infectivity assays of HIV-1HXB3. At the lowest cell density, the biological blocking activity of sCD4 agrees with the chemical K_{assoc} to within a standard deviation [$(1.2 \pm 0.2) \times 10^9$ and $(8 \pm 5) \times 10^8$ M^{-1} in references 33 and 40, respectively]. With progressive assay saturation, the figure also shows marked reductions in sCD4 blocking activity. At the highest cell density, the blocking activity declined by 50-fold
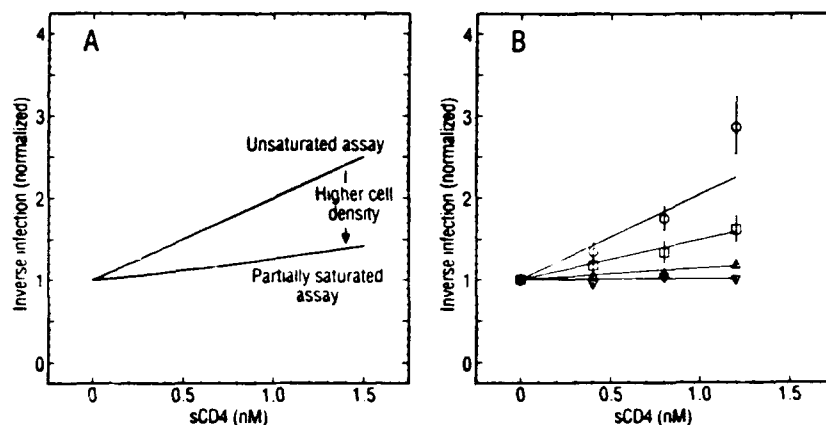
FIGURE 4   (A) Numerical solution of the model illustrating a declining slope as cell density increases.
(B)Results from quantitative infectivity assays of optimized HIV-1HXB3 stock at four target cell densities. Slopes
are weighted least squares fit to the data. Results are the mean of 8 wells; error bars show ± 1 SD. See Table I for a
summary of the biological blocking activities.

(Table I). These results from unsaturated and partially saturated assays give further evidence
that the kinetic model is basically correct.

With unsaturated assays, we have examined the biological blocking activities of three
different strains of HIV [5]. For HIV-1HXB3, HIV-1MN and HIV-2NIHZ, the biological
blocking activities were $(1.4 \pm 0.2) \times 10^9$, $(1.7 \pm 0.1) \times 10^9$ and $(8.5 \pm 0.5) \times 10^7$ M^{-1},
respectively. These values agreed, to within a factor of two, with the gp120-sCD4 K_{assoc}
from a number of independent chemical measurements [33, 40, 41, 48]. These results
support the hypothesis of equivalent and independent gp120s, and also show HIV-1 and -2
have susceptibilities to blocking that differ by 15- to 20-fold [40, 49, 50]. This finding
opens the issue that the K_{assoc} may vary widely between viral strains [51] and be an
important determinant of pathogenicity [1, 3].

Thus far we have discussed neutralization at low sCD4 concentrations, [sCD4] ×
(biological blocking activity) ≤ 1. At slightly higher sCD4 concentrations, normalized
inverse infection plots for all strains studies demonstrated an unexpected upward curvature,
indicating positive synergy in the blocking of infection by sCD4. To examine this in greater
detail, we normalized the abscissa of these plots by multiplying sCD4 concentrations by
their respective biological blocking activities. This procedure gives a numerical value of

TABLE I

Biological Blocking Activity of sCD4 Decreases with Increasing Cell Density

CEM-SS density (M1^{-1})	Symbol in Figure 4B	Biological blocking activity mean ± 1 SD (M^{-1})	Blocking activity ratio
5.6 × 10^4	○	(1.0 ± 0.1) × 10^9	1.0
1.0 × 10^5	□	(4.9 ± 0.3) × 10^8	0.49
8.0 × 10^5	△	(1.4 ± 0.2) × 10^8	0.14
6.3 × 10^6	▽	(2.1 ± 4.4) × 10^7	0.021

one to the sCD4 concentration at which half the gp120 molecules were blocked. Figure 5 shows the results of this normalization for three viral strains [5]. The line signifies inhibition that is proportional to gp120-sCD4 complex formation. As we can see, when more than half of gp120s were bound, all three strains demonstrated a similar pattern of upward curvature. Thus, at higher concentrations, the biological blocking activity of sCD4 cannot be explained simply on the basis of independent and equivalent gp120s.

The pattern of upward curvature in Figure 5 is rather surprising and eliminates a large class of plausible blocking mechanisms. For example, let us suppose that virions in an inoculum have widely divergent susceptibilities to sCD4 blocking. This could be caused by differences in K_{assoc} or by differences in the rate of infectious contact between virions and cells. In such cases, small amounts of sCD4 will easily block the most susceptible particles. As the amount of sCD4 increases, the most easily blocked particles will be eliminated and the only ones remaining will be the resistant fraction. Consequently, successive increments in blocking will become more difficult to achieve. As a result the blocking activity of sCD4 will display a marked negative synergy, which is completely inconsistent with the data.

Let us now consider plausible explanations for the upward curvature in Figure 5. The first and most obvious one is that high sCD4 concentrations accelerate gp120 shedding [18–21]. As demonstrated below, we have ruled out this explanation for our assays of HIV-1HXB3. The second explanation is that HIV requires a critical number of unblocked gp120s for efficient infection of CD4+ target cells [5]. When the number of unblocked gp120s falls below this critical number, the infection rate drops dramatically, leading to the upward curvature in Figure 5. The third explanation is that sCD4 exerts allosteric effects on the gp120 coat. In other words, by influencing neighboring gp120 molecules, gp120-sCD4 complex formation does more than just sterically hinder.

To dispense with the first explanation, we preincubated HIV-1HXB3 stock with 0, 2 and 20 nM sCD4 for 80 min at 37°C. sCD4 was then reduced ~1000-fold by ultracentrifuging the preincubated stock, removing the supernatant, and suspending the pellet in fresh media.
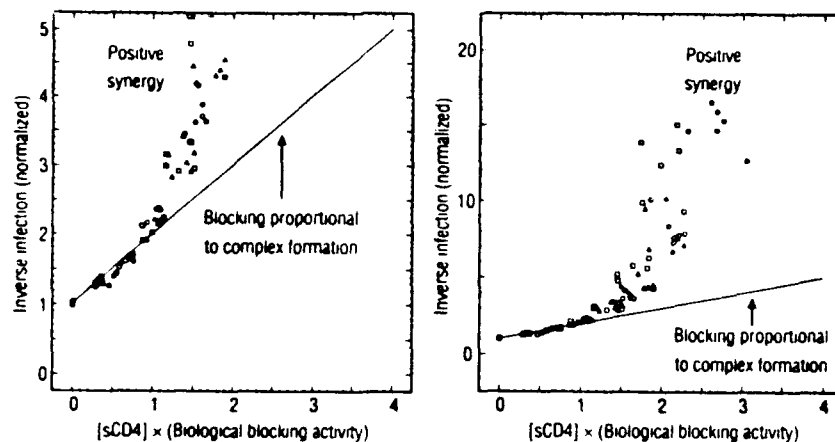

FIGURE 5   Analyzing the biological blocking activity of sCD4 for three strains of HIV. The ordinate (shown in two scales) and abscissa have been normalized to permit direct comparisons between strains. The positive synergy in the blocking of infection by sCD4 was the same for all three strains [5]. The fraction of free and complexed gp120 molecules on HIV particles is equal to $1/(1+\beta)$ and $\beta/(1+\beta)$, respectively, where $\beta = $ [sCD4] × (biological blocking activity). The line represents blocking based on independent and equivalent gp120s. The symbols denote HIV-1HXB3 (○), HIV-1MN (□) and HIV-2NIHZ (△).

Subsequently, the number of infectious units were assessed with a quantitative infectivity assay. Compared to control, 2 and 20 nM sCD4 inactivated HIV by 1.1- and 63-fold, respectively [6]. As we can see, higher sCD4 concentrations caused irreversible viral inactivation as already reported [18–21]. At the sCD4 concentrations (less than 2.4 nM) used in our assays of HIV-1HXB3, however, binding of sCD4 to viral gp120 was readily reversible by simple washing. Thus, the upward curvature in Figure 5 cannot be explained by enhanced shedding. We will further examine the critical number hypothesis and the allosteric hypothesis in subsequent experiments.

In this section, we presented evidence showing that infection kinetics are sensitive to small variations in target cell concentration, gp120-sCD4 K_{assoc} and number of unblocked gp120 molecules per virion. Contrary to the prevailing view, this demonstrates that the infection of target cells by viral particles is not an "automatic" process.

Shedding of gp120 versus Preincubation Time

The shedding of gp120 is required for our notion of auto-regulation of HIV infectivity (see introduction). Therefore, we have undertaken experiments to demonstrate that this shedding takes place on a time scale that is biologically relevant and that, in fact, it is the primary cause of viral inactivation [52].

To determine the kinetics of gp120 shedding, we rapidly grew and harvested an HIV-1HXB3 stock. This optimized stock was then incubated at 37°C. At regular intervals, aliquots of the stock were ultracentrifuged and the supernatant was separated from the pellet. Subsequently, the pellet was suspended in fresh media and both samples were frozen. At the same time, an unspun aliquot of the viral stock was also frozen and infectious viral particles were quantified with syncytial assays. To quantify the concentrations of envelope and core proteins, we then used gp120 and p24 enzyme-linked immunosorbent assays (ELISA). Figure 6A shows the results for the gp120 ELISA [53, 54] that were performed in collaboration with John Moore (Chester Beatty Laboratories, London). Figure 6B shows the res .ts for the p24 ELISA that were performed with assays from DuPont [55].

Figure 6A demonstrates that the concentration of viral-associated gp120 in the pellet (○)
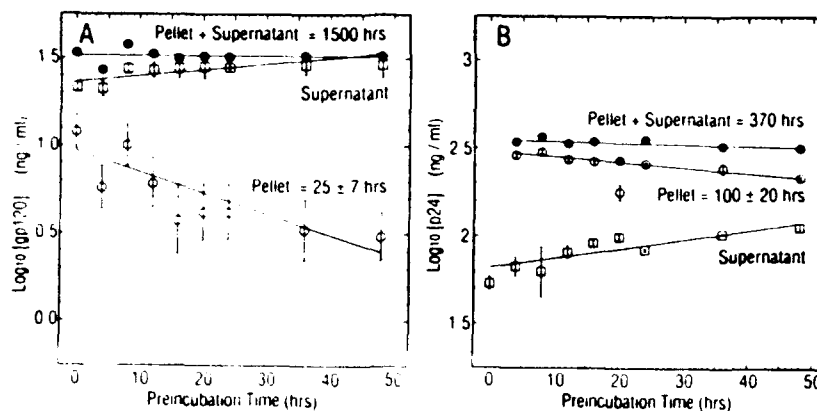

FIGURE 6   (A) ELISA measurements of gp120 concentration. (B) ELISA measurements of p24 concentration. Results for pellets are an average of replicate 9 wells; results for all other samples are an average of replicate 10 wells. Half lives (mean ± 2 SD) are weighted least squares fits to the data; error bars show ± 1 SD.

44   S. P. LAYNE AND M. DEMBO

decreased with preincubation times up to 48 hours (pellet half life = 25 ± 7 hrs). Also as
expected, the concentration of soluble gp120 in the supernatant (□) increased with time.
Summing the concentrations of gp120 in the pellet and supernatant gave a total (●) that was
conserved during the experiment (pellet + supernatant half life = 1500 hrs). This total
agreed with the concentration of gp120 in the unspun samples (data not shown), which
further confirmed that gp120 was stable with time. The least-squares fit to the pellet data (O)
yielded an excellent straight-line fit (correlation coefficient = 0.85), showing that sponta-
neous shedding of gp120 from viral particles was first-order with time. This clearly
confirms that the description of shedding in the kinetic model of infection was valid [52].

Figure 6B shows decreasing p24 in the pellet (O), that is accompanied by increasing p24
in the supernatant (□). Summing the p24 in the pellet and supernatant gave a total (●) that
was conserved with time (pellet + supernatant half life = 370 hrs). Again this total agreed
closely with p24 concentrations in unspun samples (data not shown). The rate at which p24
disappeared from the pellet (half life = 100 ± 20 hrs) was more than fourfold slower than
that of gp120. The loss of intact viral particles was therefore an insignificant factor
contributing to the decline of gp120 in Figure 6A [52].

By thin-section electron micrographs, the absolute number of virions in this stock was
5×10^9 particles ml^{-1}. Therefore, at the beginning of the incubation period, we calculated an
average of ~10 gp120 molecules per particle and ~5 × 10^{-17} g of p24 per virion. At the end
of the incubation period, we find that this average has fallen to ~2.5 gp120 molecules per
particle, with the p24 content remaining constant. To ascertain whether loss of gp120 plays
a role in the auto-regulation of HIV infectivity, it is necessary to correlate these ELISA
measurements with infectivity assays. This will be done in Figure 7.

Loss of Infectivity Versus Preincubation Time

Figure 7 shows the spontaneous decay of HIV-1HXB3 infectivity at 37°C. These data are an
average of four separate "decay" assays. Each one was conducted with a fresh viral stock
that was grown and harvested under similar conditions. In all four experiments, there was an
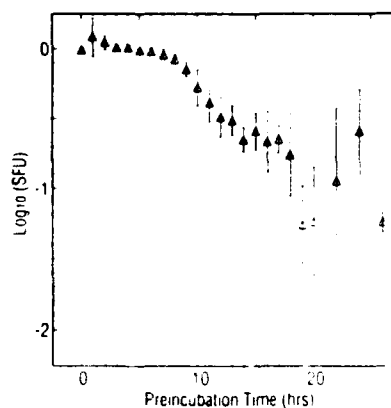initial period of slow inactivation (0 to 7 hrs) followed by a pronounced acceleration in the

FIGURE 7   The spontaneous decay of HIV-1HXB3 infectivity at 37°C. SFU are an average of four decay
experiments. Each point in the figure is the geometric mean of 16 to 32 wells, error bars show ± 1 SD. Data were
normalized to a numerical value of one at zero hours.

decay rate. This same qualitative behavior is observed regardless of the presence or absence of sCD4, and regardless of unsaturated or saturated assay conditions [6, 52]. This concave downward decay profile is most consistent with the notion of a critical number of gp120 molecules for efficient infection. The notion of a critical number explains the acceleration of the decay rate and also explains how a twofold loss of gp120 (from 0 to 25 hrs in Fig. 6) translates into a 20-fold loss of HIV infectivity (from 0 to 25 hours in Fig. 7). Once again, the allosteric model is unable to account for these observations. It would predict a mere twofold loss of infectivity over the period of the experiment.

Assay Saturation Versus Preincubation Time

In partially saturated infectivity assays, viral particles have several chances to infect before inactivation. In other words, while viral particles and target cells intermix, the average rate of collision is large enough to permit multiple infectious contacts per particle. One observable consequence of these favorable odds is that the biological blocking activity of sCD4 underestimates the K_{assoc} from chemical measurements (Fig. 4). If we now preincubate a viral stock for increasing intervals before use, particles will spontaneously shed their gp120. Thus, the average number of gp120 molecules per particle will decrease and, as a result, particles will have smaller rates of infectious contact. With increasing preincubation time, we therefore expect that effects due to assay saturation will gradually disappear [1–4].

Figure 8A illustrates this behavior for solutions of the kinetic model at two preincubation times. Without preincubation, the slope underestimates the K_{assoc} used in this simulation (1 $\times 10^9$ M^{-1}) by about fourfold. With preincubation, however, the slope increases to a level equalling K_{assoc} and remains at this numerical value with increasing time. This unchanging blocking activity reflects the fact that inhibition is proportional to gp120-sCD4 complex formation. Figure 8B demonstrate similar behavior for an HIV-1HXB3 stock. After preincubation (without sCD4) for 30 minutes at 37°C, the blocking activity (slope) underestimated K_{assoc}, which indicates partial saturation (Table II). After six hours, the blocking activity increased threefold but its value still indicates partial saturation. After 13 hours, the
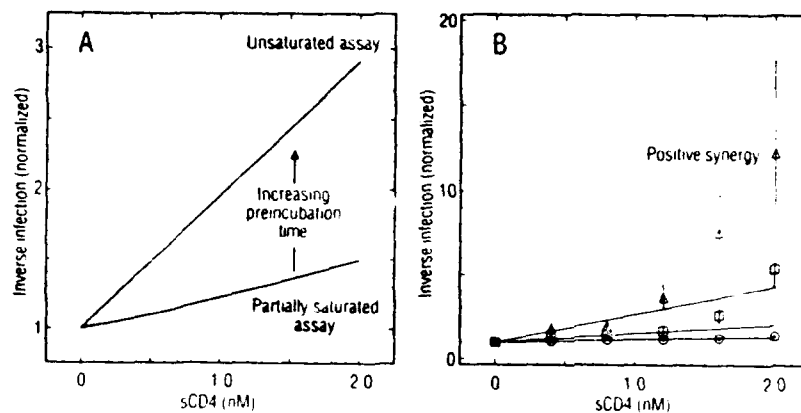

FIGURE 8 (A) Numerical solution of the model illustrating decreasing assay saturation with increasing preincubation time. (B) sCD4 blocking activity was measured after preincubating an HIV-1HXB3 stock for 0.5, 6 and 13 hours at 37°C Results are the mean of 8 microtiter wells; error bars show ± 1 SD Lines are weighted least-squares fits at the 4 lower sCD4 concentrations

46   S. P. LAYNE AND M. DEMBO

TABLE II

Biological Blocking Activity of sCD4 Increases with Preincubation Time

Preincubation time (hrs)	Symbol in Figure 8B	Biological blocking activity mean ± 1 SD (M^{-1})
0.5	o	$(1.8 \pm 0.2) \times 10^8$
6.0	□	$(5.4 \pm 0.5) \times 10^8$
13.0	△	$(1.7 \pm 0.2) \times 10^9$

blocking activity equals the gp120-sCD4 K_{assoc} derived from other unsaturated assays (Table I). This outcome clearly demonstrates that spontaneous shedding of gp120 is associated with reductions in assay saturation. Therefore, in accord with the kinetic model, aged viral particles have decreased rates of infectious contact with CD4$^+$ cells.

After preincubation for 13 hours, the data in Figure 8B curve progressively upward at higher sCD4 concentrations, indicating positive synergy in blocking [5]. This increasing synergy with aged viral stocks corroborates the hypothesis that HIV requires a critical number of free gp120 glycoproteins for efficient infection of CD4$^+$ target cells. The other hypothesis regarding allosteric interactions within the viral coat is not supported by the data in Figure 8B. Allosteric interactions should either remain constant or decline with the shedding of gp120. Therefore, we have found that the idea of "independent" gp120 molecules, though having some validity, does not completely explain HIV's infectious behavior [5, 6, 50, 56, 57].

Our original kinetic model does not account for the upward curvature in the inverse infection plots (Figs. 5 and 8B) nor does it account for discrepancies between the magnitude of gp120 shedding (Fig. 6A) and the loss of HIV infectivity (Fig. 7). We will deal with these discrepancies in the next section.

NEW KINETIC MODEL

In the quantitative infectivity experiments, most but not all predictions of the original kinetic model were corroborated By scrutinizing the departures from predicted outcomes, we were led to formulate a new model of HI' infection. This modeling work was done in collaboration with John Spouge (National Library of Medicine). Below, we describe this refined and generalized model with emphasis on the evidence that led us to propose each of its novel features.

First, in the original model, it was assumed that infection proceeded at a rate proportional to unblocked gp120 molecules. This rate was independent of the total number of gp120s in the viral envelope [1–4]. However, the positive synergy in the biological blocking activity of sCD4 (Fig. 5), the large amplification factor relating gp120 shedding to loss of infectivity (Figs. 6A and 7), and the increasing positive synergy with preincubation time (Fig. 8B) are most consistent with the notion that HIV requires a critical number of unblocked gp120 molecules for efficient infection of CD4$^+$ cells [5, 6, 52]. Therefore, in the new model, the rate of infection depends on an adjustable threshold. Above it, the rate is proportional to unblocked gp120s and below it, the rate depends on a cutoff function that is less than proportional. As discussed in the next section, there are good molecular reasons for the existence of the critical number.

Second, in the original model, the distribution of gp120 on viral particles was irrelevant because it was assumed that each gp120 was equivalent and independent in promoting infection [1–4]. Introducing a critical number, however, means that it is no longer possible to conform to this equivalent site approximation. Therefore, in the new model, any distribution of gp120 on particles (all combinations of numbers and ages) are analyzable. This flexibility is needed for studying the influence of viral stock heterogeneity on assay results. It is also useful for determining whether particular outcomes from infectivity assays are representative for all viral stocks or are stock dependent.

Third, in the old model, a single lumped parameter governed the rate of infectious collision between a viral particle and target cell. Although this was a reasonable starting point, it nevertheless did not permit us to distinguish kinetic processes taking place before a particle and cell collide from those taking place afterward. Therefore, the new model divides this lumper parameter into two components. The first characterizes the rate at which particles diffuse and collide with cells. The second characterizes the rate at which particles absorb and penetrate at cell surfaces. The relative size of these two rates permits infection to be categorized as either "collision" or "attachment" limited. In collision-limited infections [58], sCD4 will have no biological blocking activity in unsaturated assays. In attachment-limited infections [59, 60], on the other hand, sCD4 will have a blocking activity equal to the gp120-sCD4 K_{assoc}. Thus, the new model will be useful for analyzing how changes at the cell surface influence the blocking of infection, and for distinguishing pre-binding from post-binding neutralization.

Fourth, in the original model, gp120 knobs were considered as monomers. However, biochemical [61, 62] and electron microscopy [63] studies of gp120 have shown that knobs on HIV are multimers. Therefore, in the new model, we will consider a knob as a dimer, which is the simplest form of a multimer. The association constant for blocking individual gp120 monomers within a dimer may depend on whether knobs are free or half blocked. Thus, two sets of forward and reverse rate constants are defined for governing these reactions, which allows for allosteric interactions between sites.

Fifth, in the old model, the shedding rate of gp120 was independent of the formation of gp120-sCD4 complexes. However, in the background experiments, we found that biological blocking activity of sCD4 at high concentrations was noncompetitive [6]. As shown by other investigators, an enhanced rate of spontaneous shedding of gp120 accounts for this noncompetitive activity [18–21]. Therefore, in the new model, the shedding rate of a gp120 knob depends on the number of molecules bound to it. Thus, there are three separate shedding rates corresponding to free, half and fully blocked dimers. This permits greater flexibility and precision in the analysis of noncompetitive blocking activity.

Sixth, the role of nonspecific inactivation [31] is unchanged in the new model. It thus continues to represent single-hit processes that are independent of the number of gp120 dimers on a viral particle.

DISCUSSION

We have presented evidence showing that the infectious potential of an HIV particle is characterized by a critical number of gp120 molecules. Since gp120 spontaneously sheds and since this critical number is subject to variation, there are several possibilities by which the infectious potential of an HIV virion can be controlled. Also since these processes take place during the extracellular stage of the viral life cycle, they make contributions that are

48   S. P. LAYNE AND M. DEMBO

distinguishable from intracellular regulation [64–66]. To lend credence to this hypothesis, we must investigate the physical basis of the critical number and its role in pathogenesis. This leads to several questions. In their own right, these questions have immediate practical applications to standardizing infectivity assays, testing therapeutic agents that bind to viral gp120 and cellular CD4, and evaluating humoral responses induced by HIV vaccines.
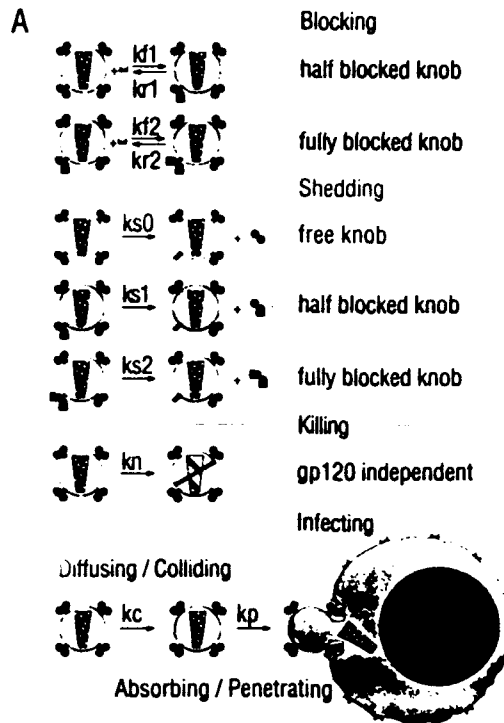
Role of the Glycocalyx

What factors on the viral envelope and cell-surface glycocalyx determine the critical number of gp120 knobs?   Cells of the immune system are finely poised between forming attachments and detachments to membrane surfaces, which permits versatility for surveillance and protection [9]. When two cell surfaces come into close proximity, repulsive forces from negatively charged surface glycocalyces are opposed by attractive ones from a repertoire of adhesion receptors. Thus factors influencing glycocalyces (hydrophylicity, compressibility, thickness and charge) and adhesion receptors (number, distribution, mobility, length and association constant) on each of the cell surfaces determine whether a threshold is reached in which stable attachment takes place [7, 8]. The large number of factors influencing these interactions suggests that one factor may substitute for another. In agreement with this concept, experiments with T cells have shown that activation of adhesion receptors was mimicked by adding positive charge to the glycocalyx or by removing the negative charge of sialic acids with neuraminidase [10]. Of equal importance, the demonstration of threshold phenomena in these interactions also suggests that the glycocalyx, which enshrouds the cell, provides protective barrier against invasion. Pathogens like bacteria and viruses would be excluded from entering an immune cell unless repulsive forces were overcome by attractive ones [67].

Let us now consider how this perspective applies to HIV particles and CD4+ cells. A gp120 molecule consists of approximately 520 amino acids and has a molecular weight of 1.2×10^5 daltons. Based on an average of 125 daltons per peptide, we calculate that approximately half of gp120's weight is composed of polysaccharides. A significant fraction of these polysaccharides are sialic acids [68]. Thus, as with immune cells, the surface of HIV is covered by a thick glycocalyx with appreciable negative charge. Established roles for this covering on lentiviruses include protection against enzymatic attack by proteases and interference with the binding of immunoglobulins to surface glycoproteins [69, 70]. In addition to these, however, we assert that viral-cell repulsions will select for particular types of infectious collisions and viral-viral repulsions will serve to reduce the physical clumping of particles, facilitating dispersal. Therefore, in molecular terms, we postulate that the critical number of gp120 knobs for efficient infection arises from repulsive forces between viral and cellular glycocalyces and attractive ones between gp120 and CD4 (Fig. 9). In order to overcome the protective barrier, a critical number of gp120-CD4 interactions must form. Once gp120 falls below the critical number, a virion may still infect a cell (for example, by colliding with cells or regions on cells having thinner glycocalyces) but the odds of this happening will be slim (Fig. 10).

This molecular mechanism for generating the critical number is consistent with three observations. First, results from infectivity assays have shown that treatment of CD4+ cells with DEAE-dextran increases the number of infectious units in HIV stocks compared to untreated cells [45, 46, 52]. Second, infectivity assays have also shown that dextran sulfate [71–73] and other sulfated polymers [74–76] decreases the number of infectious units compared to controls. Third, flow cytometric [77] measurements of virus-cell interactions

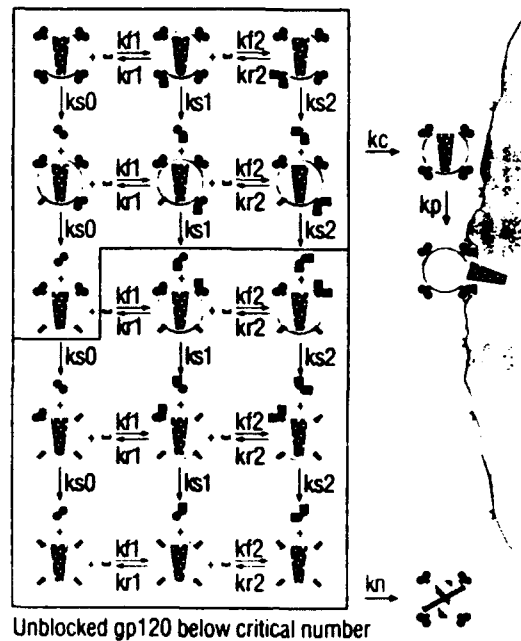AUTO-REGULATION MODEL OF HIV   49

FIGURE 9   (A) Basic reactions in the new kinetic model. k_{f1} and k_{f2} are rates for the formation of half-blocked and fully-blocked gp120 dimers, respectively. k_{r1} and k_{r2} are rate constants for the dissociation of half-blocked and fully-blocked gp120 dimers, respectively. k_{s0}, k_{s1} and k_{s2} are rates for spontaneous shedding of unblocked, half-blocked and fully-blocked gp120 dimers, respectively. k_c is the rate of collision between a viral particle and a cell. k_p is the rate of absorption and penetration for a viral particle at the cell surface. (B) Combined reactions in the new model. When viral particles are above a critical number of gp120 knobs (unshaded region), they infect at a rate proportional to the number of unblocked gp120s. When viral particles are below the critical fraction (shaded), they infect at a rate less than proportional to the number of unblocked gp120s. In this figure, for example, virions start out with four gp120 knobs and the critical number is two unblocked knobs.

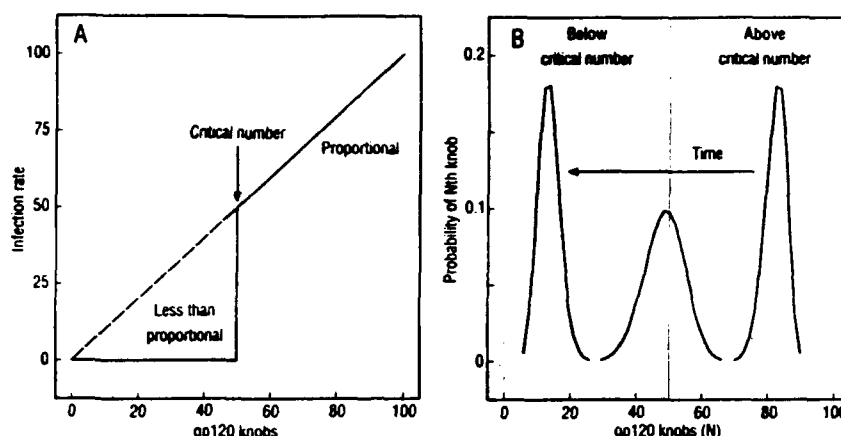50   S. P. LAYNE AND M. DEMBO

FIGURE 10   (A) Above the critical number, the infection rate is proportional to the number unblocked gp120 knobs. Below the critical number, the rate is less than proportional to the number unblocked gp120 knobs. That is, the actual infection rate falls somewhere within the triangle. (B) As viral particles age, they spontaneously fall below the critical number by the shedding of gp120. The figure illustrates a hypothetical distribution of gp120 on particles at three preincubation times. Initially, all particles are above the critical number. At the intermediate time, equal numbers of particles are above and below this number. At the longer preincubation time, all particles are below the critical number.

have shown that sulfated polymers inhibit the binding of HIV to CD4+ cells. DEAE-dextran is a cationic polysaccharide that adds positive charges to the glycocalyx. Conversely, dextran sulfate and related compounds are anionic polysaccharides that add negative charges to the glycocalyx. Therefore, in agreement with our hypothesis, it appears that this class of agents work by altering the charge of the glycocalyx [78, 79]. DEAE-dextran lowers whereas dextran sulfate and related compounds raises the threshold for the critical number of gp120-CD4 interactions.

We have found that sCD4 exhibits a "threshold" effect in the blocking of HIV infection (Fig. 5). Below threshold, blocking is proportional to the formation of gp120-sCD4 complexes [5]. Above threshold, there is a positive synergy in blocking due to the critical number of gp120s for efficient infection of CD4+ cells [6]. At even higher sCD4 concentrations, viral particles are irreversibly inactivated by enhanced shedding of gp120 [6, 18-21]. It remains to be determined how these "reversible" and "irreversible" components of biological blocking activity apply to immunoglobulins in general. If the reversible component primarily describes immunoglobulins, then the humoral response that a gp120-based vaccine must induce and maintain will be related to the critical number. Large critical numbers will require correspondingly small humoral responses and vice versa. In other words, we conceive a relationship between vaccine efficacy and the critical number. It is thus important to determine how the critical number varies between divergent wild-type strains and whether physiologic modulation of the glycocalyx—for example, by T cell activation [80, 81]-alters the critical number.

HIV primarily infects CD4+ cells, although certain CD4- cells are susceptible to infection [82-85]. For these cells, it has been suggested that a second receptor on the cell surface mediates absorption and penetration [86, 87], or that infection takes place via receptor-mediated endocytosis [88]. It is also tempting to speculate, however, that the

glycocalyx of these cells may provide reduced degrees of protection against invasion by pathogens [67]. This could be due, for example, to relatively thin or patchy glycocalyx, or to a glycocalyx with reduced negative charge [52].

Particular amino acid sequences within gp120, located outside the CD4 binding domain, have been shown to influence viral tropism [89–92]. It has been shown that these sequences influence the early phase of viral infection, taking place before reverse transcription, although the exact basis for their action has not been established. For these sequences, it is also tempting to consider whether changes in the properties of the viral glycocalyx—for example, by altering its net negative charge—may play a role in tropism.

Examining Physiologic Target Cells

Does the model of HIV infection kinetics apply to other types of target cells? The background experiments were based on CEM-SS cells. As discussed previously, this $CD4^+$ human cell line was selected because it facilitated the conduct of quantitative infectivity assays with good precision and reproducibility. As a result, we identified agreements and disagreements with the original kinetic model, refined experimental techniques, and reduced the effects of extraneous variables. Since our initial task of testing the model has been completed, it is now time to consider more "physiologic" target cells.

Cells that are mainly infected by HIV *in vivo* include $CD4^+$ PBMCs [93–96], monocytes and macrophages [97, 98]. We have already conducted a small number of infectivity assays with human PBMC that yielded similar results to CEM-SS cells [52]. Therefore, to further clarify the various issues raised by the above question, it will be necessary to conduct quantitative infectivity assays with freshly isolated human PBMC, monocytes and macrophages. These assays should repeat the ones described in the background section: (a) over what range of cell densities are assays unsaturated and partially saturated; (b) for unsaturated assays, does the biological blocking activity of sCD4 equal the gp120-sCD4 K_{assoc} from chemical measurements; (c) is assay saturation accompanied by reductions in the blocking activity of sCD4; (d) does HIV require a critical number of gp120 molecules for efficient infection of primary cells; and (e) does primary cell "activation" or "differentiation" influence the outcome of questions *a–d*?

Our investigations with CEM-SS cells demonstrated that sCD4 blocking activity declined at cell densities ranging from 10^5 to 10^6 ml^{-1}. These densities are tenfold smaller than those found in blood and ten- to 1000-fold smaller than those found in lymph node [6, 17] At present, two sCD4-based drug trials in humans have found that nanomolar sCD4 lev⋅ is in plasma had no appreciable therapeutic effects [99, 100]. As suggested by Daar *et al.* [101] and others [51], one feasible explanation for this outcome was that wild-type strains have gp120-sCD4 K_{assoc} much smaller than laboratory-adapted strains. In follow-up studies of this matter by Ashkenazi *et al.* [41] and Brighty *et al.* [48], however, it was demonstrated that recombinant envelope proteins from these wild-type strains had gp120-sCD4 K_{assoc} that were similar to laboratory strains. Therefore, a more straightforward explanation for the failure of these drug trials is that sCD4 exerts little or no blocking activity at physiologic cell densities [6]. The decline in biological blocking activity with increasing target cell density may also explain the relative inefficiency of sCD4 in inhibiting infection by "monocyte-tropic" HIV strains in monocytes and T cells [102]. Because of these findings, it will be important to determine the range of cell densities at which the biological blocking activity of sCD4 decreases with freshly isolated human cells.

52   S. P. LAYNE AND M. DEMBO

Another possible explanation for the failure of sCD4-based trials, which has been heretofore overlooked, is that sCD4 interferes with the extracellular auto-regulation of HIV infectivity. This paradoxical action could occur by the formation of complexes between sCD4 and soluble gp120. Such a binding reaction would effectively block auto-regulation by sequestering soluble gp120, thereby preventing it from performing its inhibitory functions at the target cell membrane (Fig. 11). This could greatly increase the lytic potential of HIV in tissues with high viral burdens and, perversely, result in increased rather than decreased pathology.

For unsaturated assays with CEM-SS cells, we found that sCD4 blocking activity equaled the gp120-sCD4 K_{assoc} from chemical measurements [5, 6]. This quantitative agreement between biological activity and chemical measurements demonstrated that the rate of infection was proportional to unblocked gp120 molecules on viral particles. In other words, for CEM-SS cells there were no significant routes of infection bypassing interactions between viral gp120 and cellular CD4. If infection had been mediated by CD4-independent pathways or limited merely by collisions between particles and cells, the biological blocking activity of sCD4 would have been less than its chemical K_{assoc}. We can thus make use of this relationship in detecting CD4-independent [86–88] and collision-limited infections [58]. Consequently, for primary cells, it will be important to determine whether unsaturated infectivity assays yield blocking activities equalling the chemical K_{assoc}. Conceivably, CD4-independent or collision-limited routes of infection could provide yet another explanation for the failure of sCD4-based drug trials in humans.
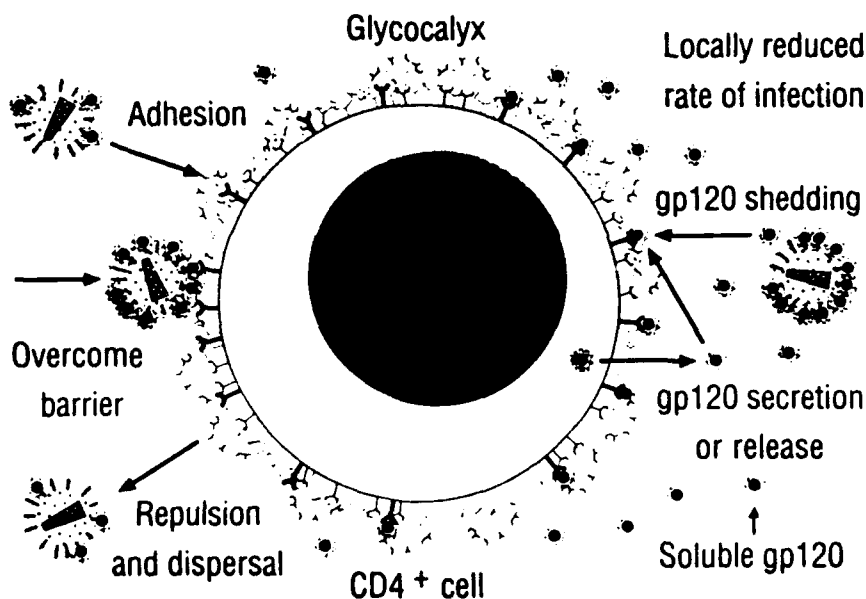

FIGURE 11   The critical number of gp120s for efficient infection of CD4+ cells arises from a balance of forces. Repulsive forces from viral and cellular glycocalyces are opposed by attractive ones from gp120 and CD4 interaction. The shedding of gp120 from particles and its secretion or release from infected cells results in high local concentrations of gp120 and the blocking of CD4 receptors on cell surfaces. This will locally reduce the rate of infection, prevent superinfection of progenitor cells, and promote viral export from infected tissues. These actions will permit HIV infection to persist within the host without causing excessive cytolytic damage or cell fusion, which is characteristic of lentiviral infections [163].

Characterizing Immunoglobulin Blocking Activity

Are neutralization mechanisms by sCD4, monoclonal immunoglobulins and polyclonal sera from HIV-infected persons similar or fundamentally different?   In our initial experiments [5, 6, 52], all assessments of biological blocking activity were undertaken with sCD4 [33–37, 103–105]. As discussed, the initial goal of understanding monovalent blocking of the CD4-binding region on gp120 has been realized. Thus the time has come to extend the analysis of blocking activity to other regions on gp120. A number of studies have shown that immunoglobulin block infection by binding to various regions on gp120. These include the CD4-binding domain [106–110], third variable (V3) region [111–117], conformational epitopes [13, 118–120], and other conserved sequences [121–123]. Therefore, to clarify the various issues raised by the third question, it will be necessary to conduct and analyze quantitative infectivity assays with a variety of monoclonal immunoglobulins [124–131] and polyclonal sera.

In this regard, Tilley *et al.* [132] reported an enhanced biological blocking activity of a human monoclonal immunoglobulin when used in the presence of sCD4 (*i.e.*, positive synergy). Since sCD4 was found to compete with this monoclonal for binding, it was concluded that both agents act at overlapping sites on gp120. In view of the finding that sCD4 is synergistic with itself (Fig. 5), it seems clear that the monoclonal was acting simply as a surrogate for additional sCD4. Tilley *et al.* [132] results thus confirm our initial observations of positive synergy [5] and also show that synergy occurs with the binding of an immunoglobulin to gp120—not merely with the binding of sCD4. Based on our notion of the critical number, we expect that other immunoglobulins directed against the CD4-binding site will also show positive synergy with sCD4. In contrast, we predict immunoglobulins directed against other epitopes will not show such synergies.

Despite vigorous humoral responses, humans do not clear their initial episode of HIV viremia [133]. Several explanations for this failure of protection by immunoglobulins have been proposed. One is that a rapid rate of amino acid substitution in gp120 permits HIV to outmaneuver the immune system. As with other lentiviruses, the continuous generation of small antigenic changes allows HIV to stay ahead of the appearance of neutralizing immunoglobulins [134–136]. A second explanation is that the initial stage of HIV infection is associated with immune dysfunction [22–26]. In this case, polyclonal B cell activation results in the overproduction immunoglobulins and the disruption of "normal" maturation of humoral responses [137–143]. A third explanation is that HIV induces a state of "original antigenic sin" [144]. That is, HIV somehow limits the output of B cells to a narrow repertoire of immunoglobulins. Subsequent changes in HIV epitopes are then met by the same old humoral response.

We do not dispute these "classic" explanations of viral persistence [23]. However, if the biological blocking activities of gp120-binding immunoglobulins are similar to those of sCD4, then our background experiments show that they will provide little or no humoral protection to the spread of infection in lymphoid compartments [6].

The initial phase of HIV infection can be likened to a branching process [1]. In this process (Fig. 12), each infected target cell generates an average number of progeny virions, V_n, that are released into the extracellular medium. These virions, in turn, infect new target cells with an average probability, I_n. If the branching number (*i.e.*, the average number of successfully infecting progeny virions) is $V_n \times I_n > 1$, then a growing infection will develop. On the other hand, if the branching number is $V_n \times I_n < 1$, then the initial infection will eventually extinguish. Table III summarizes some of the extracellular parameters that
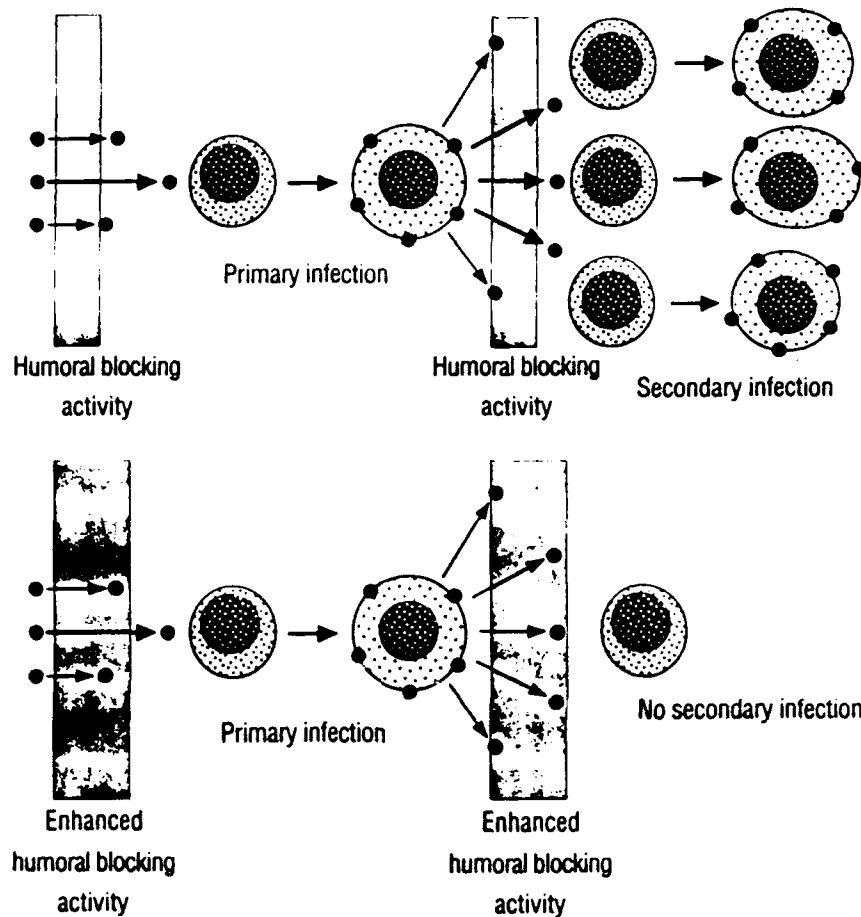
FIGURE 12   The initial growth of HIV infection *in vitro* and *in vivo* can be likened to a branching process. Such a process also describes the reactions taking place during nuclear fission. In this case, target cells are analogous to fissionable nuclei, progeny virions are analogous to neutrons, and humoral blockers are analogous to control elements. The figure illustrates the effects of humoral blocking activity. Lower levels of blocking activity (above) permit growth of infection whereas higher levels (below) halt the initial infection. Note that the spread of HIV infection can be arrested even after an initial infectious event. Table III summarized other extracellular parameters that influence whether a chain reaction is achieved or not.

determine whether an initial infectious event will result in a "bomb" or "dud." Note that increased humoral blocking activity and increased killing of infected target cells (the latter is not discussed in this review) will act in concert to reduce the branching number.

Immunoglobulins (Ig) have the ability to form multivalent attachments, which can increase binding affinities by orders of magnitude [32]. For HIV, however, there is no information on whether immunoglobulins in fact take advantage of this potential mechanism. For effective bivalent attachments by Ig to occur, for example, binding sites must be separated by 60 to 80 Å [145]. With monoclonal Ig, we thus have an opportunity to determine whether monovalent Fab fragments block infection with an activity that is similar to intact Ig. If both activities are similar, the monoclonal Ig blocks monovalently. On the

TABLE III

Extracellular Parameters Determining Whether
the Initial Branching Process Leads to a "Bomb" or "Dud"

Factors promoting the growth of infection
* increased target cell density (i.e., infection in lymphoid organs)
* increased number of progency virions
* increased gp120 on active virions
* increased lifetime of infectious particles
* decreased critical number

Factors promoting the extinction of infection
* increased humoral blocker concentration
* increased gp120-blocker K_{max}
* increased gp120 shedding rate
* increased nonspecific viral inactivation rate
* increased critical number
* increased killing rate of infected target cells (i.e., cell-mediated immunity)

---

other hand, if the activity of intact Ig is much greater than its Fab fragment, the monoclonal Ig blocks bivalently. Conceivably, the inability to produce immunoglobulins with multi-valent activity could provide yet another reason for the failure of humoral responses [146]. This could also apply to humoral responses induced by HIV vaccines [147–151].

Variations Between HIV Strains

What range of critical numbers, shedding rates and neutralization susceptibilities typify wild-type strains of HIV? In the background experiments, all investigations were conducted with laboratory-adapted strains of HIV-1 and HIV-2. We initially chose to study laboratory strains because they replicated to high titer and formed well-defined syncytia. This facilitated good precision and accuracy in quantitative infectivity assays [5, 6]. Quite often, however, the characteristics of laboratory strains differ from those commonly infecting humans [152, 153]. Thus, the aim of the fourth question is to ascertain the range of kinetic parameters that characterize wild-type strains of HIV. More specifically, this question can be expressed as:(a) how much does the critical number vary between wild-type strains; (b) in unsaturated assays, how much does the biological blocking activity of sCD4 vary between wild-type strains; and (c) how much does the spontaneous shedding rate of gp120 vary between wild-type strains?

A perplexing issue in HIV research concerns the selection of viral strains for screening therapeutic agents and developing vaccines. In other words, how do we select a small number of "model" HIV strains for subsequent use in detailed and costly studies? A customary approach has been to survey viral strains from infected individuals and to select the most prevalent ones. Based on this, strains have been selected by using panels of typing sera and by sequencing small segments of the viral genome. For example, the V3 loop has been sequenced with the aim of identifying the single most prevalent strain [111]. Based on the kinetic model and background experiments, however, another criteria for selection is to choose those strains that represent the most formidable targets for attack. Hence, strains with the smallest critical number, the lowest biological blocking activity, and the slowest gp120 shedding rate are good candidates.

As an example of this notion, let us consider the relevance of gp120 shedding to the

56   S. P. LAYNE AND M. DEMBO

testing and development of HIV vaccines [6]. Animal testing will be necessary step in developing such a vaccine [154–156]. Like experimental transmission, human transmission probably takes place with HIV particles having different ages (time elapsed after budding). Consequently, immunoglobulins induced by a vaccine will have to block particles of all ages [6]. Figure 8B shows that newer HIV particles will be more difficult to block than older ones. Thus aged animal challenge stocks may give inappropriately high estimates of humoral efficacy in animals. This effect will be the most prominent for viral strains with the fastest rates of gp120 shedding. Therefore, in selecting HIV strains for animal challenge stocks [157], prevalent strains having the slowest rates of gp120 shedding will provide the most discriminating tests of vaccine efficacy.

STANDARDIZING HIV STOCKS AND INFECTIVITY ASSAYS

Quantitative infectivity assays are indispensable tools for HIV research. They are used for screening therapeutic agents, evaluating responses to vaccines, and examining immuno-globulins from infected individuals. The amount of reliable data derived from infectivity assays, however, is undoubtedly limited by a lack of standard viral stocks and assay methods [158]. Nearly every laboratory uses its own "home grown" HIV stocks to conduct assays. Individual batches vary considerably in viral titer, gp120 and p24 protein concentra-tions. Also nearly every laboratory uses a different type of viral infectivity assay. Time and again, researchers commiserate that they cannot quantitatively compare infectivity assay results between themselves. Based on the background experiments and their comparison to the kinetic model, we now have several clear explanations for these shortcomings. The good news is that there are practical solutions for standardizing HIV stocks and assay conditions. The bad news is that standardization will entail more preparatory work for HIV researchers and the interpretation of previous data will require a thorough rehashing.

Let us now review the experiments and analyses that have led to this perspective. At low target cell densities, sCD4 blocks a small number of infectious collisions between viral particles and cells. Consequently, the biological blocking activity of sCD4 corresponds to the gp120-sCD4 K_{assoc} [5, 6]. At high target cell densities, on the other hand, sCD4 must block a large number of infectious collisions. In this instance, sCD4 blocking activity falls below the K_{assoc} from chemical measurements (Fig. 4B and Table I). In addition to this, we have seen that spontaneous shedding of gp120 leads to decreased rates of infectious collision between viral particles and cells (Fig. 7). As a result, infectivity assays performed at high target cell densities will demonstrate increasing sCD4 blocking activity as viral stocks age (Fig. 8B). Also because HIV requires a critical number of gp120s, sCD4 blocking activity will demonstrate a pronounced positive synergy with continued aging of the stock. Thus, as shown in Figure 13, the opposing effects of target cell density and viral stock age can lead to ambiguous and confounding assessments of sCD4 blocking activity in assays lacking proper controls.

To directly compare the biological blocking activity of one agent against different viral strains or of several agents against one strain, all infectivity assays must be unsaturated [6]. Practical approaches for meeting this requirement are to produce and store large volumes of viral stocks in small aliquots. Subsequently, a series of "pilot" assays can be performed with the goal of determining cell densities at which the biological blocking activity of agents, such as sCD4, equal the K_{assoc} from chemical measurements. If K_{assoc} data are not available, assays can then be performed at cell densities where the blocking activity is
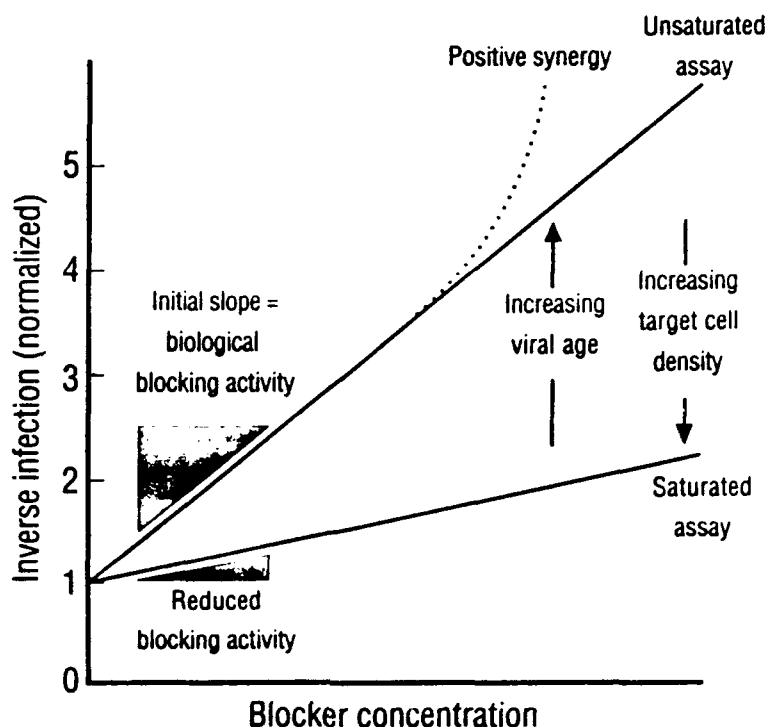
FIGURE 13   Summary of the opposing effects of target cell density and viral stock age.

independent of density. Under either circumstance, the initial slope yields biological blocking activities that are derived from unsaturated assays (Fig. 13).

The *in vitro* blocking activity of sCD4 [5, 49, 50, 57] and immunoglobulins [135, 136] varies considerably between HIV types and isolates. In terms of gp120 structure, these variations have been attributed to different glycoprotein conformations [13] and amino acid sequences [51]. In terms of physical chemistry [1-4], these variations have been ascribed to different gp120-blocker K_{assoc} [51]. However, without the stringent use of unsaturated infectivity assays, it is impossible to distinguish whether antigenic factors or assay conditions are the authentic explanation for these variations [6]. For many previous studies of HIV neutralization that have been published, we perceive that it is not feasible to ascertain whether infectivity assays were unsaturated or not. Moreover, since the requisite "saturation" and "age" controls (outlined above) are infrequently performed, it is unlikely that retrospective examination of the raw data will clarify this issue significantly. We must therefore reconsider whether previous interpretations of the humoral responses to natural infection are indeed accurate.

A rather disconcerting finding is that sCD4-like blockers may exert little or no biological blocking activity at 10^7 to 10^9 target cells ml^{-1} [6]. Therefore, we believe that humoral-blocking therapies based on soluble forms of viral receptors [159, 160] may have to be reevaluated altogether [161, 162]. At present, it remains to be conclusively demonstrated whether immunoglobulin blocking activities in general are similar to those of sCD4 or not [6]. If they are alike, however, we must also recognize that humoral blocking may not

58   S. P. LAYNE AND M. DEMBO

protect once HIV enters lymphoid organs [6]. In addition, the local CD4+ cell density where HIV first enters the body (*e.g.*, infiltrated sites in genital ulcers versus non-infiltrated abrasions) may determine whether vaccine-induced immunoglobulins can extinguish the initial rounds of infection (Fig. 12 and Table III).

Finally, since HIV requires a critical number of gp120 molecules for efficient infection, the use of aged vaccine challenge stocks (or stocks from chronic cultures) may lead to overestimates of vaccine efficacy [6]. Therefore, vaccine challenges with cell-free virus are best performed with viral stocks that are rapidly grown and harvested.

Acknowledgments

References

1. Layne, S. P., Spouge, J. L., and Dembo, M. Quantifying the infectivity of human immunodeficiency virus. *Proc. Natl. Acad. Sci. USA* **86**, 4644–4648, 1989.
2. Spouge, J. L., Layne, S. P., and Dembo, M. Analytic results for quantifying HIV infectivity. *Bull. Math. Biol.* **51**, 715–730, 1989.
3. Layne, S. P., Dembo, M., and Spouge, J. L. Kinetics of HIV infectivity. *Los Alamos Science* **18**, 90–109, 1989.
4. Layne, S. P., Spouge, J. L., and Dembo, M. Measuring HIV infectivity. In: *Lecture Notes in Biomathematics 83*, edited by C. Castillo-Chavez. New York: Springer-Verlag, 1989, pp. 80–110.
5. Layne, S. P., Merges, M. L., Dembo, M., Spouge, J. L., and Nara, P. L. HIV requires multiple gp120 molecules for CD4-mediated infection. *Nature* **346**, 277–279, 1990.
6. Layne, S. P., Merges, M. L., Spouge, J. L., Dembo, M., and Nara, P. L. Blocking of human immunodeficiency virus infection depends on cell density and viral stock age. *J. Virol.* **65**, 3293–3300, 1991.
7. Bell, G. I., Dembo, M., and Bongrand, P. Cell adhesion: competition between nonspecific repulsion and specific binding. *Biophys. J.* **45**, 1051–1064, 1984.
8. Dembo, M., and Bell, G. I. The thermodynamics of cell adhesion. *Current Topics in Membranes and Transport* **29**, 71–89, 1987.
9. Springer, T. A. Adhesion receptors of the immune system. *Nature* **346**, 425–434, 1990.
10. Plunkett, M. L., Sanders, M. E., Selvaraj, P., Dustin, M. L., and Springer, T. A. Rosetting of activated human T lymphocytes with autologous erythrocytes. *J. Exp. Med.* **165**, 664–676, 1987.
11. Dulbecco, R., Vogt, M., and Strickland, A. G. R. A study of the basic aspects of neutralization of two animal viruses, western equine encephalitis virus and poliomyelitis virus. *Virology* **2**, 162–205, 1956.
12. Della-Porta, A. J., and Westaway, E. G. A multi-hit model for the neutralization of animal viruses. *J. Gen. Virol.* **38**, 1–19, 1977.
13. Nara, P. L., Smit, L., Dunlop, N., Hatch, W., Merges, M., Waters, D., Kelliher, J., Gallo, R. C., Fischinger, P. J., and Goudsmit, J. Emergence of viruses resistant to neutralization by V3-specific antibodies in experimental human immunodeficiency virus type I IIIB infection of chimpanzees. *J. Virol.* **64**, 3779–3791, 1990.
14. Maddon, J. P., Dalgleish, A. D., McDougal, J. S., Clapham, P. R., Weiss, R. A., and Axel, R. The T4 gene encodes the AIDS virus receptor and is expressed in the immune system and the brain. *Cell* **47**, 333–348, 1986.
15. Ho, D. D., Pomerantz, R. J., and Kaplan, J. C. Pathogenesis of infection with human immunodeficiency virus. *N. Engl. J. Med.* **317**, 278–286, 1987.
16. Nara, P. L. AIDS Viruses of Animals and Man: Nonliving Parasites of the Immune System. *Los Alamos Science* **18**, 54–89, 1989.
17. Butcher, E. C., and Weissman, I. L. Lymphoid tissues and organs. In: *Fundamental Immunology*, 2nd edition, edited by W. E. Paul, New York: Raven, 1989, pp. 117–137.
18. Moore, J. P., McKeating, J. A., Weiss, R. A., and Sattentau, Q. J. Dissociation of gp120 from HIV-1 virions induced by soluble CD4. *Science* **250**, 1139–1142, 1990.

19. Moore, J. P., McKeating, J. A., Norton, W. A., and Sattentau, Q. J. Direct measurement of soluble CD4 binding to human immunodeficiency virus type 1 virions: gp120 dissociation and its implications for the virus-cell binding and fusion reactions and their neutralization by soluble CD4. *J. Virology* **65**, 1133–1140, 1991.

20. Kirsh, R., Hart, T. K., Ellens, H., Miller, J., Petteway, S. A., Lambert, D. M., Leary, J., and Bugelski, P. J. Morphometric analysis of recombinant soluble CD4-mediated release of the envelop glycoprotein gp120 from HIV-1. *AIDS Res. Hum. Retrovir.* **6**, 1209–1212, 1990.

21. Hart, T. K., Kirsh, R., Ellens, H., Sweet, R. W., Lambert, D. M., Petteway, S. R., Leary, J., and Bugelski, P. J. Binding of soluble CD4 proteins to human immunodeficiency virus type 1 and infected cells induces release of envelope glycoprotein gp120. *Proc. Natl. Acad. Sci. USA* **88**, 2189–2193, 1991.

22. Fauci, A. S. The human immunodeficiency virus: infectivity and mechanisms of pathogenesis. *Science* **239**, 617-622, 1988.

23. Oldstone, M. B. A. Viral persistence. *Cell* **56**, 517–520, 1989.

24. Narayan, O., and Clements, J. E. Lentiviruses. In: *Fields Virology*, 2nd edition, vol. 2, edited by B. Fields, New York: Raven, 1990, pp. 1571–1589.

25. Siliciano, R. F., Lawton, T., Knall, C., Karr, R. W., Berman, P., Gregory, T., and Reinherz, E. L. Analysis of host-virus interactions in AIDS anti-gp120 T cell clones: effect of HIV sequence variation and a mechanism for CD4+ cell depletion. *Cell* **54**, 561–575, 1988.

26. Lanzavecchia, A., Roosnek, E., Gregory, T., Berman, P., and Abrignani, S. T cells can present antigens such as HIV gp120 targeted to their own surface molecules. *Nature* **334**, 530–532, 1988.

27. Gelderblom, H. R., Reupke, H., and Pauli, G. Loss of envelope antigens of HTLV-III/LAV, a factor in AIDS pathogenesis? *Lancet* **ii**, 1016–1017, 1985.

28. Schneider, J., Kaaden, O., Copeland, T. D., Oroszlan, S., and Hunsmann, G. Shedding and interspecies type sero-reactivity of the envelope glycopolypeptide gp120 of the human immunodeficiency virus. *J. Gen. Virol.* **67**, 2533–2538, 1986.

29. Gelderblom, H. R., Hausmann, E. H. S., Özel, M., Pauli, G., and Koch, M. A. Fine structure of human immunodeficiency virus (HIV) and immunolocalization of structural proteins. *Virology* **156**, 171–176, 1987.

30. Gelderblom, H. R. Assembly and Morphology of HIV: potential effect of structure on function. *AIDS* **5**, 617–638, 1991.

31. Nara, P. L., Dunlop, N. M., Robey, W. G., Callahan, R., and Fischinger, P. J. Lipoprotein-associated oncornavirus-inactivating factor in the genus *Mus*: effects on murine leukemia viruses of laboratory and exotic mice. *Cancer Res.* **47**, 667–672, 1987.

32. Day, E. D. *Advanced Immunochemistry*, 2nd edition, New York: Wiley-Liss, pp. 295–350, 1990.

33. Smith, D. H., Byrn, R. A., Marsters, S. A., Gregory, T., Groopman, J. E., and Capon, D. J. Blocking of HIV-1 infectivity by a soluble, secreted form of the CD4 antigen. *Science* **238**, 1704–1707, 1987.

34. Fisher, R. A., Bertonis, J. M., Meier, W., Johnson, V. A., Costopoulos, D. S., Liu, T., Tizard, R., Walker, B. D., Hirsch, M. S., Schooley, R. T., and Flavell, R. A. HIV infection is blocked *in vitro* by recombinant soluble CD4. *Nature* **331**, 76–78, 1988.

35. Hussey, R. E., Richardson, N. E., Kowalski, M., Brown, N. R., Chang, H.-C., Siliciano, R. F., Dorfman, T., Walker, B., Sodroski, J., and Reinherz, E. L. A soluble CD4 protein selectively inhibits HIV replication and syncytium formation. *Nature* **331**, 78–81, 1988.

36. Deen, K. C., McDougal, J. S., Inacker, R., Folena-Wasserman, G., Arthos, J., Rosenberg, J., Maddon, P. J., Axel, R., and Sweet, R. W. A soluble form of CD4 (T4) protein inhibits AIDS virus infection. *Nature* **331**, 82–84, 1988.

37. Traunecker, A., Lüke, W., and Karjalainen, K. Soluble CD4 molecules neutralize human immunodeficiency virus type 1. *Nature* **331**, 84–86, 1988.

38. Wang, J., Yan, Y., Garrett, T. P. J., Liu, J., Rodgers, D. W., Garlick, R. L., Tarr, G. E., Husain, Y., Reinherz, E. L., and Harrison, S. C. Atomic structure of a fragment of human CD4 containing two immunoglobulin-like domains. *Nature* **348**, 411–418, 1990.

39. Ryu, S.-E., Kwong, P. D., Truneh, A., Porter, T. G., Arthos, J., Rosenberg, M., Dai, X., Xuong, N-h., Axel, R., Sweet, R. W., Hendrickson, W. A. Crystal structure of an HIV-binding recombinant fragment of human CD4. *Nature* **348**, 419–425, 1990.

40. Moore, J. P. Simple methods for monitoring HIV-1 and HIV-2 gp120 binding to soluble CD4 by enzyme-linked immunosorbent assay: HIV-2 has a 25-fold lower affinity than HIV-1 for soluble CD4. *AIDS* **4**, 297–305, 1990.

41. Ashkenazi, A., Smith, D. H., Marsters, S. A., Riddle, L., Gregory, T. J., Ho, D. D., and Capon, D. J. Resistance of primary isolates of human immunodeficiency virus type 1 to soluble CD4 is independent of CD4-rgp120 binding affinity. *Proc. Natl. Acad. Sci. USA* **88**, 7065–7060, 1991.

42. Dimitrov, D. S., Hillman, K., Manischewitz, J., Blumenthal, R., and Golding, H. Kinetics of sCD4 binding to cells expressing HIV-1 envelope [.....] ... . press

43. Kärber, G., Beitrag zur kollektiven behandlung pharmakologisher Reihenversuche [Methods for collective analysis of pharmacologic data from serial samples]. *Arch. f. Exp. Pathol. Pharmakol.* **162**, 480–483, 1937.

44. Spearman, C. The method of wright and wrong cases (constant stimuli) without gauss's formulae. *Brit. J. Psychol.* **2**, 227–242, 1908.

60   S. P. LAYNE AND M. DEMBO

45. Nara, P. L., Hatch, W. C., Dunlop, N. M., Robey, W. G., Arthur, L. O., Gonda, M. A., and Fischinger, P. J. Simple, rapid, quantitative, syncytium-forming microassay for the detection of human immunodeficiency virus neutralizing antibody. *AIDS Res. Hum. Retrovir.* **3**, 283–302, 1987.

46. Nara, P. L., and Fischinger, P. J. Quantitative infectivity assay for HIV-1 and -2. *Nature* **332**, 469–470, 1988.

47. Efron, B., and Tibshirani, R. Statistical data analysis in the computer age. *Science* **253**, 390–395, 1991.

48. Brighty, D. W., Rosenberg, M., Chen, I. S. Y., and Ivey-Hoyle, M. Envelope proteins from clinical isolates of human immunodeficiency virus type 1 that are refractory to neutralization by soluble CD4 possess high affinity for the CD4 receptor. *Proc. Natl. Acad. Sci. USA* **88**, 7802–7805, 1991.

49. Clapham, P. R., Weber, J. N., Whitby, D., McIntosh, K., Dalgleish, A. G., Maddon, P. J., Deen, K. C., Sweet, R. W., and Weiss, R. A. Soluble CD4 blocks the infectivity of diverse strains of HIV and SIV for T cells and monocytes but not for brain and muscle cells. *Nature* **337**, 368–370, 1989.

50. Looney, D. J., Hayashi, S., Nicklas, M., Redfield, R. R., Broder, S., Wong-Staal, F., and Mitsuya, H. Differences in the interaction of HIV-1 and HIV-2 with CD4. *J. AIDS.* **3**, 649–657, 1990.

51. Ivey-Hoyle, M., Culp, J. S., Chaikin, M. A., Hellmig, B. D., Matthews, T. J., Sweet, R. W., and Rosenberg, M. Envelope glycoproteins from biologically diverse isolates of immunodeficiency virus have widely different affinities for CD4. *Proc. Natl. Acad. Sci. USA* **88**, 512–516, 1991.

52. Layne, S. P., Merges, M. L., Conley, S. R., Moore, J. P., Renz, H., Gelderblom, H. R., Spouge, J. L., Dembo, M., and Nara, P. L. Spontaneous shedding of gp120 from HIV-1 modulates infectivity. *J. Exp. Med.* (submitted).

53. Moore, J. P., and Jarrett, R. F. Sensitive ELISA for the gp120 and gp160 surface glycoproteins of HIV-1. *AIDS Res. Hum. Retrovir.* **4**, 369–379, 1988.

54. Moore, J. P., Wallace, L. A., Follett, E. A. C., and McKeating, J. A. An enzyme-linked immunosorbent assay for antibodies to the envelope glycoproteins of divergent strains of HIV-1. *AIDS* **3**, 155–163, 1989.

55. DuPont Chemical. *HIV-1 p24 core profile ELISA.* Catalog number NEK-060A.

56. Byrn, R. A., Sekigawa, I., Chamow, S. M., Johnson, J. S., Gregory, T. J., Capon, D. J., and Groopman, J. E. Characterization of in vitro inhibition of human immunodeficiency virus by purified recombinant CD4. *J. Virol.* **63**, 4370–4375, 1989.

57. McKeating, J. A., McKnight, A., and Moore, J. P. Differential loss of envelope glycoprotein gp120 from virions of human immunodeficiency virus type 1 isolates: effects on infectivity and neutralization. *J. Virol.* **65**, 852–860, 1991.

58. Berg, H. C., and Purcell, E. M. Physics of chemoreception. *Biophys. J.* **20**, 193–219, 1977.

59. Goldstein, B. Diffusion limited effects of receptor clustering. *Comments on Theoretical Biol.* **1**, 109–127, 1989.

60. Goldstein, B., Posner, R. G., Torney, D. C., Erickson, J., Holowka, D., and Baird, B. Competition between solution and cell surface receptors for ligand. *Biophys. J.* **56**, 955–966, 1989.

61. Schawaller, M., Smith, G. E., Skehel, J. J., and Wiley, D. C. Studies with crosslinking reagents on the oligomeric structure of the env glycoprotein of HIV. *Virology* **172**, 367–369, 1989.

62. Earl, P. L., Doms, R. W., and Moss, B. Oligomeric structure of the human immunodeficiency virus type 1 envelope glycoprotein. *Proc. Natl. Acad. Sci. USA* **87**, 648–652, 1990.

63. Gelderblom, H. R., Özel, M., Hausmann, E. H. S., Winkel, T., Pauli, G., and Koch, M. A. Fine structure of human immunodeficiency virus (HIV), immunolocalization of structural proteins and virus-cell relation. *Micron Microscopica* **19**, 41–60, 1988.

64. Temin, H. M. Is HIV unique or merely different. *J. AIDS* **2**, 1–9, 1989.

65. Wong-Staal, F. Human Immunodeficiency Viruses and Their Replication. In: *Fields Virology*, 2nd edition, vol. 2, edited by B. Fields, New York: Raven, 1990, 1529–1543.

66. Greene, W. C. The molecular biology of human immunodeficiency virus type 1 infection. *N. Engl. J. Med.* **324**, 308–317, 1991.

67. Isberg, R. Discrimination between intracellular uptake and surface adhesion of bacterial pathogens. *Science* **252**, 934–938, 1991.

68. Fenouillet, E., Clerget-Raslain, B., Gluckman, J. C., Guétard, D., Montagnier, L., and Bahraoui, E. Role of N-linked glycans in the interaction between the envelope glycoprotein of human immunodeficiency virus and its cellular CD4 receptor. *J. Exp. Med.* **169**, 807–822, 1898.

69. Huso, D. L., Narayan, O., and Hart, G. W. Sialic acids on the surface of caprine arthritis-encephalitis virus define the biological properties of the virus. *J. Virol.* **62**, 1974–1980, 1988.

70. Jolly, P. E., Huso, D., Hart, G., and Narayan, O. Modulation of lentivirus replication by antibodies: non-neutralizing antibodies to caprine arthritis-encephalitis virus enhance early stages of infection in macrophages but do not cause increased production of virions. *J. Gen. Virol.* **70**, 2221–2226, 1989.

71. Ueno, R., and Kuno, S. Dextran sulphate, a potent anti-HIV agent in vitro having synergism with zidovudine. *Lancet* **i**, 1379, 1987.

72. Ito, M., Baba, M., Sato, A., Pauwels, R., De Clercq, E., and Shigeta, S. Inhibitory effects of dextran sulfate and heparin on the replication of human immunodeficiency virus (HIV) in vitro. *Antiviral Res.* **7**, 361–367, 1987.

73. Mitsuya, H., Looney, D. J., Kuno, S., Ueno, R., Wong-Staal, F., and Broder, S. Dextran Sulfate suppression of viruses in the HIV family: inhibition of virion binding to CD4+ cells. *Science* **240**, 646–649, 1988.

74. De Clercq, E. Basic approaches to anti-retroviral treatment. *J. AIDS* 2, 1-9, 1991.

75. Schols, D., Pauwels, R., Desmyter, J., and De Clercq, E. Dextran sulfate and other polyanionic anti-HIV compounds specifically interact with the gp120 glycoprotein expressed by T-cells persistently infected with HIV-1. *Virology* 175, 556-561, 1990.

76. Parish, C. R., Low, L., Warren, H. S., and Cunningham, A. L. A polyanion binding site on the CD4 molecule: proximity to the HIV-gp120 binding region. *J. Immunol.* 145, 1188-1195, 1990.

77. Schols, D., Baba, M., Pauwels, R., and De Clercq, E. Flow cytometric method to demonstrate whether anti-HIV-1 agents inhibit virion binding to T4+ cells. *J. AIDS* 2, 10-15, 1989.

78. Callahan, L. N., Phelan, M., Mallinson, M., and Norcross, M. A. Dextran sulfate blocks antibody binding to the principal neutralizing domain of human immunodeficiency virus type 1 without interfering with gp120-CD4 interactions. *J. Virol.* 65, 1543-1550, 1991.

79. Pharmacia Fine Chemicals. *Dextran Fractions, Dextran Sulphate, DEAE-Dextran: Defined Polymers for Biological Research.* Uppsala, Sweden, 1974.

80. Gowda, S. D., Stein, B. S., Mohaghegphour, N., Benike, C. J., and Engleman, E. G. Evidence that T cell activation is required for HIV-1 entry in CD4+ lymphocytes. *J. Immunol.* 142, 773-780, 1989.

81. Mohagheghpour, N., Chakrabarti, R., Stein, B. S., Gowda, S. D., and Engleman, E. G. Early activation events render T cells susceptible to HIV-1-induced syncytia formation. *J. Biol. Chem.* 266, 7233-7238, 1991.

82. Cheng-Mayer, C., Rutka, J. T., Rosenblum, M. L., McHugh, T., Stites, D. P., and Levy, J. A. Human immunodeficiency virus can productively infect cultured human glial cells. *Proc. Natl. Acad. Sci. USA* 84, 3526-3530, 1987.

83. Tateno, M., Gonzalez-Scarano, F., and Levy, J. A. Human immunodeficiency virus can infect CD4-negative human fibroblastoid cells. *Proc. Natl. Acad. Sci. USA* 86, 4287-4290, 1989.

84. Harouse, J. M., Kunsch, C., Hartle, H. T., Laughlin, M. A., Hoxie, J. A., Wigdahl, B., and Gonzalez-Scarano, F. CD4-independent infection of human neural cells by human immunodeficiency virus type 1. *J. Virol.* 63, 2527-2533, 1989.

85. Cao, Y. Z., Friedman-Klein, A. E., Huang, Y. X., Li, X. L., Mirabile, M., Moudgil, T., Zucker-Franklin, D., and Ho, D. D. CD4-independent, productive human immunodeficiency virus type 1 infection of hepatoma cell lines in vitro. *J. Virol.* 64, 2553-2559, 1990.

86. Harouse, J. M., Bhat, S., Spitalink, S. L., Laughlin, M., Stefano, K., Silberberg, D. H., and Gonzalez-Scarano, F. Inhibition of entry of HIV-1 in neural cell lines by antibodies against galactosyl ceramide. *Science* 253, 320-323, 1991.

87. Bhat, S., Spitalnik, S. L., Gonzalez-Scarano, F., and Silberberg, D. H. Galactosyl ceramide or a derivative is an essential component of the neural receptor for human immunodeficiency virus type 1 envelope glycoprotein gp120. *Proc. Natl. Acad. Sci. USA* 88, 7131-7134, 1991.

88. Levy, J. A. Changing concepts of HIV infection: challenges for the 1990s. *AIDS* 4, 1051-1058, 1990.

89. Cordonnier, A., Montagnier, L., and Emerman, M. Single amino-acid changes in HIV envelope affect tropism and receptor binding. *Nature* 340, 571-574, 1989.

90. O'Brien, W. A., Koyanagi, Y., Namazie, A., Zhao, J.-Q., Diagne, A., Idler, K., Zack, J. A., and Chen, I. S. Y. HIV-1 tropism for mononuclear phagocytes can be determined by regions of gp120 outside the CD4-binding domain. *Nature* 348, 69-72, 1990.

91. Hwang, S. S., Boyle, T. J., Lyerly, H. K., and Cullen, B. R. Identification of the envelope V3 loop as the primary determinant of cell tropism in HIV-1. *Science* 253, 71-74, 1991.

92. Shioda, T., Levy, J. A., and Cheng-Mayer, C. Macrophage and T cell-line tropisms of HIV-1 are determined by specific regions of the envelope gp120 gene. *Nature* 349, 167-169, 1991.

93. Schnittman, S. M., Psallidopoulos, M. C., Lane, H. C., Thopmson, L., Baseler, M., Massari, F., Fox, C. H., Salzman, N. P., and Fauci, A. S. The reservoir for HIV-1 in human peripheral blood is a T cell that maintains expression of CD4. *Science* 245, 305-308, 1989.

94. Ho, D. D., Moudgil, T., and Alam, M. Quantitation of human immunodeficiency virus type 1 in the blood of infected persons. *N. Engl. J. Med.* 321, 1621-1625, 1989.

95. Coombs, R. W., Collier, A. C., Allain, J.-P., Nikora, B., Leuther, M., Gjerset, G. F., and Corey, L. Plasma viremia in human immunodeficiency virus infection. *N. Engl. J. Med.* 321, 1626-1631, 1989.

96. Schnittman, S. M., Greenhouse, J. J., Psallidopoulos, M. C., Baseler, M., Salzman, N. P., Fauci, A. S., and Lane, H. C. Increasing viral burden in CD4+ T cells from patients with human immunodeficiency virus (HIV) infection reflects rapidly progressive immunosuppression and clinical disease. *Ann. Intern. Med.* 113, 438-443, 1990.

97. Meltzer, M. S., Skillman, D. R., Gomatos, P. J., Kalter, D. C., and Gendelman, H. E. Role of mononuclear phagocytes in the pathogenesis of human immunodeficiency virus infection. *Ann. Rev. Immunol.* 8, 169-194, 1990.

98. Gendelman, H. E., and Meltzer, M. S. Mononuclear phagocytes and the human immunodeficiency virus. *Curr. Opinions Immunol.* 2, 414-419, 1990.

99. Schooley, R. T., Merrigan, T. C., Gaut, P., Hirsch, M. S., Holodniy, M., Flynn, T., Liu, S., Byington, R. E., Henochowicz, S., Gibish, E., Spriggs, D., Kufe, D., Schindler, J., Dawson, A., Thomas, D., Hanson, D. G., Letwin, B., Liu, T., Gulinello, J., Kennedy, S., Fisher, R., and Ho, D. D. Recombinant soluble CD4 Therapy

62   S. P. LAYNE AND M. DEMBO

in patients with the acquired immunodeficiency syndrome (AIDS) and AIDS-related complex. *Ann. Intern. Med.* **112**, 247–253, 1990.

100. Kahn, J. O., Allan, J. D., Hodges, T. L., Kaplan, L. D., Arri, C. J., Fitch, H. F., Izu, A. E., Mordenti, J., Sherwin, S. A., Groopman, J. E., and Volberding, P. A. The safety and pharmacokinetics of recombinant soluble CD4 (rCD4) in subjects with the acquired immunodeficiency syndrome (AIDS) and AIDS- related complex. *Ann. Intern. Med.* **112**, 254–261, 1990.

101. Daar, E. S., Li, X. L., Moudgil, T., and Ho, D. D. High concentrations of recombinant soluble CD4 are required to neutralize primary human immunodeficiency virus type 1 isolates. *Proc. Natl. Acad. Sci. USA* **87**, 6574–6578, 1990.

102. Gomatos, P. J., Stamatos, N. M., Gendelman, H. E., Fowler, A., Hoover, D. L., Kalter, D. C., Burke, D. S., Tramount, E. C., and Meltzer, M. S. Relative inefficiency of soluble recombinant CD4 for inhibition of infection by monocyte-tropic HIV in monocytes and T cells. *J. Immunol.* **144**, 4183–4188, 1990.

103. Traunecker, A., Schneider, J., Kiefer, H., and Karjalainen, K. Highly effective neutralization of HIV with recombinant CD4-immunoglobulin molecules. *Nature (London)* **339**, 68–70, 1989.

104. Capon, D. J., Chamow, S. M., Mordenti, J., Marsters, S. A., Gregory, T., Mitsuya, H., Byrn, R. A., Lucas, C., Wurm, F. M., Groopman, J. E., Broder, S., and Smith, D. H. Designing CD4 immunoadhesins for AIDS therapy. *Nature* **337**, 525–531, 1989.

105. Byrn, R. A., Mordenti, J., Lucas, C., Smith, D., Marsters, S. A., Johnson, J. S., Cossum, P., Chamow, S. M., Wurm, F. M., Gregory, T., Groopman, J. E., and Capon, D. J. Biological properties of CD4 immunoadhesin. *Nature* **344**, 667–670, 1990.

106. Clayton, L. K., Hussey, R. E., Stienbrich, R., Ramachandran, H., Husain, Y., and Reinherz, E. L. Substitution of murine for human CD4 residues identifies amino acids critical for HIV-gp120 binding. *Nature* **335**, 363–366, 1988.

107. Landau, N. R., Warton, M., and Littman, D. R. The envelope glycoprotein of the human immunodeficiency virus binds to the immunoglobulin-like domain of CD4. *Nature* **334**, 159–162, 1988.

108. Lifson, J. D., Hwang, K. M., Nara, P. L., Fraser, B., Padgett, M., Dunlop, N. M., and Eiden, L. E. Synthetic CD4 peptide derivatives that inhibit HIV infection and cytopathicity. *Science* **241**, 712–716, 1988.

109. Nara, P. L., Hwang, K. M., Rausch, D. M., Lifson, J. D., and Eiden, L. E. CD4 antigen-based antireceptor peptides inhibit infectivity of human immunodeficiency virus in titer at multiple stages of the viral life cycle. *Proc. Natl. Acad. Sci. USA* **86**, 7139–7143, 1989.

110. Hayashi, Y., Ikuta, K., Fujii, N., Ezawa, K., Kato, S. Inhibition of HIV-1 replication and syncytium formation by synthetic CD4 peptides. *Arch. Virol.* **105**, 129–135, 1989.

111. LaRosa, G. J., Davide, J. P., Weinhold, K., Waterbury, J. A., Profy, A. T., Lewis, J. A., Langlois, A. J., Dreesman, G. R., Boswell, R. N., Shadduck, P., Holley, L. H., Karplus, M., Bolognesi, D. P., Matthews, T. J., Emini, E. A., and Putney, S. D. Conserved sequence and structural elements in the HIV-1 principal neutralizing determinant. *Science* **249**, 932–935, 1990.

112. Javaherian, K., Langlois, A. J., LaRosa, G. J., Profy, A. T., Bolognesi, D. P., Herlihy, W. C., Putney, S. D., and Matthews, T. J. Broadly neutralizing antibodies elicited by the hypervariable neutralizing determinant of HIV-1. *Science* **250**, 1590–1593, 1990.

113. Javaherian, K., Langlois, A. J., McDanal, C., Ross, K. L., Eckler, L. I., Jellis, C. L., Profy, A. T., Rusche, J. R., Bolognesi, D. P., Putney, S. D., and Matthews, T. J. Principle neutralizing domain of the human immunodeficiency virus type 1 envelope protein. *Proc. Natl. Acad. Sci. USA* **86**, 6768–6772, 1989.

114. Goudsmit, J., Debouck, C., Meleon, R. H., Smit, L., Bakker, M., Asher, D. M., Wolff, A. V., Gibbs, C. J., and Gajdusek, D. C. Human immunodeficiency virus type 1 neutralization epitope with conserved architecture elicits early type-specific antibodies in experimentally infected chimpanzees. *Proc. Natl. Acad. Sci. USA* **85**, 4478–4482, 1988.

115. Parker, T. J., Clark, M. E., Langlois, A. J., Matthews, T. J., Weinhold, K. J., Randall, R. R., Bolognesi, D. P., and Hayes, B. F. Type-specific neutralization of the human immunodeficiency virus with antibodies to env-encoded synthetic peptides. *Proc. Natl. Acad. Sci. USA* **85**, 1932–1936, 1988.

116. Putney, S. D., Matthews, T. J., Robey, W. G., Lynn, D. L., Robert-Guroff, M., Mueller, W. T., Langlois, A. J., Ghrayeb, J., Petteway, S. R., Weinhold, K. J., Fischinger, P. J., Wong-Staal, F., Gallo, R. C., and Bolognesi, D. P. HTLV-III/LAV-neutralizing antibodies to an E. coli-produced fragment of the virus envelope. *Science* **234**, 1392–1395, 1986.

117. Rusche, J. R., Javaherian, K., McDanal, C., Petro, J., Lynn, D. L., Grimaila, R., Langlois, A., Gallo, R. C., Arthur, L. O., Fischinger, P. J., Bolognesi, D. P., Putney, S. D., and Matthews, T. J. Antibodies that inhibit fusion of human immunodeficiency virus-infected cells bind a 24-amino-acid sequence of the viral envelope, gp120 *Proc. Natl. Acad. Sci. USA* **85**, 3198–3202, 1988.

118. Goudsmit, J., Kuiken, C. L., and Nara, P. L. Linear versus conformational variation of V3 neutralization domains of HIV-1 during experimental and natural infection. *AIDS (suppl 1)* **3**, S119–S123, 1989.

119. Haigwood, N. L., Barker, C. B., Higgins, K. W., Skiles, P. V., Moore, G. K., Mann, K. A., Lee, D. R., Eichberg, J. W., and Steimer, K. S. Evidence for neutralizing antibodies directed against conformational epitopes of HIV-1 gp120. *Vaccines* **90**, 313–320, 1990.

120. Ho, D. D., McKeating, J. A., Ling, X. L., Moudgil, T., Daar, E. S., Sun, N.-C., and Robinson, J. E.

Conformational epitope on gp120 important in CD4 binding and human immunodeficiency virus type I neutralization identified by a human monoclonal antibody. *J. Virology* **65**, 489–493, 1991.

121. Chanh, T. C., Dreesman, G. R., Kanda, P., Linette, G. P., Sparrow, J. T., Ho, D. D., and Kennedy, R. C. Induction of anti-HTLV-III/LAV neutralizing antibodies by synthetic peptides. *EMBO J.* **5**, 3065–3071, 1986.

122. Ho, D. D., Kaplan, J. C., Rackauskas, I. E., and Gurney, M. E. Second conserved domain of gp120 is important for HIV infectivity and antibody neutralization. *Science* **239**, 1021–1023, 1988.

123. Ho, D. D., Sarngadharan, M. G., Hirsch, M. S., Schooley, R. T., Rota, T. R., Kennedy, R. C., Chanh, T. C., and Sato, V. Human immunodeficiency virus neutralizing antibodies recognize several conserved domains on the envelope glycoproteins. *J. Virol.* **61**, 2024–2028, 1987.

124. Mizukami, T., Fuerst, T. R., Berger, E. A., and Moss, B. Binding region for human immunodeficiency virus (HIV) and epitopes for HIV-blocking monoclonal antibodies of the CD4 molecule defined by site-directed mutagenesis. *Proc. Natl. Acad. Sci. USA* **85**, 9273–9277, 1988.

125. Kinney-Thomas, E., Weber, J. N., McClure, J., Clapham, P., Singhal, M., Shriver, K., and Weiss, R. A. Neutralizing monoclonal antibodies to AIDS virus. *AIDS* **2**, 25–29, 1988.

126. Matsushita, S., Robert-Guroff, M., Rusche, J., Koito, A., Hattori, T., Hoshino, H., Javaherian, K., and Putney, S. Characterization of a human immunodeficiency virus monoclonal antibody and mapping of the neutralizing epitope. *J. Virol.* **62**, 2107–2114, 1988.

127. Sun, N.-C., Ho, D. D., Sun, C. R. Y., Liou, R.-S., Gordon, W., Fung, M. S., Li, X.-L., Ting, R. C., Lee, T.-H., Chang, N. T., and Chang, T.-W. Generation and Characterization of monoclonal antibodies to the putative CD4-binding domain of human immunodeficiency virus type 1 gp120. *J. Virol.* **63**, 3579–3585, 1989.

128. Lindsey, P. S., Ledbetter, J. A., Kinney-Thomas, E., and Hu, S.-L. Effects of anti-gp120 monoclonal antibodies on CD4 receptor binding by the env protein of human immunodeficiency virus type 1. *J. Virology* **62**, 3695–3702, 1988.

129. Scott, C. F., Silver, S., Profy, A. T., Putney, S. D., Langlois, A., Weinhold, K., and Robinson, J. E. Human monoclonal antibody that recognizes the V3 region of human immunodeficiency virus gp120 and neutralizes the human T-lymphotropic virus type IIIMN strain. *Proc. Natl. Acad. Sci. USA* **87**, 8597–8601, 1990.

130. Skinner, M. A., Ting, R., Langlois, A. J., Weinhold, K. J., Lyerly, H. K., Javaherian, K., and Matthews, T. J. Characteristics of a neutralizing monoclonal antibody to the HIV envelope glycoprotein. *AIDS Res. Human Retrovir.* **4**, 187–197, 1988.

131. Gorny, M. K., Xu, J.-Y., Gianakakos, V., Karwowska, S., Williams, C., Sheppard, H. W., Hanson, C. V., and Zolla-Pazner, S. Production of site-selected neutralizing human monoclonal antibodies against the third variable domain of the human immunodeficiency virus type 1 envelope glycoprotein. *Proc. Natl. Acad. Sci. USA* **88**, 3238–3243, 1991.

132. Tilley, S. A., Honnen, W. J., Racho, M. E., Hilgartner, M., and Pinter, A. A human monoclonal antibody against the CD4-binding site of HIV1 gp120 exhibits potent, broadly neutralizing activity. *Res. Virol* **62**, 000–000, 1991.

133. Clark, S. J., Saag, M. S., Decker, W. D., Campbell-Hill, S., Roberson, J. L., Veldkamp, P. J., Kappes, J. C., Hahn, B. H., and Shaw, G. M. High titers of cytopathic virus in plasma of patients with symptomatic primary HIV-1 infection. *N. Engl. J. Med.* **324**, 954–960, 1991.

134. Narayan, O., Zink, M. C., Huso, D., Sheffer, D., Crane, S., Kennedy-Stoskopf, S., Jolly, P. E., and Clements, J. E. Lentiviruses of animals are biological models of the human immunodeficiency viruses. *Microbial. Pathogenesis* **5**, 149–157, 1988.

135. Saag, M. S., Hahn, B. H., Gibbons, J., Li, Y., Parks, E. S., Parks, W. P., and Shaw, G. M. Extensive variation of human immunodeficiency virus type-1 in vivo. *Nature* **334**, 444–447, 1988.

136. Fisher, A. G., Ensoli, B., Looney, D., Rose, A., Gallo, R. C., Saag, M. S., Shaw, G. M., Hahn, B. H., and Wong-Staal, F. Biologically diverse molecular variants within a single HIV isolate. *Nature* **334**, 444–447, 1988.

137. Lane, H. C., Masur, H., Edgar, L. C., Wahlen, G., Rock, A. H., and Fauci, A. S. Abnormalities of B-cell activation and immunoregulation in patients with the acquired immunodeficiency syndrome. *N. Engl J. Med.* **309**, 453–458, 1983.

138. Schnittman, S. M., Lane, H. C., Higgins, S. E., Folks, T., and Fauci, A. S. Direct polyclonal activation of human B lymphocytes by the acquired immune deficiency syndrome virus. *Science* **233**, 1084–1086, 1986.

139. Heriot, K., Hallquist, A. E., and Tomar, R. H. Paraproteinemia in patients with acquired immunodeficiency syndrome (AIDS) or lymphadenopathy syndrome (LAS). *Clin. Chem.* **31**, 1224–1226, 1985.

140. Yarchoan, R., Redfield, R. R., and Broder, S. Mechanisms of B cell activation in patients with acquired immunodeficiency syndrome and related disorders. Contribution of antibody-producing B cells, of Epstein-Barr virus-infected B cells, and of immunoglobulin production induced by human T cell lymphotropic virus type III/lymphadenopathy associated virus. *J. Clin. Invest.* **78**, 439–447, 1986.

141. Amadori, A., De Rossi, A., Faulkner-Valle, G. P., and Chieco-Bianchi, L. Spontaneous in vitro production of virus-specific antibody by lymphocytes from HIV-infected subjects. *Clin. Immunol. Immunopathol.* **46**, 342–351, 1988.

64   S. P. LAYNE AND M. DEMBO

142. Pahwa, S., Chirmule, N., Leombruno, C., Lim, W., Harper, R., Bhalla, R., Pahwa, R., Nelson, R. P., and Good, R. A. In vitro synthesis of human immunodeficiency virus-specific antibodies in peripheral blood lymphocytes of infants. *Proc. Natl. Acad. Sci. USA* **86**, 7532–7536, 1989.

143. Amadori, A., Zamarchi, R., Ciminale, V., Del Mistro, A., Siervo, S., Alberti, A., Colombatti, M., and Chieco-Bianchi, L. HIV-1-specific B-cell activation: a major constituent of spontaneous B-cell activation during HIV-1 infection. *J. Immunol.* **143**, 2146–2152, 1989.

144. Nara, P. L., and Goudsmit, J. Clonal dominance of the neutralizing response to the HIV-1 V3 epitope: evidence for "original antigenic sin" during vaccination and infection in animals, including humans. *Vaccines* **91**, 37–44, 1991.

145. Day, E. D. Advanced immunochemistry, 2nd edition, New York: Wiley-Liss, 1990, pp. 183–255.

146. Dimmock, N. J. Mechanisms of neutralizing animal viruses. *J. Gen. Virol.* **65**, 1015–1022, 1984.

147. Hu, S.-L., Fultz, P. N., McClure, H. M., Eichberg, J. W., Thomas, E. K., Zarling, J., Singhal, M. C., Kosowski, S. G., Swenson, R. B., Anderson, D. C., and Todaro, G. Effects of immunization with a vaccinia-HIV env recombinant on HIV infection of chimpanzees. *Nature* **328**, 721–723, 1987.

148. Arthur, L. O., Pyle, S. W., Nara, P. L., Bess, J. W., Gonda, M. A., Kelliher, J. C., Gilden, R. C., Robey, W. G., Bolognesi, D. P., Gallo, R. C., and Fischinger, P. J. Serological responses in chimpanzees with human immunodeficiency virus glycoprotein (gp120) subunit vaccine. *Proc. Natl. Acad. Sci. USA* **84**, 8583–8587, 1987.

149. Berman, P. W., Groopman, J. E., Gregory, T., Clapham, P. R., Weiss, R. A., Ferriani, R., Riddle, L., Shimasaki, C., Lucas, C., Lasky, L. A., and Eichberg, J. W. Human immunodeficiency virus type 1 challenge of chimpanzees immunized with recombinant envelope glycoprotein gp120. *Proc. Natl. Acad. Sci. USA* **85**, 5200–5204, 1988.

150. Arthur, L. O., Bess, J. W., Waters, D. J., Pyle, S. W., Kelliher, J. C., Nara, P. L., Krohn, K., Robey, W. G., Langlois, A. J., Gallo, R. C., and Fischinger, P. J. Challenge of chimpanzees (pan troglodytes) immunized with human immunodeficiency virus envelope glycoprotein gp120. *J. Virology* **63**, 5046–5053, 1989.

151. Berman, P. W., Gregory, T. J., Riddle, L., Nakamura, G. R., Champe, M. A., Porter, J. P., Wurm, F. M., Hershberg, R. D., Cobb, E. K., and Eichberg, J. W. Protection of chimpanzees from infection by HIV-1 after vaccination with recombinant glycoprotein gp120 but not gp160. *Nature* **345**, 622–625, 1990.

152. Wain-Hobson, S. HIV genome variability in vivo. *AIDS* (suppl 1) **3**, S13–S18, 1989.

153. Fenyö, E. M., Albert, J., and Åsjö, B. Replicative capacity, cytoplasmic effect and cell tropism of HIV. *AIDS (suppl 1)* **3**, S5–S12, 1989.

154. Koff, W. C., and Hoth, D. F. Development and testing of AIDS vaccines. *Science* **241**, 426–432, 1988.

155. Burke, D. S. (ed.). U.S. Army Medical Research and Development Command Retrovirus Research Program Five-Year Plan: FY 89–FY 93. Report of a Conference of Walter Reed Army Medical Center Physicians and Scientists. Hagestown, Maryland. November, 2–4, 1988.

156. Schild, G. C., and Minor, P. D. Human immunodeficiency virus and AIDS: challenges and progress. *Lancet* **335**, 1081–1084, 1990.

157. Cohen, J. Is NIH failing an AIDS "challenge"? *Science* **251**, 518–520, 1991.

158. Newmark, P. AIDS: Complexities and strategies. *Nature* **341**, 566–567, 1989.

159. Ward, R. H. R., Capon, D. J., Jett, C. M., Murthy, K. K., Mordenti, J., Lucas, C., Frie, S. W., Prince, A. M., Green, J. D., and Eichberg, J. W. Prevention of HIV-1 IIIB infection in chimpanzees by CD4 immunoadhesin. *Nature* **352**, 434–436, 1991.

160. Putkonen, P., Thorstensson, R., Ghavamzadeh, L., Albert, J., Hild, K., Biberfeld, G., and Norrby, E. Prevention of HIV-2 and SIVsm infection by passive immunization in cynomolgus monkeys. *Nature* **352**, 436–438, 1991.

161. Moore, J. P., and Weiss, R. A. Passive primate protection. *Nature* **352**, 376–377, 1991.

162. Kaplan, G., Peters, D., and Racaniello, V. R. Poliovirus mutants resistant to neutralization with soluble cell receptors. *Science* **250**, 1596–1599, 1990.

163. Ahmed, R., and Stevens, J. G. Viral persistence. *Fields Virology*, 2nd edition, vol. 1, edited by B. Fields et al., New York: Raven, 1990, pp. 241–266.